Sedimentology, hydrology, and climatic environment of alluvial fans on Earth and Mars

Alexander Michael Morgan

Belmont, California

B.S., University of California Santa Cruz, 2010

A Dissertation presented to the Graduate Faculty

of the University of Virginia in Candidacy for the

Degree of Doctor of Philosophy

Department of Environmental Sciences

University of Virginia

December, 2017

Abstract

A global survey doubles the number of previously identified alluvial fans and deltas on Mars. Alluvial fans are far more widespread than previously reported but are not uniformly distributed. Fans within craters show a favored N-S orientation, but there is a lack of correlation between fan morphometry and local geography or topography. An investigation into the sedimentology of the alluvial fans in Saheki crater provides insights into the climatic environment during deposition. Fan forming discharges consisted of the channelized transport of primarily sand- and gravel-sized sediment as bedload coupled with extensive overbank mud-rich flows depositing planar beds of sand-sized or finer sediment. A comparison with fine-grained alluvial fans in the Chilean Atacama Desert constrains the interpretation of processes responsible for constructing the Saheki crater fans. Flow events are inferred to have been of modest magnitude (probably less than ~60 m^3/s), of short duration, and probably occupied only a few distributaries during any individual flow event. The most likely source of water to form the martian fans is inferred to be snowmelt released after annual or epochal accumulation of snow in the headwater source basin on the interior crater rim. Crater count derived ages of the fans in Saheki crater yield an age of early Amazonian, and a vast majority of fans across Mars superpose Hesperian or Amazonian terrains.

A new landform evolution model is presented that simulates the formation of fine grained alluvial fans. The model generalizes the hydrodynamics of flow and sediment transport while incorporating multiple sizes of sediment, channelized and overbank sediment deposition, and multiple active distributaries. The sediment depositional model is based on interpretations of alluvial fans in Saheki crater and the Chilean Atacama Desert. When subjected to variant boundary conditions such as input discharge and sediment load, the model responds in a similar manner to natural alluvial fans, indicating that it can provide qualitative and quantitative insights into linkages between alluvial fan processes, morphology, and stratigraphy.

A series of previously unstudied fans along the Hilina Pali escarpment on the Island of Hawaii are characterized by their steep slopes, coarse grain sizes, and lobate surface morphology. On the basis of exposed stratigraphy, geologic setting, and calculated flow discharges the fans are interpreted to be forming predominately from sieve lobe deposition, a style of bedload transport that has fallen out of use in the alluvial fan literature due to a perceived lack of field examples.

Acknowledgements

First and foremost, I would like to thank my advisor, Alan Howard, for his mentorship, guidance, encouragement, and patience going back to before I had even arrived at the University of Virginia. I would also like to thank all of my committee members: Pat Wiberg, Paolo D'Odorico, and Bob Johnson.

The research within this dissertation could not have been completed had it not been for the help of many individuals. I thank my NASA Graduate Student Researchers Program mentor Jeff Moore and Smithsonian Institution advisor Bob Craddock. I would also like to thank Dan Hobley (Cardiff), Yo Matsubara (Smithsonian), Orkan Umurhan (NASA Ames), Marisa Palucis (Dartmouth), Bill Dietrich (UC Berkeley), Becky Williams (PSI), Devon Burr (University of Kentucky), Reid Parsons (Fitchburg State), Elizabeth Murphy (UVA), David Seekell (Umeå University), and Michael Morgan for their assistance in the field and sharing their knowledge and experience. I would also like to thank Sharon Wilson (Smithsonian), Ross Irwin (Smithsonian), Ross Beyer (SETI Institute), Erik Asphaug (ASU), and Francis Nimmo (UCSC) for the engaging conversations, assistance with data analysis, and general inspiration.

It has been a great pleasure to be a part of this department. The Department of Environmental Sciences may have a shortage of planetary scientists, but that did not prevent me from making friends and building relationships that I am sure will continue to strengthen throughout my career. I very much appreciate all of the students, faculty, and staff who suffered through my ramblings about Mars with a smile. I would particularly like to thank Jessica Gephart, Michael Saha, and Kyle Emery for the lively conversations during lunch and teatime.

Finally, I would like to thank Alex Bijak for her patience and support while I completed this work, and my parents for instilling in me a love of the outdoors from an early age. I cannot

help but think that our family trips throughout the Sierra Nevada and California Coast Ranges had something to do with my desire to study the rocks both under our feet and amongst the stars.

Per aspera ad astra

Alex Morgan

November 30, 2017

Table of Contents

List of Figures

List of Tables

Chapter 1

Alluvial fans on Earth and Mars

1.1. Context

There is a historical trend in which early researchers study processes on the finer scale, and over time scientific advances allowed them to view the world from a wider perspective. When William Maclure compiled the first geologic map of the United States in 1809, he personally crossed the Allegheny Mountains over fifty times, mapping geologic contacts by hand. Subsequent scientists could use previously collected data to get a broader view of what they were studying, and it was not until the latter half of the twentieth century that modern remote sensing allowed scientists to study the Earth as a global system. This historical transition from finer to broader scale observations is true across many scientific disciplines, with modern tools and methods being used to connect local measurements into a more comprehensive understanding of the natural world.

Planetary geology has largely progressed in the opposite direction. Mars has been studied since the 1600s, but the first telescopic observations were of such broad scale and low resolution that the concept of an extraterrestrial constructed, planet-wide canal network was considered a real possibility until the early 1900s. Flyby and orbital spacecraft in the 1960s and 1970s put to rest any idea of finding little green men in our cosmic neighborhood, characterized the planets thin CO_2 atmosphere, and identified evidence for crater degradation, volcanism, and possible water flow through the outflow channels. Since the arrival of high resolution instruments in the late 1990s fluvial landforms have been identified at a range of scales, including lake basins, deltas, valley networks, and alluvial fans.

Except in the very rare cases of in situ observations by a robotic rover or lander, our understanding of Mars' geology is based on the interpretation of orbital remote sensing observations. By characterizing the conditions that prevailed when these features formed, we can piece together the billions of years of geologic and climatic history that are recorded onto the martian surface. A particularly intriguing piece of this record are the alluvial fans. These features are enigmatic, as their large size, intricate stratigraphy, and partially infilled embedded craters suggest that they formed over a prolonged period, but crater statistics indicate they formed relatively late in Mars' history. The ability to infer process from form is also a challenge in our understanding of terrestrial fan dynamics, and the lack of data linking flow state and subsequent sedimentary deposits remains one of the major barriers in alluvial fan research.

1.2. Geologic and climatic history of Mars

The history of water on the martian surface, and in particular the fate of Mars' climate, remains one of the premier topics of study in the planetary sciences. While the surface of modern Mars cannot sustain liquid water, widespread fluvially modified landscapes suggest that the planet was once warmer and wetter. The effects of water on a landscape are the most unambiguous markers of past climate, and while difficult to decipher, understanding the processes responsible for their formation can provide clues into Mars' climatic history.

The geomorphic evidence for such fluvial activity on early Mars is unequivocal. Branching valley networks and associated overflowed basins required abundant surface water and aquifer recharge (Bhattacharya et al., 2005; Fassett and Head, 2008; Grant, 2000; Gulick, 2001; Irwin et al., 2005b; Matsubara et al., 2013). Tributary heads near drainage divides and erosion of topographic highs show that the atmosphere sustained a hydrologic cycle (Carr, 2002; Craddock and Howard, 2002; Luo et al., 2017; Masursky et al., 1977). The dimensions of relict river channels suggest runoff production rates of up to a centimeter per day (Irwin et al., 2005a), and deltas record deposition into standing bodies of water (Goudge et al., 2017; Irwin et al., 2014).

Mars today is a cold, dry, and hypobaric desert world, with a surface temperature and pressure of 215 K and 6.1 mbar. The thin carbon dioxide atmosphere is insufficient to sustain liquid water on the surface, conditions which climate models suggest should have been more prevalent in the planet's earlier history. The standard solar evolution model indicates the sun had a luminosity of only ~70% its current value at around 3.8 giga-annum (Ga) (Gough, 1981). To compensate for this "faint young sun," the atmosphere would need to trap 85% of the Sun's incoming radiation, significantly higher than modern Earth's 56% (Haberle, 1998). Climate modelers have suggested that the early martian atmosphere must have been denser, perhaps up to 10 bars (Pollack et al., 1987), but this is problematic because clouds condensing from this dense CO_2 atmosphere could reduce the convective lapse rate and, thus, the planetary radiation budget (Kasting, 1991). A variety of greenhouse gases have been proposed to warm the surface, but most of these are typically short-lived (e.g., ammonia, carbonyl sulfide, methane, or sulfur dioxide) and would need a mechanism to be replenished (Wordsworth, 2016). The climate modeling community has not reached a consensus about Mars' climatic evolution. The onus gets back to the geology, which can provide important constraints for the climatic conditions necessary to form the observed landforms.

The geophysical, geochemical, and geomorphological evidence has been pieced together over the past several decades to reconstruct the geologic history of Mars. The relative density of craters on martian terrains divides the planet's history into three periods, the Noachian, Hesperian, and Amazonian (Figure 1.1). Absolute ages for these periods are based on radioactive dating of lunar samples, relative cratering rates between the Moon and Mars, and the long-term evolution of the inner solar system impactor population (Neukum et al., 2001). These parameters are regularly reassessed and exact absolute ages remain uncertain, but it is generally agreed that the Noachian-Hesperian boundary is at ~3.7 Ga and the Hesperian-Amazonian boundary is ~2.9 to 3.3 Ga (Platz et al., 2013).

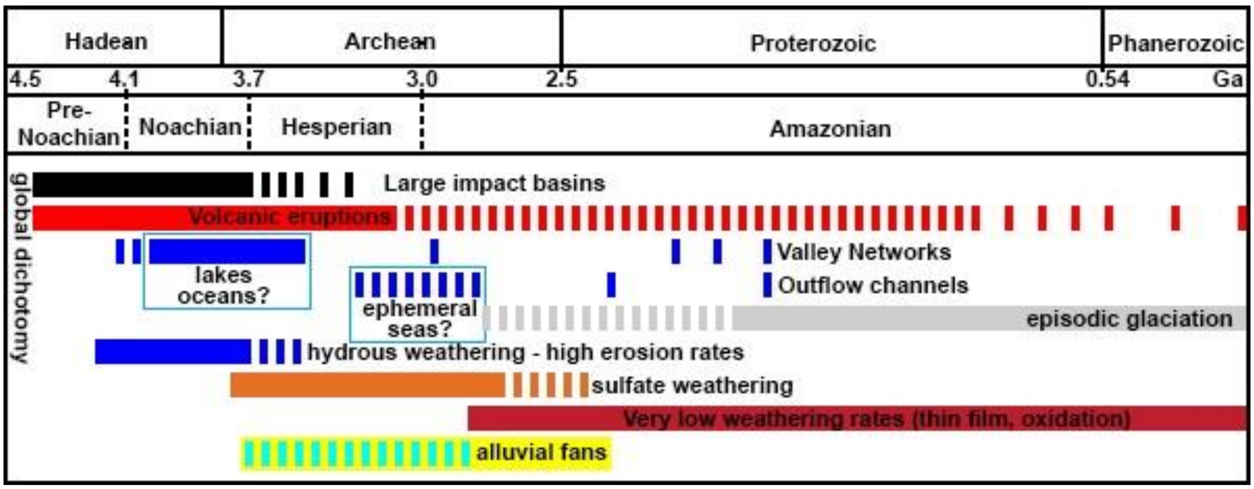

Figure 1.1. Mars geologic timescale. Adapted from Carr and Head (2010) and Ehlmann and Edwards (2014).

The Noachian period featured extensive impact cratering and relatively high erosion rates. Most of the observed fluvial modification to the martian surface occurred during this era, with a spike in activity around the time of the Noachian-Hesperian boundary (Howard et al., 2005; Irwin et al., 2005b). Following the Noachian, erosion rates decreased by two to five orders of magnitude (Golombek et al., 2006). Volcanism became the dominant processes on the martian surface during the Hesperian Period, and outgassing of sulfur dioxide caused a transition in mineralogy from Noachian-aged phyllosilicates to evaporitic minerals such as sulfates as liquid water became more acidic (Bibring et al., 2006; Ehlmann and Edwards, 2014; Murchie et al., 2009). Volcanic activity has become even less frequent during the Amazonian period, and a persistent cold and dry climate has resulted in very little surficial fluvial activity, with the possible exception of gullies along interior crater walls, which remain active in the present day (Harrison et al., 2015).

Recent age reassessments of many fluvial features challenges this paradigm. Alluvial fans (Grant and Wilson, 2011, 2012; Morgan et al., 2014), deltas (Lewis and Aharonson, 2006; Moore et al., 2003) and small shallow valleys (Fassett et al., 2010; Howard and Moore, 2011; Wilson et al., 2016) have been dated to the Hesperian or Amazonian, and may therefore be representative of the last episodes of widespread fluvial modification to the martian surface. The large size of many martian alluvial fans necessitates significant volumes of surficial water (Moore and Howard, 2005; Morgan et al., 2014; Palucis et al., 2014) and analysis of superposed embedded craters indicates that they formed over a prolonged period of tens to hundreds of millions of years (Kite et al., 2017b). Together, these observations raise significant questions about Mars' late-stage hydrologic cycle and potential habitability.

1.3. Alluvial fan processes, morphology, and evolution

Alluvial fans form at the base of mountain fronts as a channel debouches onto a valley floor. The flow loses competence and capacity due slope reduction and the lateral expansion of flow, and sediment is deposited into a semi-conical shape. Alluvial fans are found in all environments with topographic relief, occasional catastrophic discharge, and high sediment production in the source catchment (Blair and McPherson, 2009). Terrestrial alluvial fans span a wide range of sizes and slopes, from steep, sub kilometer cones to large fans of shallow gradient and tens of km in length (Figure 1.2). This variability is a function of depositional process, catchment lithology, tectonism, and climate (Blair, 1999; Blair and McPherson, 2009; Bull, 1977; Harvey, 2004; Harvey et al., 2005; Ritter et al., 1995).

Alluvial fans form from a variety of depositional processes, which can be generalized as avulsing channelized streams, sheetfloods, and debris flows (Blair and McPherson, 2009; Harvey, 2011; Stock, 2013). Understanding the dynamics of alluvial fan flow events has significant implications to human populations. As relatively low-relief features in otherwise mountainous areas, fan surfaces can be desirable locations for development, and portions of rapidly growing metropolises in the American West are built directly on top of alluvial fans. Land-use changes in fan catchments (including deforestation or grazing), as well as changing weather patterns due to climate change, can increase sediment discharge by over 1000% (Coulthard et al., 2000). Areas of Las Vegas, Salt Lake City, and Phoenix have all suffered alluvial fan flooding in recent years (French, 1987; Schumm et al., 1996). Additionally, alluvial fan deposits are reservoirs of water, petroleum, and aggregate materials, but their resource potential is dependent on their composition, which is a function of their formative dynamics.

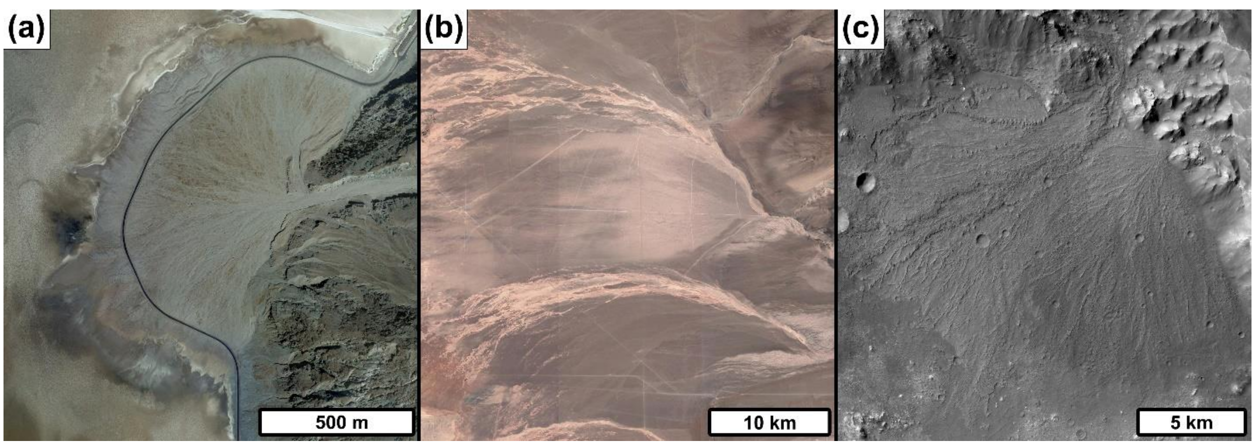

Figure 1.2. Examples of alluvial fans. From left to right: (a) the small Badwater fan in Death Valley National Park. Length .6 km, slope 7°, centered on 36.22°N, 116.77°W. (b) Large alluvial fans in the Atacama Desert, Chile. Length ~35 km, slope 1.1°, centered on 20.75°, 69.40°W. (c) An alluvial fan in Harris crater, Mars. Length 22 km, slope 1.6°, centered on 21.50°S, 67.20°E.

Arid alluvial fan flows are highly episodic and mostly unpredictable, so there is a poor understanding of the relation between a flow's hydrologic and sedimentologic properties and the subsequent deposits. In addition, channel avulsion generally occurs on a century to millennia timescale and cannot be readily observed in the field. The lack of direct observations is further complicated by secondary weathering and the erosional reworking of fan surfaces, which can mask the dominant processes (de Haas et al., 2014; Frankel and Dolan, 2007). This means that despite over a century of study there are still a number of controversies around alluvial fan research, including whether dominant transporting flows are channelized or sheetflood, whether there is a systematic downstream fining of bedload sediment, whether particular fans are characterized by fluvial, debris, or sheet flows, and the effects of external forcings on fan morphology (Blair and McPherson, 2009; Harvey et al., 2005; Stock, 2013).

Alluvial fans appear to be ubiquitous in environments having fluvial flow and sediment transport, existing not only on Mars but also Titan (Birch et al., 2016). Martian fans have been identified within 30-150 km diameter craters across the southern highlands (Kraal et al., 2008; Moore and Howard, 2005; Wilson et al., 2012). Fan-bearing craters are reported to be geographically clustered (Moore and Howard, 2005), and close-proximity craters contain vastly different numbers and sizes of fans (Morgan et al., 2014). In the first global survey for martian alluvial fans, Moore and Howard (2005) suggested that this geographic localization could be due to restricted erosion, previously formed sedimentary basins (underlying the fan-hosting crater), formation of duricrusts, or orographic controls on precipitation. The presence of distributary channel networks (now expressed in inverted relief as ridges) with bedforms such as scroll bars suggested flow was likely fluvial rather than debris flows. They concluded that the fans were formed from many hundreds to thousands over tens to hundreds of thousands of years.

Alluvial fans are one of the few classes of depositional sedimentary landforms on Mars and the host craters into which most fans have deposited are an inherently closed sedimentological and hydrological system requiring sufficient runoff to erode and transport material from the alcove catchments while not being so abundant as to produce deep lakes within the craters. As depositional features in close proximity with a sediment source, alluvial fans have long been recognized as records of environmental change during the transport and deposition of sediment (Harvey, 2004; Harvey and Wells, 2003, 1994; Haug et al., 2010; Salcher et al., 2010). The martian fans therefore contain clues into a critical time in the Red Planet's history when it transitioned from a potentially wet and warm early state to the cold and dry world we observe today.

1.4. General objectives and dissertation outline

This dissertation is centered around two main objectives:

(1) Establish constraints on Mars' climate during the era of fan formation

(2) Characterize the role process has in shaping alluvial fan morphology

This is addressed through remote sensing observations, field work, and numerical modeling. In this chapter I present the overarching theme of this dissertation, and give an overview of Mars' climatic and geologic history. I summarize the dominant processes that form alluvial fans and detail gaps in our understandings of fan dynamics that this dissertation aims to address.

Chapter 2 introduces a newly compiled catalogue of martian alluvial fans and deltas. This database doubles the number of previously identified fans and addresses a need to identify the locations of such features on Mars in order to constrain controls on their distribution and morphology. This dataset includes a number of morphometric measurements, including fan area, gradient, length, catchment area, and catchment relief, which are used in conjunction with host crater properties to constrain formative conditions and the ages of the fan deposits.

Chapter 3 is an investigation of the large alluvial fans in Saheki crater, Mars. Extensive aeolian erosion and subsequent impact cratering has exposed the intricate stratigraphic layering allowing for a study into formative sedimentologic and hydrologic environment during deposition. A process analog fan in the Chilean Atacama Desert is used to characterize flow conditions, and inferences are made on the range of climatic factors that may have been present during martian fan deposition.

Chapter 4 presents a new numerical landform evolution model to study alluvial fan formation. This model incorporates both channelized and overbank sediment transport and the essential parameters to understand the interactions between flow hydraulics, overbank deposition, and avulsion processes. It is an advanced tool that can be used for studying fine-grained alluvial fans on both Earth and Mars. Results are presented showing the effects of extrinsic forcings on fan morphology.

Chapter 5 describes the geomorphological processes responsible for the formation of a series of alluvial fans on the south side of the Big Island of Hawaii, with an interpretation that the fans are deposited almost exclusively by sieve lobe deposition. This process was once widely accepted in alluvial fan depositional models but has fallen out of use in recent years due to a perceived lack of clear field examples.

Chapter 6 is a summary and synthesis of this dissertation, with a discussion of the implications of the research findings and possible directions for future research.

Chapter 2

Global distribution and morphometric properties of fan landforms on Mars

Abstract. A global survey of alluvial fans and deltas using Context Camera image data doubles the number of such features from previous surveys. Fans are not uniformly distributed across Mars, but are far more widespread than previously reported. Alluvial fans within craters show a favored N-S orientation, which is more pronounced for close proximity fan hosting craters. Relative to their source catchments, martian fans are larger than those on Earth, which is likely a consequence of no tectonic subsidence. There is a lack of correlation between fan morphometry and geographic or local topographic properties. The orientation directionality and inferred long formation timescales lead us to favor snowpack accumulation and melt as the runoff source. Crater count derived ages yield an age of early Amazonian, and a vast majority of fans superpose previously mapped Hesperian or Amazonian terrains.

2.1. Introduction

Alluvial fans are sedimentary landforms that form where a channel exits a mountain front and the sharp decrease in slope forces the deposition of sediment into a semi-conical shape (Figure 2.1). Terrestrial alluvial fan research has long focused on the varying roles of climatic, tectonic, and lithologic factors in controlling their formation. As depositional landforms, alluvial fans preserve a record of these controls in their stratigraphy, and by deciphering this record we can characterize the prevailing environment during deposition. Alluvial fans are ubiquitous in environments featuring fluvial transport and topographic relief, and have been identified on Mars

(Kraal et al., 2008; Moore and Howard, 2005) and Titan (Birch et al., 2016; Radebaugh et al., 2016), the two planetary bodies other than Earth known to have had surficial fluid flow.

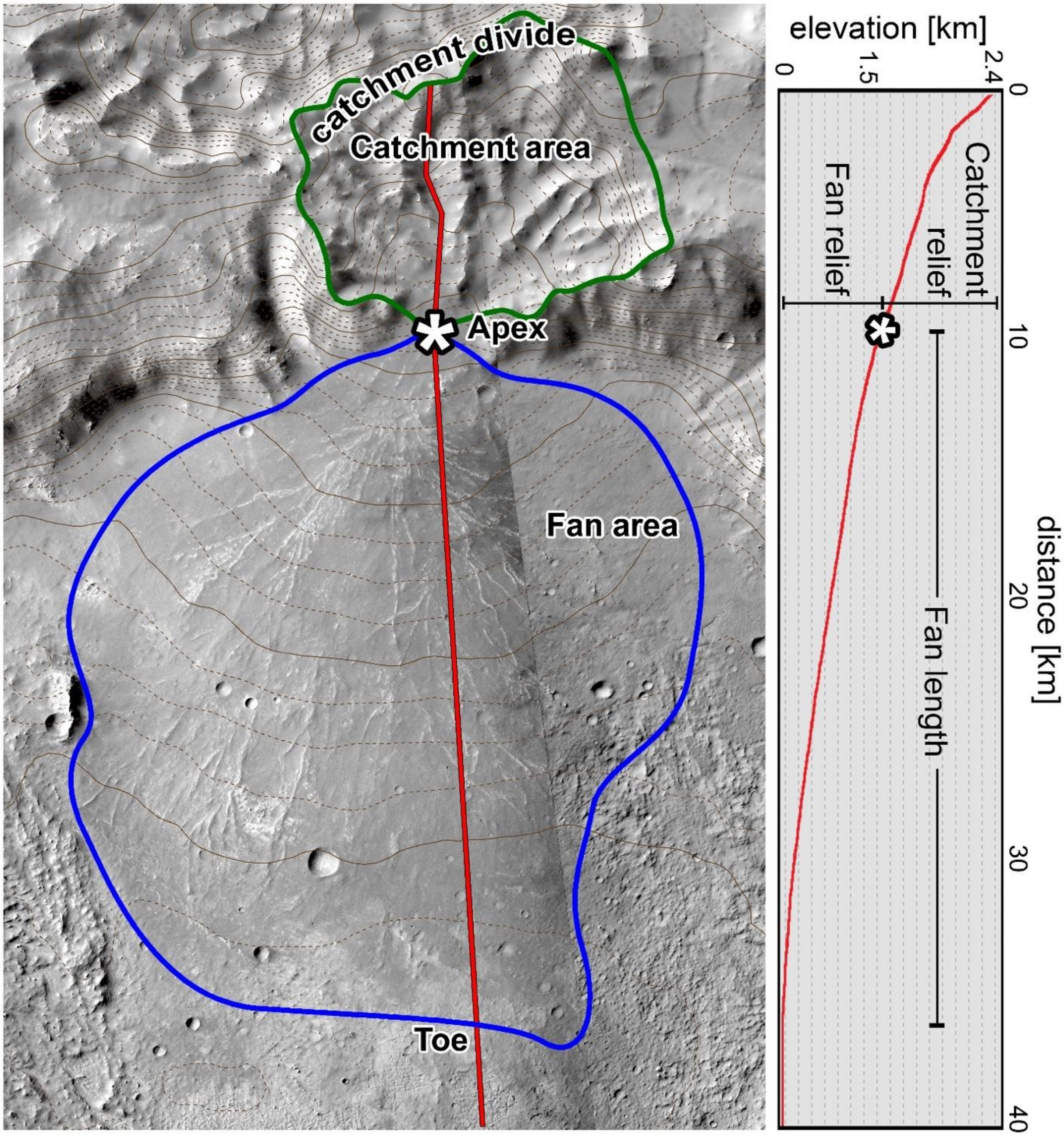

Figure 2.1. CTX mosaic of the alluvial fan in Baum crater, Mars, illustrating major fan features. Fan is outlined in blue, catchment in green, and the red line is the elevation profile from catchment divide to beyond the fan toe. Brown solid and dashed lines are 50 m contours. Image centered on 24.45°S, 28.28°W, north is up. The apex elevation is 1500 m. Note the shift in contour orientation at the fan apex from convergent to divergent flow, the lighter colored distributary network on the fan, and the slope breaks at the fan apex and fan toe. CTX images B17_016300_1559_XN_24S331W and P13_006213_1561_XN_23S332W, image credit: NASA/JPL-Caltech/MSSS.

Alluvial fans on Mars are enigmatic; their large size suggests a prolonged hydrologic cycle, but crater age statistics indicate that some may have formed well after the Noachian-Hesperian transition at ~3.7 giga-annum (Ga)[1] (Grant and Wilson, 2011, 2012; Morgan et al., 2014), during an era that paradigm has accepted to be cold and dry (Carr and Head, 2010). Alluvial fans, along with deltas (e.g. Hauber et al., 2013) and shallow incised valleys (e.g. Howard and Moore, 2011; Wilson et al., 2016), may be representative of the last vestiges of widespread fluvial modification to the martian surface. Deciphering the conditions present during fan formation may reveal how Mars transitioned from a potentially wet and warm early history to the dry and cold world we observe today.

In particular, the distribution, orientation, and varying size of martian fans may provide insights into the spatial heterogeneity of post-Noachian Mars' climate, and the modern availability of high resolution global visual and topographic datasets allows for such an investigation. Moore and Howard (2005) conducted the first survey for alluvial fans, searching through all available Thermal Emission Imaging System (THEMIS, spatial resolution ~100 m) (Christensen et al., 2004) daytime infrared (IR) imagery between 0°-30°S. They identified ~50 fans in 18 craters, which were concentrated in three regions: southern Margaritifer Terra, southwestern Terra Sabaea, and southern Tyrrhena Terra (Figure 2.2). Using Mars Orbital Laser Altimeter (MOLA, spatial resolution ~463 m) (Zuber et al., 1992) topographic data, they compiled morphometric measurements for 31 of the fans and compared them with terrestrial alluvial fans, terrestrial alluvial ramps, and eroded interior martian craters, finding similar morphometric relations martian and terrestrial fans. They found that martian fans are larger than terrestrial fans relative to their catchment sizes, and that martian catchments are of greater relief

[1]All absolute ages in this paper are based on the Neukum chronology system (Hartmann and Neukum, 2001; Ivanov, 2001), and geologic periods are defined according to dating by Platz et al. (2013).

than terrestrial fans in active tectonic settings. Finding bedforms such as scroll bars, Moore and Howard (2005) surmised that the martian fans are constructed of gravel sized sediment transported by dominantly fluvial (as opposed to debris flow) processes.

Kraal et al. (2008) conducted a follow-up global survey using the expanded THEMIS daytime IR dataset, increasing the fan inventory compiled by Moore and Howard (2005) to about 65. They likewise found fans to be concentrated in southern Margaritifer Terra, southwest Terra Sabaea, and southern Tyrrhena Terra, but not exclusively, and inferred that this regional concentration may imply some sort of control on fan formation location that may be lithologic, topographic, or climatologic. Somewhat surprisingly, they found that fans did not have any favored orientations along their host crater interior rim, and larger fan sizes did not correlate with larger host craters. Kraal et al. (2008) did find, however, that fans within larger craters are more likely to share similarly shaped long profiles, which may imply a similar depositional process (Williams et al., 2006).

Using the expanded Context Camera (CTX, spatial resolution ~7 m) (Malin et al., 2007) coverage, Wilson et al. (2012) undertook a new survey of fan deposits between 0° and 40°S, and identified ~450 fans within ~125 craters. This survey also included deltas, defined as fan shaped landforms at the lower end of a valley (as opposed to fans, which source from sharply defined catchments along interior crater rims). They found that alluvial fans are not restricted to the three regions identified by Moore and Howard (2005) or Kraal et al. (2008), but are scarce on Hesperian (3.71-3.37 Ga) and Amazonian (3.37 Ga to present) terrains. They observed that fans are more likely to be sourced from northern and southern crater rims, which they inferred to be evidence of an obliquity or insolation control.

These global surveys have been subsequently used for more detailed studies. Williams et al. (2011) undertook a detailed geomorphic analysis of the large alluvial fan in Harris crater (labeled “M” by Moore and Howard (2005)) and found that the fan formed from multiple events over thousands of years. Grant and Wilson (2011) utilized the Kraal et al. (2008) database to establish a Hesperian to Amazonian age for fans in southern Margaritifer terra, adding to the growing appreciation that Mars may have had habitable conditions during the post-Noachian. Morgan et al. (2014) used high resolution imagery and DTMs, along with a field analogue in the hyperarid Atacama Desert, to characterize fan-forming processes in Saheki crater (labelled “K” by Moore and Howard (2005)), finding that flows were of modest magnitude, likely sourced from snowmelt, and formed over many hundreds of separate flow events. Kite et al. (2017b) used the Wilson et al. (2012) database to search for partially infilled embedded craters on alluvial fan surfaces, and established a minimum formation timescale of 20 Myr, with a more likely duration of 100-300 Myr.

The near-global availability of high resolution datasets offers new opportunities for conducting global surveys of landforms on Mars (e.g. valley networks (Hynek et al., 2010), crater central mounds (Bennett and Bell, 2016), or gullies (Harrison et al., 2015)). All previous fan surveys were impeded by low resolution or spatially incomplete datasets. In addition, the wide spacing between MOLA shots limits the size range of fans that can be studied morphometrically, a problem that is partially remedied by the availability of higher resolution DTMs generated from High Resolution Stereo Camera (HRSC, spatial resolution of available data varies from 50 to 225 m) (Jaumann et al., 2007) data. Here, we use the near global availability of high-resolution CTX imagery with MOLA and HRSC topographic data products to identify, map, and measure properties of ~1300 martian fan landforms. As opposed to previous studies that surveyed only for alluvial fans (Kraal et al., 2008; Moore and Howard, 2005) or deltas (e.g. Irwin et al., 2005b), we include all fan shaped sedimentary depositional landforms because the formative hydrologic conditions for features on Mars generally cannot be constrained without detailed stratigraphic analysis (e.g. Goudge et al., 2017). This survey has two objectives: (1) to compile a comprehensive database of all fan shaped sedimentologic landforms on Mars for future workers to utilize in deciphering the environmental conditions at each location, and (2) use this database to constrain the sources of runoff, controls of geographic distribution, and spatial heterogeneity of fans on Mars.

2.2. Methods

This survey utilizes data from the CTX, THEMIS, MOLA, and HRSC instruments. First, using Google Earth, we conducted a systematic global survey of fan-shaped landforms, searching within moving windows of 15° latitude and 30° longitude. We used both the CTX global mosaic and THEMIS daytime IR layers, and utilized previously constructed databases of alluvial fans (Kraal et al., 2008; Moore and Howard, 2005; Wilson et al., 2012), deltas (Irwin et al., 2005b), valley networks (Hynek et al., 2010), and lakes (Fassett and Head, 2008) for context in identifying fan landforms. Due to the limited coverage of the CTX layer in Google Earth (~45% between +-60°N, relative to the total coverage of >90%), we marked all visible fans as well as all locations where it looked as though there might potentially be a fan based on the qualitatively assessed state of crater degradati on and proximity of other fluvial features in the THEMIS daytime IR layer. Google Earth is limited in its GIS functionality, so all potential fans were loaded into ArcGIS, and we downloaded CTX and HRSC DTM data covering the vicinity of each possible fan. The availability and spatial resolution of the HRSC DTMs varied (Table 2.1).

DTM Resolution (m)	50	75	100	125	150	175	200	225	MOLA
% fans w/ coverage	3.9	27.8	10.5	11.8	4.8	1.8	0.1	0.2	39.2
% fan catchments w/ coverage	4.8	31.6	11.1	12.9	5.5	1.9	0.1	0.3	31.9

Table 2.1. Breakdown of the best available topographic coverage for the fans and catchments in this survey.

Using CTX imagery and 25 m contours derived from the MOLA and HRSC topographic data, we mapped the apex and areal extent of every visible fan. Putative fans were identified on a number of observations, including (1) break in slope from at the fan toe (see Figure 2.1 for fan terminology), (2) textural changes, as fans typically have smooth surfaces unless they have been eroded, and (3) patterns in contour orientation. The criteria used to add a putative fan to the survey database included the following: a landform must (1) be sourced from an eroded catchment and either (2a) be identifiable in CTX imagery (based on observations such as downfan trending ridges, convergent to divergent flow at apex, or a toe transition from fan to crater floor material) or (2b) be identifiable by convex oriented contours. While these criteria may exclude features that were originally deposited as alluvial fans or deltas, this methodology is necessary to identify features that are indeed fans and are not simply degraded craters. We discuss the limits of our selective criteria in Section 2.4. Many small features that might be better classified as gully debris aprons were included in our survey, but were marked as a separate class from larger fans and due to their small size are not included in the quantitative analyses below.

We defined the fan apex as the location where contours transitioned from concave (convergent flow in the source catchment) to convex (divergent flow on the fan) orientation. Using standard ArcHydro procedures we delineated source basins catchments from the underlying DTMs. This worked well for the higher resolution DTMs, but for the fans covered only by MOLA topographic data we mapped fan catchments by hand using basin divides in the visual CTX imagery. The heavily eroded terrain in many parts of upper interior crater rims made it difficult to define some catchments, and we only mapped those for which the boundary could be clearly identified. Using the Robbins crater database (Robbins and Hynek, 2012) we obtained properties of the host craters, including crater diameter, depth, and degradation state.

An alluvial fan's radial profile is both an effect of and a driver of depositional processes. Along each fan's radial long profile from the apex to the lowest point along the fan outline, we measured elevations using a minimum point spacing equal to 2x the underlying DTM topography (e.g. every 100 m for the 50 m HRSC DTM) and a maximum spacing of 5% of the total fan length. We excluded all fans from this analysis for which there would be fewer than 5 data points along the profile. Following the methodology of Moore and Howard (2005) and Kraal et al. (2008), we measured concavity B through regression analysis by finding the best fit to the equation

$$z = z_0 + (z_a - z_0)\exp[-B(x - x_a)] \tag{2.1}$$

where z is the local elevation, z_0 is the elevation just beyond the fan toe, z_0 is the apex elevation, and x is the distance along the profile from the apex at x_a.

2.3. Results

Figure 2.2 shows the results from the global survey. Fans are mostly, but not exclusively, restricted to the southern cratered highlands. As found by previous surveys, the vast majority of fans are found within crater interiors. We identified ~1300 fan landforms in 315 craters, plus an additional few fans that lie outside of a crater, such as along the walls of Ganges Chasma.

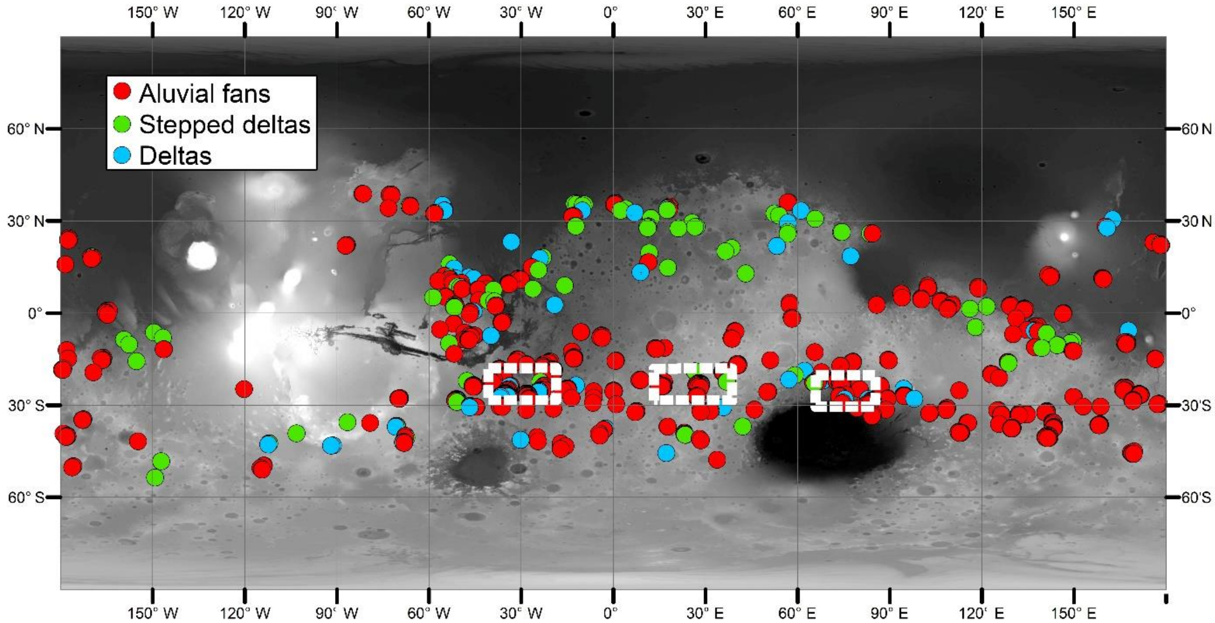

Figure 2.2. Global distribution of fan landforms on Mars. Dots indicate fan apices. Red dots are alluvial fans, green are stepped deltas, and blue are branched and unbranched deltas. White boxes indicate the three regions identified by Moore and Howard (2005) as having concentrations of large alluvial fans, from west to east these are Margaritifer Terra, southwestern Terra Sabaea, and southern Tyrrhena Terra. Base map MOLA (NASA/JPL-Caltech).

2.3.1. Morphology

Based on size, gradient, and morphology we categorized the fan landforms into 4 classes: alluvial fans, stepped deltas, branched deltas, and smooth deltas (Figure 2.3). This classification is primarily made on the basis of appearance of HRSC DTM-derived morphometric properties and observations of CTX imagery, and do not necessarily imply a genetic process. We use the terms "alluvial fan" and "delta" largely to compare features with those identified in other studies (e.g. de Villiers, 2009), and stress that detailed studies are necessary to characterize fan depositional setting and formative process (e.g., Goudge et al., 2017; Lewis and Aharonson, 2006; Morgan et al., 2014; Palucis et al., 2014).

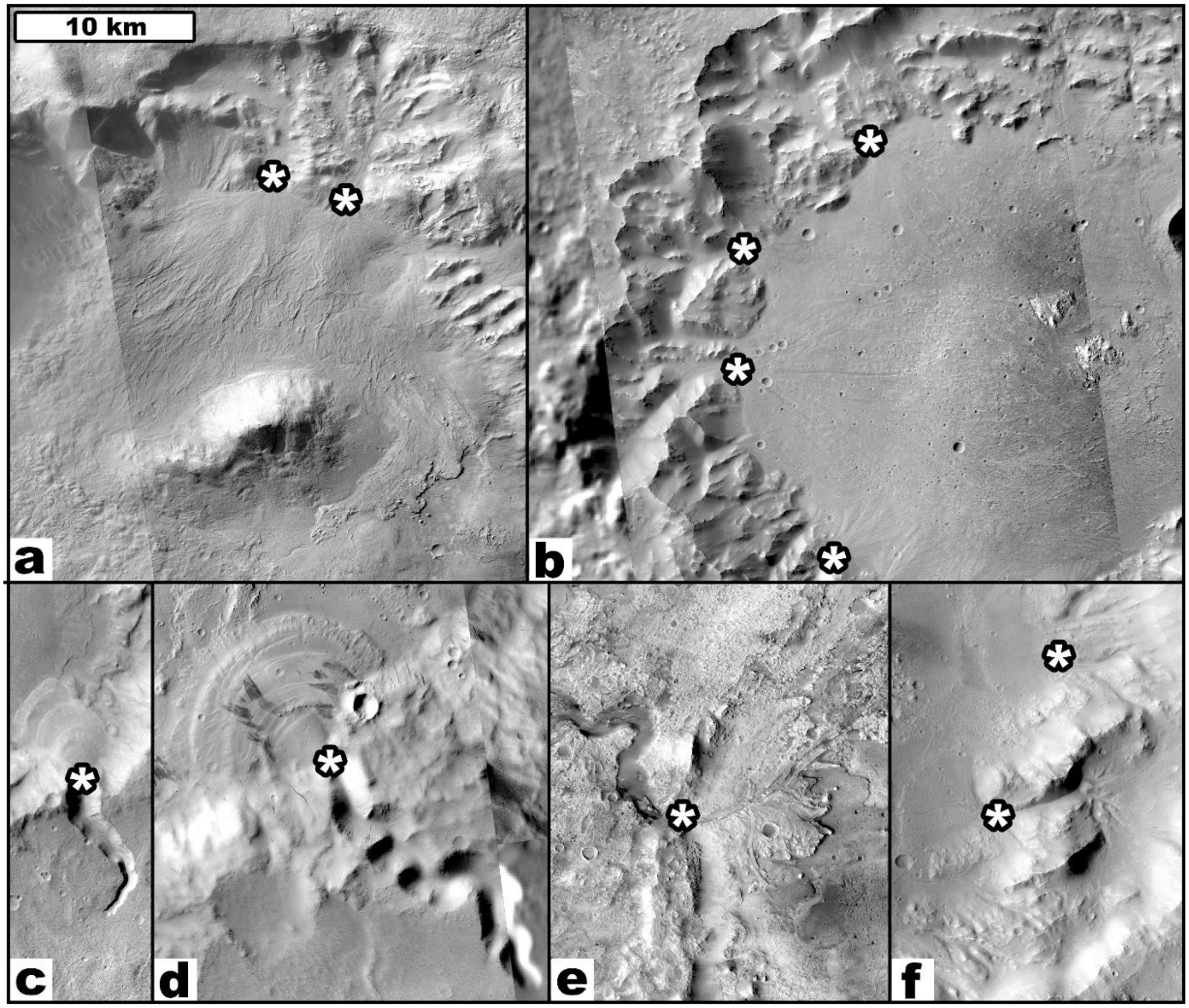

Figure 2.3. Examples of fan landforms included in this survey. All images are at the same scale, north is up. Fan apices are marked with *. (a) Two coalescing alluvial fans in Majuro crater. Alluvial fans are generally sourced from well-defined catchments carved into the interior crater rim. Note the distal fan deposits to the southeast of the central peak. (b) A bajada (a series of coalescing alluvial fans) in an unnamed crater in SW Tyrhenna Terra. This crater is in one of the regions identified by Moore and Howard (3005) and Kraal et al (2008) as containing a high concentration of alluvial fans, but was missed in their surveys, demonstrating the benefit of using higher resolution CTX imagery for landform identification. (c) Stepped delta in Dukhan crater. Note the short, steep walled, unbranched source valley typical of stepped delta catchments. (d) Stepped delta in an unnamed crater south of Medusae Fossae. (e) The well-studied branched delta in Jezero crater. This class of deltas generally source from long, relatively well integrated valley systems. (f) Two smooth, flat top deltas in an unnamed crater in northern Noachis Terra. CTX images (a) P18_008070_1450_XI_35S275W and P22_009573_1474_XI_32S276W, (b)D16_033559_1585_XI_21S283W and G22_026834_1573_XN_22S283W, (c) G01_018544_1878_XN_07N039W, (d) P17_007736_1713_XI_08S159W, (e) P04_002664_1988_XI_18N282W, and (f) J04_046525_1554_XN_24S014W. Image credit: NASA/JPL-Caltech/MSSS.

Alluvial fans make up the bulk of the identified landforms. These are classic, semi-conal features that range in length from hundreds of meters to tens of kilometers with average slopes of ~4°. Prominent, well known examples include the Peace Vallis fan in Gale crater (Palucis et al., 2014), the large fans in Saheki (Morgan et al., 2014) and Harris (Williams et al., 2011) craters, and the many fans in Holden crater (Pondrelli, 2005). This class includes all of the features identified by Moore and Howard (2005) and Kraal et al. (2008). Alluvial fans usually source from deeply eroded alcoves carved into the interior crater rim, and do not appear to have had a sediment or runoff source beyond the crater. Many alluvial fans have been extensively eroded, with aeolian processes resulting in tens of meters of deflation (e.g. Morgan et al., 2014).

Stepped deltas are characterized by their terraced topographic profile, typically steep slope (>7°, but gradients vary widely), and deeply incised, low order source valleys. A prominent example of this class is the landform in Coprates Catena (Di Achille et al., 2006). The processes that form these features are enigmatic as they have no clear terrestrial analogs, and previous workers have suggested a range of formative mechanisms, including mass wasting (Malin and Edgett, 2003), sheetflood dominated alluvial fan deposition (Di Achille et al., 2006), and deltaic deposition into a rising lake (De Villiers et al., 2013). These deposits are typically fed by wide v-shaped incised valleys that cross the host crater's rim and cut into its ejecta. These valleys often terminate in an amphitheater-shaped headwall, with only a few short, stubby tributary valleys (i.e., a low drainage density).

Both branched and smooth deltas have low surface gradients of ~1-2°. Branched deltas include the famous landforms in Eberswalde and Jezero crater. These are generally found at the lower end of larger valley network systems, which is in stark contrast to the short drainages that feed the other fan types. However, most valleys on Mars do not have depositional sedimentary landforms at their mouths. Smooth deltas have a rounded, triangular, or projecting platform, and show little evidence for channelization, segmentation, or scarp dissection. A prominent example is the "Pancake Delta" in Gale crater (Palucis et al., 2015).

We include all of the above class types in the fan database since in many cases it is difficult to determine whether a feature is an alluvial fan or delta. Our analyses here focus on the features that appear to definitively be alluvial fans.

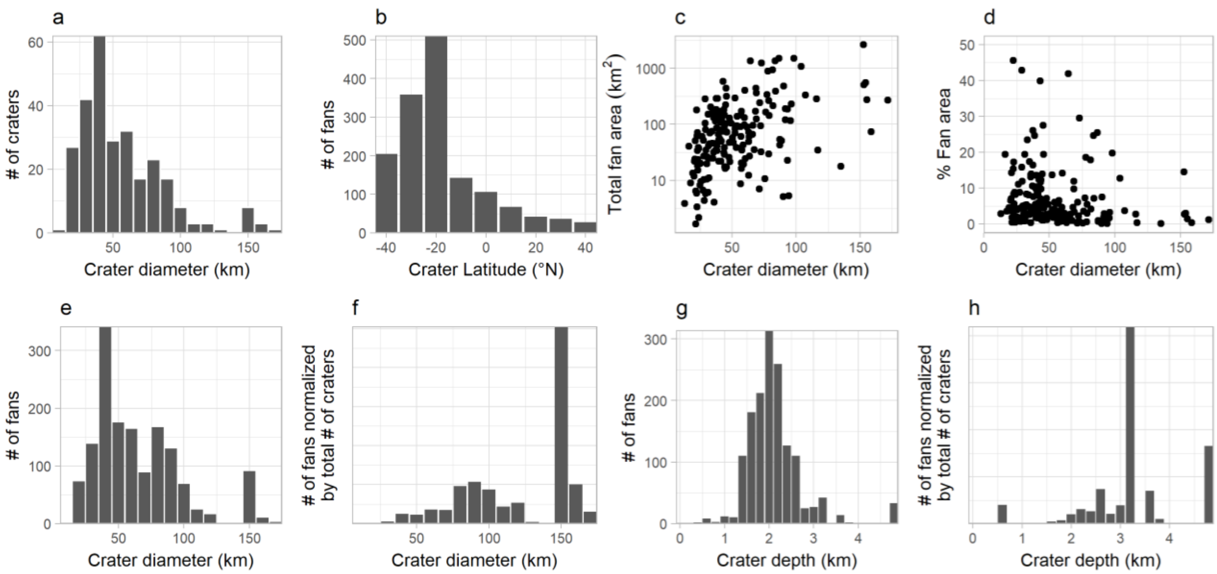

Figure 2.4. Properties of alluvial fan host craters. (a) Histogram of alluvial fan-bearing crater diameters. (b) Number of fans per 10 ° latitude bin. Fans are concentrated in the southern equatorial and mid latitudes. (c) Total alluvial fan area within a crater relative to the crater diameter. Larger craters contain larger fans. (d) Fraction of a crater interior (inside of the rim edge) that is covered by fan deposits relative to crater diameter. (e) Number of alluvial fans per 10-km crater diameter bin, and (f) normalized to the total number of craters in that diameter bin (Robbins and Hynek, 2012). The large spike at 150 km is Holden crater (g) The number of fans as a function of crater depth (average rim elevation – average floor elevation), and (f) normalized to the relative number of craters within each depth bin (Robbins and Hynek, 2012). The large spike at 3.2 km is Bakhuysen crater.

2.3.2. Geographic distribution

Fan-hosting craters span a range of sizes (Figure 2.4a). Craters of diameter 30-60 km appear to be the most likely to host alluvial fans, but when the distribution is normalized to the total crater population of a size bin (Figure 2.4f) it is apparent that this is due to the greater number of smaller craters on Mars. Alluvial fans are largely concentrated in the southern highlands (Figure 2.4b), but we identified a number of fans that are in the northern hemisphere. Alluvial fans are more widespread than originally reported, but as stated in previous surveys

(Kraal et al., 2008; Moore and Howard, 2005, Wilson et al., 2012) are indeed not globally distributed. Unsurprisingly, the total fan area increases with host crater diameter size.

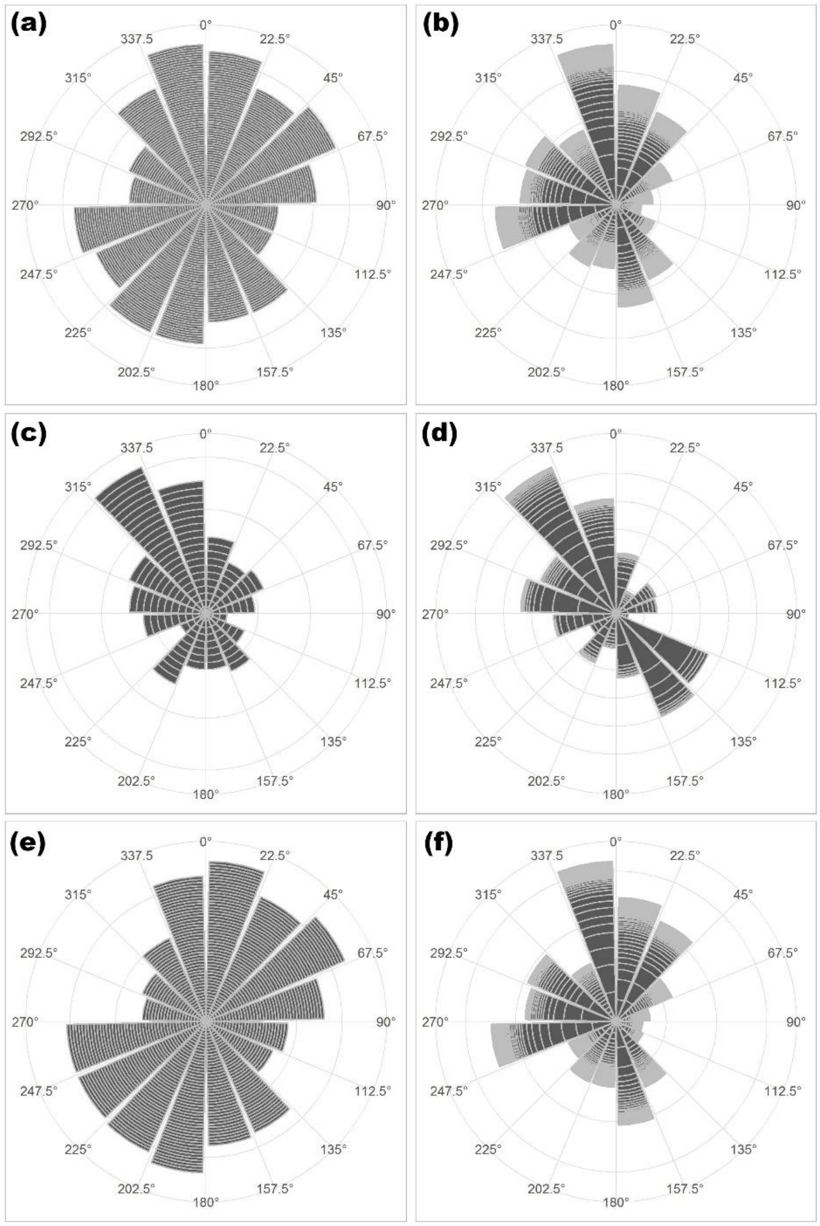

Figure 2.5. Orientations of alluvial fans along interior crater rims. Plots in the left column are raw values, and those in the right column are weighted by fan area. Each dark grey area indicates a different fan, with larger fans plotted as larger grey areas. (a and b) Total distributions. (c and d) Northern hemisphere alluvial fans (d and e) Southern hemisphere alluvial fans.

To examine what geographic properties might be controlling the spatial distribution of the alluvial fans, we used exploratory ordinary least squares regression to test for all possible combinations between the response variables fan gradient, fan area, and fan concavity, and the predictor variables crater relief, crater diameter, crater depth, apex latitude, and apex elevation. We did not find significant high correlations in any of 1310 models between the predictor and response variables. We comment on this paucity of relation in Section 2.4.1.

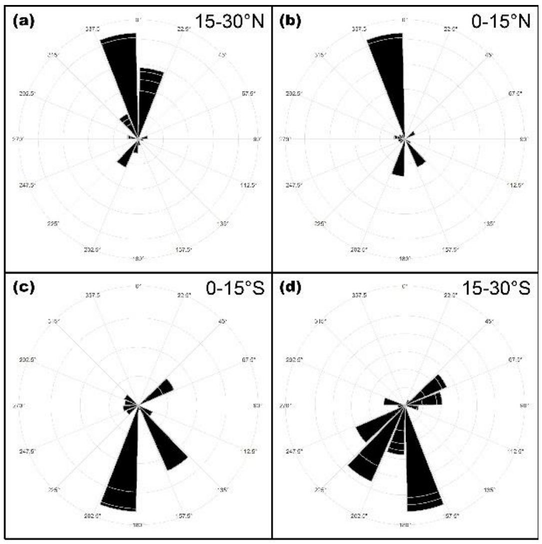

Figure 2.6. Orientations of fans in 20 craters between longitudes 150° and 180°W. Within a local area, fan orientations have a higher degree of non-uniformity. All plots are weighted by fan area. (a) 4 craters, 15-30°N, (b) 4 craters, 0-15°N, (c) 6 craters, 0-15°S, (d) 7 craters, 15-30°S

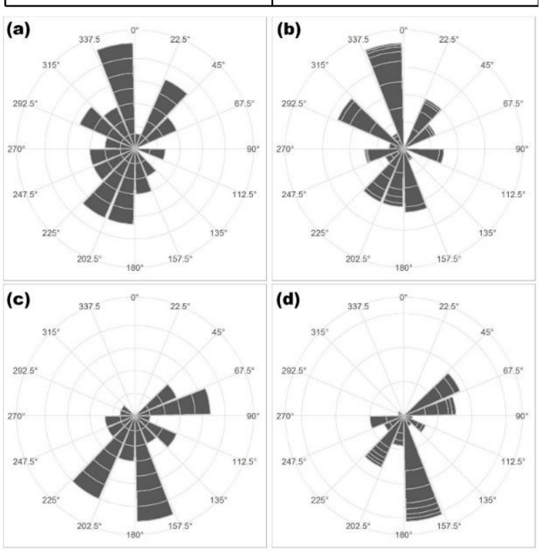

Figure 2.7. Orientations of stepped deltas along interior crater rims. Each dark grey segment represents a fan. On the left are raw orientations, on the right are weighted by fan area, with larger grey areas indicating larger fans. (a and b) northern hemisphere (b and c) southern hemisphere.

We excluded non-crater fans from any orientation analyses since many are in Ganges Chasma, which is an E-W oriented canyon, and would bias the results. For the alluvial fans that do lie within craters, we compiled the location of the fan apex along the interior crater rim. At first glance, the raw fan locations around the crater rim show a broad distribution of azimuth (Figure 2.5a), but a clear deficiency in E-W orientation, in contrast to the lack of preferred orientation in the findings of Kraal et al (2008). When the fans are weighted based on their area, there is a prominent N-S trend (Figure 2.5b). We used a Rao's Spacing Test to assess the uniformity of the azimuthal distribution. This test aggregates the deviations between consecutive points under the assumption that if the distribution is uniform the points should be equally spaced apart (Rao, 1976). We find that all of the crater orientations show significant (at the 5% level of significance) directionality. The degree of directionality increases for fans within a local area (Figure 2.6). Stepped deltas also show a clear orientation bias in both the northern and southern hemispheres (Figure 2.7). Southern hemispheric stepped deltas almost exclusively are found on the southern interior rim of their host craters. Northern hemispheric stepped deltas are more varied in their orientation but are most commonly on the northern interior rim.

Alluvial fans are commonly characterized by the relations between fan area or gradient and catchment area, expressed as

$$A_f = p_1 {A_c}^{q_1} \tag{2.2}$$

and

$$S_f = p_2 {A_c}^{q_2} \tag{2.3}$$

where A_f is the fan area, A_c is the catchment area, S_f is the fan slope, and p_1, p_2, q_1, and q_2 are parameters that describe the relation's slope and intercept (Harvey, 2011). For terrestrial fans q_1 is often below 1, signifying that fan area is typically less than catchment area. Statistically significant regression fits to these relations for the martian fans are in Table 2.2. Martian fans are large relative to terrestrial catchments but have similarly scaled gradients. Fans vary widely in concavity, but in general larger fans have lower concavities, and the average concavity of fans within a host crater decreases with increasing crater size (Figure 2.9).

Dependent variable	Independent variable	p	q	R^2
Fan area	Catchment area	1.63	0.79	0.42
Fan area	Catchment gradient	3.77	-0.87	0.11
Fan area	Catchment relief	0.35	0.54	0.04
Fan slope	Catchment area	0.17	-0.29	0.38
Fan slope	Catchment gradient	0.18	0.61	0.41
Fan gradient	Catchment relief	0.08	-0.45	0.50

Table 2.2. Statistically significant morphometric relations fit to the equation $Y = pX^q$, where p an q are coefficients that describe the slope and intercept of the power relation between Y and X.

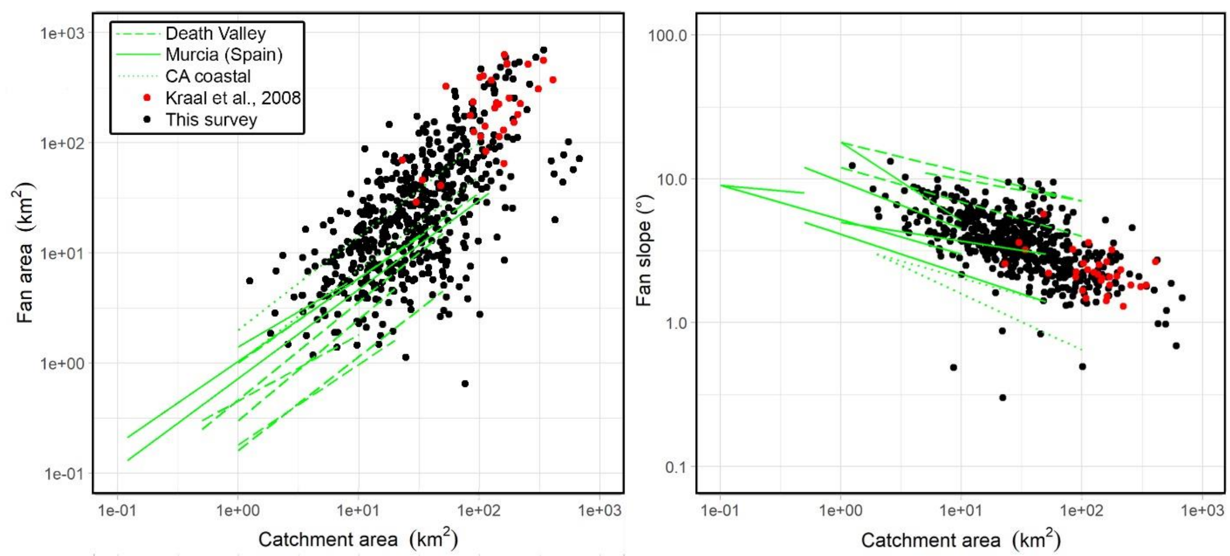

Figure 2.8. Martian fan morphometric relations. In both figures black are alluvial fans from this survey, red are alluvial fans from previous surveys, and green lines are terrestrial relations. Martian fans follow similar trends to terrestrial fans, but are generally larger relative to their source catchments.

2.4. Discussion

2.4.1. Geologic and morphologic observations

From this survey we can conclude that while alluvial fans are more widespread than previously reported, they are not distributed globally on Mars. Fans are concentrated in the southern hemisphere, which may be related to the higher number of large craters which provide high relief surfaces against which the fans can form. Typically, fans are found within craters with depths (rim to floor elevation) of >2 km. We did not identify any fans south of ~50°S, but it is not clear if this restriction is due to some control on fan formation processes or if fans are simply not preserved at higher latitudes due to polar processes. The region south of ~45° is covered by a kilometer thick mantle (Kreslavsky and Head, 2000), which could obstruct the identification of alluvial fans. Fans are also uncommon in the northern lowlands and the Tharsis region.

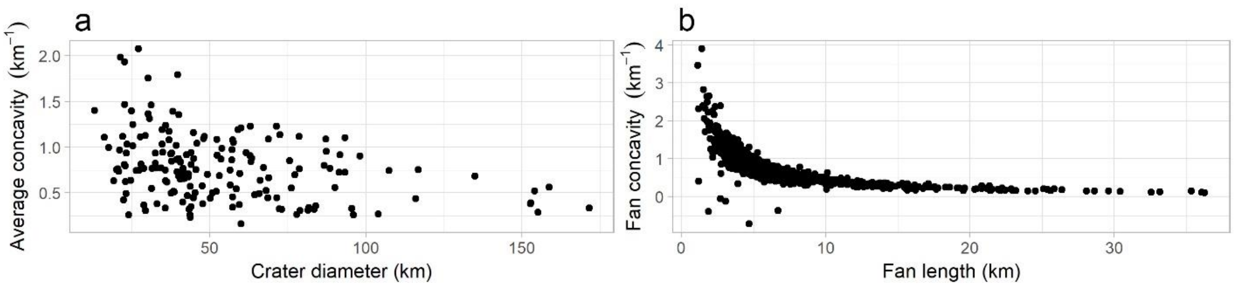

Figure 2.9. (a) Average fan concavity within a crater as a function of crater diameter. Larger craters have a lower variability of fan concavity. (b) Fan concavity as a function of fan length. Larger fans are less concave.

Our criteria in discerning fans likely excludes a number of features that formed as fans but have subsequently been eroded. Large alluvial fans in crater interiors that have been degraded to a piedmont surface (e.g. Craddock et al., 1997) would not be identifiable as fans in the topographic data and were excluded from this survey. In addition, it is likely that many small fans formed during the era of fan deposition but have since been eroded, may have aeolian surface mantles, or simply be below the resolution scale of MOLA or HRSC topographic data. There are hundreds of small alluvial fans in the <5 Ma Mojave crater (Werner et al., 2014), presumably because they have not had the time to be covered by dust and masked in visual imagery, and they do not exhibit convex oriented contours in the MOLA data due to their small size.

Moore and Howard (2005) observed that most martian fans derived both sediment and water from deeply eroded alcoves carved into the interior crater rim. They found that typical catchments have ~ 1 km relief and ~6.7° slope. In our expanded database we find this to be true for fans across Mars, with catchments averaging 1.1 km and 9.65° in relief and slope. Alluvial fans mostly source from these scalloped alcoves, in contrast to stepped deltas and branched deltas, which respectively source from steep walled canyons or longer valley systems. Also in agreement with Moore and Howard (2005), we find that relative to their source basins, martian fans are larger than those on Earth. This is to be expected due to the lack of tectonics on Mars, as a decrease in subsidence rate is correlated with a larger fan to catchment area ratio (Dade and Verdeyen, 2007). For a fan to prograde and increase in area, the net deposition rate must exceed the subsidence rate, a condition that is not met for many fans in tectonically active settings on Earth (Hooke, 1972).

2.4.2. Flow processes

The dominant flow regime for the martian fans is uncertain, and likely varied spatially and temporally. Active processes on alluvial fans can be broadly distinguished into dominantly debris flow or dominantly fluvial flow (Blair and McPherson, 2009). Fluvial flows generally contain <20% sediment by volume and deposit in the channel bed and overbank as broad sheets of moderately sorted, clast supported sand and gravel (Blair and McPherson, 2009). Debris flows have a sediment concentration in excess of 40%, a significant portion of which is silt and clay which lowers the flow's permeability, increasing pore pressure and allowing for the flow to act as a non-Newtonian, highly viscous, low turbulence material (Costa, 1988).

Fan surface topography can be indicative of the dominant formative process, with terrestrial debris flow fans being shorter and steeper (>5-10°) than their fluvially dominated counterparts (Harvey, 1992; Stock, 2013; Stock et al., 2008; Williams et al., 2006). Moore and Howard (2005) found that most fans had a slope of ~2°. From the new database, we find that alluvial fans surface slopes average ~3°-4°, which is similar to the slopes measured on the Peace Vallis fan (0.5°-2°) (Palucis et al., 2014), the Saheki crater fans (2°) (Morgan et al., 2014), and the NE Harris crater fan (2.3^{o}) (Williams et al., 2011). However, surface slopes can be modified by secondary processes that can mask the dominant facies making up the fan (de Haas et al., 2014). Martian fans have undergone extensive erosion since the time of deposition, with some fans having undergone tens of meters of deflation (Grant and Wilson, 2012; Morgan et al., 2014). The low resolution of globally available topographic data, combined with uncertainty in how process would affect depositional form due to both Mars' lower gravity and the dominant basaltic lithology of the transported sediment, inhibits the ability to determine whether a certain fan on Mars was dominantly formed from a fluvial or debris flow. It is interesting that larger craters have a smaller variability in concavity (Figure 2.9), a property that has been proposed to be indicative of dominant formative process (Williams et al., 2006). Assuming fans within a given crater underwent a similar amount of erosion, this may be indicative of similar depositional processes at work in larger craters.

As has been noted in previous studies (e.g. Grant and Wilson, 2012; Morgan et al., 2014; Williams et al., 2011), many fans have linear and platform features that trend downslope from the apex with generally uniform widths, and contain bedform features such as scroll bars (Morgan et al., 2014; Palucis et al., 2014; Williams et al., 2011). These features have been interpreted as fluvial distributaries that carried coarse sediment down-fan and have since been inverted by aeolian erosion (Grant and Wilson, 2011; Moore and Howard, 2005; Williams et al., 2011, 2009). The elevated channel beds (now ridges) also indicate that a large amount of the deposited material was finer-grained overbank sediments within flood flows, capable of being swept away by wind. Fine-scale layering observed in HiRISE imagery might be related to breaks between individual flow events (Morgan et al., 2014). Taken together, the low fan slopes and presence of paleo-channels suggest that many of these mid-latitude fan systems were fluvially-dominated (Moore and Howard, 2005; Morgan et al., 2014; Palucis et al., 2014; Williams et al., 2011), and that these features were deposited over multiple flow events. Smaller, steeper fans (Palucis et al., 2015; Williams and Malin, 2008) are possibly of debris flow origin, as debris flows on Mars may require steeper slopes in order for the shear stresses to overcome the flow's yield strength.

Detailed analyses that are beyond the scope of this chapter are necessary to constrain the range of processes that may have been involved in the construction of an individual fan. Even if we could decipher the dominant flow regime, this would only allow inferences on the environment during the upper few tens of meters of deposition, and would not necessarily give any insights into the prevailing climate at the time of deposition. While numerous studies have demonstrated the effects of climatic change in alluvial fan sedimentation processes (Bull, 1991; Harvey et al., 1999; Harvey and Wells, 2003; Wells et al., 1987), the primary processes forming alluvial fans differ little in different climatic settings. Fans in humid and arid regions form from largely similar processes (Blair and McPherson, 2009; Harvey et al., 2005).

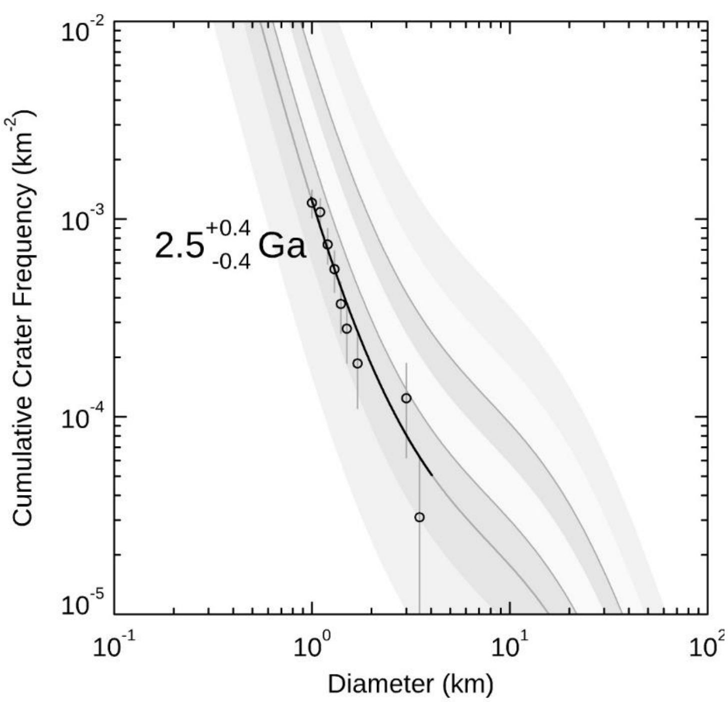

Figure 2.10. Cumulative crater statistics for all alluvial fans, assuming contemporaneous deposition (see text for discussion), using the production function of Ivanov (2001), chronology function of Hartmann and Neukum (2001), and epoch boundaries of Michael (2013).

2.4.3. Water source

Whatever the dominant process regime, the volume of water forming the fans was prodigious. To estimate water discharge on Mars, common practice has been to either (1) assume that channel bed gravels and cobbles are transported when a critical shear stress is reached and that this occurs at bankfull discharge, or (2) utilize relations between hydraulic properties such as channel geometry, meander wavelength, and stream discharge (Dietrich et al., 2017). Discharges were estimated to be 10 to 100 m^3/s for the fans in Saheki and Gale crater, which equates to ~1 mm/hr runoff from their upslope catchments (Morgan et al., 2014; Palucis et al., 2014). These values can be compared to snowmelt and runoff models, such as that of Kite et al. (2013), which predicts average snowmelt rates of ~1 mm/hr in the equatorial highlands of Mars under certain obliquities and a faint young sun.

These approaches can yield a total water volume by assuming a water to rock ratio, although values for this relation are approximate and depend on the interpreted depositional processes. For example, Moore et al. (2003) assumed 0.05, Mangold et al. (2012b) used 0.0005 for dilute flows and 0.02-0.3 for dense flows, Palucis et al. (2014) used 0.002 on the basis of pebble conglomerate outcrops bserved by *Curiosity*, and Morgan et al. (2014) chose 0.2, as the Saheki crater fans were interpreted to be partly built by mudflows. Minimum estimated water volumes for formation of the 500 km^3 Saheki crater fans were ~2500 km^3 (Morgan et al., 2014), and ~600 km^3 for the smaller Peace Vallis fan.

Possible sources of runoff that drove fan formation could be melting of ground ice, groundwater flow or seepage, rainfall, or snowmelt. The melting of ground ice following a bolide impact has been proposed as a formative mechanism for water formed features on modern (cold and dry) Mars. An impact event is over in minutes, but the energy delivered from the impact, hot ejecta blanket, or uplifted geothermal gradient can initiate a post impact hydrothermal system of sufficient energy to drive gully incision (Abramov and Kring, 2005) or possibly the formation of small alluvial fans (Williams and Malin, 2008). However, such activity would not provide the estimated fan forming volumes of water (Barnhart et al., 2010), and would not explain the long period of time over which fans were active (Kite et al., 2017b).

Groundwater discharge has been cited as an unlikely source of runoff for many fan systems based on the geometry of the channel network, the lack of an elevated groundwater source area (as crater rims are typically a local topographic high), and the large water volume requirements and rates to transport boulder sized particles across a fan surface (Moore and Howard, 2005; Morgan et al., 2014; Palucis et al., 2014). Groundwater could be a viable runoff source for many of the possible deltaic systems, as the feeder valleys are often minimally branched andcharacterized by their amphitheater headwalls, possibly suggesting seepage erosion of loose material (Laity and Malin, 1985).

The only other mechanism for producing sufficient discharge rates is precipitation, either in the form of rain or snow. The possible Hesperian to Amazonian age (see Section 2.4.4) of many of the fans may makes rain unlikely, as both the atmospheric pressure and temperature are thought to be too low to support rainfall (Forget et al., 2013; Wordsworth et al., 2013), leading us to conclude that snowmelt is therefore the most viable runoff source for fan formation. The orientation directionality (Figures 2.5-2.7) is a strong indication of climatic control through solar insolation. Pre-existing crater morphology might play a key role in fan formation, as snow within a crater could potentially drift into pre-eroded sections of crater rims. There it could be protected from sunlight and build up with time, until volcanic activity, impact events (Segura et al., 2008), methane release (Kite et al., 2017a), obliquity shifts (Laskar et al., 2004), or some other climatic forcing warmed the planet, causing melt and runoff. This could create a positive feedback, where snow accumulation would lead to increased runoff, which would enlarge the alcove, trapping more snow. Runoff might also be enhanced due to the steep topography and exposed bedrock in the eroded crater rim.

Previous workers have noted a lack of fluvial modification outside of fan host craters, (Grant and Wilson, 2012, 2011; Kraal et al., 2008; Moore and Howard, 2005), which has been presented as problem for precipitation as a water source. There are in fact numerous examples of small-scale fluvial activity, such as channels, in close proximity to alluvial fans (e.g. the upper right of Figure 2.1), but these features would have been less resistant to erosion than the larger fans and may have been eroded or buried by subsequent aeolian activity. Regardless, if snowmelt drove fan sedimentation, and if precipitation rates were low, runoff from thin snowpacks might not be sufficient (either in duration or magnitude) to leave a geomorphic record of fluvial activity. In contrast, melt from thick snowpacks that accumulated over a longer period in protected alcoves would generate enough runoff to transport sediment downfan, forming larger, more resistant landforms.

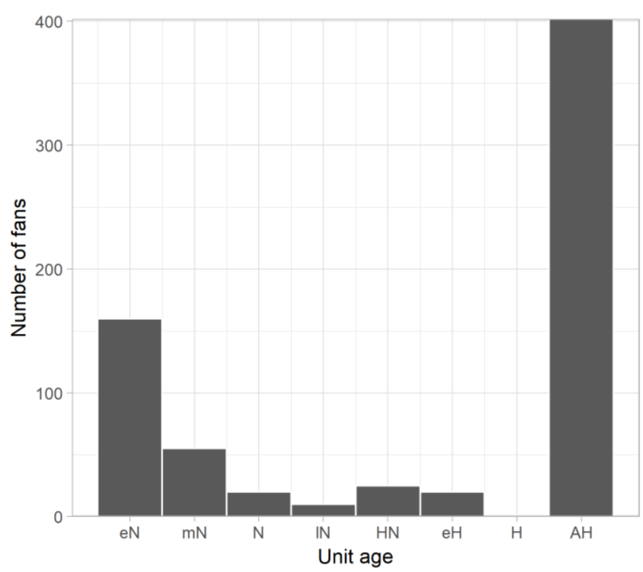

Figure 2.11. Number of alluvial fans on different aged landforms, as mapped by Tanaka et al. (2014). The vast majority of fans superpose Amazonian and Hesperian aged landforms.

2.4.4. Age

The timing of fan formation has significant implications for Mars' climatic history. Moore and Howard (2005) inferred that the alluvial fans were contemporaneous with valley network formation, during a period of enhanced fluvial activity across Mars (Howard et al., 2005; Irwin et al., 2005b), and that the highly-eroded craters from the early to mid Noachian were unable to provide the relief needed for fan formation due to degradation (Craddock et al., 1997). More recent studies of fans and deltas suggest that they were deposited some time closer to the Hesperian-Amazonian transition (Grant et al., 2014; Grant and Wilson, 2011; Morgan et al., 2014), an era long considered to be unfavorable to fluvial activity due to a thick and horizontally stratified global cryosphere (Carr and Head, 2010). Assuming that all fans formed concurrently (which has not been confirmed), 39 craters larger than 1 km diameter superpose the fans, suggesting an age of 2.5 Ga, or early Amazonian (Figure 2.10). We reach similar results by comparing fan locations with the geologic units of the most recent global geologic map of Mars (Tanaka et al., 2014). The bulk of the fans are atop surfaces mapped as Amazonian-Hesperian in age (Figure 2.11). Recent analysis of partially infilled craters reveals that the fans were likely active for greater than 100-300 Myr (Kite et al., 2017b), which challenges the long-held paradigm of Mars being a continuously cold and dry world since the Noachian period.

2.5. Conclusions

Alluvial fans on Mars are a testament to the planet's wetter history. Martian alluvial fans are widespread across the equatorial and low midlatitudes, but are not globally distributed. Fan morphology is not correlated with elevation, latitude, or crater properties, but fans do exhibit a favored N-S orientation. Martian fans are, on average, larger but of similar gradient relative to their source catchments than terrestrial alluvial fans. Snowmelt is the most likely runoff source for forming the fans. Statistics of crater densities on both the fans and underlying terrains yield an age of late Hesperian to Amazonian. Future work will utilize this dataset in delving deeper into the heterogeneity of boundary conditions and processes responsible for fan formation. This study demonstrates the utility of global high-resolution datasets, and the Mars science community would greatly benefit from a global CTX mosaic, similar in coverage and ease of access as the Global Land Survey.

Chapter 3

Sedimentology and climatic environment of alluvial fans in the martian Saheki crater and a comparison with terrestrial fans in the Atacama Desert

Published as: Morgan, A. M., Howard, A. D., Hobley, D. E. J., Moore, J. M., Dietrich, W. E., Williams, R. M. E., Burr, D. M., Grant, J. A., Wilson, S. A., Matsubara, Y. (2014). Sedimentology and climatic environment of alluvial fans in the martian Saheki crater and a comparison with terrestrial fans in the Atacama Desert. *Icarus*, 229, 131–156. DOI:10.1016/J.ICARUS.2013.11.007

Abstract. The deflated surfaces of the alluvial fans in Saheki crater reveal the most detailed record of fan stratigraphy and evolution found, to date, on Mars. During deposition of at least the uppermost 100 m of fan deposits, discharges from the source basin consisted of channelized flows transporting sediment (which we infer to be primarily sand- and gravel-sized) as bedload coupled with extensive overbank mud-rich flows depositing planar beds of sand-sized or finer sediment. Flow events are inferred to have been of modest magnitude (probably less than ~60 m^3/s), of short duration, and probably occupied only a few distributaries during any individual flow event. Occasional channel avulsions resulted in the distribution of sediment across the entire fan. A comparison with fine-grained alluvial fans in Chile's Atacama Desert provides insights into the processes responsible for constructing the Saheki crater fans: sediment is deposited by channelized flows (transporting sand through boulder-sized material) and overbank mudflows (sand size and finer) and wind erosion leaves channels expressed in inverted topographic relief. The most likely source of water was snowmelt released after annual or epochal accumulation of snow in the headwater source basin on the interior crater rim during the Hesperian to Amazonian periods. We infer the Saheki fans to have been constructed by many hundreds of separate flow events, and accumulation of the necessary snow and release of meltwater may have required favorable orbital configurations or transient global warming.

3.1. Introduction

An alluvial fan is a semi-conical landform that develops where a channel exits a confined valley, and through avulsions and channel branching spreads sediment across the unconfined terrain (Blair and McPherson, 2009). The combination of slope reduction and lateral spreading reduces the carrying capacity and forces progressive sediment deposition. Martian alluvial fans have been identified ranging in scale from sub-kilometer (Williams and Malin, 2008) to a few kilometers (Burr et al., 2009) to tens of kilometers (Moore and Howard, 2005; Kraal et al., 2008; Anderson and Bell, 2010; Grant and Wilson, 2011, 2012). The well-preserved, mid-latitude fans of the Hesperian (and perhaps even younger) (Grant and Wilson, 2011; Kraal et al., 2008; Moore and Howard, 2005, Morgan et al., 2012a,b) are of particular interest because they, along with deltas (e.g., Malin and Edgett, 2003; Moore et al., 2003; Lewis and Aharonson, 2006; Pondrelli et al., 2008,2011; Mangold et al, 2012b; Wilson et al., 2013; Chapter 2) and small valleys in the mid-latitude regions (e.g., Hynek et al., 2010; Fassett et al., 2010; Howard and Moore, 2011; Mangold, 2012), may represent a widespread episode of large-scale fluvial landform construction and modification on Mars occurring well after the Late-Noachian to Early Hesperian epoch of valley network incision (Grant and Wilson, 2011; Howard and Moore, 2011). This later period of fluvial activity occurred in an environment thought to be characterized by a relatively thin atmosphere and global cryosphere (Carr and Head, 2010; Fassett and Head, 2011; Lasue et al, 2013). Although difficult to decipher, the effects of water (both fluid and ice) on a paleo-landscape are the most unambiguous markers of past climatic environment and have significant potential to further our understanding of the climate evolution and potential late-stage habitability of Mars.

Almost all mapped martian alluvial fan systems have been found to be enclosed within basins (craters) and source from deeply incised crater rim alcove basins (Moore and Howard, 2005; Kraal et al., 2008; Wilson et al., 2013; Chapter 2)., which strongly constrains both the hydrological and sedimentary environments. The association between the sediment and water source areas in the dissected crater wall and the fan system is short and direct. The presence of a large alluvial fan in an enclosed basin limits the possible range of the hydrologic regime; on the low end it is constrained by the necessity to erode and transport sediment from the headwater source and on the high end by the apparent absence of coincident deep lakes within the crater. Previous work on the larger equatorial fans has concluded that they formed during periods of enhanced precipitation (probably as snowfall) primarily through hundreds of flow events over tens of thousands (to perhaps millions) of years (Armitage et al., 2011; Grant and Wilson, 2011, 2012; Moore and Howard, 2005).

This study focuses on Saheki crater (85 km-diameter, 21.7°S, 73.2°E), one of several fan-bearing craters along the northern rim of the Hellas basin (Figures 3.1 and 3.2). Fans in this crater are among the largest catalogued by Kraal et al. (2008) and Moore and Howard (2005) and contain the clearest exposed stratigraphy yet identified on Mars (Table 3.1). The studies of alluvial fans in southern Margaritifer Terra (Grant and Wilson, 2011, 2012) revealed that the fans and fan-deltas of this region date to the Late Hesperian to Early Amazonian rather than being coeval with the extensive valley networks of Late Noachian to Early Hesperian, which had been suggested by Howard et al. (2005). The exquisite alluvial fan stratigraphy exposed in craters of the Hellas north rim (Figure 3.1), and Saheki crater in particular (Figure 3.2), permits a comprehensive assessment of several unresolved issues concerning martian alluvial fans, including the mode of sedimentation (e.g., fluvial versus debris flows), the magnitude, frequency and duration of formative flows, the age of the alluvial fans and the associated climatic environment. We address these issues through a detailed stratigraphic analysis, crater count-derived ages, quantitative interpretation of the flows (velocity and discharge) forming the fans, and a comparison with a terrestrial analog fan system in the Chilean Atacama Desert. This is followed by our synthesis of the fan sedimentology, geologic history of fan deposition, and the associated hydrologic and climatologic environment. We conclude that the Saheki crater fans were deposited by a combination of channelized fluvial and muddy overbank flows by many separate flow events numbering in the hundreds to thousands over an extended time period around the Hesperian-Amazonian boundary. Snowmelt sourced from upper crater walls is found to be the most tenable water source.

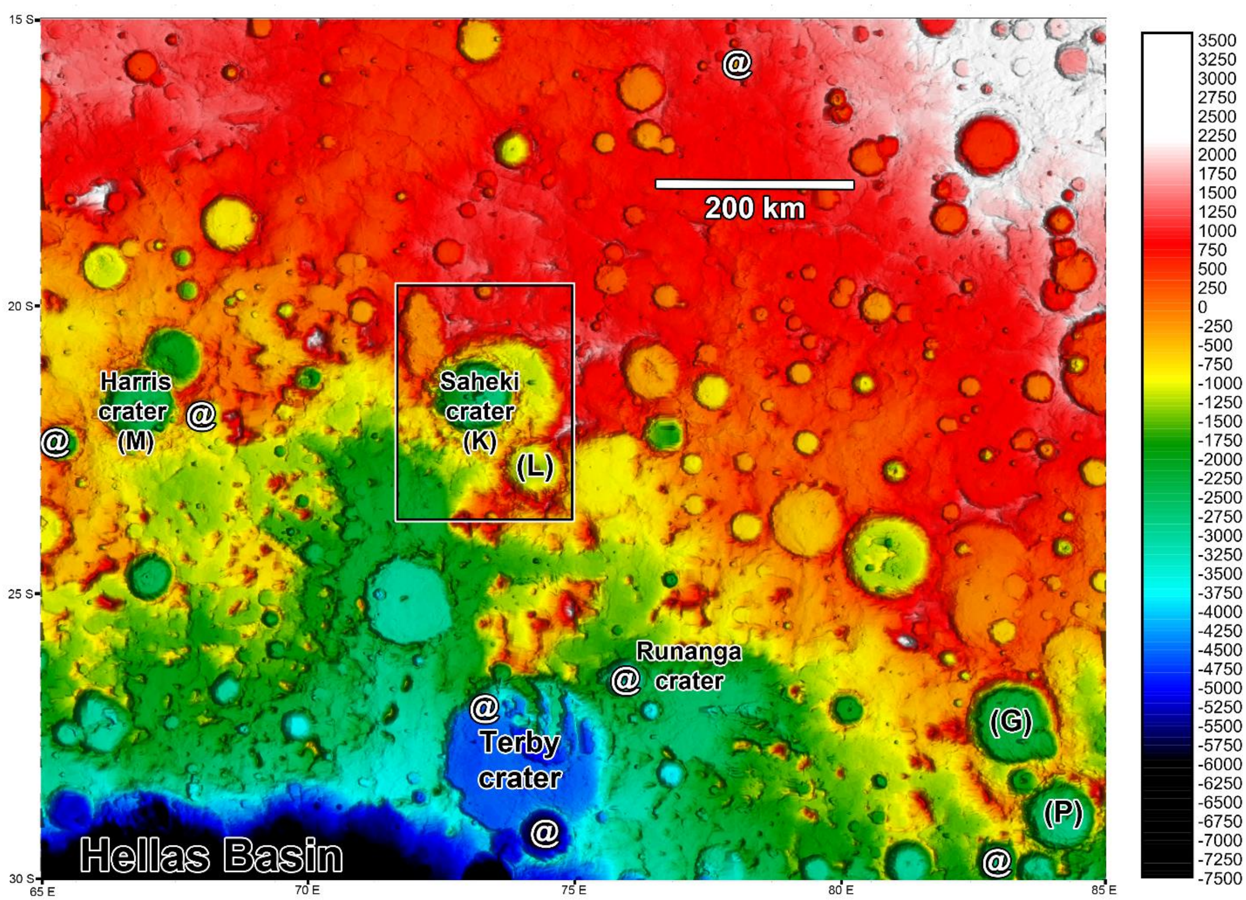

Figure 3.1. Regional digital elevation location map of the northern Hellas rim. Image extends from 15°S to 30°S and 65°E to 85°E, Mercator projection. Letters in parentheses indicate crater designation in *Moore and Howard* (2005). "@" symbols show craters hosting fans identified by *Kraal et al*. (2008) and *Wilson et al*. (2007, 2013). Box shows location of Figure 3.2. Topographic scale is in meters to Mars datum. North is up in this and all following figures (excluding photographs).

3.2. Observations and interpretations

3.2.1 Geologic setting and data used

Six fan-bearing craters, labeled “G”, “K” (since named Saheki by the IAU), “L”, “M” (since named Harris by the IAU), “P”, and “X” (Figure 3.1) have been identified in the far western Terra Tyrhenna (Moore and Howard, 2005; Kraal et al., 2008; Williams et al., 2011). As part of a new global inventory of alluvial fans (Wilson et al., 2013; Chapter 2), several additional fan-hosting craters have been identified in the north Hellas rim region (“@” symbols in Figure 3.1). Our morphologic and stratigraphic study primarily focuses on the fans within Saheki.

Saheki crater is superimposed onto a larger ~100 km crater to the east and an elongated elliptical basin measuring 90 km by 45 km to the northwest. It contains two prominent fans (K1 and K2 in Figure 3.2) sourcing from its western rim and one much smaller fan sourcing from the southeastern rim. The Saheki fans are of shallow gradient (~0.03) and large size (greater than 750 km^2) (Table 3.1), comparable to dimensions of other alluvial fans in the region. Localized fluvial dissection occurs on the craters’ ejecta as well as within the main cavity and is of an uncertain age relationship to the fans. The southern rim of Saheki features large slumps presumably formed by failure of the steep transient crater wall shortly after the crater itself was formed. These slumps have been modified by mass wasting and fluvial erosion and based on their superposition must pre-date the fan deposits discussed (Figure 3.3). All of the large fans in this region are sourced from steep-walled, sharply defined alcoves carved into the crater rim that act as the sole sediment source region and drainage basin supplying the fan.

Figure 3.2 (next page). Close up of boxed area of Figure 3.1. Saheki crater exhibits poorly expressed proximal crater ejecta, a total floor to rim relief of ~2.5 km, and a central peak that rises approximately one kilometer above the crater floor. Crater “L” is 20 km to the southwest of Saheki. Individual fans and source basins are outlined in white and are marked with asterisks and arrows, respectively. Small fans denoted by “@”. Fan notation follows Moore and Howard (2005). Scale is in meters to Mars datum.

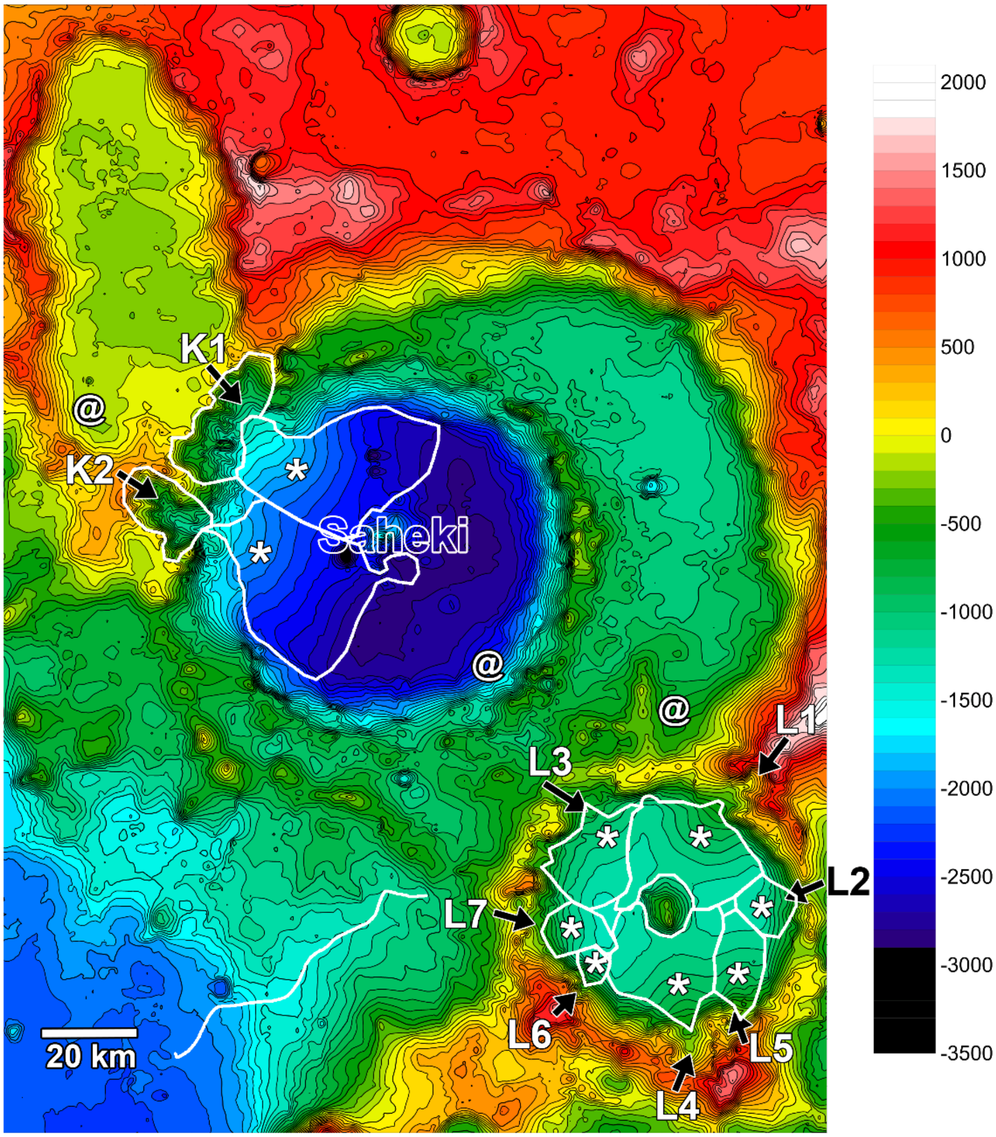

The Saheki fans have been completely imaged by the Mars Reconnaissance Orbiter's (MRO) CTX camera (Context Camera, resolution ~6 meters/pixel) (Malin et al., 2007) and have varying degrees of HiRISE coverage (High Resolution Imaging Science Experiment, resolution ~30 cm/pixel) (McEwen et al., 2007). We have produced digital elevation models (DEMs) from select HiRISE and CTX stereo pairs with the Ames Stereo Pipeline software package (Morato et al., 2010). MOLA topographic data (Zuber et al., 1992) was used for areas not covered by our DEMs. Spectral data from the Thermal Emission Imaging System (THEMIS) (Christensen et al., 2004) and the Compact Reconnaissance Imaging Spectrometer for Mars (CRISM) (Murchie et al.,

2007) datasets were not useful in this investigation; two CRISM images covering the fans indicated the presence of hydrated minerals but did not resolve any spatial pattern that could be correlated with visible features.

Property	K1 Fan	K2 Fan	Average Mars Fan[a]	Atacama Fan 1	Atacama Fan 2
Catchment Size, km^2	501	319	149	910	328
Catchment Relief, km	1.5	2.3	1.6	3.7	3.0
Catchment Gradient	0.096	0.089	0.118	0.050	0.084
Fan Size, km^2	813	750	251	199	215
Fan Relief, km	1.33	1.22	0.72	0.3	0.38
Overall Fan Gradient	0.030	0.031	0.041	0.0094	0.018
Mid-Fan Gradient	0.038	0.030	---	0.02[b]	0.028[b]
Fan Length, km	44.8	40.1	18.74	30.0	20.5
Fan Concavity[c]	0.0193	0.0045	0.0700	0.048	0.072

[a]Average of 31 large fans reported in Moore and Howard (2005)
[b]Fan gradient near apex
[c]Fan concavity is measured by $-(d^2z/dx^2)/(dz/dx)$, where z is surface elevation (m) and x is distance from the fan apex (km), estimated from measurements at the fan apex, midpoint, and termination (Moore and Howard, 2005).

Table 3.1. Properties of Saheki crater fans and terrestrial Atacama Desert fans.

3.2.2. Fan morphology and stratigraphy

The fans in Saheki, particularly the more southern of the two principal fans (K2, Figure 3.3) exhibit surface texture and erosion-accentuated bedding at hectometer scale (Moore and Howard, 2005) that is far more pronounced than observed on other martian fans. Both the K1 and K2 fans (Figure 3.2) form typical conical morphology and are sourced from deeply dissected source basins on the northwestern and western crater rim. The K1 and K2 fans merge concordantly at their lateral boundaries, but no clear superposition relationship was identified and they likely formed simultaneously, resulting in interfingered deposits. The two fans are of similar size, surface gradient and source basin characteristics (Table 3.1). The surface of the upper parts of the K1 fan is relatively featureless at the decameter scale except for superimposed impact craters and a 650 m wide valley extending about 10 km into the fan from the apex. Several indistinct shallow valleys radiate from this incised valley. The eastern, distal 10 km of the K1 fan has been wind-dissected into linear ridges similar to those on the K2 fan (discussed below). In contrast, the upper portion of the K1 fan appears to be relatively unaffected by wind erosion, but meter to decameter features of the original fan surface have been obscured by post-fan impact gardening and modest aeolian deposition, largely occurring as scattered transverse aeolian ripples (TARs) (Wilson and Zimbelman, 2004; Balme et al., 2008; Berman et al., 2011). As a result, fluvial morphology and stratigraphy is poorly exposed, so this study emphasizes the better exposures on the K2 fan.

Particle Size (mm)	Main Class	Subclass	Secondary Class
4096			
		Boulder	
256			
		Cobble	
64	Gravel		
4		Pebble	
			Granule
2			
		Coarse Sand	
0.5			
	Sand	Medium Sand	
0.25			
		Fine Sand	
0.0625			
	Silt[a]		
0.0039			
	Clay[a]		

[a]Silt and clay grouped together are termed “mud”.

Table 3.2. Terminology for grain sizes used in this paper based on the Wentworth (1922) classification.

The K2 fan surface features prominent ridges radiating from the fan apex (Figure 3.3). These ridges have the greatest relief and continuity on the southern and eastern distal portions of the fan. Clear exposures of layered deposits on the sides of the inverted ridges indicate that winds keep exposures free of dust and that wind is the likely erosional agent inverting the ridges (Figure 3.4). TARs with a dominant E-W orientation mantle much of the depressed inter-ridge surfaces, although whether winds were northerly or southerly is uncertain. Layer exposures on the south side of the dominantly E-W trending ridges are generally clearer than on the north side, suggesting that the strongest winds are southerly. Consistent with this interpretation, composite IRB HiRISE images (composites with the near-IR, red, and blue–green images displayed in red, green, and blue channels, respectively) indicate a distinct bluish cast on the north side of some ridges indicative of a different composition, which, when coupled with obscuration of layers, suggests aeolian accumulation on the sheltered side (Figure 3.4). The TARs suggest a high availability of sand-to granule size sediment (our terminology for grain size is summarized in Table 3.2) to aid aeolian scour, and because the TARs are concentrated on the fan surfaces rather than on the exposed crater floor, the fan deposits are a likely sediment source.

Thicknesses of the Saheki fans were estimated by comparing topographic profiles of the nearly flat eastern half of the crater floor to profiles through the fans (Figure 3.5), so that the fans are likely 800-850 m thick near the apices and approximately 300 m thick where they impinge upon the central peak. The volume of the fan deposits was estimated in two ways. The first method gives an order of magnitude estimate by multiplying an assumed average fan thickness (400 m) by the combined surface area of K1 and K2 fans (1563 km^2) giving 525 km^3. Another estimate is based on circular projection of the profiles A through E in Figure 3.5 to produce the estimated basal fan topography and calculating the volumetric difference with the modern DEM, giving 586 km^3. This second value is likely a slight underestimate because valley fill deposits above the fan apex were not accounted for. Unfortunately, the MOLA DEM has insufficient resolution to estimate the eroded volume of the source basin, and higher resolution stereo imaging was not available there.

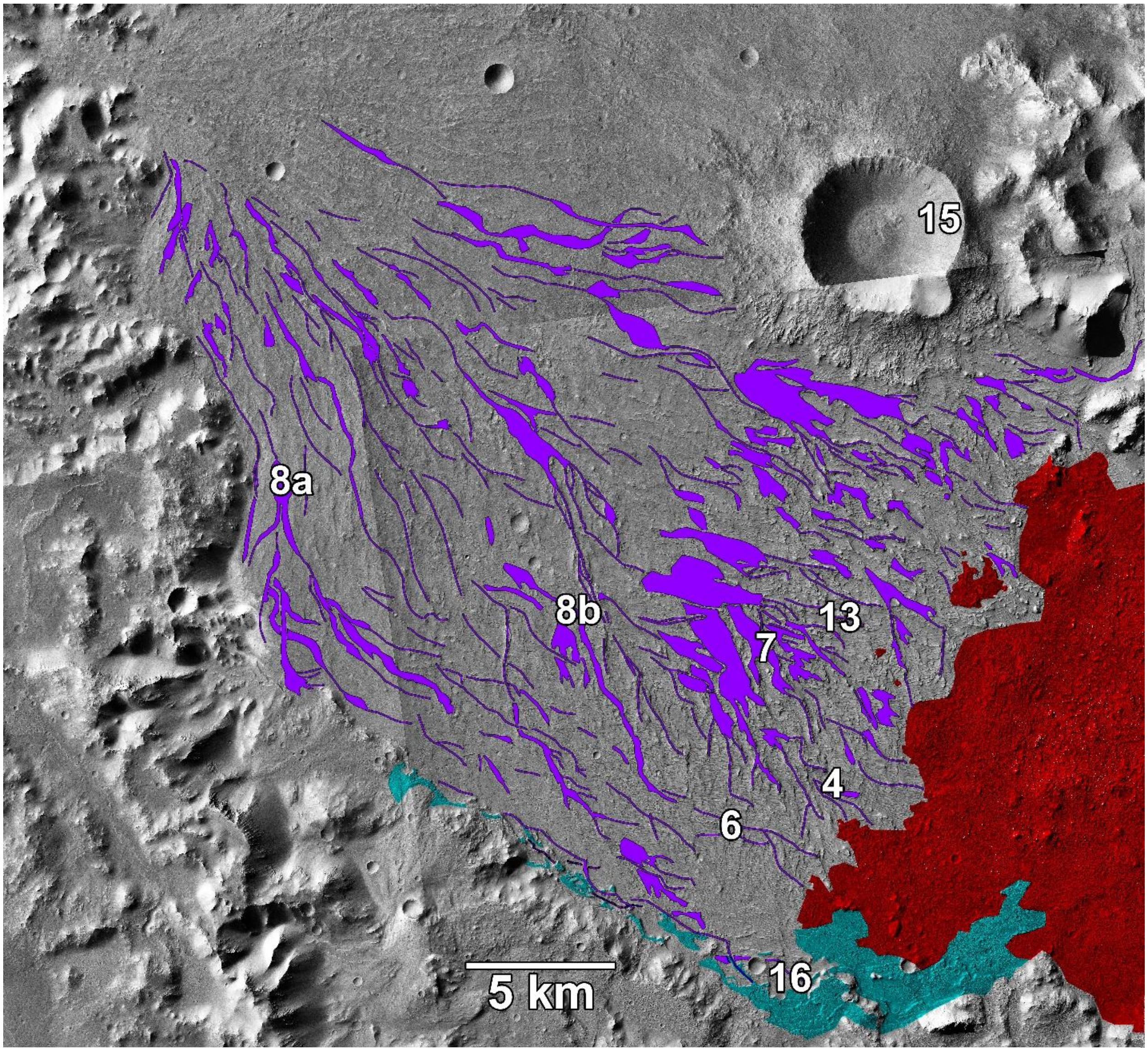

Figure 3.3. Interpretive map of southern portion of the Saheki crater K2 fan and related features. The central peak and degraded interior rim are in the upper right and lower left, respectively. Also along the southern edge of the fan are slumps sourced from the crater walls which pre-date the fan material. Numbers indicate locations of additional figures in this chapter. Purple lines and areas are raised ridges and platforms interpreted to be fluvial distributaries radiating from the fan apex at the upper left. Where the linear ridges or paired ridges are less than about 100 m in width they are shown as purple lines, but broader ridges and level platforms are portrayed as purple areas. Aeolian erosion has raised these into varying degrees of inverted relief. Red areas are crater floor materials interpreted to be megabreccia. Cyan features along southern margin of fan are flat-topped benches interpreted to be lacustrine or playa deposits contemporaneous with the fan. Uncolored areas on the fan are discontinuous distributaries and low areas partially mantled by transverse aeolian ridges (TARs). Mosaic of ~6 m/pixel CTX images P17_007543_1586, P19_008545_1576, and B09_007543_1586 centered at 21.96°S, 72.81°E.

Three distinct geomorphic and associated sedimentary features are associated with the Saheki fans, each of which is described below: 1) linear ridge and broad platform features and associated deposits that locally broaden into nearly flat benches with rough-textured surfaces; 2) fine-textured layered deposits largely exposed on side-slopes beneath ridges and platforms; and 3) level benches at distinct elevations bordering the fan deposits at their southern and eastern margin.

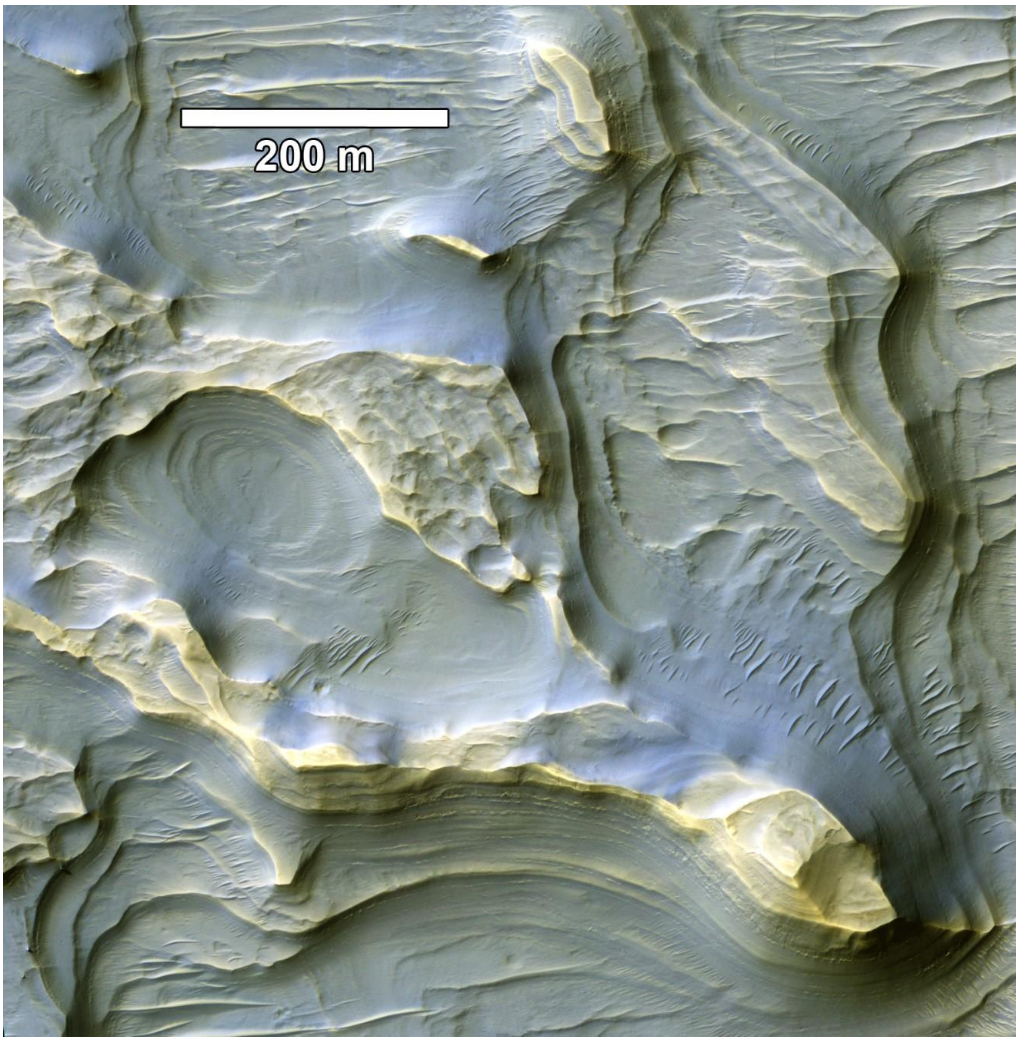

Figure 3.4. Detail of inverted ridges and interbedded fine sediment exposed on subjacent slopes Sediment capping ridge crests have yellowish cast relative to fine sediment. Fine aeolian sediment concentrated on north side of ridges has distinct bluish tone. Note scalloped indentations on ridge crests, presumably due to wind scour. Part of IRB color ~.3 m/pixel HiRISE image PSP_007688_1575 centered on 22.092°S, 72.966°E, with colors stretched for clarity. Portions of low areas are occupied by TAR ridges.

3.2.2.1. Linear and platform features

We broadly define this class of features as downslope-oriented ridges or depressions radiating from the fan apex and traceable over kilometer or longer distances (Figures 3.6-3.8). These features occur as four subtypes. The dominant morphology occurs as linear to modestly sinuous (<1.2), narrow (10s of meters in width) ridges that stand up to 70 m above the surrounding terrain. With distance downslope, ridges often become narrower, discontinuous, and higher relative to their surroundings, although the ridge tops define an accordant, sloping surface. A second, less common morphology consists of two parallel ridges that are separated by a few 10s of meters. A third morphology comprises linear depressions generally 100 m or more across. In a few cases, a systematic down-fan transition from a depression through parallel ridges to a single ridge is observed, although unequivocal examples are rare (Figure 3.6). Individual linear features can locally be traced 15 km or more down-fan, but none of the features extends from the fan apex to the distal fan margin (Figure 3.3). A fourth morphology occurs as broad, nearly level platforms that display a ridge and swale topography, generally with the long axis oriented downstream although sometimes displaying a curved pattern (Figure 3.7). Ridges are typically spaced a few 10s of meters apart and platforms commonly connect to linear ridges upslope or downslope (Figure 3.3). In the mid-section of the fan, these platforms mostly occur as isolated features, often widening downstream in small flared forms (Figure 3.8) that are usually dissected at their downstream ends (black arrows in Figure 3.8). About 10 km from the distal end of the fan, the platforms become broader, more numerous, and interfinger at different stratigraphic levels (e.g., Figures 3.7 and 3.9). Comparing the actual elevations of the lower fan surface to a virtual conic surface projected from the upper fan suggests that as much as 120 m of sediment may have been wind-eroded from low regions between ridges (Figure 3.9).

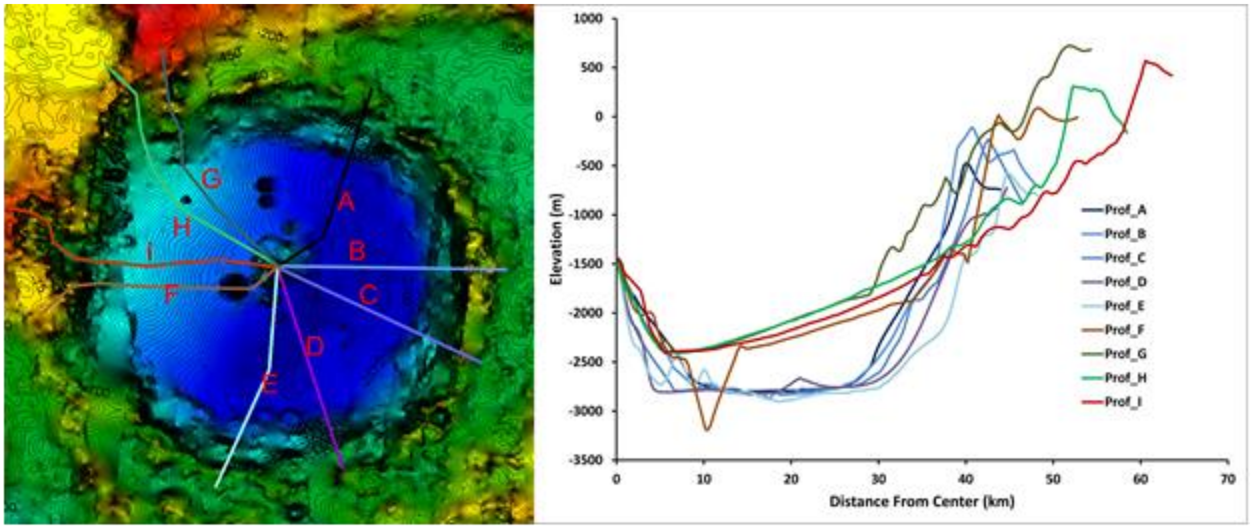

Figure 3.5. Radial topographic profiles through Saheki crater. Saheki crater is approximately circular and the eastern half of the crater floor is nearly flat, making radial profiles A through E nearly coincident, whereas F to I cross the K1 and K2 fans permitting depth estimates assuming a symmetrical initial crater. Difference between the two sets of profiles provides an estimate of fan deposit thickness, reaching a maximum of about 850 m near the fan apices. Profiles H and I approximately follow the main valley axes of the source basins upstream from the K1 and K2 fans. Topography from interpolated MOLA PEDR data.

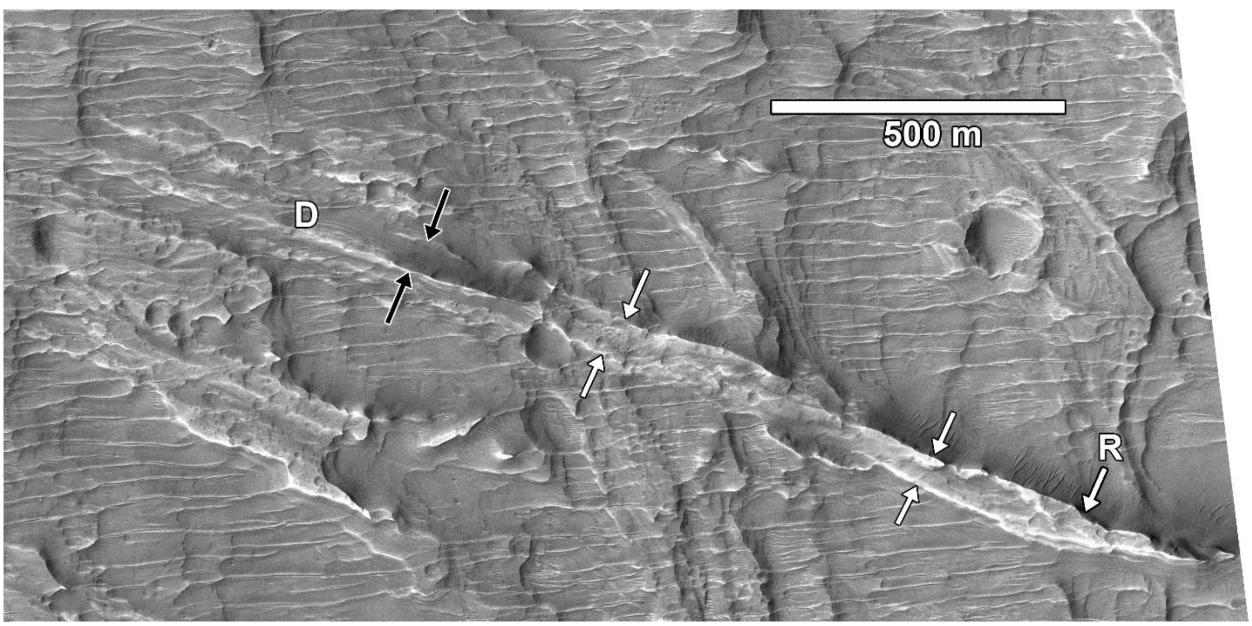

Figure 3.6. Down-fan transition from a linear depression (D) through a U-shaped trough (delimited by black arrows) to a linear ridge (R) delimited by white arrows. Feature is interpreted as a fluvial channel with increasing degree of exposure and inversion down-fan due to increasing depth of aeolian deflation. Parallel ridges (black arrows) may be narrow natural levees. Part of ~.3 m/pixel HiRISE image ESP_029788_1575, centered at 22.123°S, 72.906°E.

Onlap and superposition relations are visible locally all over the fan surface (Figures 3.3, 3.7, 3.9). In almost every case, each linear ridge projects downstream to a higher elevation than ridges originating farther downstream. Although superposition relationships are evident locally, correlations across the entire fan surface are not possible. Essentially all of the linear ridges and depressions are oriented downslope, but ridges at different levels occasionally cross at acute angles. Definitive examples of ridge intersections at an accordant level are sparse. Where they occur, they generally exhibit downslope branching, although rare braiding patterns occur.

The top surface of the linear ridges typically has a scalloped appearance at decameter scales (Figures 3.3 and 3.10). Blocks up to several meters in diameter are visible locally on the ridge surfaces, and in numerous locations the surface shows occasional ~1 m blocks interspersed with a characteristic mottling or speckling (Figure 3.10 inset) that appears to be limited in occurrence to the ridge surfaces. Elsewhere, the ridge crests are relatively smooth at meter to sub-meter scales. To establish the distribution and setting of the blocks, we mapped occurrences by careful examination of three HiRISE images covering the K2 fan surface (Figure 3.11). Concentrations of blocks occur almost exclusively on the tops of linear ridges or as exposures on the top few meters of side-slopes at the edge of the ridges. Block exposures are generally elongated along the direction of the ridge crests and often occur in close association with mottled/speckled surfaces. Both blocks and mottling become less frequent towards the distal end of the K2 fan, so that ridge crests are smooth at meter scale (although frequently scalloped at decameter scale).

Figure 3.7 (next page). Flat platforms on the K2 fan. We interpret the ridges to be mantled with gravelly sediment deposited by low-sinuosity meandering or braiding streams during deposition. An interpreted meander bend is shown by dashed white lines, and possible point-bar deposits interior to the bend occur near the asterisks, with black arrows pointing in the direction of inferred meandering. Paired white arrows on right hand of image shows ridges representative of those sampled to determine original widths. Paired black arrows show paired narrow ridges interpreted to be natural levees exposed through partial aeolian distributary exposure. Part of ~.3 m/pixel HiRISE image PSP_007588_1675, centered at 22.016°S and 72.936°E.

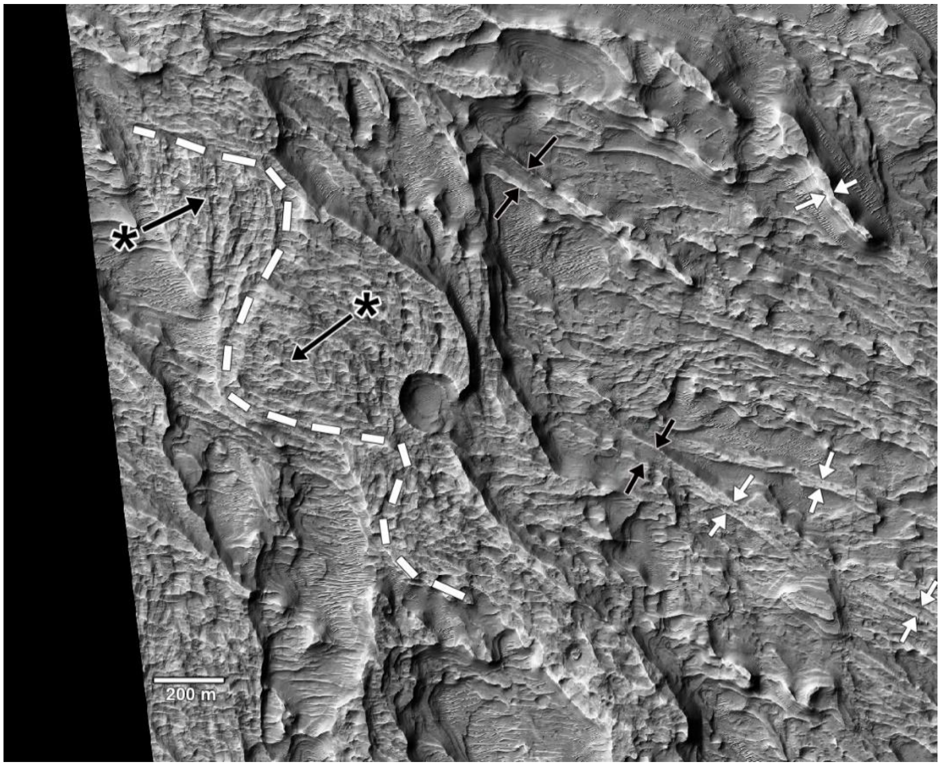

3.2.2.2. Interpretation of linear and platform features

The linear and platform features radiate from the apex, trend downslope, and generally exhibit nearly uniform widths downstream. Consistent with channelized flow, we interpret these features as fluvial distributaries constituting the sediment dispersal backbone of the alluvial fans (Grant and Wilson, 2012; Moore and Howard, 2005; Williams et al.,2011) and the fact that most of these linear features are exposed as ridges to indicate they have been inverted by differential aeolian erosion. The channelized distributaries must have been embedded within finer and/or more poorly cemented deposits that were preferentially stripped. The characteristics of these easily eroded deposits are discussed in Section 2.2.4.

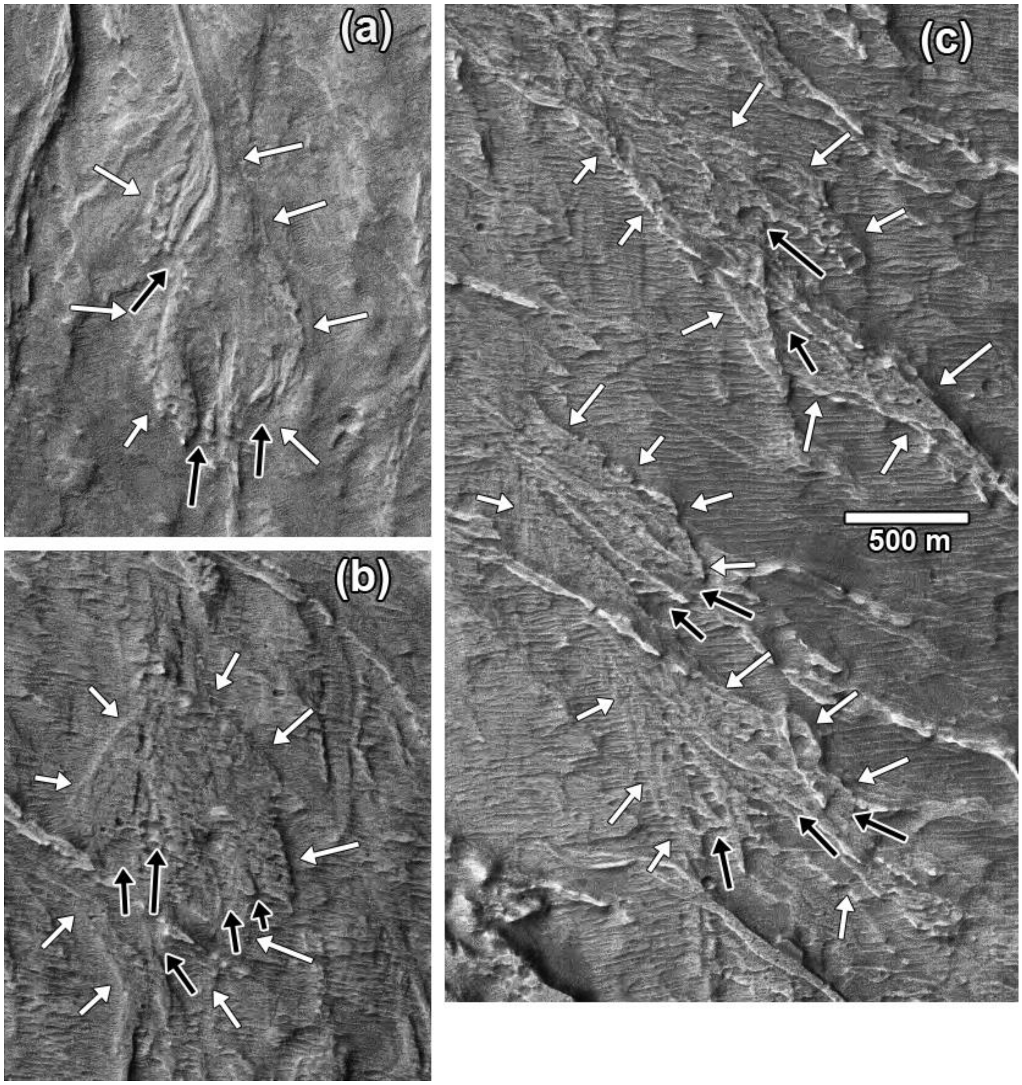

Figure 3.8. Splay-like inverted platforms. White arrows show outer limits of splay. Ridges on surface of ridge suggest a spreading, possibly avulsive set of channels. Splays generally terminate down-fan in multiple finger-like ridges, separated by incised linear depressions (black arrows point upstream). All images at same scale. These structures are interpreted as fluvial deposits generally fed by a single channel upstream that spread into local depressions on the fan surface, or as autogenic transverse bars causing upstream deposition. Flows across the splay deposit eventually incise into the distal end of the deposit (black arrows). Images are part of ~6 m/pixel CTX image P14_006686_1579. (a) Centered at 21.927°S 72.634°E, (b) at 22.019°S, 72.811°E, and (c) at 22.141°S, 72.863°E.

Boulders on the Saheki fan surface might have originated through a variety of processes, such as fluvial deposition, through cementation of a deposit and its subsequent weathering into blocks, or as impact ejecta. We, however, interpret the visible blocks exposed on the ridges (Figure 3.10) to be fluvially transported and deposited boulders ranging from 0.25 – 4 m in diameter.

Blocks are largely absent in the depressions between ridges, although the frequent mantling by TARs could obscure some deposits. Exposures of coarse-grained material occur primarily from the K2 fan apex to about 10 km from the distal margin of the fan (Figure 3.11), and are positively correlated with an apparent increase in total incision into the fan surface (Figure 3.9). This observation is consistent with a downstream fining of channel bed sediment, with boulders giving way to finer gravel and sand as the distance from the fan apex increases, as sometimes observed in terrestrial fluvial fans (Stock et al., 2008; Stock, 2013). On terrestrial fans dominated by debris flows, systematic downstream changes in grain size would not be expected, reinforcing our interpretation that these Saheki fans are not debris flow fans (Blair and McPherson, 2009). The observation that fluvial conglomerates are present on an alluvial fan in Gale crater (Williams et al, 2013) supports the interpretation that runoff on martian alluvial fans was capable of transport of gravel.

On portions of the distributary deposits near the downstream end of areas with visible boulders, the ridge tops are commonly mottled or speckled at 30 cm/pixel HiRISE resolution (Figure 3.10). Mottling in images could result from a variety of surface morphologies, including wind ripples and patterned ground, but the association of these mottled surfaces with visible coarser-grained material in nearby exposures suggests that they are gravels below the limit of HiRISE resolution (see Section 3.3.2.2). Distributary ridges that do not display either visible boulders or a mottled surface are presumably deposits finer than a few tens of cm in diameter.

Distributary ridges are often discontinuous (Figure 3.7), implying that ridges can be eroded, either by direct removal by wind erosion and/or by lateral backwasting of hillslope scarps. The resistance of the fluvial distributaries to wind erosion that results in their topographic inversion could be due either to diagenetic cementation or to a component of the fluvial sediment being coarser than a few mm in diameter (the effective limit to wind transport (Greeley et al., 1976;

Zimbelman et al., 2009; Gillies et al., 2012;). Sand and gravel in fluvial deposits, being permeable, often become cemented from percolating groundwater, whereas interbedded and largely impermeable fine deposits are not (Spötl and Wright, 1992). The decameter-scale fluting on the surface of many of the inverted channels suggests a loose component of the sediment that can be deflated; in such locations cementation is probably less important than the presence of a component of coarse sediment that can form a wind-resistant pavement. Similar wind fluting occurs on fine, apparently modestly cemented deposits in Terby crater (Ansan et al., 2011; Wilson et al., 2007) and on fine-grained deposits on Atacama Desert fans (discussed in Section 3.3.1.1). The local presence of fluvially-deposited boulders (Figure 3.10) suggests that mass wasting must dominate ridge backwasting at least locally because wind cannot strip such coarse debris.

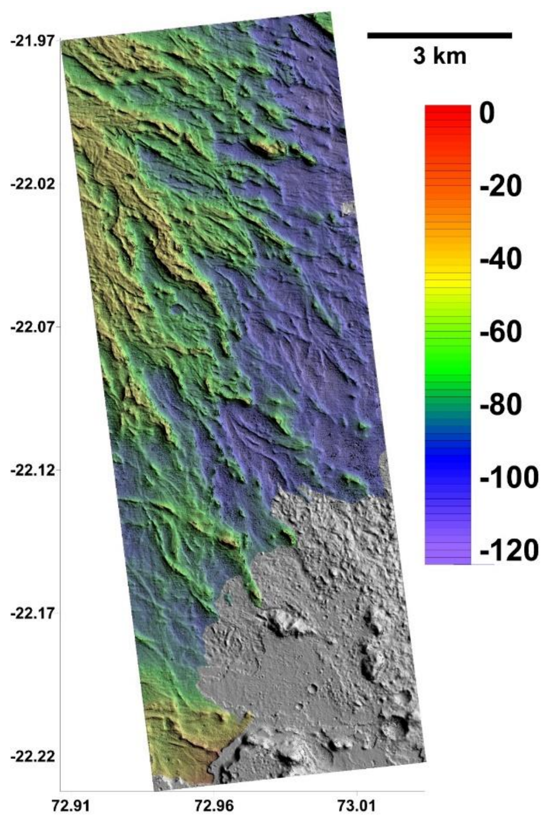

Figure 3.9. Shaded relief image of the distal end of the Saheki K2 fan from ~3 m DEM constructed from HiRISE stereo image pair PSP_7688_1575 and PSP_008545_1575, centered at 22.10°S, 72.97°E. A plane fit to the overall dip (0.03 ESE) and strike (NNE) of the fan surface was subtracted from the DEM, and elevations (in meters) relative to that plane are indicated in color shading. Portions of the fan surface at approximately equal stratigraphic level have the same relative elevation. This indicates that the depth of aeolian erosion increases towards the distal end of the fan, which is accordant with higher ridge inversion near the distal end of the fan. Axis labels in degrees North and East. Portions of image not mantled with fan deposits are uncolored.

The pattern shown in Figures 3.3 and 3.6 in which distributaries emerge from beneath stratigraphically higher deposits, increase in relative height and height of inversion downslope, and terminate before reaching the distal fan edge indicate that the degree of aeolian stripping increases systematically towards the distal end of the K2 fan. Near the apex of the K2 fan, distributaries are in low relative relief and difficult to differentiate. This muted topography would be expected near a fan apex, where distributaries shift frequently (thereby covering a greater area with coarser material) and where deposition would likely be dominated by coarse-grained channel deposits.

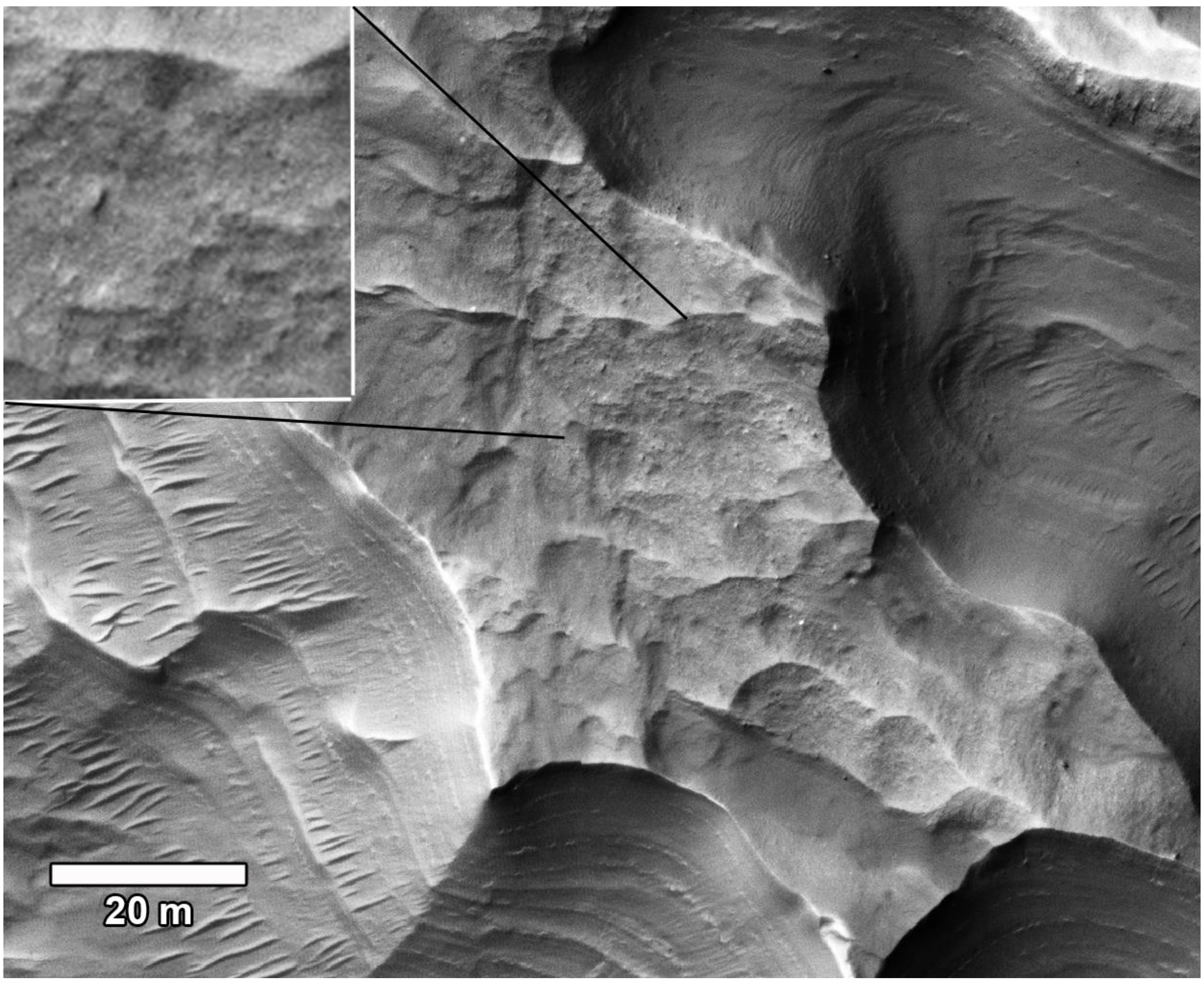

Figure 3.10. Detail of inverted ridge showing gravelly sediment and wind scoured surface. Inset is magnified 3x. Layered sediments exposed on slopes below ridge. Part of ~.3 m/pixel HiRISE image PSP_007688_1575 centered at 22.049°S and 72.944°E.

Occasionally the K2 fan surface has eroded into two parallel ridges which typically transition down-fan into raised ridges of similar width (black arrows in Fig 6 and red arrows in

Figure 3.7) but which often become indistinct hollows when traced upstream (Figure 3.6). We interpret these parallel ridges to be narrow natural levees that would be the first coarse-grained component of an overbank channel deposit to emerge during wind scour, with the finer distal overbank deposits being preferentially removed. Likewise, the interiors of such channels were presumably filled with finer, more readily-eroded sediment after abandonment.

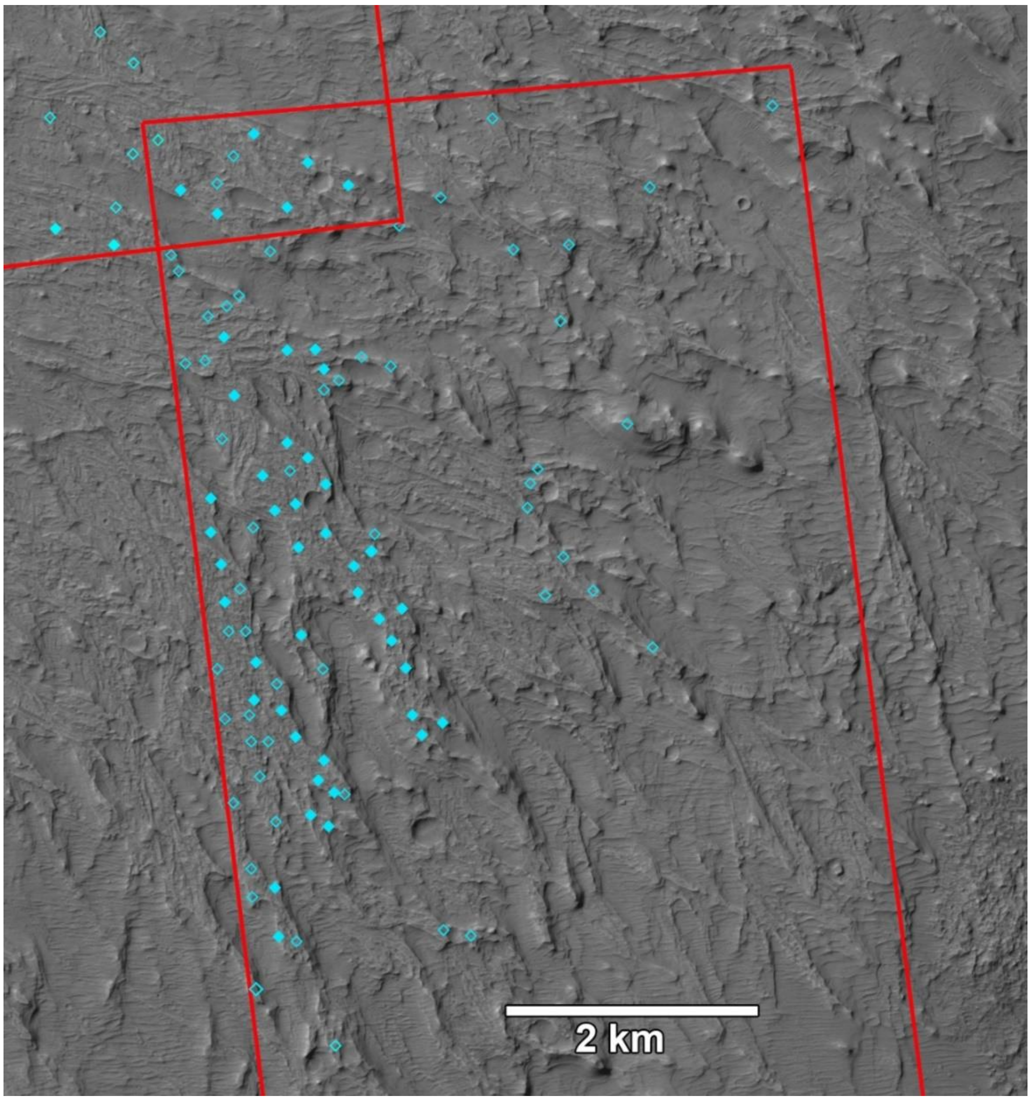

Figure 3.11. Distribution of coarse-grained deposits on part of the Saheki K2 fan. These occurrences were mapped on 0.25 m/pixel HiRISE images PSP_007686_1575 (lower red outlined area) and PSP_006686_1580 (upper left red area). Mapping additionally included the remainder of these images and HiRISE image PSP_007899_1580 near the apex of the K2 fan (not shown). Visible coarse deposits and characteristic mottling or speckling in HiRISE images indicated by solid and hollow diamonds, respectively. These are interpreted as deposits of gravel just below the limit of resolution of individual boulders. Image base is CTX image P19_008545_1576 centered at 22.02°S, 92.96°E.

The wider platform features mapped in Figure 3.3 are interpreted as fluvial deposits created either by multiple, braided channels (Figure 3.8) or by a single, slightly sinuous channel that migrates laterally, leaving scroll-bar ridges (Figure 3.7), as suggested by Moore and Howard (2005). Similar inverted features interpreted as scroll bars occur on the Eberswalde crater delta (Malin and Edgett, 2003; Moore et al., 2003) and sinuous channels in the Aeolis-Zephyria region (Burr et al., 2009, 2010). It is likely that flow did not occupy the entire width of these broad expanses at any given time.

The isolated platform deposits in the mid-section of the K2 fan (Figures 3.3 and 3.8) might form by two processes, one related to avulsion and the other to autogenic processes. The avulsion scenario would accompany distributary shifts into a new course. As fans aggrade, the inactive portions of the fan become relative depressions. When an avulsion penetrates into a depression, splay-like bedload deposition may occur until the depression becomes filled and material can be transported further down-fan. Subsequent fluvial erosion downstream from the relative depression can result in entrenchment of the splay deposits or abandonment due to an avulsion. The second scenario involves local flow expansion, transverse gravel bar deposition, infilling of the resultant upstream depression, and eventual breaching and trenching of the bar (Field, 2001; Stock, 2013).

The broad band of overlapping platform deposits about 5-10 km upstream from the distal end of the fan might have resulted from the effects of a rising temporary lake (playa) base level at the fan terminus which would encourage enhanced deposition and a spreading flow pattern. The high relief on the distal end of the fan suggests that wind erosion has stripped at least 70 m and perhaps up to 120 m of fan and basin-floor deposits, indicating a higher base level when the uppermost fan deposits were laid down (Figure 3.9). As discussed in Section 3.2.2.7, benches along the southern margin of the fan also suggest a higher base level was present during deposition of the youngest fan deposits. It is also possible that decreasing grain size downstream simply led to reduced formation of levees around the channels, resulting in more sheet-like and laterally unconstrained flow and deposition.

3.2.2.3. Distributary widths

Information on distributary widths is important for analysis of flow discharges. The aeolian erosion that inverts the distributaries serves to expose the channels, but may also narrow them as a result of lateral backwasting of the channel edges by mass wasting triggered by aeolian erosion of weaker surrounding layers. Burr et al. (2010) conclude that many inverted meandering channels in the Aeolis Dorsa/Zephyria Plana region have been significantly narrowed because of an observed meander wavelength to preserved ridge width that significantly exceeds the typical terrestrial value of about 10-14 (Knighton, 1998, p. 215). In some environments, however, wavelength/width ratios can reach 20-25, as along the low gradient, mud-bank Quinn River in Nevada (Matsubara et al., 2012). If the interpretation of the meander pattern in Figure 3.7 is correct, the wavelength of about 750 m divided by an average distributary width of 40 m gives a meander wavelength/width ratio of about 19. Although we suspect large observational variance and perhaps some bias in resolving distributary width, a best estimate will serve to calculate approximate formative discharges. Width measurements of 68 inverted channel segments on the K2 fan where ridge tops are flat with well-defined margins with consistent widths over reasonable (> 500 m) distances (Figure 3.7) yielded no systematic spatial trend with position on the fan. The distribution of these widths has a sharp, well-defined peak at 38 m (Figure 3.12), though with a significant positive skew of apparently wider channels. This tail may be in part due to misidentification of wider platforms as single-thread instead of braided channels or to lateral migration of meandering channels. In the few cases where ridges measured for width can be traced upstream to parallel ridges (presumed to be levees), the ridge spacing is approximately equal (within several meters) to the ridge width. Limited HiRISE coverage over other fans in the vicinity of Saheki (Figure 3.1) and the lack of additional well-preserved flat-topped ridges in other fan systems prevents a thorough assessment of channel widths elsewhere, though channel widths appear to be qualitatively similar (Burr et al., 2010; Grant and Wilson, 2012).

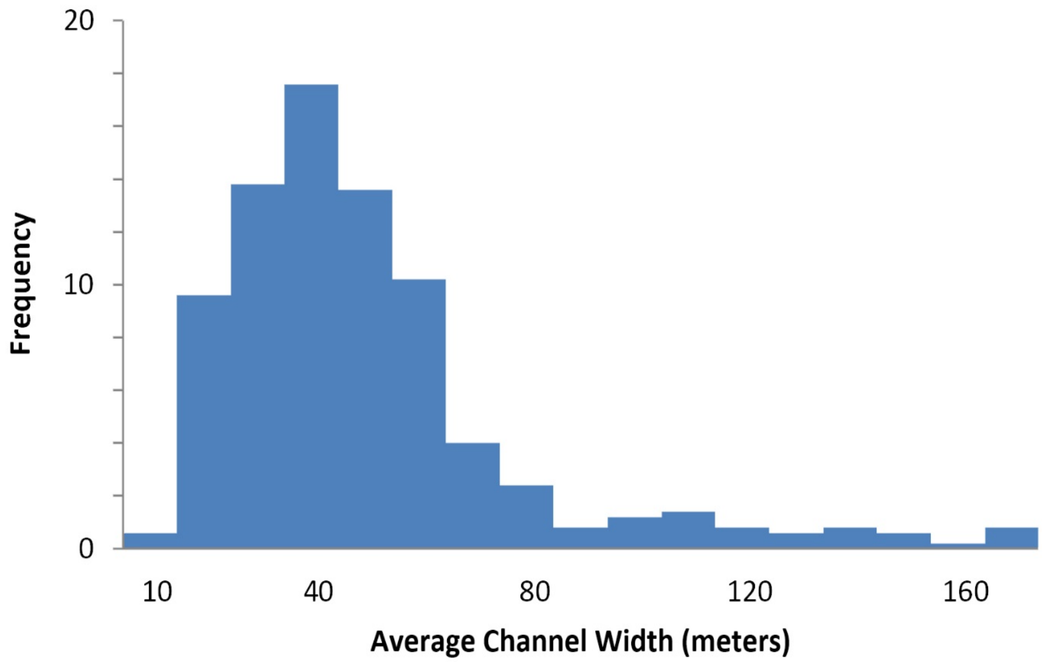

Figure 3.12. Histogram of measured channel widths. Average width of segments is 38 meters.

3.2.2.4. Fine-textured, layered fan deposits

The topographic inversion of the distributary fluvial deposits and the presence of broad depressions between individual distributaries imply that wind erosion has excavated extensive deposits of erodible sediment interbedded with the channel deposits. In most locations, exposures of these deposits are largely obscured by the TAR bedforms mantling inter-ridge depressions. However, at the distal end of the K2 fan, the extensive wind erosion has inverted the fluvial ridges into as much as 70 m of relative relief. Exposures of layered deposits are common on the sideslopes below the ridges (Figures 3.4, 3.10, 3.13). These sideslopes are generally smoother at multi-meter scales than the scalloped ridge crests and typically the slopes exposing the layers incline close to the angle of repose for loose sediment (~30°). Resolvable layers are typically 2-3 m thick, although image resolution may limit detection of finer-scale bedding. The beds are commonly massive in appearance and contain no blocks visible at HiRISE resolution (Figure 3.13). Beds are often separated by thin light layers that appear to be slightly more resistant to wind erosion and are less continuous, possibly nodular or upward-scalloped (Figures 3.13 and 3.14). Well-exposed individual layers can be traced for several hundred meters but with subtle pinching out occurring locally (Figure 3.13b). Thick layered sequences of very similar beds are exposed on the interior walls of several craters that are superimposed onto the K1 and K2 fans. A ~300 m thick section of the distal fan exposed in a crater wall near Saheki's central peak indicates the finest resolvable layers are ~2 m thick, and many individual layers can be traced several kilometers along the crater wall (Figure 3.15). This exposure reveals no resolvable meter-scale blocks except at the base of the section where probable central peak materials appear to be exposed.

The beds exposed on the slopes below the inverted ridges are largely conformable in their dip to the gradient of the ridges (e.g., Figure 3.13c). Individual beds cross-cut elevation contours along the trend of the ridge seen in Figure 3.13c, with an interpreted gradient of about 0.021 to the southeast following the general dip of the fan using individual prominent beds crossing multiple mapped contours. Similar measurements of bed dips at eight locations elsewhere on the portion of the fan covered by the HiRISE DEM yielded dips ranging from 0.025 to 0.041; the mean for the nine total measurements is 0.032, very close to the ~0.03 gradient of the entire K2 fan surface as measured from MOLA tracks.

Figure 3.13. (next page) Layered deposits exposed on slope below narrow ridge. (a) Exposed layers. Note thick, medium toned layers about 2-3 m thick separated by thin, light-toned layers with nodular or discontinuous presentation. (b) Interpretation of layering in (a), showing layer pinch-out locations indicated with an asterisk. (c) Contours from a 3 m/pixel DEM (pink) from HiRISE stereo pair PSP_7688_1575 and PSP_008545_1575 DEM superimposed on layer drawing. Ten meter contour interval. Note very shallow dip of layers broadly to the SE. Box at lower right indicates location of Figure 3.14. Image scale is reduced in (c) relative to (a) and (b). Part of HiRISE image PSP_007688_1575, centered at 22.007°S, 72.975°E.

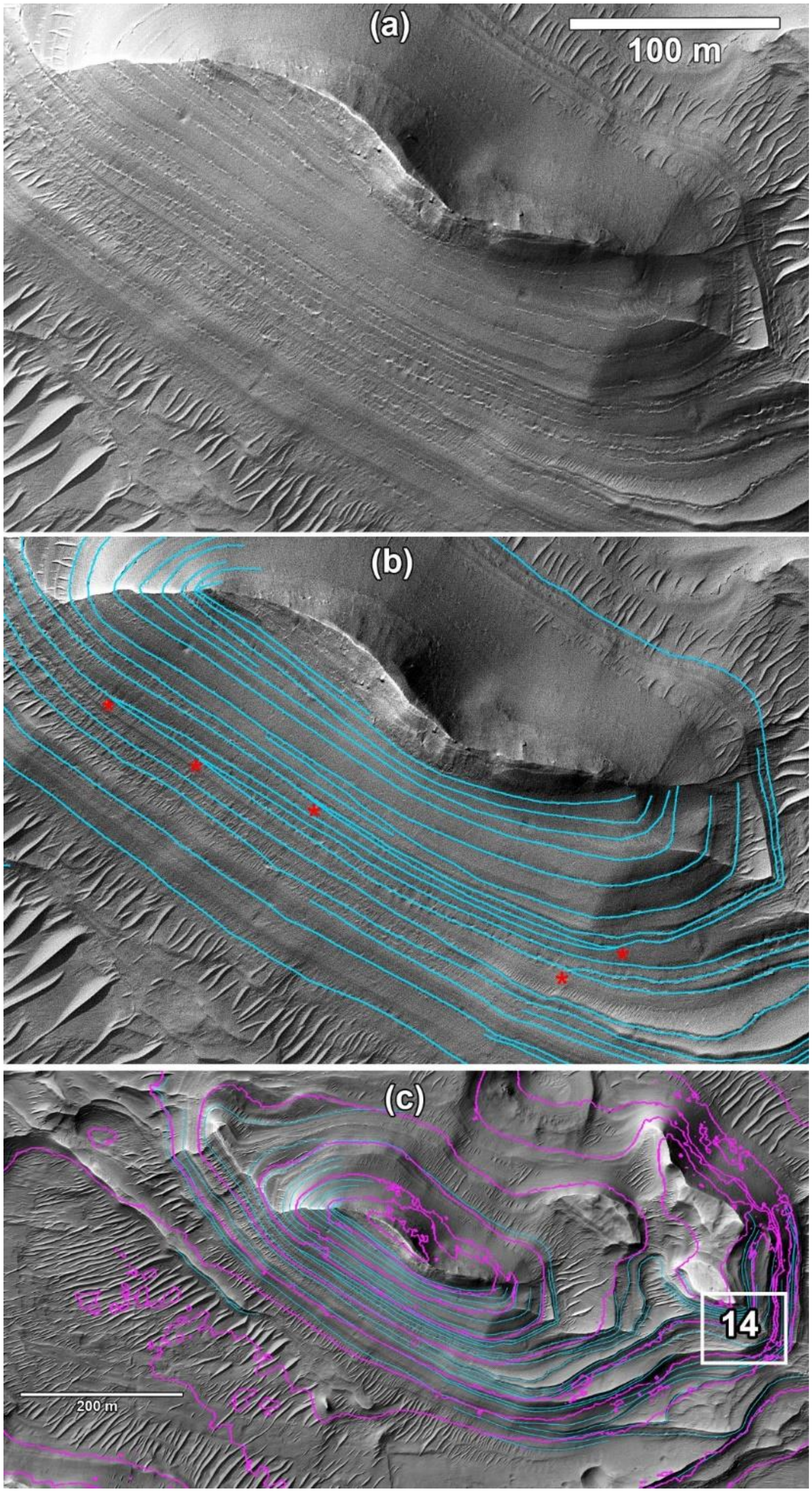
(a)
100 m
(b)
(c)
14
200 m

3.2.2.5. Interpretation of fine-textured deposits

The ease by which wind can erode the layered deposits and the near absence of exposed blocks (save for the thin interbeds) suggests that these deposits are sand size or smaller in dominant grain size. If the deposits were loose sand, however, wind erosion would probably readily sculpt the deposits into dunes. Also, if sand were the principal component of the layers, appreciable accumulation of sand dunes might be expected within the Saheki crater, but are not found. The observed TARs comprise a small volume of material compared to the total wind-eroded volume. This proportionality suggests an appreciable component of silt and possibly clay within the layered deposits that can be removed in suspension.

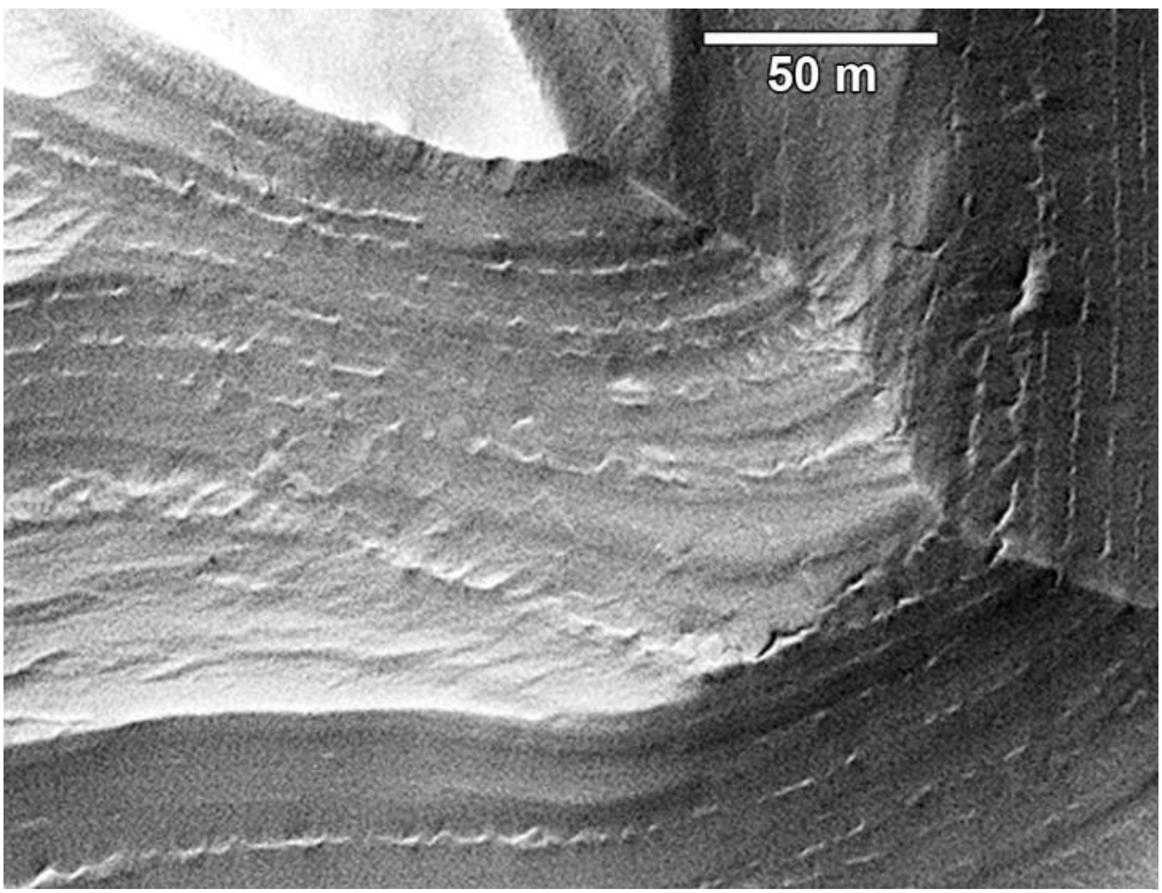

Figure 3.14. Detail of thin, light-toned layers interbedded with thicker, massive layers (see Figure 3.13 for context). Note the discontinuous appearance of the layers and indications of concave-upward layer cross-section. Part of HiRISE image PSP_007688_1575, centered at 22.008°S, 72.982°E.

The observation that the fine-textured layers dip concordantly with the superjacent ridges eliminates the possibility that they are exposures of layering pre-dating the fluvial fan ridges, e.g., lacustrine deposits. Rather, the finer-textured deposits must be a distinct facies generally coeval to the channel deposits. We interpret the layered sediment to be deposited by overbank flows sourced from flows within distributary channels that are sufficiently deep to spread across the adjacent fan surface, analogous to overbank deposits on floodplains. Such deposits are likely to be continuous over long distances downstream and to border the source distributaries, but thin laterally. The subtle pinch-outs of layers shown in Figure 3.13b may reflect the limited lateral extent of deposition from an individual distributary channel. The apparent thickness of 2-3 m for individual layers could indicate deep, long-duration flows through individual distributaries with large concentrations of suspended sediment. Because of limited image resolution, however, individual visible beds may be composed of many thin layers from multiple smaller flow events. Because exposed layers are stratigraphically lower than the superjacent channel deposit capping the ridges (e.g., Figures 3.4, 3.10, 3.13), we infer they are would have been sourced from a different channel at the same stratigraphic level as the exposed layer rather than being related to the superjacent ridge.

The thin, light-toned, and possibly nodular layers that separate the smoother, darker, and thicker (~2-3m) units in layered exposures (Figures 3.13 and 3.14) may result from processes occurring on the fan surface in the time intervals between overbank flooding events, or possibly are some form of graded bedding. However, their thinness compared to the more massive units, the sharpness of their expression and lack of gradual transitions to the overlying or underlying massive beds argues against graded bedding. If, as we postulate, the character of the beds represents post-depositional modification, this alteration likely occurred during times when depositional activity has shifted to other parts of the fan, or during periods of fan inactivity associated with quasi-cyclical climatic variations orbital variations (Laskar et al., 2004; Ward, 1979). Such processes could include wind erosion and surface concentration of granule layers, surface cementation, wetting and drying events, or cold-climate processes. The concave scalloping of some of the light-toned layers has an apparent spatial scale of 2-5 m (Figure 3.14), and might be the result of desiccation-crack development, which occurs at spatial scales ranging from centimeters to tens of meters (El Maarry et al., 2012; Harris, 2004; Neal et al., 1968; Weinberger, 1999), teepee structures from chemical precipitates (Dixon, 2009; Shaw and Thomas, 1989), or patterned ground from thermal cycling or ice-related processes (Chan et al., 2008; Korteniemi and Kreslavsky, 2012; Levy et al., 2009; Mangold et al., 2004; Mellon, 1997). There are no obvious vertical structures in the sediment beneath the scalloped layer edges, however, so that direct evidence for any of these mechanisms is lacking.

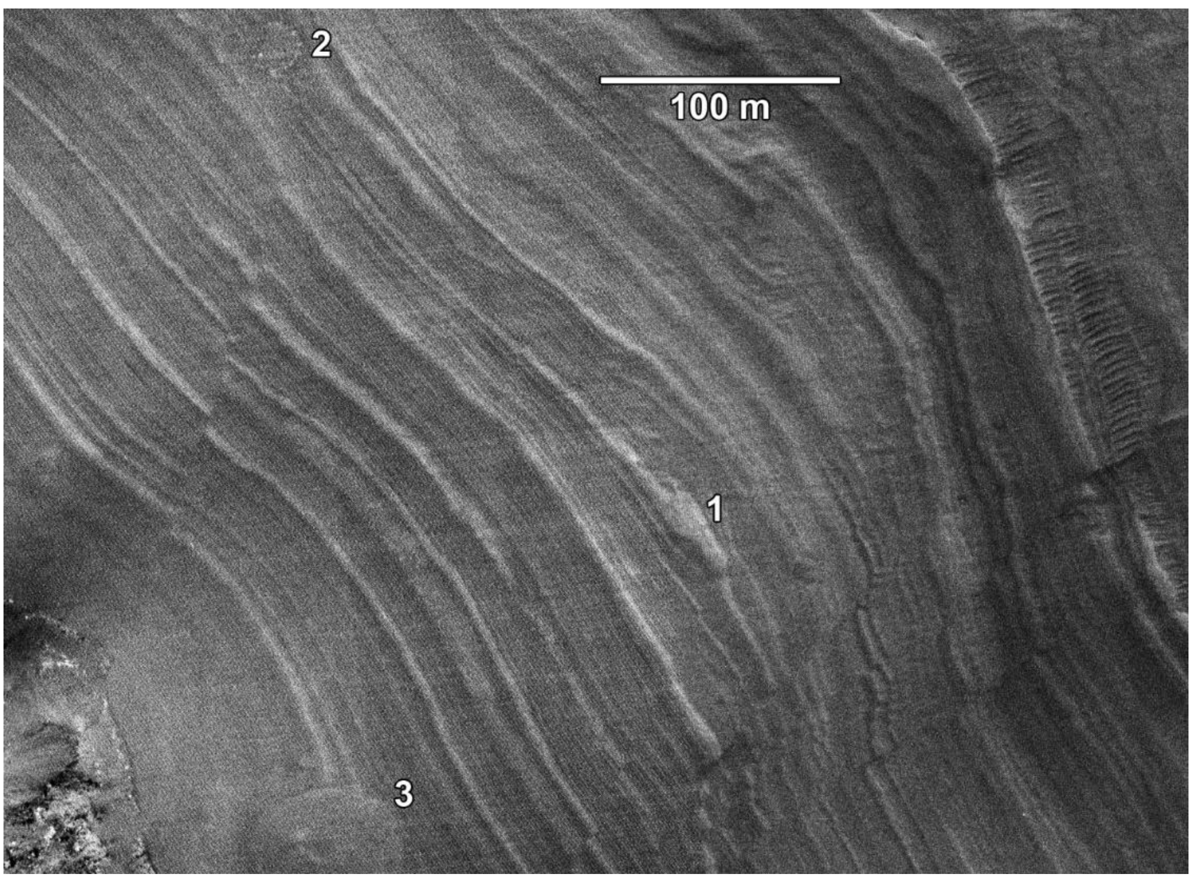

Figure 3.15 (previous page). Thick sequence of beds in eastern wall of a 5.3 km diameter crater superimposed onto fan deposits adjacent to Saheki central peak. Finest visible beds are ~2 m thick. Thicker blobs, as near “1” may be channel deposits. Circular features 2 and 3, obscuring bedding, may be scars of small impacts into interior crater wall. Note faulting in near left and right side of image, presumably due to impact deformation. Bottom of layer sequence at lower left of image where coarse crater floor or central peak materials are exposed. Image DN highly stretched to emphasize layering. Part of HiRISE image ESP_013226_1580, centered at 21.762°S, 73.046°E.

The clearest exposures of layered deposits occur on 25-35° side slopes of flanking ridges capped by fluvial deposits. No interbedded boulders are visible at HiRISE scale. The exposure of layering indicates the slopes are not deeply mantled with debris. Gradients close to the angle of repose of loose sediment (~32-35°) and the smoothness of the side slopes, however, suggest that the exposures may be shallowly, and possibly discontinuously, mantled by debris mass-wasted from the ridge-capping fluvial deposits plus sediment derived from the beds themselves. Such threshold slopes are common on terrestrial badlands (e.g., Howard, 2009). Despite the shallow mantling, indurated beds are often exposed in outcrop, helping to define the stratigraphic relationships. The thin, light-toned layers visible in Figures 3.10, 3.13, and 3.14 are probably such examples. In some situations the apparent mantling obscures expression of the layering (e.g., the northerly slope of the hill near (a) in Figure 3.13), but it is likely that at least discontinuous mantling occurs on the southwest-facing slope in Figures 3.10 and 3.13 to account for the uniformity of the slope. The sediment may be friable and thus easily eroded, although some weathering of the layered deposits, forming a thin regolith similar to that observed in terrestrial badlands, might be necessary prior to their erosion by wind.

3.2.2.6. Benches

A vertically-stacked series of nearly horizontal benches border the southern margin of the K2 fan against the Saheki crater interior wall (Figures 3.3 and 3.16). HiRISE stereo imaging of part of this bench complex (Figure 3.9) demonstrates that the individual bench surfaces are essentially flat-lying with a slope of less than 0.5%. At meter to decameter scales, the surfaces of the benches are quite rough, with numerous quasi-circular depressions (Figure 3.17). The surface is littered with numerous angular, meter-scale blocks and the outer edges of the benches form abrupt scarps with irregular outlines. Angular blocks that apparently mass-wasted from the bench surface often discontinuously mantle the steep sideslopes of the benches. Where not mantled by debris, the subjacent slopes are smooth and express subtle layering that appears to be conformable with the overlying terraces (Figure 3.17). This layering is very similar to the fine-textured layers exposed on the sides of inverted fan distributary ridges upslope (Figure 3.13). The highest bench within the HiRISE DEM is about 85 m above the similarly-textured basin floor surface, although a slightly higher bench lies just to the south of the DEM. Along the southern margin of the K2 fan some linear ridges interpreted as distributary channels appear to overlie or to merge accordantly with the rough-textured benches, and in such locations the ridges take on the rough texture of the benches. Fine-textured layered deposits also locally superpose the benches. Similar surfaces appear elsewhere, including the lowest point of the eastern half of the nearby “L” crater where a rough, flat-lying surface occurs at the terminus of four large fans (Figure 3.18). Part of the Saheki crater floor immediately adjacent to the fan deposits also has a similar flat surface at 100+ meter scale that is rough at decameter scale, although it has not been eroded laterally to form a bench (Figure 3.3). Similarly rough-textured surfaces also occur in small depressions along channels dissecting the southwestward flank of Saheki crater.

3.2.2.7. Interpretation of benches

We interpret the benches to be underlain by playa and/or possibly shallow lacustrine sediments sourced by runoff from the adjacent fans. Their level surface implies they are probably composed of fine sediment deposited from suspension. Alluvial fans in enclosed basins typically terminate in nearly level playas that receive fine suspended sediment that is carried beyond the end of the fan (Shaw and Thomas, 1989). Although the higher benches in Saheki crater are spatially limited to bordering the southern crater rim (Figure 3.3), and are thus largely isolated from the fan system, the similar-appearing bench in “L” crater clearly occupies a basin-central position where playa or lacustrine sedimentation would be expected (Figure 3.18).

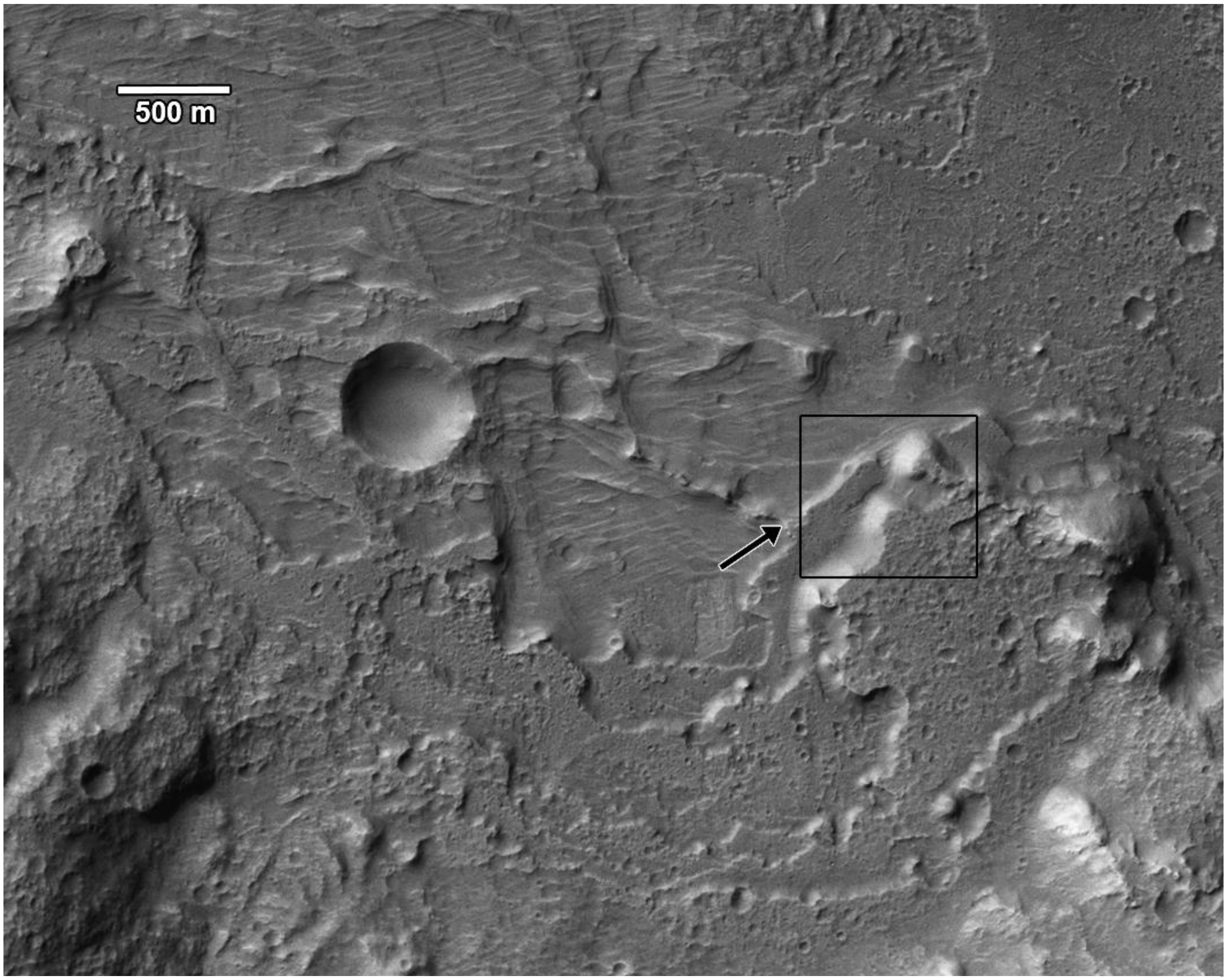

Figure 3.16. Flat-topped benches at boundary between southern K2 fan deposits and Saheki crater wall. Note multiple levels and irregular terrace edges. Arrow points to location where inverted fan ridge may be at the same elevation at the adjacent terrace. Box shows location of Figure 3.17. Part of CTX image P19_008545_1576_XI_22S287W centered at 22.216°S and 72.946°E.

The bench surfaces appear to be thin, nearly horizontal resistant layers that have been laterally eroded, shedding boulders onto subjacent slopes. The numerous rounded depressions (Figures 3.17 and 3.18) suggest that the roughness of the surface is due to impact gardening forming a blocky regolith. The resistant layers are underlain by apparently conformable layers that are more easily eroded by wind. We interpret the benches and other rough-textured level surfaces in the region to be chemically-cemented layers that have been subsequently broken up. They occur at topographic lows, or, where the benches occur at higher levels, what might have been low points prior to aeolian stripping.

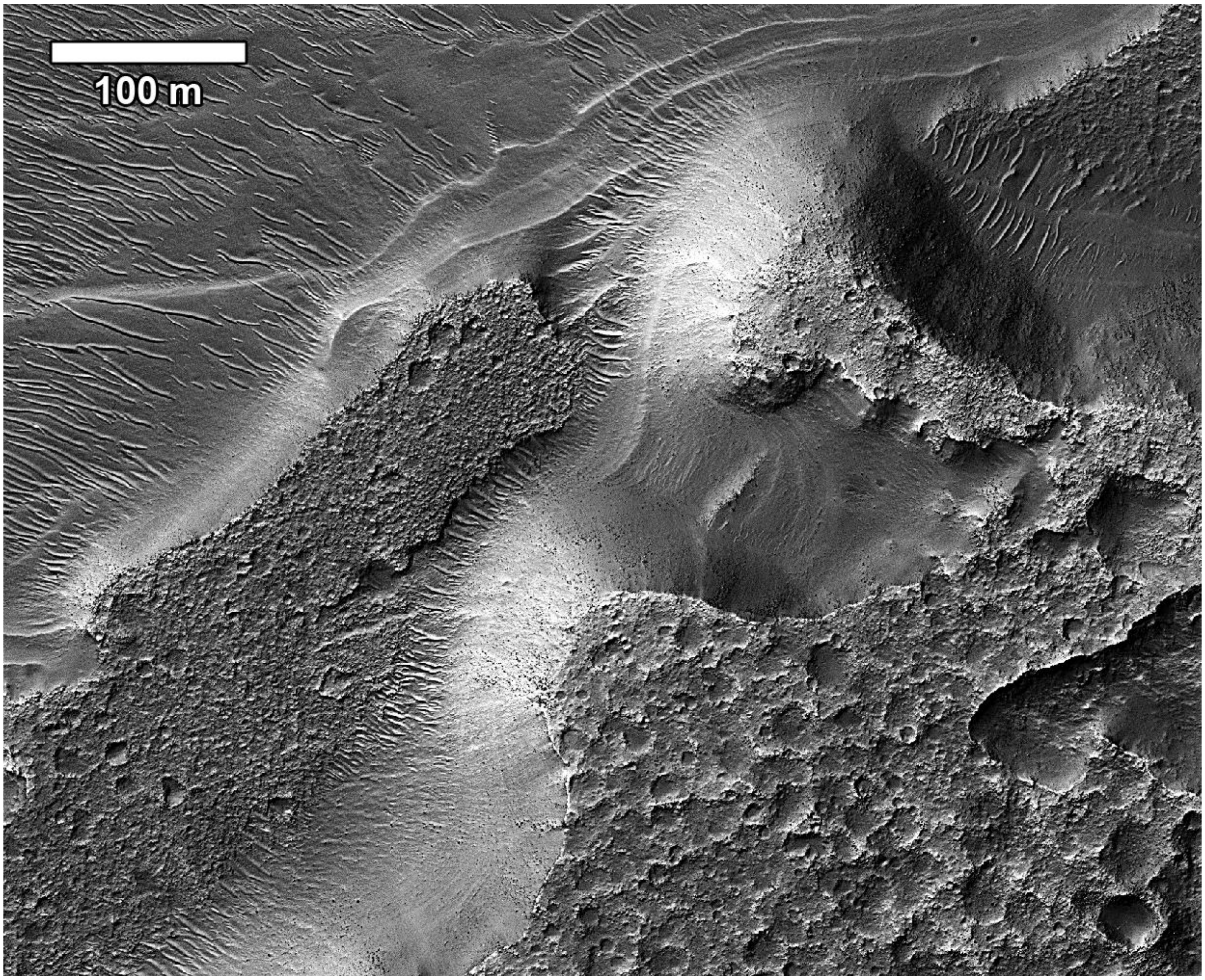

Figure 3.17. Benches at two levels (see Figure 3.16 for context). Note pitted surface, interpreted to be the result of impact gardening. The bench surface is mantled with coarse blocks, which are mass-wasted onto slopes at terrace edges. Fine, layered sediment that is largely conformable with overlying benches is exposed on slopes below benches. Benches are interpreted to be chemically-cemented lacustrine or playa deposits. Part of HiRISE image PSP_007688_1575.

Being the endpoint for both suspended and dissolved loads, playa sediments are commonly rich in salts concentrated from evaporation of ephemeral shallow lakes or delivered by groundwater (Dixon, 2009; Langer and Kerr, 1966; Shaw and Thomas, 1989; Yechieli and Wood, 2002). Solute-cemented playa deposits are common in the southwestern United States and in the salars of the Atacama Desert. In the Atacama and similar desert settings elsewhere, the segregation of mineral precipitates within the sediments often results in volumetric expansion and small-scale deformation of the surface sediments, resulting in chaotic surface topography at meter to decameter scales (e.g., the "Devil's Golf Course" in Death Valley National Park (Hunt et al., 1966; Smoot and Castens-Seidel, 1995) and similar forms in Atacama salars (Stoertz and Ericksen, 1974). The roughness of the Saheki bench surfaces may thus be a combination of chemical cementation, small-scale deformation associated with playa sedimentation, and disturbance by impact gardening.

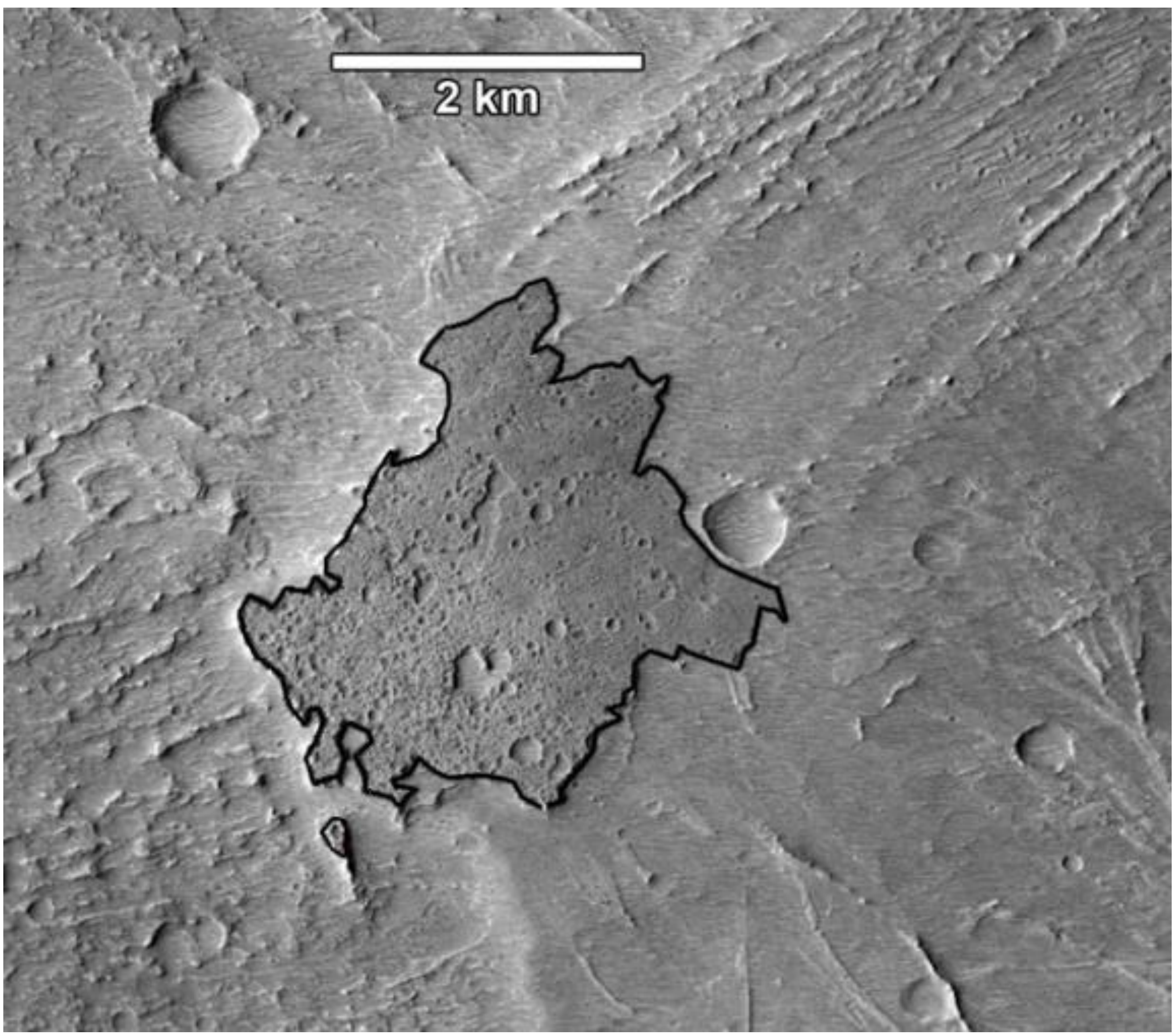

Figure 3.18 (previous page). Rough-textured, nearly level surface in the interior of “L” crater (red outlining), located at the point of convergence of several fans. Surface of deposit as well as ridges on surrounding fans are slightly inverted due to aeolian erosion. Deposit is interpreted as cemented playa or shallow lacustrine sediments sourced from runoff from the adjacent fans. Note the similarity in morphology to benches in Figures 3.16 and 3.17 in Saheki crater. Part of map-projected CTX image P3_002295_1568, centered at 23.060°S, 74.030°E.

In terrestrial enclosed basins, the fan and playa deposits interfinger during basin infilling (e.g., Shaw and Thomas, 1989). The stratigraphy of terminal deposits in enclosed basin centers often alternates between playa and lacustrine sediments, with varying degrees of interbedded and co-deposited chemical precipitates (Pueyo et al., 2001; Smith, 1957, 1974). This complex stratigraphy reflects climatic changes and the simplest explanation to account for the multiple planar benches in Saheki crater would be that the successively higher playa surfaces formed sequentially as the center of the basin became infilled. Episodes of playa cementation alternated with periods of sediment input without appreciable chemical co-deposition (creating the less indurated layers revealed below the erosional edges of the terraces, Figure 3.17). Subsequent aeolian deflation would have had to remove at least 100 m of basin fill sediments in the vicinity of the benches based upon their relief relative to the present basin floor (Figure 3.9). By this interpretation the highest benches have experienced greater erosion and backwasting than lower benches as a result of undermining by erosion of the non-indurated finer interbeds, and the lower, younger indurated playa deposits would have extended beneath the remnant higher benches. Note that this implies an age sequence with the highest bench being youngest, inverse to the usual sequence of fluvial terraces increasing vertically in age. The “L” crater basin floor (Figure18) would presumably resemble the basin floor at the south end of Saheki crater prior to the period of intense aeolian deflation. More complicated scenarios are also possible involving declining or varying basin floor levels in which fan and playa deposition alternate with episodes of aeolian erosion or in which the bench-forming deposits did not extend across the basin floor.

3.2.3 Source basins

The large alluvial fans in the southern highlands on Mars are generally sourced from steep dendritic valley networks incised into the interior crater walls of large, deep, relatively fresh martian craters (Mangold et al., 2012b; Moore and Howard, 2005). This is clearly the case for fans in Saheki and "L" craters (Figure 3.2). Within individual craters, the largest drainage networks and largest associated fans are generally sourced from the highest portions of the hosting crater rim. The only exception to this pattern is that the K1 source basin occurs along a low rim section contiguous with a degraded elliptical basin beyond the NW rim of Saheki. Source basin and corresponding fan and gradients areas for the K1 and K2 fans are summarized in Table 3.1, with comparative average statistics for all of the fans surveyed by Moore and Howard (2005).

We find no evidence for valleys incised into the Saheki fans from runoff sourced on the fan itself. The deep aeolian erosion on the K2 fan could have erased evidence for such local runoff, but the relatively pristine K1 fan surface shows all distributaries radiating from the fan apex. Likewise, other large martian fans appear to have received little runoff directly on the fan surface because the surfaces exhibit no channelized erosion initiating from mid-fan sources– the basin headwaters (fan-hosting crater walls) were overwhelmingly the source of runoff (Grant and Wilson, 2012; Moore and Howard, 2005).

3.2.4 Age relationships

Crater density counts are a standard method of determining the relative ages of planetary surfaces. Absolute model ages can then be estimated by comparing these counts to the lunar surface, which has been radiometrically dated. The fan-bearing craters in the region lie on terrain that has been mapped as Noachian (Greeley and Guest, 1987; Irwin et al., 2013). Using a CTX basemap within ArcGIS, our crater count analysis incorporated craters with a diameter of larger than 200 meters to avoid complications arising from the preferential erosion of smaller craters and the increasing influence of secondaries with decreasing diameter (McEwen et al., 2005; McEwen and Bierhaus, 2006). Central peaks, obvious secondary craters, and the interior rims of the host crater were excluded from the analysis. Crater statistics were compiled using CraterStats software (Michael and Neukum, 2010), using the production function of Ivanov (2001) and the chronology function of Hartmann and Neukum (2001). When using craters to derive ages, the surface area over the feature of interest must be large enough to obtain a sufficient sample of craters, and there are inherent accuracy issues with deriving ages when using craters smaller than D<1km (McEwen et al., 2005), although recent studies largely confirm the use of smaller craters (Hartmann, 2007; Hartmann et al., 2008; Hartmann and Werner, 2010; Michael and Neukum, 2010; Werner et al., 2009).

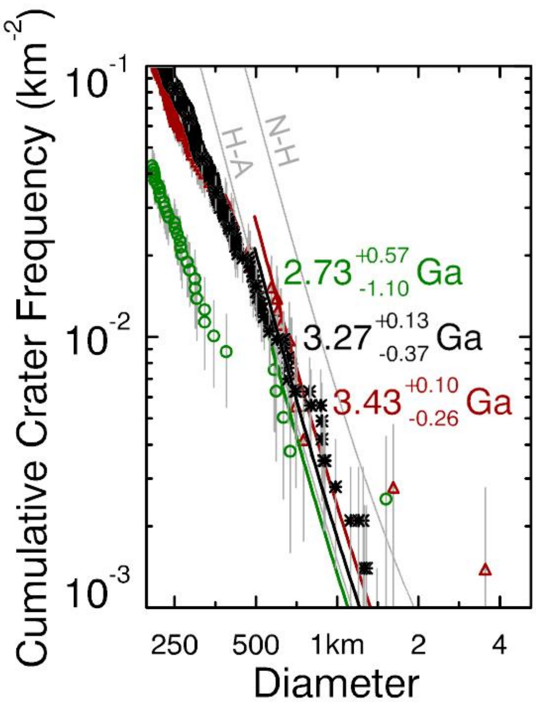

Figure 3.19. Crater age determination plots. N-H and H-A indicate Noachian-Hesperian and Hesperian-Amazonian boundaries. Absolute age determination used craters greater than 500 meters in diameter to avoid errors arising from aeolian erosion (see text for discussion). **Red:** K1 fan. **Black:** Aggregate of four fans in “L” Crater. **Green:** K2 fan. The young age and large error bars for the K2 fan can likely be attributed to high amount of aeolian modification.

These limitations considered, the fan surfaces in Saheki and “L” crater date to the Mid to Late Hesperian, and in the case of fan K2, as late as the Early Amazonian (as defined by Tanaka (1986) and Werner and Tanaka (2011)) (Figure 3.19). In fitting ages to the cumulative frequency curves in Figure 3.19, we utilized craters greater than 500 m in diameter to minimize effects of crater degradation and we did not include the three large (>1.4 km diameter) craters with large error bars. These ages are indistinguishable from those obtained for fans in Margaritifer Terra (Grant and Wilson, 2011). The K2 fan surface has a crater retention age (Early Amazonian) that is notably younger than that of K1, which is probably due to the different degrees of aeolian erosion. Ridges on the K2 fan rise as much as 70 m above the surrounding fan surface. If we assume a crater depth/diameter ratio of 1:5 (Garvin et al., 2003), we conservatively infer that craters smaller than 350 m in diameter would be completely erased from the surface record. If the estimate of ~100 m of stripping from Figure 3.9 is accurate, this erosion could eradicate craters up to diameters of ~0.5 km; deposition of dust would cause further infilling and obliteration of potentially even larger craters. In a number of places, stratigraphically higher surfaces that have not been eroded preserve significantly higher densities of craters than the underlying eroded fan surfaces (e.g., Figure 3.18), confirming qualitatively that this effect is important, and that the apparent age difference is due to subsequent amount of erosion of the fan. We have detected no craters embedded in layer exposures, so that wind-exhumed craters probably contribute little to inferred ages.

3.3. Discussion

The Saheki K2 fan has a strongly bimodal character, comprising a radiating network of long distributaries and broader platforms capped by coarse (sand and cobble) fluvial bedload (possibly indurated) interspersed with finer, wind-erodible layered sediment. The strong component of fine sediment deposition in the Saheki fan complex contrasts with the types of terrestrial alluvial fans most discussed in the literature, which emphasizes steep fans in high-relief terrain. On these fans, sedimentation most frequently occurs either as coarse-grained bedload deposited by wide, often braided or sheetflood distributaries or as equally coarse debris flows (e.g., Blair and McPherson, 2009; Harvey, 1999; Stock, 2013). In such settings, the associated fine sediment is primarily deposited either in a debris flow matrix or in basin-center playas. In neither case would wind erosion be capable of creating the characteristic inverted distributary system seen in Saheki and several other craters.

The intense aeolian deflation that has affected the K2 fan at the southern end of Saheki crater must have resulted in removal of a vast volume of sediment. We conservatively estimate this volume to be about 10 km^3, assuming 25 m of deflation over the distal 400 km^2 of the K2 fans surface. A small fraction of this sediment remains trapped in the numerous TARs covering the fan surface. Because there are no major dune fields within Saheki crater, we infer that the majority of the eroded sediment must be composed of grains fine enough (sand size or smaller) to have been swept by winds out of the crater. This inference underscores our interpretation that the majority of the layered sediment in the Saheki fans is composed of fine sediment deposited from overbank sedimentation and in playa deposits. Some of this sediment appears to have been redeposited in the source basins on the crater walls, which appear to be partially infilled with fine-grained sediment.

The deflated material from the ridges and to some degree from the finer layered interbeds is interpreted to be the sediment source for the widespread TAR megaripples present between ridges (Figures 3.4, 3.6-3.8). By analogy with megaripples observed by both of the MER rovers (Jerolmack et al., 2006; Sullivan et al., 2008), we interpret them to contain a significant granule sized component. We have also observed similar local sourcing of granules to form aeolian ripples occurring in our analogue field site in the Atacama Desert (see Section 3.3.1.1).

3.3.1. Possible terrestrial analog fans

In only a few cases have terrestrial fans with sedimentary characteristics similar to those inferred for the Saheki K2 fan been discussed. Bull (1962, 1963) describes fan sedimentation in the western Central Valley of California sourced from headwaters underlain by sandstone, shale and siltstone bedrock. Both fluvial and mudflow deposits occur on these fans. Mudflow deposits are unsorted, typically containing 54% mud (clay and silt), 40% sand, and 6% gravel. Clay percentages range from 12-76%, averaging 31%. Mudflow deposits generally decrease in thickness downstream from 0.5 m to 0.1 m, with abrupt terminal edges that range from 0.3 cm to 2.5 cm in thickness. Mudflows are transported through a channelized fluvial system. In upstream portions of the fan, the mudflow deposits occur as lobate overbank deposits thicker on outside channel bends, but they terminate downstream as sheet-like deposits. Mudflows develop polygonal shrinkage cracks upon drying. Some flows across the fan have a more fluvial character, creating well-sorted, thin deposits dominated by sand with typically less than 10% mud and less than 10% gravel. Fluvial flows are typically up to 0.15 m deep and occur as braided channels or sheetflows.

Blair (2003) discusses the sedimentology of the Cucomungo Canyon fan in California as characterized by both fluvial and mudflow deposits. The dimensions of this fan approach that of the Saheki crater fans, being 15 km in length, with an areal extent of 119 km^2, a concave profile, and an average fan gradient of 0.03. The fan is sourced from strongly weathered granitic bedrock. Mudflow deposits are typically 10% mud, 70% sand, and 20% gravel (Table 3.3). Mudflow deposits on this fan are thicker than those described by Bull, ranging from 10-100 cm thick with 10-40 cm high abrupt, rounded lateral edges and terminations. Mudflows source from feeder channels and are typically 50-300 m wide but extend the length of the fan. The mudflows surfaces are smooth and develop narrow polygonal shrinkage cracks. Feeder channels are typically 5-30 m wide (width decreasing down-fan) and 2-6 m deep (also decreasing depth down-fan), with smaller secondary channels. Such channels cover less than 10% of the fan surface, and deposit well-sorted deposits ranging from pebbly sand to cobbly pebble gravel. Fluvial and mudflow facies are interbedded in the fan deposits, with the proportion of fluvial gravels decreasing down-fan. A field reconnaissance conducted by the authors in 2012 on the Cucomungo Canyon fan suggests, however, that fluvial deposits are volumetrically more important than mudflow deposits on this fan, particularly on the downstream portions of the fan.

Description	**Property**	**Clay**	**Silt**	**Fine-Medium Sand**	**Coarse Sand**	**Pebbles**
Upstream Mudflows	Average[a]	16.68	30.75	18.85	12.91	20.81
	Minimum	9.99	21.36	11.27	0.00	0.00
	Maximum	27.53	60.95	35.52	29.30	40.01
Channel Bank Deposits	Average[b]	15.30	30.92	33.15	11.35	9.28
	Minimum	1.09	6.25	12.97	0.02	0.00
	Maximum	25.95	55.52	80.61	37.36	53.73
Overbank Sediment	Average[c]	16.74	42.53	37.64	3.09	0.00
	Minimum	12.35	34.12	12.36	0.00	0.00
	Maximum	24.28	63.37	49.27	6.75	0.00
Cucomungo Fan Deposits[d]	Average	1.06	8.50	42.11	29.52	18.80
	Minimum	0.60	5.40	24.80	1.30	0.00
	Maximum	2.20	21.80	74.70	44.50	35.50

[a]Sample size=11; [b]Sample size=22; [c]Sample size=5
[d]Summarized from Table 4 of Blair (2003)

Table 3.3. Grain size characteristics of Atacama fan sediment expressed as percentages with comparative values from the Cucomungo fan of California.

A third potential analog for the Saheki fans is a suite of fans in the Atacama Desert of Chile. These fans contain similar bimodal fluvial and mudflow deposits but also display the relief inversion due to aeolian deflation that is characteristic of the Saheki K2 fan. Because of this close morphologic analogy, the Atacama fans are described in detail below, and used to better understand the formative processes of the Saheki fans.

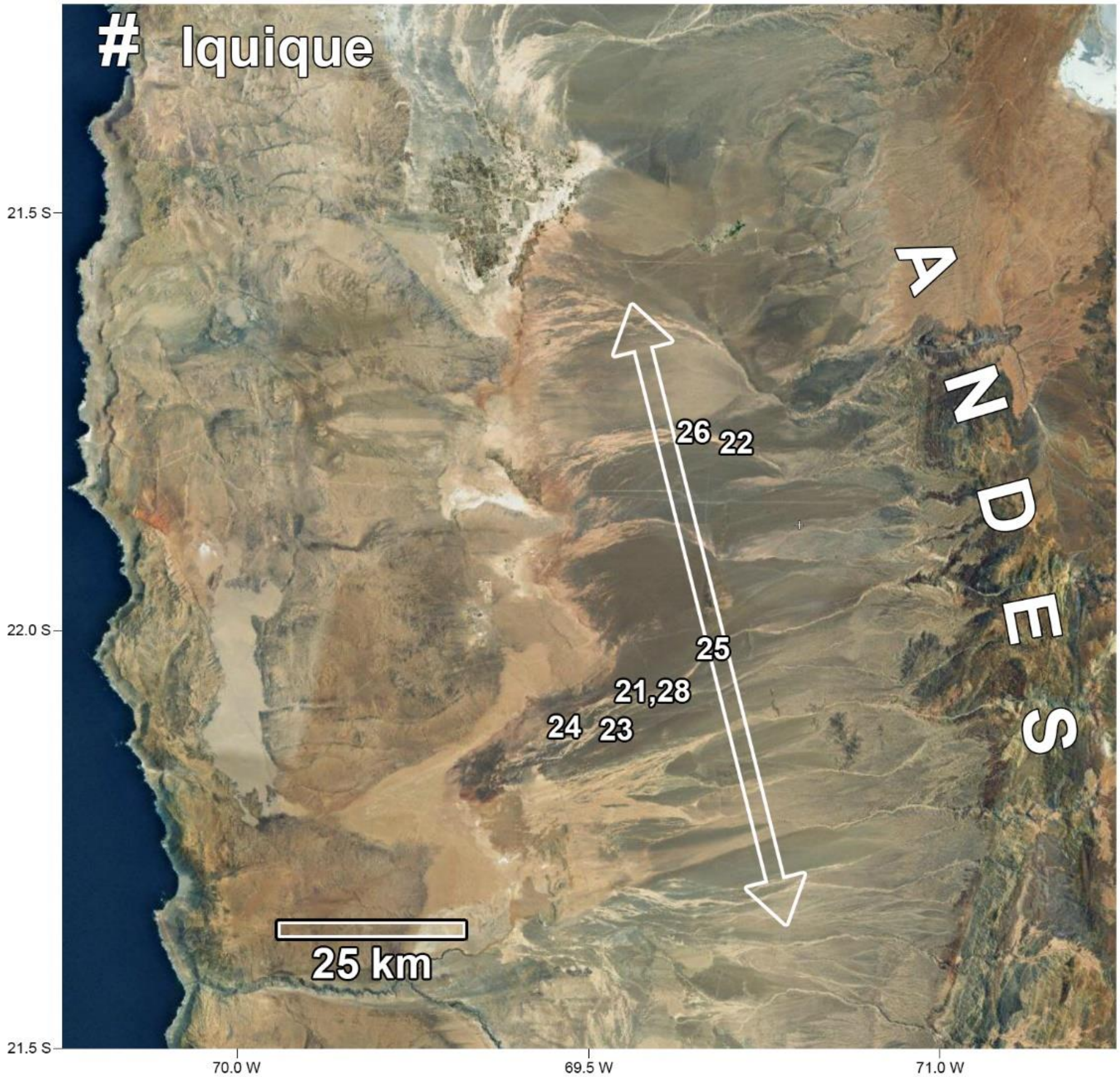

Figure 3.20. Overview of geographic setting of fine grained fans in the Pampa del Tamarugo region of northern Chile, centered at 20.87°S, 69.55°W. Arrow shows lateral extent of fan complexes. Numbers show approximate location of other figures in this chapter. Light-toned regions on fans have received recent deposition, whereas dark-toned areas are inactive and have accumulated a granule surface layer die to aeolian deflation. City of Iquique indicated. Base map from Yahoo! Maps.

3.3.1.1. A Chilean terrestrial analog

The alluvial fans of the Pampa del Tamarugal region of the Chilean Atacama Desert (Figure 3.20) appear to constitute a close analog in morphology and formative processes to the Saheki crater fans in the following ways:

1. The fan gradients, areas, and concavity of two representative Atacama fans fall within the range of martian fans, although the Atacama fans are somewhat smaller, steeper, and more concave that the K1 and K2 fans (Table 3.1).
2. The Atacama fans in the area of study have channels ranging from sand to boulder beds, with mud-rich overbank deposits (Figures 3.21, 3.22, and Table 3.3), mirroring what we have inferred for the Saheki fans.\
3. Inactive parts of the Atacama fans are wind eroded (Figure 3.23), resulting in 1-2m of inverted channel relief (Figure 3.24), consistent with the erodibility of the fine-grained overbank deposits. The Saheki fans are likewise inverted, although surface relief is greater (as much as 70m).
4. Overbank deposits on the Atacama fans exhibit no evidence for fluvial reworking by local runoff subsequent to deposition.
5. The Atacama fans terminate in mixed playa/lake "salars" (salt-rich enclosed basins) (Amundsen et al., 2012); the K2 Saheki crater distributaries terminate at possibly analogous flat-lying deposits (Sections 2.2.6 and 2.2.7).

Because of these similarities, analysis of sedimentary processes and landforms on the Atacama fans has the potential to yield insights into the mechanics and environment forming large martian fans. The fans are located along a ~140 km transect of the western slopes of the Andes centered at about 21°S, 69°W (Figure 3.20), radiating westward from the Andean mountains onto a hyperarid upland plateau. The fans experience only a few millimeters of direct precipitation annually and almost no locally-generated runoff (Amundson et al., 2012). Despite the hyperaridity of the immediate fan environment, flood events sourced from the superjacent Andes occur with appreciable frequency as evidenced by disruption of vehicle tracks, footprints on recent deposits, and sediment deposition on roads and railroad tracks (Houston, 2006) (see also Figure 3.26).

Our study of the Atacama fans is based on a combination of reconnaissance field investigations plus remote sensing interpretation. During a field season in 2012, we surveyed fan cross-sections and longitudinal profiles using differential Global Positioning Satellite observation, excavated pits and streambank exposures, collected sediment samples, and made Ground Penetrating Radar transects across portions of the fans. Sediment grain size distributions (Table 3.3) are based on laser diffraction analysis of dispersed samples.

Figure 3.21. Fan distributary, showing fine-grained cohesive banks and extensive overbank deposits. Bank crest to bank crest about 3 m. Photo by A. Howard. Location at about 21.097°S, 69.486°W.

The fine sediment comprising these Atacama fans is originally derived from erosion of fine-grained deposits including mudstones, sandstones and volcanic ash, exposed on the flanks of the Andes to the east of the fans (Servicio Nacional de Geologia y Mineria, 2003). A representative canyon (Quebrada de Guatacondo) heading in the Andean foothills (location 25 and upstream in Figure 3.20) that feeds a fan gives evidence of a spectrum of flows with markedly different properties (Figure 3.25). The channel bed exposes clean sub-meter gravels and cobbles indicating that normal fluvial floods are common. The channel walls, however, are plastered with remnants of at least three recent mudflows that occurred in early 2012. The mudflows are typically nearly 50% mud (clay and silt), 30% sand, and 20% pebbles (Table 3.3). The same event in 2012 deposited an extensive deposit on another fan (Figure 3.21) that is likewise characterized by both channelized and overbank flows. As in the canyon flows shown in Figure 25, later (waning stage?) deposits were lighter colored and more confined to distinct channels.

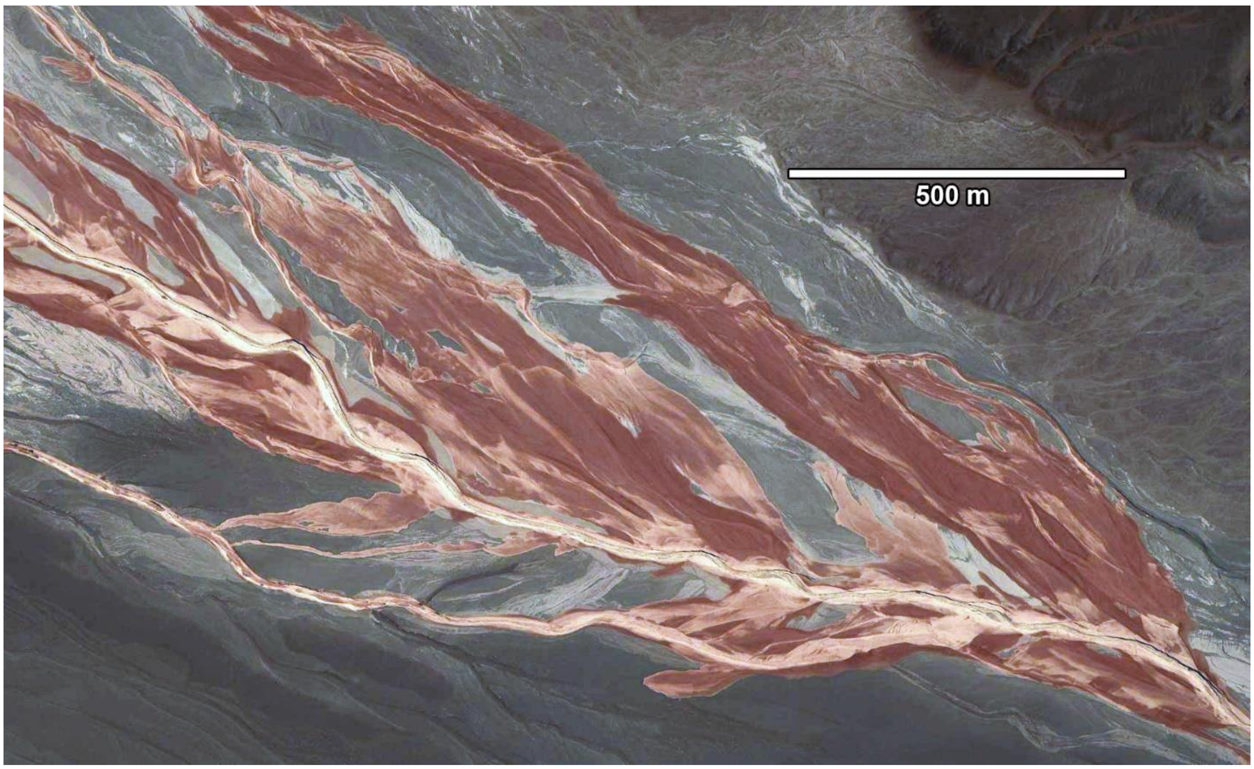

Figure 3.22. Atacama fan flood deposits. Red-toned deposits deposited by an early 2012 flood sourced from the Andes foothills to the east. Deposits radiate from the end an entrenched channel section at left boundary. Broad sheet deposits source from overflow of main distributary channels. Earliest deposits are darkest red, with later overflows and channelized flow being lighter pink. Main distributary averages about 12 m wide. Flooding and sediment deposition continued for 25 km downstream, spanning the length of the alluvial fan. Center of image at 20.765°S, 69.311°W. North is up. Iconos 0.8 m/pixel image, taken 12/27/2012.

Where flows spread onto the aggrading fan, a distinctive and repeated pattern of deposition occurs. The differences in color resulting from variations in sediment color and darkening by aeolian erosion suggest that during an individual flow event only a few distributary channels are active, with widths typically in the range of 3-10 m and depths of up to a meter. The channel bed deposits consist of a mixture of grain sizes, dominated by pebble and finer sediment but containing occasional cobble and boulder bars with median grain size of about 100 mm. Undercut banks of distributaries expose layered sediment averaging about 45% mud, 45% sand, and 10% pebbles (Table 3.3). However, beds of well-sorted sand or pebbles are interbedded with the muddier layers. Individual layers range from a few centimeters to 20 cm in thickness. A similar facies association of channel gravels and overbank mudflows has been described for other fans in the Pampa del Tamarugal region (Kiefer et al., 1997; Houston, 2002).

Large flow events through distributaries spread overbank, depositing sheet-like mud deposits extending a few meters to 150 m bilaterally around the distributary (Figures 3.21, 3.22, 3.26). Locally, however, these mudflows may extend several hundred meters to a kilometer or more across the surrounding fan surface as broad depositional lobes (Figures 3.22, 3.26). The overbank deposits typically contain 60% mud and 40% sand, although a few beds contain granules and fine pebbles (Figure 3.27). These deposits harden to adobe-like consistency typically with well-developed mudcracks. Individual deposits are nearly homogeneous and range up to 25 cm in thickness. The beds generally thin away from the distributary, generally with abrupt, rounded edges a few cm high. Repeated flows gradually develop broad natural levees extending >150 m to either side of the distributary (Figure 3.28). Deposits from individual overbank events are generally easily distinguished by sharp flow margins and, often, color differences between deposits from different events (Figure 3.26). We have described the formative flows as mudflows because they have abrupt, rounded lateral and downstream boundaries. Also, vertical surfaces inundated by the mudflows retain coatings several millimeters thick. Both observations indicate the flows displayed finite yield strength. However, the flows have low viscosity relative to many terrestrial mudflows as indicated by their thin terminal edges.

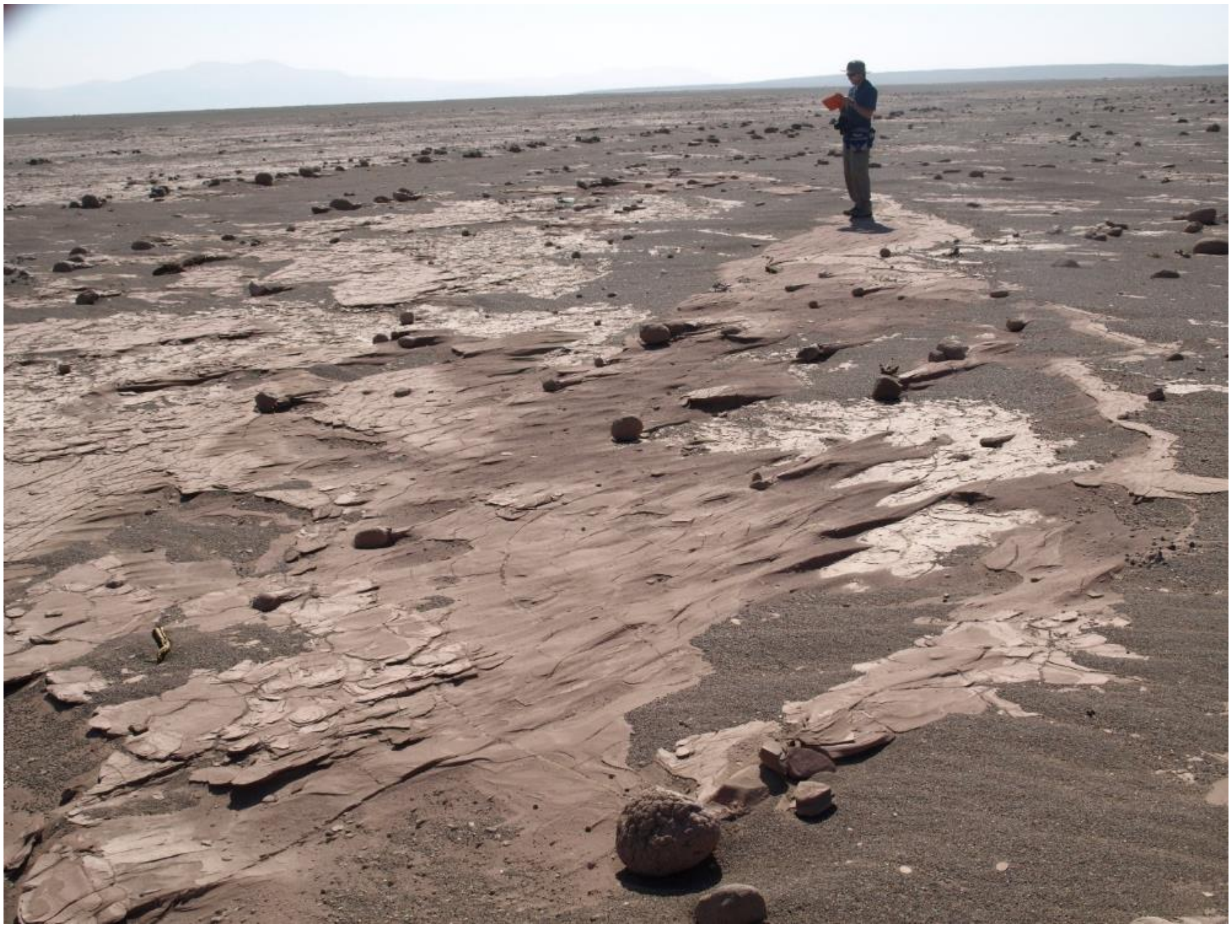

Figure 3.23. Wind-scoured surface of an Atacama fan. Reddish and light-toned surfaces expose fine-grained overbank sediments, scoured by winds directed to the right. Rounded balls of mud locally protect the surface from erosion, producing elongated tails. Darker granule-covered aeolian ripples mantle parts of the surface as well as infilling the channel in the middle distance. Boulders aligned along the margins of the channel were deposited by overbank flows in proximal parts of levees. Photo by A. Howard. Location 21.121°S, 69.527°W.

Locally the distributaries exhibit modest sinuosity, although vertical aggradation probably dominates over lateral shifting. As with fluvial channels in general, distributary widths are determined by the balance of erosion and deposition of the fine-grained deposits forming the channel banks. Their width is remarkably constant downstream despite the significant lateral leakage of flow that must accompany the mudflows that deposit the overbank deposits. This consistency of width suggests that formative discharges may consist of a sediment-laden early peak flow overflowing to form lateral deposits followed by slowly receding flow largely contained within the channel and responsible for determining channel width.

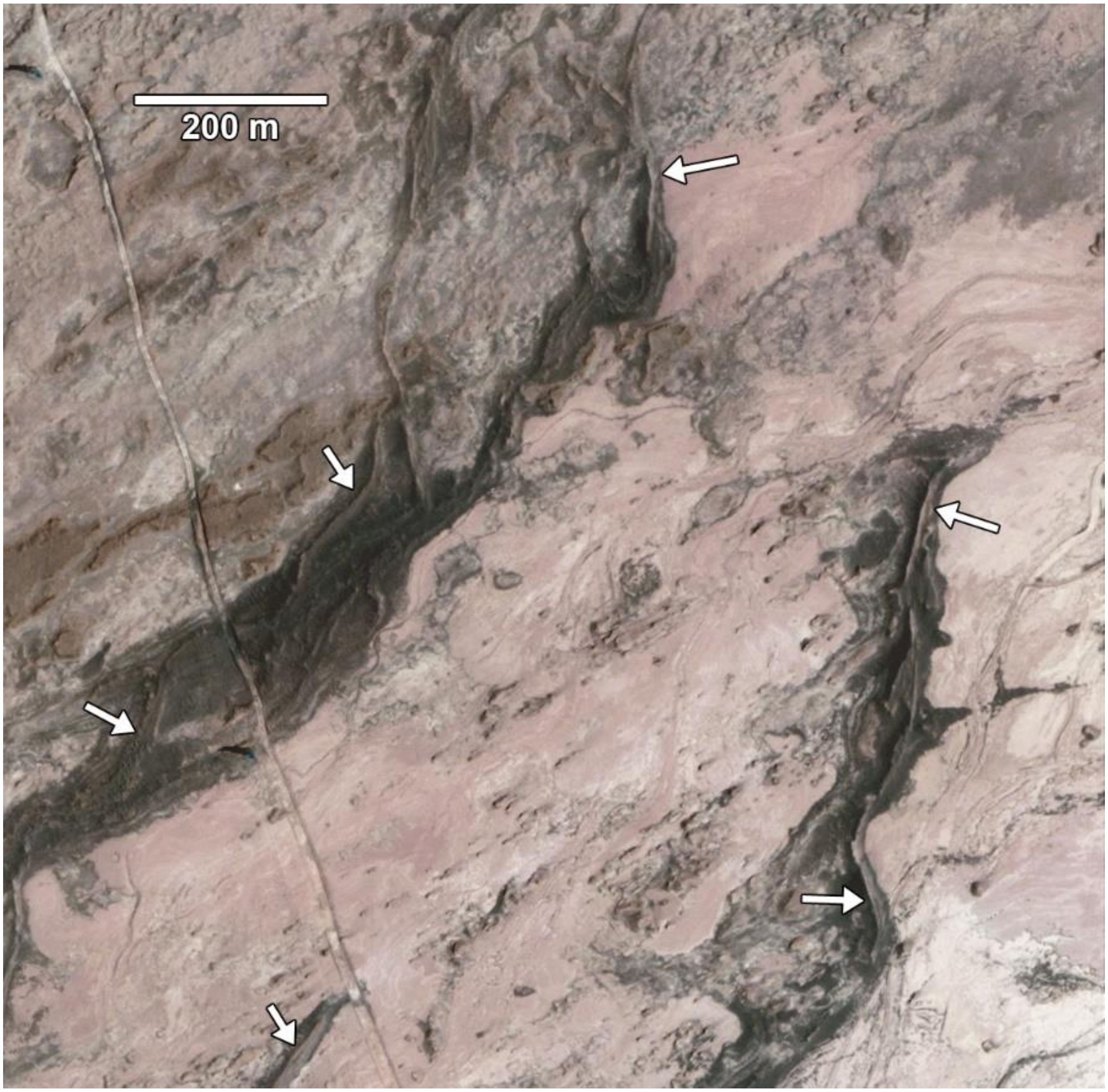

Figure 3.24. Channels inverted by aeolian erosion. Arrows point to representative inverted channels. Dark coloration in vicinity of channels is granule deposits winnowed from the channel deposits. Inversion is due to coarser grain size of the channel deposits, protecting them from wind erosion and possibly chemical cementation. Note dirt track crossing image. Recent overbank deposits are pinkish. Older overbank deposits (upper left) are lightly mantled with winnowed granules as in Figure 3.21. Maximum inverted channel relief 1-2 m. GeoEye imaging from Google Earth centered at 21.115°S, 69.576°W.

As channels and their natural levees aggrade though multiple flow events, the channel floor may rise ~1 m above the fan surface within a 150-200 m radius (Figure 3.28). This resultant relief can lead to avulsions, trenching of a new flowpath through the natural levee, a new distributary channel on the fan surface, and infilling of the abandoned distributary below the avulsion point.

The stratigraphy resulting from multiple such events is characterized by gradually tapering layers separated by diastems (minor hiatuses).

The net result of multiple avulsions is a fan surface consisting of a complex network of active and abandoned channel segments (Figure 3.26). Avulsions may lead to reoccupation of abandoned distributary channels that have gradually become topographically low relative to adjacent actively aggrading distributaries. Other inactive channel segments become buried by subsequent deposition.

Figure 3.25. View looking upstream along the Quebrada de Guatacondo channel. Three mudflows are labeled with oldest being number one. Note that mudflows coat steep banks. Channel floor is composed of clean fluvially transported coarse sediment (gravel, cobbles, and occasionally boulders). Photo by A. Howard. Location 21.024°S, 69.367°W.

Although the overbank deposits harden to such consistencies that blocks must be excavated by pickaxe, they are easily eroded on a grain-by-grain basis by wind-driven saltating grains (Figure 3.23). These grains, up to a few millimeters in size, are derived from the eroding overbank deposits, and over a period of time lag layers and megaripples of granules create a thin (0-10 cm) pavement away from the fluvially active areas, progressively covering the overbank deposits. Burial by later overbank deposits can create diastems demarcated by granule layers.

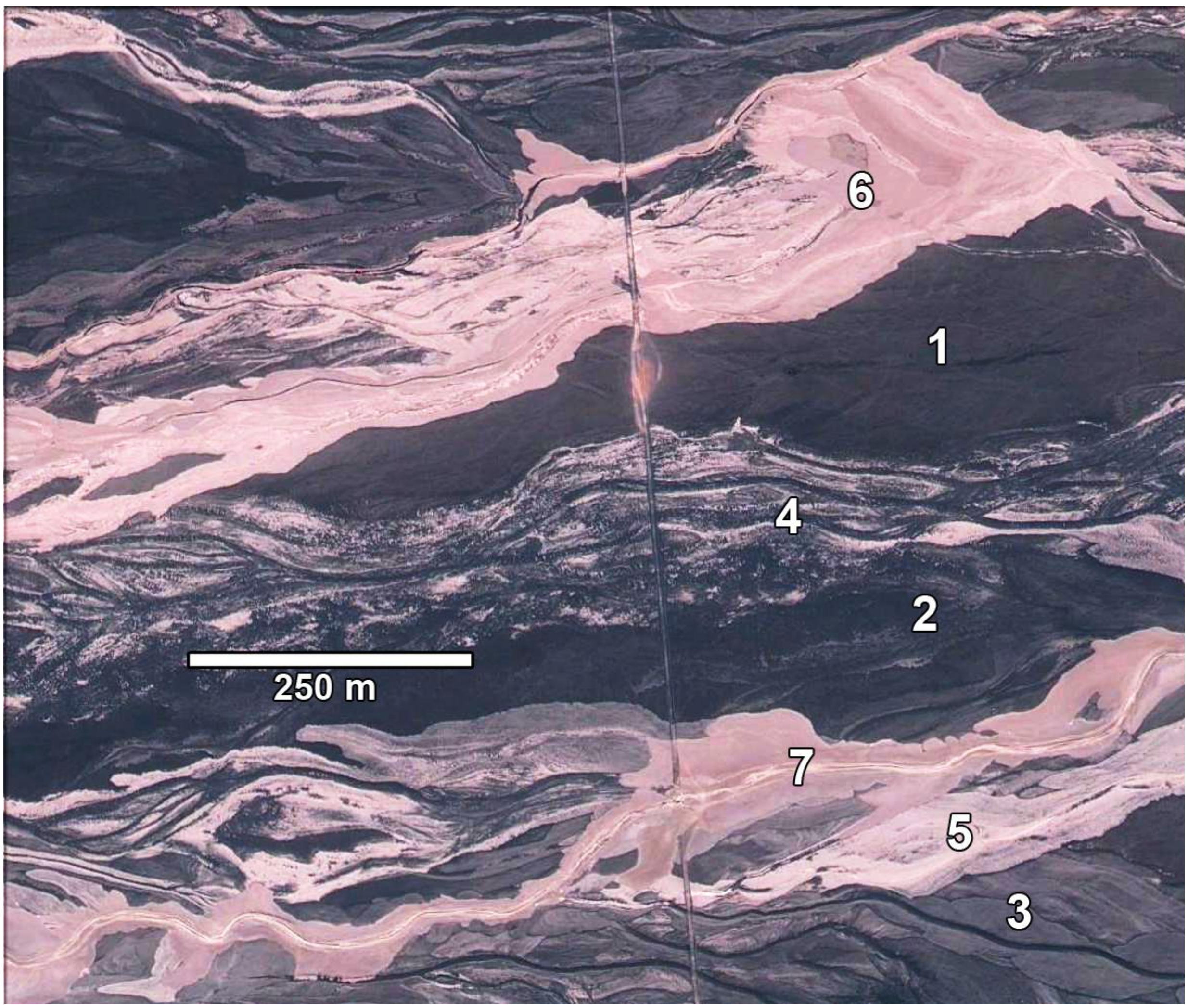

Figure 3.26. Complex history of distributary history on part of a fan surface. Numbers indicate sequence of fan activity (1 is oldest). Note that flow 7 has covered the railroad track crossing the image. Inactive parts of fan become darker due to progressive mantling by granule ripples derived from overbank deposits. GeoEye imaging from Google Earth centered at 20.75°S, 69.40°W, taken prior to the 2012 flood deposition.

On the Atacama fans, the granules forming the pavement are dark colored relative to the bulk overbank deposits. Thus, recently active portions of the fan systems are light-colored, but inactive portions gradually become darker as the percentage cover by granules increases (Figures 3.23 and 3.26). This natural color-coding permits easy recognition of the relative ages of sections of fan surfaces (Figure 3.26). Satellite imagery of the fans show that deposition is typically active (lacking dark sediment cover) over zones 1-5 km wide (measured normal to the flow direction) of the 10-20 km width of individual fan complexes, and within these zones of recent activity individual flood deposits occupy a cumulative width of a few hundred meters or less. The channels range from 3 to 10 m wide. The spatial relationship of these features indicates that fans are built though hundreds or thousands of individual flow events often separated by several years.

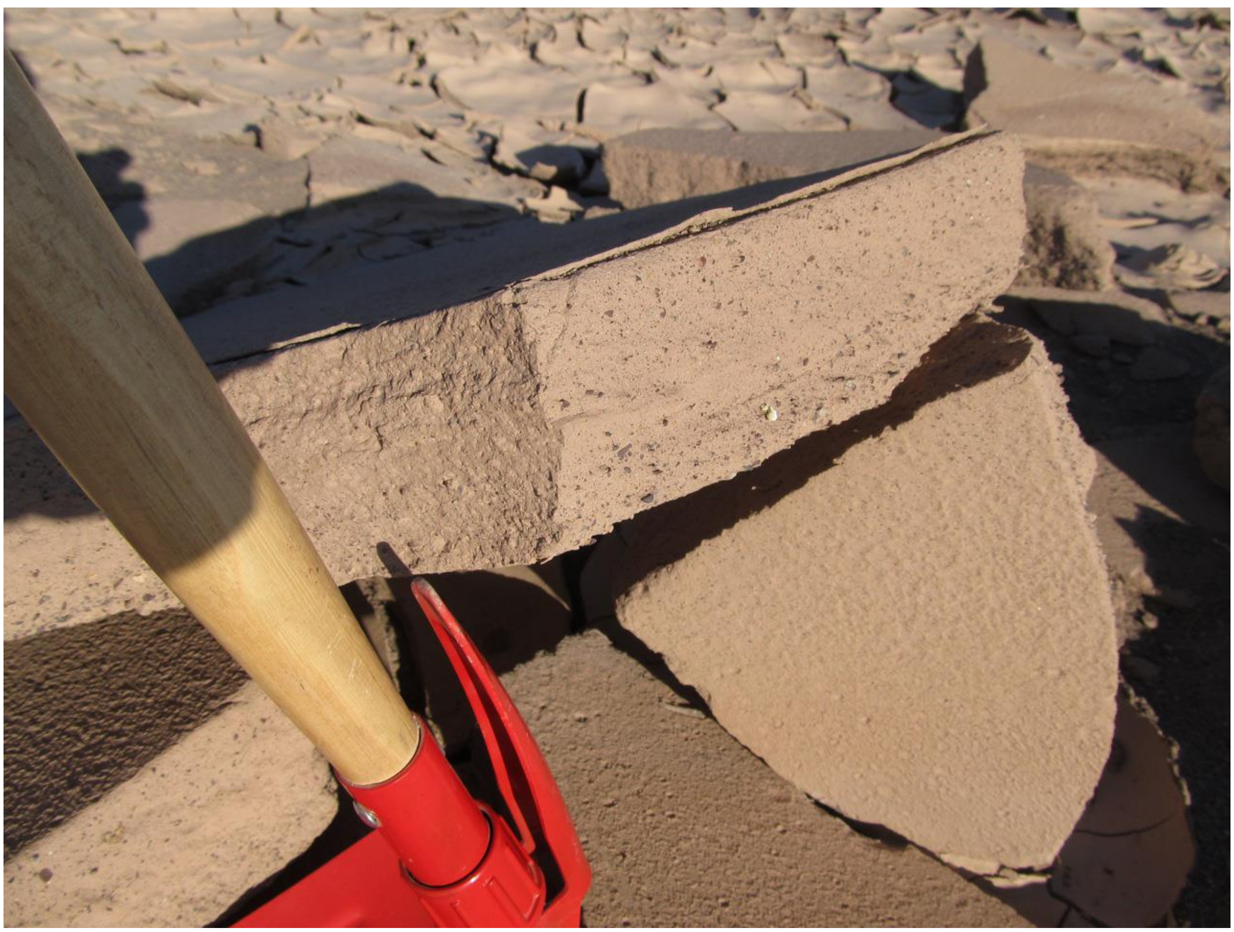

Figure 3.27. Cross section of an overbank deposit containing sparse granules. Note mudcracking of overbank sediments in background. Photo by W. E. Dietrich.

Inactive portions of the fan complex become modified by aeolian deflation, resulting in inverted topography as the channels containing gravel resist erosion, whereas sand saltation readily abrades the muddy overbank sediments (Figures 3.23 and 3.24). Granules deflated from the channel and coarser overbank deposits are swept into megaripples less than 10 cm high that form a distributed pavement limiting the rate of aeolian erosion. On the Atacama fans, the inverted channel relief is generally limited to 2 meters or less, set by the depth of erosion of overbank deposits required to generate a coherent granule pavement and possibly by the duration of wind erosion.

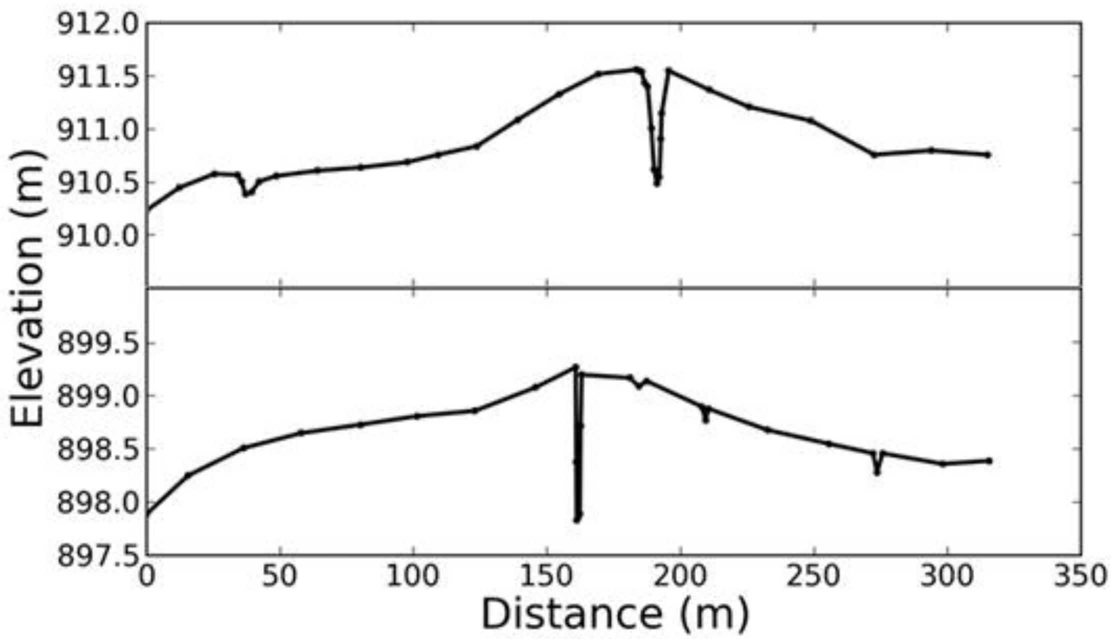

Figure 3.28. Surveys across channel and overbank deposits of distributary shown in Figure 3.20, showing broad natural levees. Top cross section centered on 21.093°S, 69.478°E, bottom cross section centered on 21.100°S, 69.490°E. The bottom of the channel in the top survey is higher than the surrounding fan surface. Note 25x vertical exaggeration.

The strong sedimentological and morphological similarity between the Atacama and Saheki crater fan complexes are used to formulate several working hypotheses for the Saheki fans:

1. The Saheki fans are formed through many hundreds of flow events, often with long intervals between flow events.

2. Only a small portion of a fan complex receives flow and sedimentation during any event.
3. The bulk of the deposited sediment consists of fine-grained overbank deposits.
4. Individual overbank deposits may extend long distances downslope but likely thin and feather out laterally.
5. Avulsions are common as channels and natural levees aggrade, and individual distributary segments may be reoccupied during later flow events, resulting in a complex intertwining of channel deposits.
6. Flows vary in intensity and fine sediment content. Gravel and boulder deposits in distributaries may only be transported during the largest flow events whereas overbank mudflow deposition may occur during more frequent flows.

As with any terrestrial analog to martian landforms, there are limits to the process, material, and morphological similarities:

1. The strong tonal contrast between bright recent overbank deposits and the darker granule pavement that develops during wind erosion is much less obvious on the TARs partially mantling the wind-eroded Saheki fan than for the Atacama fans. This difference in tonal contrasts may be due to lithologic differences, smaller clay content on the martian fans, possible biofilms on the terrestrial granules, or a smaller component of granule-sized overbank sediment on Mars. A lower granule component in the Saheki deposits would limit pavement formation and promote deeper deflation of fan surfaces as observed.
2. Distributaries on the Atacama fans are narrower than estimates of the Saheki crater inverted channels (3-10 m for the Atacama fans (Figure 3.25, 26) versus an average of ~38m for Saheki; (Figure 3.12)). This dissimilarity could be due to greater discharges on the martian fans, to less sediment concentration in formative flows, or to a smaller proportion of cohesive clays contributing to deposition on channel banks.

3. Individual overbank layers deposited on the Atacama fan are generally less than 25 cm thick and generally much thinner near flow margins, whereas observed layering in Saheki crater deposits is typically 2-3 m thick. The degree to which this thickness difference is due to freshness of exposures or to image resolution limitations is uncertain.

3.3.1.2. Summary of terrestrial fan analogs

The terrestrial fans described above are relatively unusual relative to the total population of alluvial fans in having a combination of gravel-bedded distributaries with fine-grained overbank sediments deposited by mudflows. This is inferred to also characterize the Saheki crater fan sediments. Mudflows are characterized by finite yield strength, and imply an appreciable mud fraction (silt and clay). Unlike more viscous debris flows, however, they normally do not transport sediment coarser than pebbles. The mudflow deposits of the Atacama and those described by Bull (1962, 1963) contain an appreciable fraction (>10%) of clay, whereas the Cucomungo Canyon fan deposits (Blair, 2003) typically have about 1% clay and only 10% total mud, indicating that a high concentration of clay and silt is not necessary to support mudflow overbank transport. While the fine sediment composition of the Saheki crater overbank deposits is uncertain, it likely falls within the range of the terrestrial mudflow fans.

3.3.2. Interpretation of Saheki fan stratigraphy and evolution

The observations in Section 3.2 and on possible terrestrial analogs indicate that the Saheki crater fans are composed of a network of fluvial distributaries formed by channelized flows with associated fine overbank mudflow deposits, and, at the fan terminus, playa or shallow lake sediments with some chemically-cemented interbeds. The coexistence of fluvial distributaries with gravel beds and mudflow-dominated overbank deposits might seem contradictory because debris flow dominated terrestrial alluvial fans typically are largely composed of unsorted matrix supported deposits with lobate flow terminations (Blair and McPherson, 2009). The flows on the terrestrial analog channels discussed earlier, however, have aspects of both fluvial and mass flows. Debris flows and presumably the finer grained mudflow events commonly occur as deep, viscous noses followed by long, more watery terminal flows (Costa, 1984, 1988; Johnson, 1984) that are more channelized and winnow fine material from the bed. In addition, large discharge, deep mudflows are commonly interspersed with more frequent, lower magnitude fluvial flows. Either trailing or subsequent-event fluvial flows could be responsible for the relatively clean gravel bed of the Atacama channel shown in Figure 3.25.

In the next two sections, we interpret the stratigraphy of the Saheki crater fans and their erosion by the wind in a simplified cross-sectional model, followed by a discussion of the formative hydrological and climatic environment.

3.3.2.1. Interpretive model of Saheki fan surface erosion

An interpretive, semi-quantitative 2D cross-sectional model detailing the inferred fan stratigraphy undergoing aeolian deflation in Saheki (Figure 3.29) is used to evaluate the viability of our interpreted fan history and material properties of the fan sediment (see Appendix A for full details of model). The model was developed to illustrate three aspects of our interpretation of the alluvial fan composition and subsequent fan erosion: (1) the fan deposits can be interpreted as the two facies of resistant channel deposits and wind-erodible overbank deposits; (2) the erosional processes include interacting processes of aeolian stripping, shallow mass wasting, and undermining of the caprock; and (3) the surface area covered by exposed channel deposits considerably exceeds their volumetric proportion within the fan deposits.

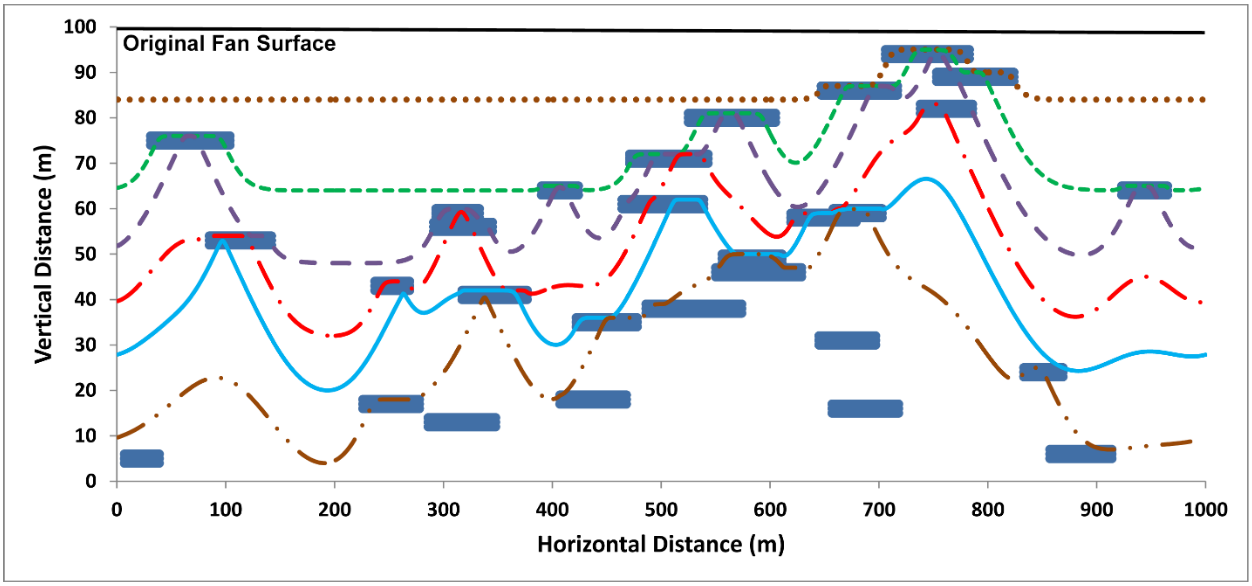

Figure 3.29. Interpretive model of aeolian fan erosion in Saheki crater. A hypothetical along-strike cross section of the fan is pictured, with white being fine-grained, wind-erodible overbank sediment, and blue being randomly seeded channel gravels. Wind erosion starts from the black horizontal upper surface and colored profiles show successive stages of modeled wind erosion. See Section 3.3.3.1 in text and Appendix A for further discussion.

The model takes as its starting condition an idealized hypothetical cross-section of the lower part of fan K2, comprising a randomly distributed set of rectangular "channel bodies" (blue) composed of fluvial sands and gravels scattered through a more easily eroded muddy overbank stratigraphy (uncolored). Aeolian inversion is mimicked by a set of rules for the vertical removal of the overbank material at a rate in part dependent on the local surface curvature (convex-upwards surfaces erode more easily due to greater exposure to the wind), but the channel bodies containing coarser sediment cannot be directly wind-eroded. Instead, they can erode only by hillslope mass wasting, with the resulting material being transferred diffusively down sideslopes. This mass wasting exposes the overbank deposits and moves material into the adjacent topographic lows as well as becoming covered by TARs, both of which decrease the rate of wind erosion (idealized by having the rate of wind erosion diminish in concave upwards locations).

The initial surface is the horizontal black line at the top of the cross section in Figure 3.29. The colored and dashed curves show the surface profile at successive times during the simulation.

The model indicates that, as would be expected, erosion of channel gravels lags behind lowering of the adjacent overbanks until eroded laterally by mass wasting. Exposure of the overbank deposits occurs primarily on slopes subjacent to the gravel ridges and on low-relief surfaces in between ridges. An important effect of wind erosion is to magnify the fraction of gravel on the surface relative to its volumetric fraction. In this simulation, channel deposits occupy 25-36 % of the land surface (locations where the land surface is in the blue deposits in Figure 3.29) in the later stages of wind erosion compared to the 5% volumetric fraction proscribed at the start of the run. This change of proportionality over time due to the exposure of buried channels is likely true for the wind-eroded portions of the Saheki fans. We suggest that the present pattern of inverted ridges gives a false impression of what the density of channels on the active fan may have been, possibly overestimating it several-fold.

3.3.2.2. Interpreted hydrological environment of Saheki fans

In this section, we use observations and measurements of the fan slopes and channel widths with inferences about likely channel bed grain sizes and sediment loads to quantitatively interpret the discharges and flow velocities in the distributary channels at peak discharge. This information allows us to discriminate between the various possible environments of formation for the fans. We then employ these estimates to assess formation timescales for the fans, addressing in particular whether the fans could have formed by one or a few, long-duration flows, or alternatively would have required many cycles of sedimentation over perhaps thousands or tens of thousands of years.

The estimated age of the Saheki crater fans (Mid to Late Hesperian) is a time period when both the atmospheric pressure and temperature are thought to be too low to support precipitation other than as snow (Carr, 2006; Forget et al., 2013; Wordsworth et al., 2013). Groundwater discharge has been considered to be a possible water source for martian valley networks as well as modern gullies (Malin and Carr, 1999; Malin and Edgett, 2000; Harrison and Grimm, 2009; Goldspiel and Squyres, 2000, 2011). The dendritic structure of the source basins, and especially the stream heads descending from narrow ridge spurs away from the walls of the craters, argues strongly for a spatially distributed surface water source. In addition, with the exception of the K1 fan, which has an elevated degraded crater behind the crater rim source basin, all of the source basins in the Saheki and "L" crater fans are eroded into the highest parts of the crater rim with negligible potential groundwater source areas beyond the head of the incised basins. Therefore, in our analysis we assume that flows eroding the source basins and delivering sediment to the fans derives from melting of ice and snow by solar insolation at the surface, a conclusion also reached by Grant and Wilson (2012).

Our method mirrors the approach of Kleinhans (2005), in that we explicitly model the effects of channel bed roughness into our discharge calculations. We assume that the flow during fluvial transport is primarily contained within the distributary channels. Because flows clearly become overbank when depositing the fine-grained inter-channel deposits, this assumption provides a minimum estimate of formative flow magnitude. In addition, we also incorporate additional constraints based on a critical Shields stress in the channels, assuming that the coarsest sediment is transported primarily by the high flows responsible for creating the observed channel geometry. This approach yields internally consistent flow velocities and discharges commensurate with what we know of terrestrial coarse bed alluvial streams.

We aim to model discharges on a single fan (K2) in Saheki crater where we have a high density of HiRISE observations from which to draw data, and where we can adequately constrain the drainage basin structure feeding the fan. Flow velocity, u, in streams can be modeled based on channel hydraulic radius, h, channel slope, S, and some measure of channel bed roughness. From these velocities discharges, Q, can be derived by conservation of mass,

$$Q = uhW \tag{3.1}$$

where W is the channel width.

The local splaying (Figures 3.7 and 3.8) suggests wide channels that are close to the threshold of braiding, so we assume that channels are much wider than they are deep. Under this assumption, the hydraulic radius converges with the channel depth, and we use the terms interchangeably. We also demonstrate below the channels likely have large width-to-depth (aspect) ratios (>20). Even for narrow channels, making this assumption introduces only a few percent bias. A large number of formulations exist in the literature describing calculations of flow velocity. Most follow either the form of the Manning equation,

$$u = \frac{h^{0.67}S^{0.5}}{n} \tag{3.2}$$

where n is an empirically determined channel roughness; the Chezy equation,

$$u = C\sqrt{hS} \tag{3.3}$$

where C is another empirically determined channel roughness term; or the Darcy-Weisbach equation,

$$u = \sqrt{\frac{8ghS}{f}} \tag{3.4}$$

where f is the Darcy-Weisbach friction factor, and g the gravitational acceleration. Following Kleinhans (2005) and Wilson et al. (2004), we work only with the Darcy-Weisbach formulation. This equation makes explicit the dependence of the flow velocity on g, thus allowing more reliable extrapolation of terrestrial calibrations to martian conditions (though we note by comparison of equations 3.2, 3.3, and 3.4, that n and C can also be expressed as functions of g).

Determining the friction factor f under various conditions has occupied many researchers over the years, as summarized by, e.g., Ferguson (2007) and Rickenmann and Recking (2011). This parameter integrates the interaction of flow turbulence with channel roughness across all length scales, and thus shows variability under differing hydrological conditions and fluvial environments. In particular, it incorporates both skin and form roughness, i.e., roughness of the bed at both grain scale and bedform scale (although the latter is neglected in many laboratory calibrations of *f*). The most recent forms of these equations (e.g., Ferguson, 2007; Rickenmann and Recking, 2011) seek to incorporate the effects of very high form drag throughout the flow from the largest clasts on a mixed grain size fluvial bed when flow is shallow, but recognize that flow follows logarithmic laws progressively more closely as the flow deepens and the topology of the boundary becomes less important. When compared to existing databases of terrestrial flow data, these formulations perform at least as well as the best of the older, heuristic approaches – although Ferguson (2007) notes that a factor of two error in predicted discharge should be expected in all cases.

We adopt Ferguson's favored equation for this scale-dependent roughness, which uses a power law to describe the transition zone between the "deep" and "shallow" ($h/D_{84} < 4$) flow regimes, because of both its physical basis and superior performance in terrestrial datasets. This choice is further justified by the fact that our calculated Shields stresses (see below) tell us that the relative roughness of these martian channels falls in the shallow flow regime poorly described by older approaches. The Ferguson (2007) equation is

$$\sqrt{\frac{8}{f}} = 17.7\left(\frac{h}{D_{84}}\right)\left[56.25 + 5.5696\left(\frac{h}{D_{84}}\right)^{5/3}\right]^{-0.5} \tag{3.5}$$

The equation has been calibrated across a range of gravel to boulder bed streams, with slopes 0.0007 to 0.21. These ranges bracket the measurements taken for our martian channels (see below).

To solve equation (3.4) for cross-sectional average velocity requires as inputs the channel slope, *S*, depth relative to the bed grain size, (h/D_{84}), width, and absolute channel depth. We constrain channel widths by examining and measuring the inverted ridges of the fan surface, as described in Section 3.2.3.2. From these data, we take W = 38 m as the average width of these channels on the well-constrained fan K2. Channel slope can be determined directly from MOLA digital terrain models of the fan, having established that the channels and associated overbank sediments are subparallel to the exposed fan surface, and that the channel sinuosity is negligible (Figure 3.3; <5% increase in channel length compared to a straight line). Slopes were measured along the same segments used to obtain widths, and were found to be consistent with S = 0.029 in the upper part of the K2 fan.

The relative depth of these channels, (h/D_{84}), can be constrained by assuming a critical Shields stress, τ_c^*, for the channel bed:

$$\tau_c^* = \frac{S}{r}\left(\frac{h}{aD_{84}}\right), R = \frac{\rho_s - \rho_f}{\rho_f} \tag{3.6}$$

where r is the relative submerged specific gravity of the sediment clasts, and ρ_s and ρ_f are the densities of the clasts themselves and the transporting fluid respectively. The parameter a represents the sorting of the sediment (i.e., $D_{50} = aD_{84}$), and is very poorly constrained on Mars. We here assume a = 0.5, a fairly typical value for coarse grained alluvial systems on Earth. Note that equation (3.6) is not sensitive to g, making it appropriate to apply to martian conditions. This expression was originally derived by considering the force balance on a single particle in a sediment bed, and it semi-empirically describes the threshold of motion for particles in a clast bed. Terrestrial gravel channels typically transport bed sediment at discharges just slightly exceeding the threshold of motion of the D_{50} grain size (Andrews, 1984; Dade and Friend, 1998; Howard, 1980; Parker, 1978; Talling, 2000), so that the dominant (channel-forming, bankfull) discharge corresponds to the threshold of motion, and we assume the same is true of the martian channels. The value of τ_c^* applicable to a given channel varies somewhat, and is a complex function of bed structure, grain size magnitude and distribution, and flow characteristics. However, in almost any fluvial channel it falls in the range $0.03 < \tau_c^* < 0.1$, and much of the variability in the value can be folded into the variability with channel slope (e.g., Lamb et al., 2008):

$$\tau_c = 0.15S^{0.25} \tag{3.7}$$

We adopt this relation, which indicates that on our fan (S=0.029), $\tau_c^* = 0.062$. We take $\rho_s = 3000$ kg/m^3, the approximate density of basalt. We treat ρ_f as a variable, taking $\rho_f = 1000$ kg/m^3 for assumed clear water flow as a reference case, but allowing the value to rise to represent more realistic turbid flows. Flows can retain many of the bedload transport characteristics of fluvial flows while the sediment concentration remains ~< 40% (e.g., Costa, 1988), and we adopt this value as a fairly arbitrary upper limit for the fluid density. Hence, using these values and following equation 6, $(h/D_{84}) = 2.1$ for clearwater flow, decreasing as the flow becomes more turbid, reaching $(h/D_{84}) = 0.7$ when 40% of the flow by volume is basaltic sediment.

The only remaining variable to constrain is the flow depth, which we can calculate by constraining the bed grain size. HiRISE imagery of the fans at 0.25 m/pixel scale indicates that a high proportion of the flat-topped ridges which were measured for channel width are studded with occasional boulders up to a few times the pixel width, and that the rest of the surface has a speckled appearance. This texture is qualitatively suggestive of clasts close to or slightly below the resolution limit of the camera. We place this estimate on a more quantitative footing by resampling imagery of terrestrial river bed sediment with known D_{84} to varying relative resolutions (i.e., pixel resolution/D_{84}) and comparing it to the texture seen in the HiRISE images (Figure 3.30). We infer that the speckled texture seen on the ridges (Figure 3.10) corresponds to a grain size in the range $12.5 < D_{84} < 25$ cm (i.e., 1-2 D_{84} grains/pixel), and most probably towards the higher end of that range. Using our value of (h/D84), we obtain $0.25 < h < 0.5$ m for clear water flow (and channel aspect ratios $70 < W/h < 150$, confirming our approximation that the channel depth equals the hydraulic radius). Such cobble-grade grain sizes are also consistent with our model for the fan inversion process, as described in Section 3.3.1, as the coarse sediment on the bed of the channel will not be transportable by wind.

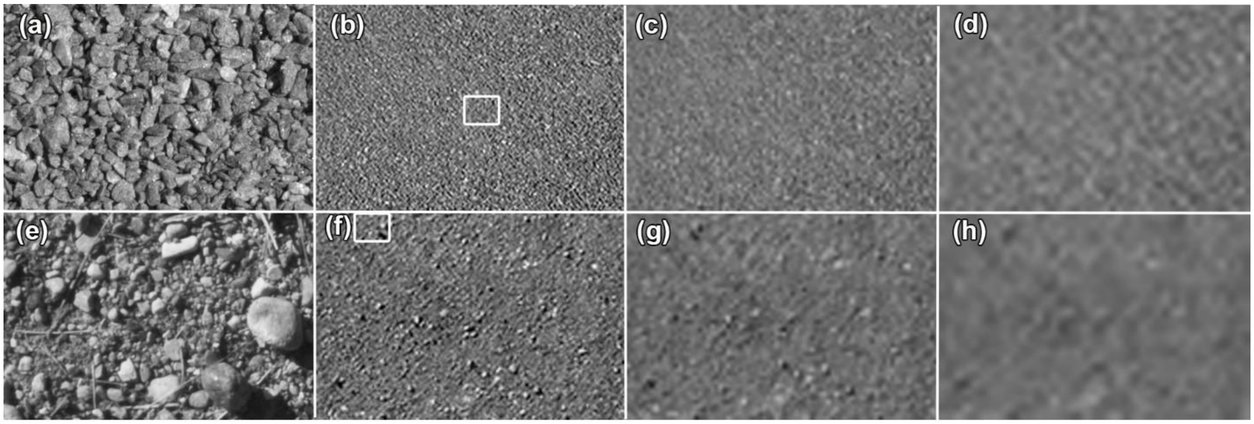

Figure 3.30. Effect of image resolution on interpretation of gravel deposits. Images (a) and (e) are snippets from larger images of gravelly sediment. Sediment in (a) is well-sorted gravel and in (e) is poorly sorted. Images (b) and (f) show reduced resolution of full images in which the particles representative of about the 84th percentile size are shown at 2 pixels per particle (for full resolution HiRISE images this would correspond to 50 cm particles). Location of snippets in (a) and (b) are shown as white boxes in (b) and (c), respectively. In (c) and (g) resolution is further reduced to 1 pixel per particle, and to ½ pixel per particle in (d) and (h). In reduced resolution images gravel shows a characteristic mottled texture. Note that scale was not provided for original images.
Source for original illustrations:
http://www.texturemate.com/content/free-gravel-texture-19-11-2011-001 (a)-(d)
http://aquaponics.wiki.com/wiki/gravel?file=Gravel_small_stones.jpg (e)-(h)

Combining equations 3.1 and 3.4-3.7, we calculate the flow velocities and corresponding dominant discharges in each of these channels (Figure 3.31). Under the range of appropriate sediment concentration and grain size values, we derive flow velocities between ~0.4 and 2.5 m/s and dominant discharge ranged from 0.5-21 m^3/s. Note that these values are also dependent on the value chosen for the sorting parameter a above; however, even if a = 1, (i.e., $D_{50} = D_{84}$, the theoretical maximum value where there is no size variation at all amongst the coarser fraction of the sediment), the maximum values we could obtain are only u = 2.0 m/s and Q = 95 m^3/s.

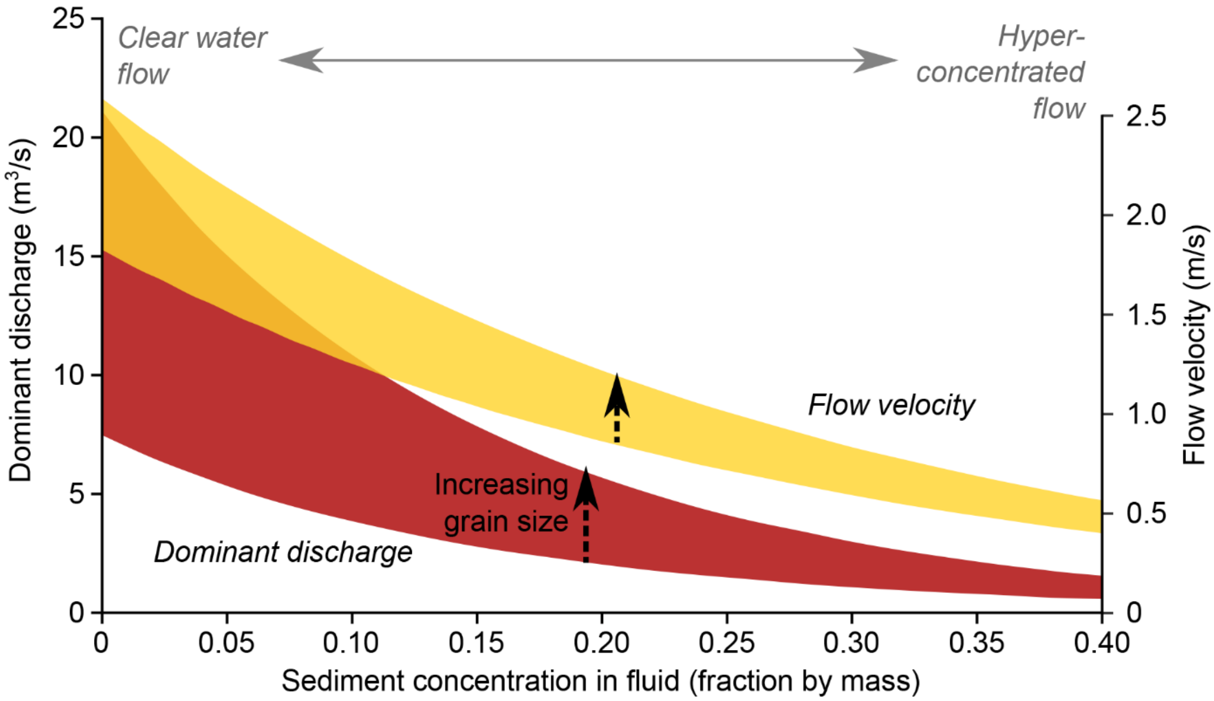

Figure 3.31. Variability of calculated dominant discharges and associated flow velocities with sediment concentration in the fluid and grain size. The fields shown correspond to the effects of varying grain size across the interval $0.125 < D_{84} < 0.25$ m, consistent with observations from HiRISE (Figures 3.10 and 3.30); higher values of discharge and velocity are derived from the coarser grain sizes.

It is uncertain how many channels on the fan were active at any given time, and it may be necessary to multiply these channel discharges by some factor to arrive at the total discharge from the source catchment per event. However, the scarcity of bifurcations seen on the channel ridges suggests that this factor should be low, probably ≤ 3 as is observed in the Atacama analog (Figure 3.25). Assuming three active channels, the coarsest possible grain sizes, *a*=1, and clearwater flow, maximum total discharge across the fan could be up to 285 m^3/s. Much more likely total discharges are probably in the range ~30-60 m^3/s, allowing for a small percentage of sediment in the fluid, and a grain size in the middle of our suggested range, a plausible particle size distribution, and 23 active channels (Figure 3.31). We also reemphasize (following Ferguson, 2007) that a factor of two error in these figures should be assumed.

We constrain the area of the source catchment of this fan as 793 km^2. In order to produce the maximum (i.e., very optimistic) discharges of 285 m^3/s, the source catchment would have to supply water at the rate of 1.3 mm/hr. Our preferred, lower discharges ~30-60 m^3/s would result in proportionally lower supply rates of ~0.1-0.2 mm/hr. These estimates are probably somewhat conservative, as we cannot account quantitatively for refreezing, evaporation, or infiltration in the system. However, if discharge is sourced from an overlying wet snowpack over permafrost, the contributions of all three loss mechanisms are likely to be relatively minor. Such discharges would have to be sustained for at least a timescale comparable with the time taken for water to move through the catchment system, to allow the discharge to integrate across the whole drainage area. For the ~20 km length K2 basin, and assuming flow velocities as seen on the fan are typical of flow velocities higher in the catchment (a conservative assumption, u ~ 1 m/s), then discharge across the catchment would have to be sustained for at least several hours.

We can however test snow or ice ablation as a mechanism for sourcing the discharges based on our data, a hypothesis for the water source for fans and deltas in the Margaritifer Terra region (Grant and Wilson, 2012), and also suggested for contemporaneous shallow channels in Newton and Gorgonum basins (Howard and Moore, 2011). Ablation of ice is fundamentally limited by the energy balance of the icepack itself, including incoming solar flux, reflection at the surface and in the atmosphere, re-radiation from the ice itself, downwelling longwave heat flux from the atmosphere (e.g., from clouds), and potentially complex effects from convection (e.g., winds), advection (e.g., water drainage, dust movements), and secular changes in the driving parameters (e.g., day/night, seasons, obliquity changes). Were all the incoming solar flux to be converted into latent heat to melt ice, we acquire a hard (and physically implausible) upper limit for water supply rates of 5.4-7.5 mm/hr, assuming solar insolation of 500-700 W under the modern orbital eccentricity of Mars (c.f., Laskar et al., 2004). Other authors have used more sophisticated energy balances to investigate the melt rates and total discharges expected from melting snow on Mars. Williams et al. (2008a, 2009a) concluded runoff > 1 mm/h at spatially averaged rates exceeding 0.25 mm/h would be readily possible in the martian midlatitudes over the past 5 Ma, and their data suggests occasionally somewhat higher rates and discharges may also be possible. Kite et al. (2013) suggest that in general across Mars' history, maximum snow melt rates should be 2-3 mm/h, with melt occurring in widely spaced discrete temporal windows, promoted by either orbital parameter variation or by transient darkening of snow surfaces by ash or ejecta.

Our estimates of runoff production rates in the catchment for the K2 fan are comparable to Williams and colleagues' (2009a) estimates for "typical" snow melt events for recent Mars, and comfortably below Kite and colleagues (2013) long term maxima for melt production rates. We thus conclude that melt by ablation of snow deposits on the crater walls is a viable mechanism for the production of the flows that built the K2 fan, and by inference, the other fans in Saheki and crater L that have relief characteristics to the K2 fan (Moore and Howard, 2005). This analysis cannot address the physics of melt production beneath a snowpack, which is likely complex and nonlinearly dependent on the timing of warming of the pack in the solar year (e.g., Williams et al., 2008a), but indicates that the flux magnitude is not sufficient to reject the snow melt hypothesis.

Large terrestrial alluvial fans form over thousands of years of seasonal or rarer flows (such as for the Atacama Desert fans discussed above). Scenarios have been proposed that martian fan deltas (Jerolmack et al., 2004; Mangold et al., 2012b) and some small channel systems (Morgan and Head, 2009; Mangold, 2012) have been created over a short time period by relatively continuous flows resulting from thermal anomalies created, for example, by energy resulting from by bolide impacts. Here we evaluate whether the Saheki fans could have formed from one or a few relatively continuous flow events. Our analysis suggests maximum flow rate to the K1 and K2 fans was unlikely to be more than ~100 m^3/s. The K1 and K2 fan volume is about 586 km^3. Assuming a generous sediment concentration of 20% of water flow volume, a continuous flow could create the fans in a minimum of ~500 Mars (~1000 Earth) years. The primary issue, however, is in generating the flows. As discussed previously, groundwater flow is an unlikely source, so precipitation on the crater walls (almost certainly as snow) would have been required. For the 20% sediment concentration across the known headwater area a total runoff depth of 3.57 km of water would be required. Given sublimation losses and the high porosity of snow, a total snow accumulation several times that figure would have been required. If, say, 10 km of snowfall were required of the headwater areas to form the fan in 500 martian years, this would require an annual snow accumulation of ~20 m. A more reasonable scenario would be seasonal snowmelt occurring for 6 hours per day, 100 days per Mars year, requiring ~3600 martian years to form the fan and an annual snow accumulation rate of ~3 m/yr. This is still a very optimistic scenario given the high average sediment loads assumed.

Another check on a minimum timescale comes from the observed layer stratigraphy. If the ~2 m-thick beds observed in HiRISE images (Figures 3.13 and 3.15) represent annual accumulations and we take an average fan thickness of ~400 m, then approximately 200 deposition events are recorded at any given location. If as much as 10% of the fan surface were active during any given year, then 2000 martian years would have been required. It is likely, however, that higher resolution imaging of clean layer exposures would reveal finer-scale layering than observed. We therefore conclude that at least a few thousand martian years was required to form the alluvial fans. More likely, given the probability of lower sediment load percentages, less frequent flow events, and thinner annual bed thickness, the fans may have required a few tens of thousands of martian years to form at a minimum. These years need not have been sequential. A fan lifetime with a small number of annual events during favorable obliquity may have been separated by long inactive periods through multiple obliquity cycles. We do note, however, that we have seen no evidence for impact cratering having disturbed visible bedding during deposition, although appreciable cratering has occurred subsequent to fan deposition.

3.3.3. Comparison with other martian fans

Large alluvial fans on Mars have morphological characteristics that vary through a narrow range of fan gradients, ratios of gradient to contributing area, and ratios of fan area to contributing basin area (Moore and Howard, 2005) (Table 3.1). These characteristics suggest very similar hydrological and sedimentary processes and materials characterized most martian fans. The “L” crater 25 km southeast of Saheki crater hosts fans that are of similar size and morphology as those of Saheki crater. The major differences appear to be the multiple fans in “L” sourcing from all quarters of the rim, and lesser aeolian stripping of the fan surface (although, as in Saheki crater, the greatest wind erosion has occurred on the southern fans). Recent high-resolution imaging, however, reveals differences in fan morphology and geologic context among other fan-bearing craters. In Harris crater (Figure 3.1), the fans show pronounced distributary patterns like Saheki, but the fan in the northeast quadrant exhibits an isolated, rough–surfaced, bouldery deposit crossing the fan with a wide, lobate planform morphology that has been interpreted as a debris flow deposit (Williams et al., 2011). The fans on the west side of this same crater overlie a light toned, layered deposit not found in Saheki crater. The fan surfaces in Runanga crater (Figure 3.1) exhibit inverted distributaries, but the interbedded layered deposits are light-toned and are broken by meter to decameter polygonal fracturing, which might be explained by either more coherent sediment or a different weathering environment. Most of the fans in Margaritifer Terra studied by Grant and Wilson (2012a) exhibit radiating distributary patterns similar to those in Saheki and “L” craters, but one set of fans terminates in steep-fronted lobes that could be explained by their deposition into a concomitant lake (with the fan-delta in Eberswalde crater being a prominent case of interaction with a lake (Malin and Edgett, 2003; Moore et al., 2003)). Finally, Holden crater features a more complicated history of successive fan development than has been proposed for Saheki crater (Grant and Wilson, 2012).

These observations illustrate a range of fan stratigraphic patterns across martian fans, perhaps reflecting local climate or differences in source materials. Nonetheless, the general pattern seen in Saheki and “L” craters - of radiating distributaries composed of wind-resistant sediment interbedded with finer, layered sediments - characterizes most martian fans which have been sufficiently exposed by aeolian erosion to reveal their stratigraphy.

3.4. Conclusions

The Hesperian Period is generally thought of as a cold and dry period dominated by extensive volcanism, canyon formation, and large outflow channels. Recent studies have suggested that fluvial activity was widespread though probably sporadic on Mars well into Hesperian and perhaps occurring as late as the Hesperian/Amazonian transition (Fassett et al., 2010; Grant and Wilson, 2011, 2012; Howard and Moore, 2011; Mangold et al., 2012a). Widespread post-Noachian fluvial features which require precipitation (probably as snow) as their water source are indicative of a global climate favorable to surface water transport as suggested by Grant and Wilson (2011, 2012) and Howard and Moore (2011).

The precipitation and discharge of water is the premier question in understanding the climatic implications to fan formation. Our calculated discharges and the origin of runoff being the highest portions of hosting crater rims effectively rule out the possibility of groundwater as a source of water feeding the fans, leaving atmospheric precipitation as the likely candidate. Given the constraints imposed by the martian climate during the Hesperian as well as the lack of fluvial channel heads on the fan surface, torrential rain is very unlikely. Our hydrological analysis (Section 3.3.2.2) shows that snowmelt appears to be adequate to drive the required discharges.

One of the most enigmatic observations of the alluvial fan systems on Mars is their highly localized distribution. On a global scale, large fans are limited to within mid-latitude band craters (Kraal et al., 2008; Moore and Howard, 2005; Wilson et al., 2012), and even within craters fans are limited in their spatial distribution. Despite being just several tens of kilometers apart, "L" crater contains seven fans sourcing from all sides of the crater rim while Saheki contains only three, one of which is too small to be of much significance. The high crater rims of the relatively young craters hosting fans may have helped to create a microclimate that could trigger appreciable snow accumulation. Restriction of fans to certain portions of crater rims may also be attributed to crater rims containing deposits susceptible to erosion by modest runoff rates, that is, predominantly fine-grained and unconsolidated materials. Both of the main Saheki fans source from a region that intersects both the western rim of a larger adjacent crater as well as the elongated basin to the northwest (Figure 3.2), both of which could be potential sites of antecedent sediment accumulation.

Fans on Mars exhibit vastly different levels of subsequent aeolian erosion. The two fans within Saheki crater have slightly different crater-derived surface ages, yet interfingering of distributaries along their border is suggestive that the fans formed at the same time and that the apparent age difference is due to the subsequent amount of erosion of the fan surface. The amount of aeolian erosion is thus not solely a function of surface age, but rather a product of other factors including sediment composition and wind direction and intensity. However, while different fans have undergone varying levels of erosion, they mostly share the same morphological characteristics. We propose many of the large fans in this latitude belt formed from similar hydrologic processes and conditions as the Saheki fans. Therefore, even though Saheki crater was chosen for detailed study due to the high amount of information revealed from surface aeolian erosion, other fans have formed through similar processes, albeit with some variations in processes, materials, and setting as indicated in Section 3.3.3.

Evidence from the fans in Saheki crater and elsewhere represent significant fluvial activity relatively late in martian history and contribute to our ever-changing understanding of the fate of Mars' climate. These fans could not have formed in a single event; their formation requires many years and multiple periods of snow accumulation and subsequent runoff. Moreover, for snow to preferentially accumulate on local topographic highs, the atmospheric pressure had to be higher during this time than at present (Wordsworth et al., 2013). The sedimentological characteristics of the Saheki and "L" crater fans indicate that flows during at least the final stages of fan activity were fluvial flows with occasional overbank mudflows, so that volumes of sediment that could be transported during individual flow events would be limited to a fraction of the discharge volumes. The modest discharges that would be available from the source basins suggests that only a few distributaries were active in any given flow event. The lack of evidence for deep lakes occupying Saheki crater during the time of fan formation indicates formative flows were of limited volume and duration, requiring many flow events to construct the fans. The thin, light-toned beds in the fine-grain deposits may relate to modifications occurring during depositional hiatuses (Figures 3.13 and 3.14). Flow events did not necessarily follow a yearly cycle; rather, there may have been epochal periods of snow accumulation followed by periods of release during favorable orbital configurations or transient aperiodic but repeated global warming events such as volcanic eruptions. In addition, occurrence of snowfall may have been tied to availability of source water, possibly related to phreatomagmatic eruptions or flood events in outflow channels.

Acknowledgements

This study was partially supported by the NASA Graduate Student Researchers Program, NASA grants NNX08AE47A, NNX08AM91G, NNX09AM02G, and NNX12AM73H, and by an award to Y. Matsubara by the Department of Environmental Sciences, University of Virginia.

Chapter 4

Simulating the formation of fine-grained alluvial fans

Abstract. We present a new landform evolution model for use in investigating alluvial fan dynamics. The model incorporates a bimodal sediment distribution and multiple active distributaries, while being computationally efficient by generalizing the hydrodynamics of flow and sediment transport. Sediment is transported across the fan as channelized bedload and fine grained mudflows that can deposit overbank, utilizing depositional processes observed on large fans in the Chilean Atacama Desert and inferred to have occurred on Mars. The simulated channel bed aggrades or degrades in proportion to the bedload flux divergence, and avulsions occur stochastically with a probability dependent on deposited levees heights and fan surface topography. The model records the fan's internal stratigraphy, allowing for investigations into patterns of bedload versus overbank deposited sediment. When subjected to variant boundary conditions such as input discharge and sediment load, tectonic tilting of the underlying basin, and deposition into a lake, the modeled fan surface behaves as expected, indicating that it can provide qualitative and quantitative insights into linkages between alluvial fan processes, morphology, and stratigraphy.

4.1. Introduction

Alluvial fans are sedimentary landforms that form when a mountain stream debouches onto broader lowland terrain. A combination of gradient reduction and lateral spreading of the flow forces the deposition of sediment into a semi-conal shape. Alluvial fans act as storage reservoirs for sediment as it makes it way from source to eventual sink, and their morphology and stratigraphy is a record of these processes. Fans have long been recognized as potential markers of past climatic change (Harvey, 2004; Ritter et al., 1995; Wells et al., 1987). The potential for paleoclimate record preservation is of particular interest in the case of alluvial fans on Mars, where the conditions present during their deposition remain unconstrained. Crater age statistics indicate that some martian alluvial fans date to the Hesperian or even Amazonian Periods (Grant and Wilson, 2011; Chapter 2), an era generally characterized as being cold and dry (Carr and Head, 2010). How conditions arose that allowed for fluvial sediment transport during this era of martian history are not well understood.

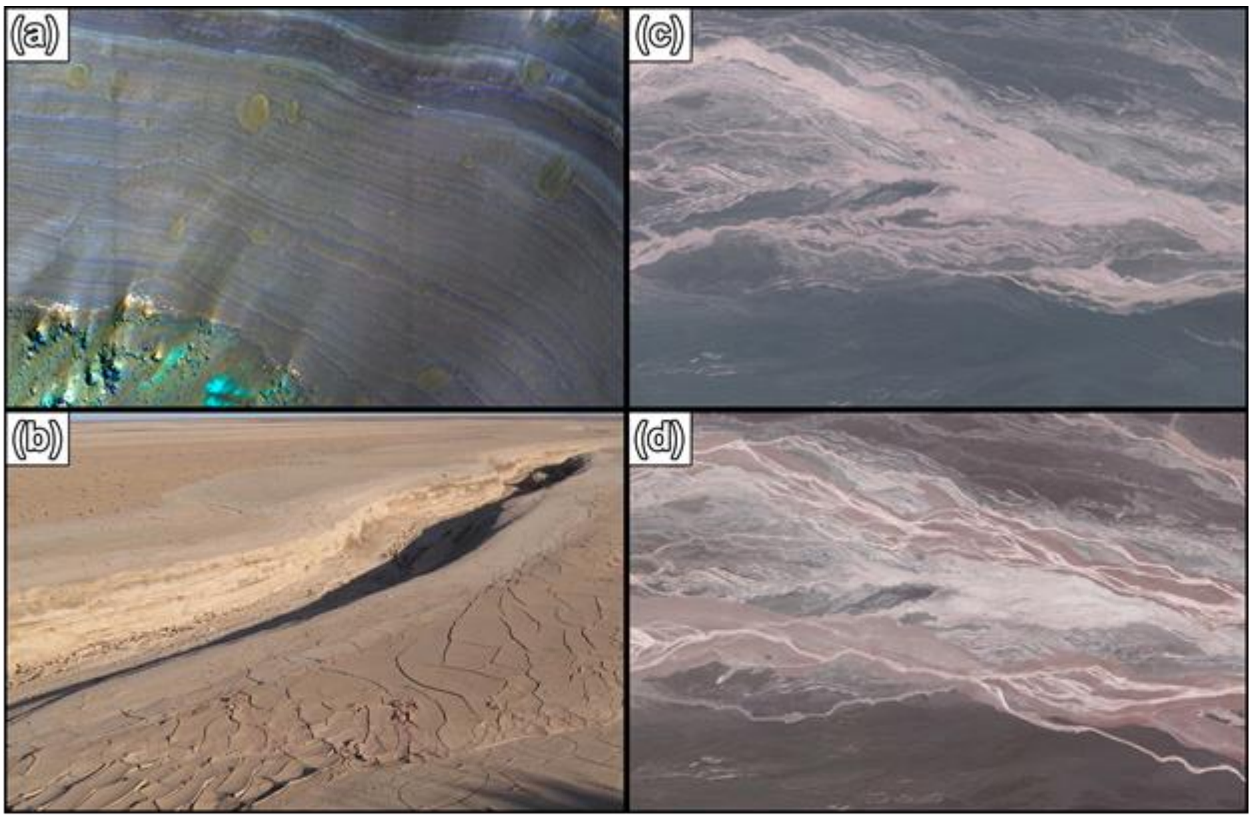

Figure 4.1. Examples of the depositional model we aim to replicate in the model. (a) Intricate layering revealed within an impact crater that punched through an alluvial fan in Saheki crater. HiRISE image ESP_049172_1585 (NASA/JPL-Caltech). (b) Photograph of overbank deposition on a large alluvial fan in the Atacama Desert. Channel is ~3m across. (c and d) Surface of alluvial fan in the Atacama in (c) 2009 and (d) 2012. Overbank deposition has flooded the fan surface around the channels. Image centered on 20.7°S, 69.38°W. Images are 3.5 km across from left to right. Accessed with Google Earth.

Landform evolution modeling (LEM) is a powerful tool for the geomorphologist to explore the long-term evolution of planetary landscapes. Previous modeling studies have investigated interactions between impact cratering and fluvial erosion (Howard, 2007), climatic conditions during valley network formation (Barnhart et al., 2009), and the degradation of impact craters (Forsberg-Taylor et al., 2004). To date, there have been limited attempts to use an LEM to examine the formation of the martian alluvial fans. Armitage et al. (2011) used an idealized 2-D model to explore the effects of precipitation and catchment erodibility on a fan's radial long profile, finding that conditions during fan formation were either arid for 10^7-10^8 yr or semiarid for 10^6 yr. However, this simplified approach was unable to examine fan topography and the effects of varying distributions of bedload and overbank sediment, which may be necessary to understand the geographic distribution of the martian fans.

Numerical models of terrestrial alluvial fan formation generally come in two types. Cellular models of channel dynamics use probabilistic rules for flow distribution and deposition, with the flow path shifting as sediment is deposited and topography is adjusted (e.g., Jerolmack and Mohrig, 2007; Karssenberg and Bridge, 2008; Murray and Paola, 1994). Models examining the morphologic evolution of an entire fan often use a diffusional approach over a time period deemed long enough to generalize the channel dynamics (e.g., Armitage et al., 2011; Nicholas and Quine, 2007; Parker et al., 1998; Swenson et al., 2000). Some models, including that of Sun et al. (2002), combine elements of both approaches, but omit overbank deposition, which is a crucial component in the case of the martian fans (Morgan et al., 2014). The model presented here expands upon the Sun et al. (2002) model by incorporating multiple grain sizes, levee and bed elevations, and overbank sediment deposition.

4.2. A process analog in the Chilean Atacama Desert

A series of large alluvial fans in the Atacama Desert appear to be a close morphological and process analog to those on Mars (Morgan et al., 2014) (Figure 4.1). Observations from a field expedition guide the approach used in modeling fan sediment deposition. The surfaces of fans in the Pampa del Tamarugal region reveal a complex network of channels, but only a few distributaries are active during a flow event. Channel bed material consists of clean (no mud) gravels and cobbles with grain-to-grain contacts (clast-supported), but mudflows are dominated by the fine-grained matrix and isolated coarser grains (matrix-supported) which are plastered onto channel walls.

The bulk of the fan appears to consist of fine-grained mudflows (hereafter referred to as overbank deposits), that deposit in sheet-like, unconfined flows extending tens to hundreds of meters laterally from the main source channel. Individual flow deposits are up to ~25 cm thick, contain 60% mud and 40% sand with occasional granules, and have thin lateral edges, implying a low viscosity relative to the mudflows caked onto the channel walls. Main channel distributary widths are relatively constant with distance downfan, as the mudflows confine the channel through which the coarser gravel sediment is transported. Waning stage flows have a lower fine-grained sediment concentration but longer duration, and erode the channel bed and transport gravels (Wells and Harvey, 1987). The stratigraphy along channel walls reveals mud layers up to tens of cm thick, with occasional well-sorted sand, pebble, and cobble interbeds, that is, an intimate sequencing of mudflow- and fluvial-dominated facies.

These observations guide several assumptions in the development of the landform evolution model. Mud free, subrounded cobbles in the channel bed and clast supported gravelly layers in section reveal channelized, fluvial processes. Overbank deposit thickness decreases with distance down the fan, suggesting that deposition rate is a function of flow discharge and depth. The base of recent overbank sheets show little evidence for scour of previously emplaced deposits, so overbank deposits are entirely depositional. Deposits thin with distance from the channel, and flow edges vary in thickness, indicating the mudflow viscosity varies between flow events.

4.3. Model approach

4.3.1. Flow routing and sediment transport

The model presented here is based upon fundamental equations of sediment transport and hydraulics, but generalizes the physics of flow and sediment discharge. Reduced complexity models have been shown to be as effective (Thomas et al., 2007) or even superior (Nicholas et al., 2012) to three dimensional hydrodynamical models in predicting the response of geomorphic systems to fluvial processes. The primary model components of channel geometries, avulsion criteria, channel cutoffs, and overbank sedimentation are based upon empirical observations expressed as heuristic rules. We explore reasonable variations in these parameters in Section 4.4.

The computational domain is a Cartesian grid of dimensions mx by my and consists of square cells of width dx. Each cell is classified as either a “channel” or “non-channel” cell, with the channel system represented as a vector network connecting channel cells to their downstream neighbors. Sediment-laden flow enters the domain at discharge Q_f through an input cell at the fan apex and is distributed through the channel network. The flow carries bedload of median grain size D_{50} that can be deposited within channels and a suspended load that is treated as a fraction of the total discharge. Channels can branch and recombine, and multiple channels can be active at a given time. At branches, the discharge is distributed based on the relative gradients of the downstream channels. For a channel in cell a that branches in k directions, discharge into adjacent cell b is

$$Q_{f_{ab}} = \sum_k Q_{f_{ak}} \frac{S_{ab}^{\gamma}}{\sum_k S_{ak}^{\gamma}} \tag{4.1}$$

where γ is a constant set to 0.5 (Murray and Paola, 1994) and S is the gradient, computed as

$$S = \frac{\eta_a - \eta_b}{L_{ab}} \tag{4.2}$$

where η is a cell's elevation and $L_{ab} = dx$ for edge adjacent cells and $dx\sqrt{2}$ for diagonal cells. Sediment transport is modeled as two end members: bedload and fine grained mudflows that can flood overbank. (Parker et al., 2007; Wilkerson and Parker, 2011) performed regression analyses on multiple data sets to derive quasi-universal relationships between discharge, channel geometry, and bedload sediment flux at bankfull conditions. Bedload sediment is transported according to the equation

$$Q_s = B\, D_{50}\, (gRD_{50})^{\frac{1}{2}}\, \alpha_i\, \alpha_c \left(\frac{g}{RD_{50}}\, S\, H - \tau_c^*\right)^{\alpha_e} \tag{4.2}$$

where D_{50} is the median grain size, g is gravity, α_i is the intermittency (the fraction of time during an iteration the fan is morphologically active), α_c is a transport constant (set to 4.0 for D_{50} >.002 and 8.0 for D_{50} <.002), α_{te} is a transport exponent (set to 1.5), and τ^*_c is the critical Shields number at the onset of sediment motion. R is the submerged specific gravity of the channel sediment, defined as

$$R = \frac{\rho_s}{\rho} - 1 \tag{4.3}$$

where ρ_s is the density of the sediment and ρ is the density of the fluid. The calculations of channel width B and depth H are dependent on the bedload median grain size, which for gravel bed rivers is

$$B = \frac{4.63}{g^{1/5}} Q_f^{0.4} \left(\frac{Q_f}{\sqrt{gD_{50}}D_{50}^2}\right)^{0.0667} \tag{4.4}$$

$$H = \frac{0.382}{g^{1/5}}\, Q_f^{2/5} \tag{4.5}$$

and for sand bed rivers is

$$B = 0.0398 \left(\frac{\sqrt{R}}{\upsilon}\right)^{0.494} g^{-0.0875}\, Q_f^{0.669}\, D_{50}^{0.0685} \tag{4.6}$$

$$H = 22.9 \left(\frac{\sqrt{R}}{\upsilon}\right)^{-0.310} g^{-0.293}\, Q_f^{0.276}\, D_{50}^{-0.155} \tag{4.7}$$

where υ is the kinematic viscosity of water (Parker et al., 2007; Wilkerson and Parker, 2011).

Channels aggrade or erode depending on a cell’s incoming and outgoing bedload sediment flux following the Exner relation of bed sediment conservation

$$\Delta\eta_a = \sum_k \frac{Q_{s\,ak}}{(dx)^2} \Delta t \tag{4.8}$$

where k is the number of upstream and downstream branches from cell a, Δt is the iteration time increment, and Q_s is positive for sediment flux into a cell and negative otherwise.

Channel geometries are updated each iteration but are time-averaged over the previous ten iterations. When the flow depth increases above the channel bank, sediment can be deposited overbank. Overbank sediment is deposited in sheets that radiate outward and thin with distance from the channel according to the equation

$$\varphi = Q_f\ \mu\, [\exp(-\zeta\, D)] exp[-\varepsilon(\eta_f - \eta_c)] \tag{4.9}$$

where μ is the suspended sediment flux, D is the distance from the channel to the floodplain cell, w is an exponent, set to 2.0, η_f and η_c are the elevations of the floodplain and channel, and ζ and ε are the exponential decay constants for the distance and elevation (Howard, 1996).

Flows can expand outward from a channel until they reach a topographic rise higher than the channel flood depth, hit a channel (it is assumed in this case that the channel captures the flood) or thin to the point where the driving shear stress $\tau = \rho_f\, g\, h\, S$ (where h is flow thickness) drops below the flow’s yield strength. The stratigraphy of the fan is recorded as the relative proportions of bedload and overbank sediment.

4.3.2. Avulsions and Channel Abandonment

Bedload deposition and aggradation causes a channel to become elevated relative to the surrounding terrain. Avulsions occur stochastically when a potential new channel direction is found to be more energetically favorable (i.e. steeper) than the current one. In river systems this generally occurs when the channel bed is about one channel depth above the surrounding floodplain (Mohrig et al., 2000). More specifically, a channel from cell *a* to cell *b* can avulse to cell *c* if

$$\frac{(\eta_a+\beta H_a)-\eta_c}{L_{ac}} > S_{ab} \tag{4.10}$$

where β is between .5 and 1 (Mohrig et al., 2000). Following an avulsion, a new channel path is routed downfan that mostly follows the path of steepest descent but allows for a degree of random deviation. For the initial direction of an avulsion, the probability that flow originating in cell *a* will flow to cell *c* out of *k* candidate cells with $\eta_k < \eta_a$ is

$$p_{ac} = \frac{S_{ac} exp\left[-\left(\frac{\theta_{ac}}{\theta_0}\right)^2\right]}{\sum_k S_{ik} exp\left[-\left(\frac{\theta_{ak}}{\theta_0}\right)^2\right]} \tag{4.11}$$

where θ_{ik} is the angle between the vectors that link cells *a*-*k* and cells *a*-*b*, and θ_0 is the standard deviation of the probability function, which following (Sun et al., 2002) is set to $\pi/(2\sqrt{2})$. The new flow path is established downfan until the route merges with another channel, reaches the fan edge, or encounters a topographic low point. The flow distribution between the subsequent branches is governed by equation 4.1.

Following an avulsion, the initial channel remains active. However, channels can be abandoned in two ways. First, for simplicity channels are not allowed to triple branch. Branching cells may undergo an avulsion, but following the new route selection, the lowest discharge third branch is abandoned. Second, channels can become abandoned if the channel discharge drops below a critical value. In natural streams this can happen if the gradient decreases to zero from overbank or gravel deposition, but in the model is generalized to occur when the discharge to the distributary drops below a fixed fraction of the total discharge entering at the fan apex.

4.4. Results

Parameter	Base value
Q_{f0}	20 m^3 s^{-1}
Q_s	.04
D_{50}	.003 m
β	.5
μ	8e-8
ε	2.8
ζ	0.01

Table 4.1. Input model parameters for the base set of conditions

The model was run using the parameter ranges specified in Table 4.1. We ran the model under a base set of boundary conditions and then modified inputs to experiment with the subsequent output morphology and stratigraphy. In all runs we used a dx = 100 m so that the cell size is always greater than the channel width and a domain size of 20 km. The input discharge varies randomly as

$$Q_{f\ input} = Q_{f0} \log(-r) \tag{4.12}$$

where r is a pseudorandomly generated number between 0 and 1 and Q_{f0} is the nominal boundary discharge. For the base case we use a Q_{f0} = 20 m^3/s. The submerged specific gravity R is set to 1.65 (quartz sand) for fluid and sediment densities of 1000 and 2650 kg m^{-3}.

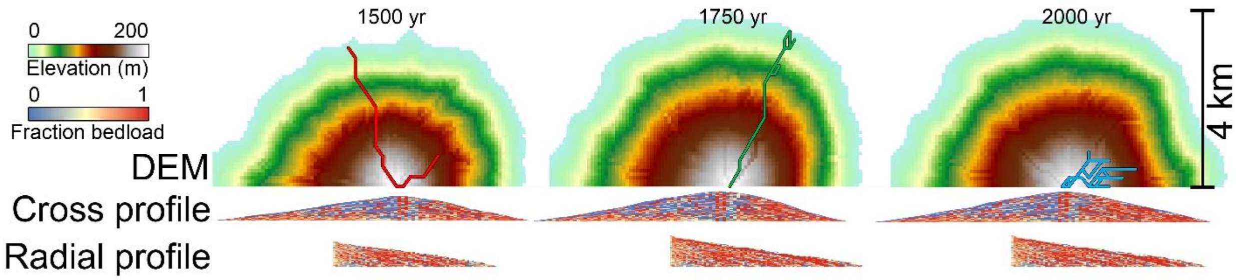

Figure 4.2. Example of model output using the base set of conditions. The DEMs represent the elevation at three iterations near the end of a simulation. The red, green, and blue lines indicate the channel network. The vertically exaggerated cross sectional profiles show the distribution of bedload and overbank deposited sediments, with red being 100% bedload deposits and blue being 100% overbank deposits. The cross profile sections are oriented horizontally across the fan 300 m from the apex, the radial profile extends vertically from the apex to the toe.

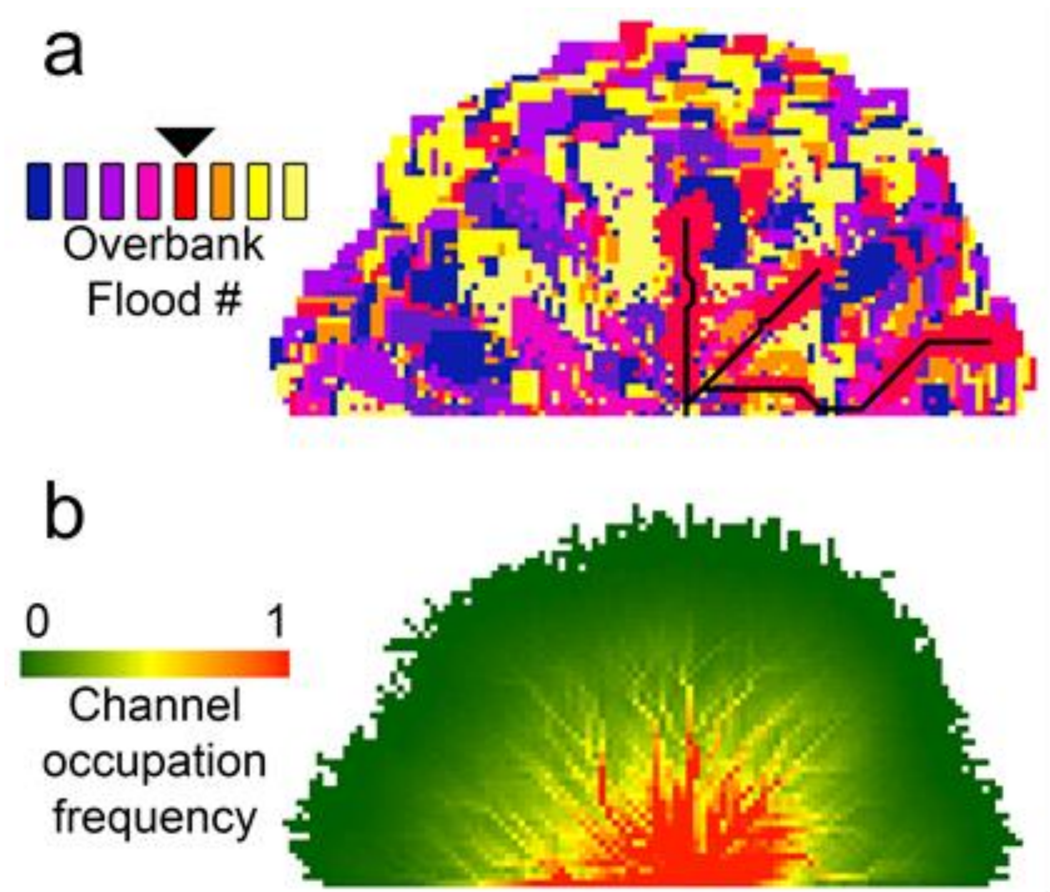

Figure 4.3. Additional results from the base set demonstrating the model output. (a) Overbank floods on the fan surface. Channel network marked by black lines. The colors indicate the flooded cells during a flood event (defined as all of the flooding that occurs in an iteration), and the color scheme resets every 8 flood events. The black arrow on the scale bar marks the most recent flood color. (b) Frequency of channel occupation per cell. Avulsions occur most often in the fan's proximal zone, and less frequently with distance downfan.

Figure 4.2 shows the output from the base set run. The final fan after 2000 yr of deposition is 4 km long with a slope of ~2.8°. The internal stratigraphy is shown as two cross sections cut through the fan. Additional model output includes the tracking of overbank flood events and the frequency a cell is occupied by the channel (Figure 4.3). The model presented here does explicitly simulate overbank deposition as it is observed to occur on the Atacama Desert fans and inferred have occurred on the martian fans. On the fans in the Atacama, flows frequently overtop their levees and spread out on inter-channel portions of the fan surface, advectively depositing sheets of fine sediment while only occasionally causing permanent avulsions. We attempted to include these as unchannelized sheet flows, but the model's cellular discretization and reduced complexity nature is not well suited to modeling complex floodplain topography, which has a topographic roughness at a scale well below *dx*. However, the overbank deposition algorithm in the current model appears to capture the essence of the Atacama flows reasonably well (compare Figure 4.3 with 4.1a,c, 3.22, and 3.26). Individual floods extend far beyond the distributary network, but overall deposit on a relatively small area of the fan surface. Avulsions modify the channel network and shift the active depositional zone across the fan.

In the following section, we describe how variations in the input parameters are expressed in the fan morphology relative to the base case. We then experiment with changing several input parameters during a model run to test how the model behaves under extrinsic and intrinsic forcings.

Figure 4.4. (next page) Effect of overbank properties on fan morphology. The only difference between these runs are the overbank flood height and distance decay rates. Boxes show the relative values of ζ and ε between runs. Overall morphology is mostly similar, but there are clear differences in channelization as a result of the low runout distance in panel (a). Elevations are all at the same scale, the apex is ~100 m and average slope is ~1.5°

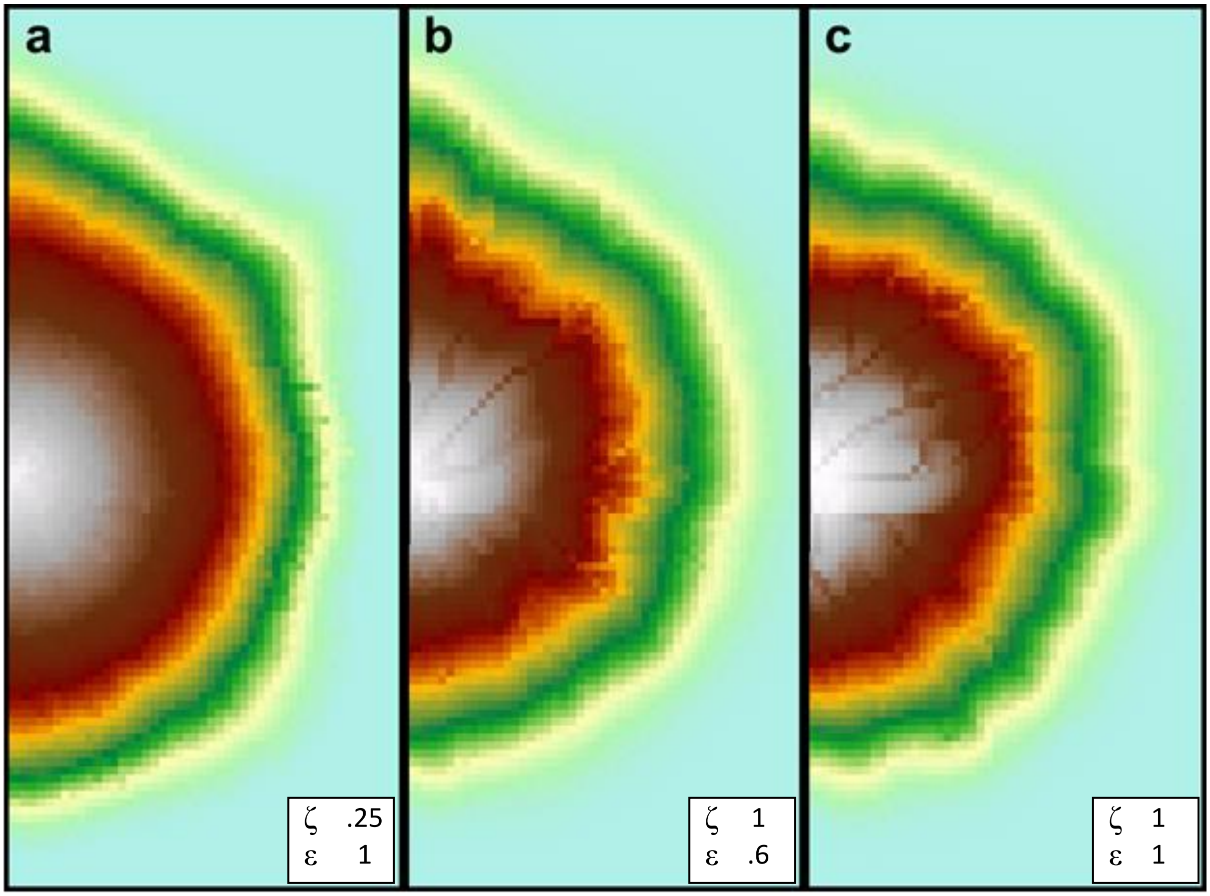

The distance and height decay rates of an overbank mudflow, which are essentially a measure of the flow's viscosity, have a major effect on the fan's surface morphology. Figure 4.4 shows the differences in fan surface from different overbank properties. Varying the distance coefficient ζ has a much larger effect on subsequent morphology than the elevation coefficient ε. Longer runout distances correlate with more developed channels due to a lower avulsion frequency.

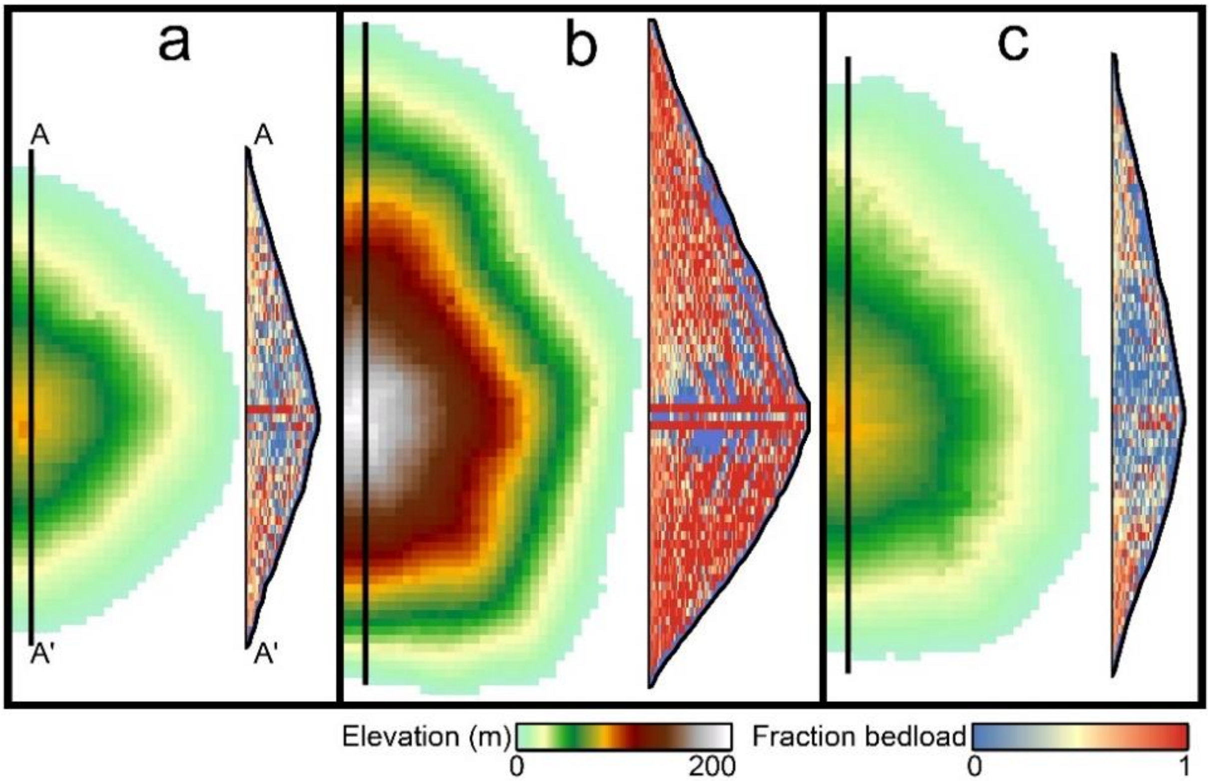

	a	b	c
D_{50}	.01	.003	.003
Q_s	.04	.07	.02

Figure 4.5. Effect of varying bedload size or volume on fan morphology. DEM on left, vertically exaggerated cross section stratigraphic profile on right. Cross section A-A' has a length of 6.5 km, all fans are shown at the same scale. The cross sections are color graded by depositional process, with blue being 100% overbank deposits and red 100% bedload deposits. All parameters other than those listed are held equal between runs. (a) Coarse bedload results in a smaller fan. (b) Relatively high bedload sediment flux. The fan is notably higher and steeper than the other two cases, and contains a much higher fraction of bedload sediment. (c) Relatively low bedload flux. The fan is large and gently sloped.

Figure 4.5 explores the effect of varying the volume and grain size of the input bedload sediment size. The fan fed by a coarse sediment size is relatively small. A large bedload sediment flux results in a large, steep (3.8°) fan, and its stratigraphy is dominated by bedload deposits. The low bedload flux fan is large with a gentle slope of 0.8°, and primarily consists of overbank deposits.

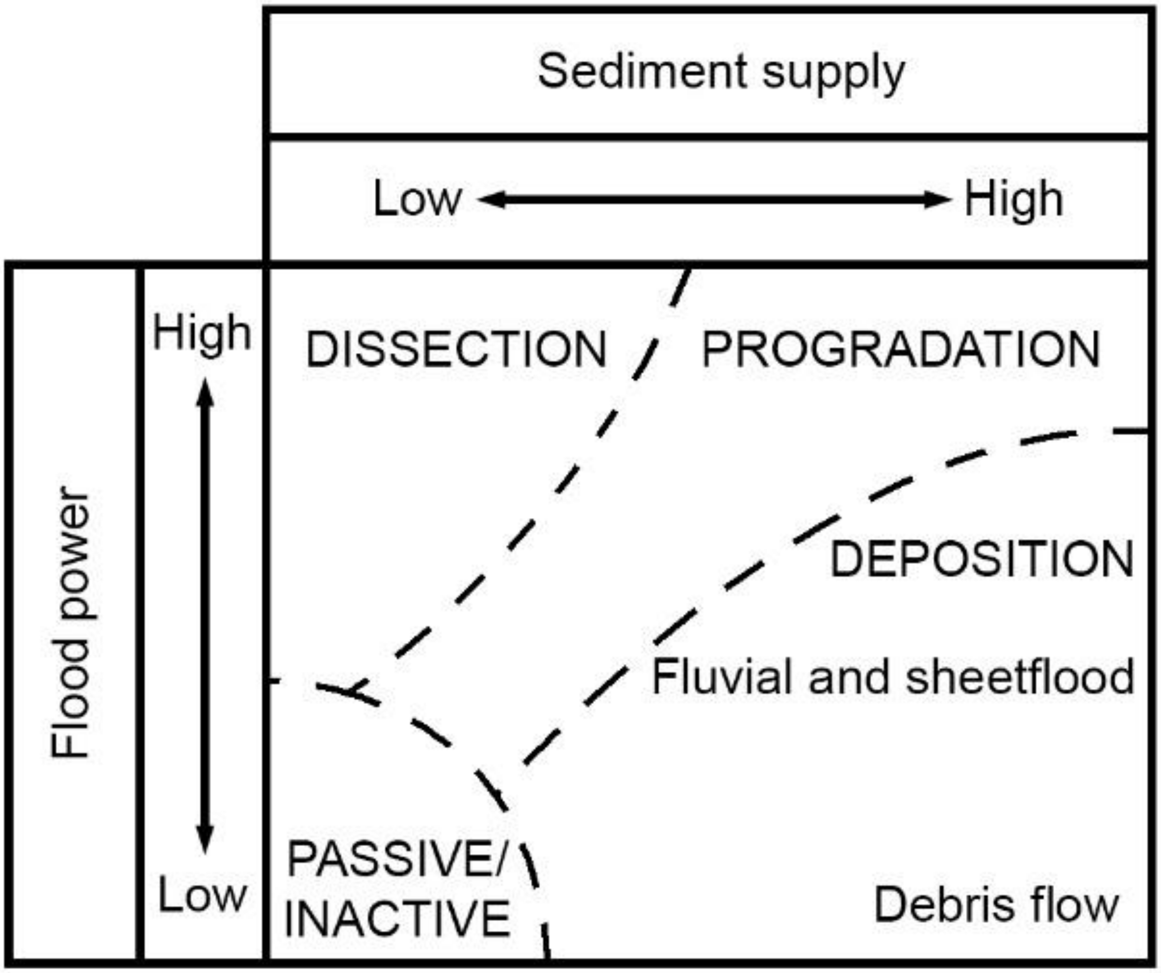

Figure 4.6. The expected response to an alluvial fan surface from changes in flood power and sediment supply. Adapted from Harvey (2012).

In a simplified model of extrinsic controls on fan surface response as shown in Figure 4.6, an increase in sediment supply leads to deposition, as the sediment load exceeds the flow capacity. Alternatively, an increase in flood power will result in dissection, and an increase in both sediment supply and flood power will result in fan progradation (Harvey, 2012). When subjected to changes in Q_f or Q_s, the model responds as expected in all three cases (Figure 4.7). With all else held equal, a doubling of input discharge promotes incision around the fan head, and previously deposited sediment is transported to the distal fan. A doubling of sediment with discharge held constant results in the infilling of channels near the apex and aggradation of the proximal fan. An increase in both discharge and sediment supply causes the fan to prograde. Interestingly, there are still well-developed channels during the progradation. On real world fans, flood power and sediment supply are controlled primarily by climate, and to a lesser degree also land use and tectonism. That the model responds appropriately to these inputs allows future use to study such processes.

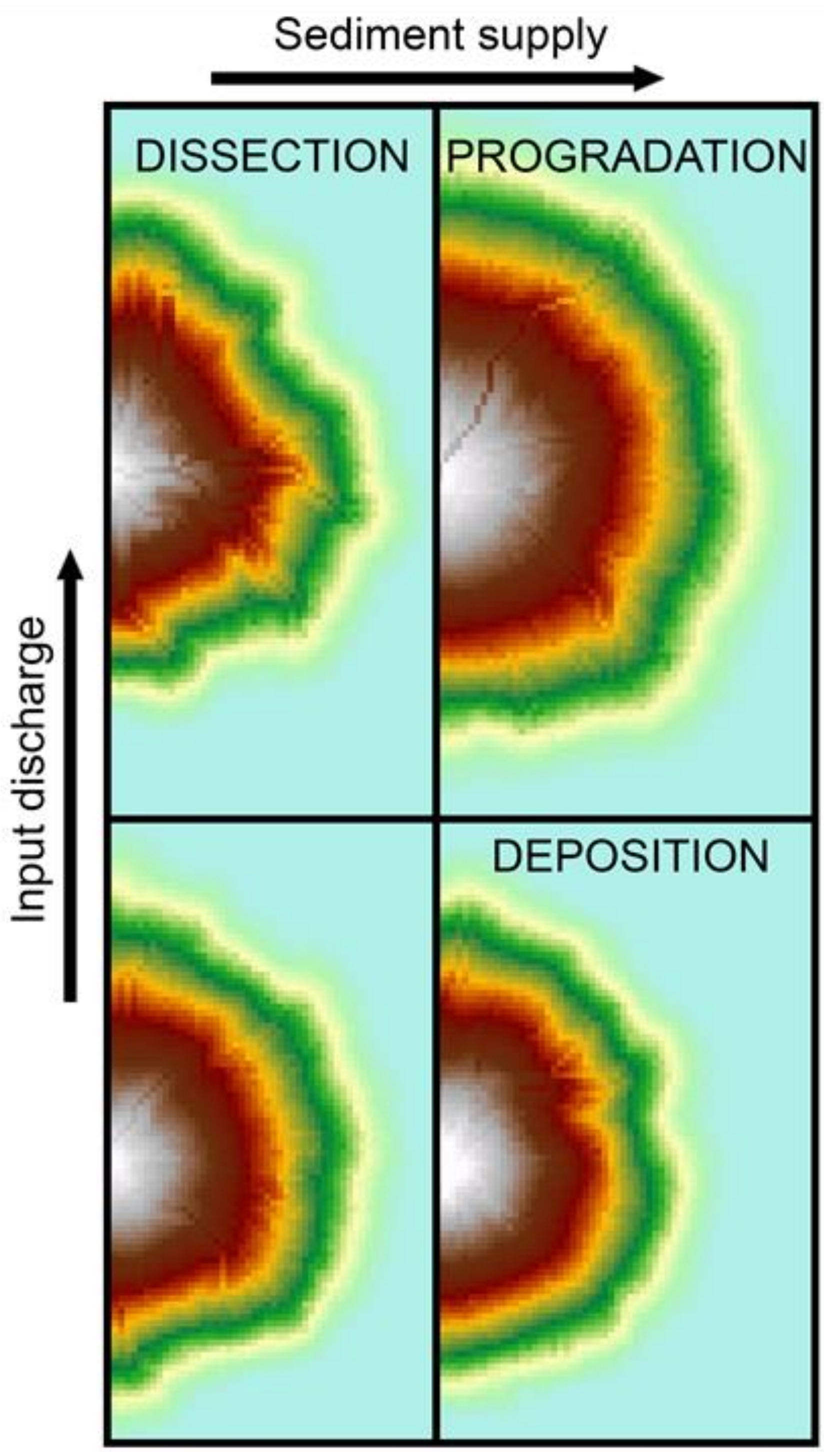

Figure 4.7. The effect of doubling discharge, sediment supply, or both on a fan's surface morphology. The length scale and elevation color gradient are arbitrary but equal for all frames. Bottom left frame is a fan 75% through a model run, and the other three frames show the fan at the end of the simulation when different boundary controls are imposed for the final 25% of the run. When discharge is increased without a corresponding increase in sediment supply, fan head trenching occurs, and sediment is removed from the proximal fan and deposited at on the distal fan (top left). When sediment supply is increased without an increase in discharge, channels at the fan head are filled in and deposition occurs near the fan apex (bottom right). An increase in both sediment supply and discharge leads to fan progradation.

4.5. Conclusions

The model successfully constructs an alluvial fan under a range of inputs, and has a realistic response to extrinsically forced changing boundary conditions. This model is a powerful tool that can be used to address a number of open questions regarding alluvial fans, including the effects of changing catchment properties to fan coupling (Harvey, 2012) and the effect of overbank deposition of fan morphology (Stock et al., 2008). When applied to Mars, the model can be used to investigate controls such as input sediment size, sediment flux, and varying discharge, which will yield insights into catchment lithology and formative climatic setting. Application to Mars will require careful approximation of input parameters such as overbank mudflow rheology and water to rock ratio. Other input parameters, including grain size, have been measured for martian fans.

Notation

a	Index denoting cell *a*
b	Index denoting cell *b*
B	Channel width
D_{50}	Grain size
dx	Cell size
g	Gravity
H	Channel depth
L_{ab}	Distance between adjacent cells *a* and *b*
mx,my	Domain dimensions
Q_f	Flow discharge
Q_s	Volume sediment discharge
r	Pseudorandom number between 0 and 1
R	Specific gravity
S	Gradient
α_c	Sediment transport constant
α_e	Sediment transport exponent
α_i	Flow intermittency
β	Avulsion parameter
γ	Flow distribution exponent
ε	Overbank elevation decay constant

ζ	Overbank distance decay constant
η	Elevation
θ_0	standard deviation of the path selection probability function
θ_{ab}	Angle between the line connecting cells a and be and the line connecting cell a to its downstream connection
ν	Fluid kinematic viscosity
ρ_f	Fluid density
ρ_s	Sediment density
τ_c^*	Critical Shields number at the onset of sediment motion
φ	Overbank sedimentation rate
μ	Suspended sediment flux

Chapter 5

Depositional processes of alluvial fans along the Hilina Pali fault scarp, Island of Hawaii

Published as: Morgan, A. M., Craddock, R. A. (2017). Depositional processes of alluvial fans along the Hilina Pali fault scarp, Island of Hawaii. *Geomorphology*, 229, 131–156. DOI: 10.1016/J.GEOMORPH.2017.08.028

Abstract. A series of previously unstudied alluvial fans are actively forming along the Hilina Pali escarpment on the south flank of Kīlauea volcano on the Island of Hawaii. These fans are characterized by their steep slopes, coarse grain sizes, and lobate surface morphology. Fans are fed by bedrock channels that drain from the Ka‘ū Desert, but sediment is mostly sourced from deeply eroded alcoves carved into the Hilina Pali. Examination of recent deposits indicates that the fans are dominantly constructed from gravel and larger sized sediment. Flow discharges calculated using field measurements of channel geometries and the Manning equation indicate that events inducing sediment transport are of high magnitude and occur during high intensity precipitation events, including Kona storms. The fans along the Hilina Pali appear to be a rare example of fans formed predominately from sieve lobe deposition owing to the area’s high slopes, high discharge, coarse bedload, and limited supply of fine-grained sediment. Given such conditions, sieve lobe deposition can form large lobes consisting of boulder-sized material, which may have implications for the identification of depositional processes when interpreting the stratigraphic record.

5.1. Introduction

Alluvial fans are depositional landforms that form where a sediment laden channel exits mountainous terrain onto a lower gradient surface. The reduction of carrying capacity and lateral spreading of the channel forces the deposition of sediment into a semi-conical shape. Alluvial fans form in environments with steep topography and sufficient sediment production and fluid discharge (Blair and McPherson, 2009). They occur in all environmental settings with fluid-driven sediment flow and sharp topographic relief, occurring not only on Earth, but also Mars (Moore and Howard, 2005) and Titan (Birch et al., 2016), the two other planetary bodies known to have had surface fluid flow.

Processes that provide sediment to alluvial fans are broadly defined as either sediment-gravity processes such as debris flows, or fluid-gravity processes, which include sheetfloods and incised channel flows (Blair and McPherson, 2009). When sediment-laden flow debouches onto a permeable, coarse-grained fan surface, water may infiltrate into the fan and the coarsest material in the flow acts as a sieve, permitting water and fines to transport through while coarser grains are deposited. Hooke (1967) described this process as sieve lobe deposition, and it was once widely used in alluvial fan literature to describe such processes and their subsequent deposits (Hooke, 1967, 1968; Bull, 1972; French, 1987; Nemec and Postma, 1993). This style of deposition is particularly prevalent in settings with a scarcity of fine-grained sediment, significant bedload, and permeable ground (Nemec and Postma, 1993). Later researchers argued that such conditions do not occur in nature and that the sieve lobe model is based on the erroneous interpretation of weathered, fine-winnowed debris flow deposits (Blair and McPherson, 1992, 1993, 2009). Following Blair and McPherson's (1992, 1993, 1994, 1995, 2009) rejection of the sieve lobe model, the term fell out of usage, but has recently been revived as a fundamental process in describing alluvial fan formation and architecture (Milana, 2010; Chen et al., 2017).

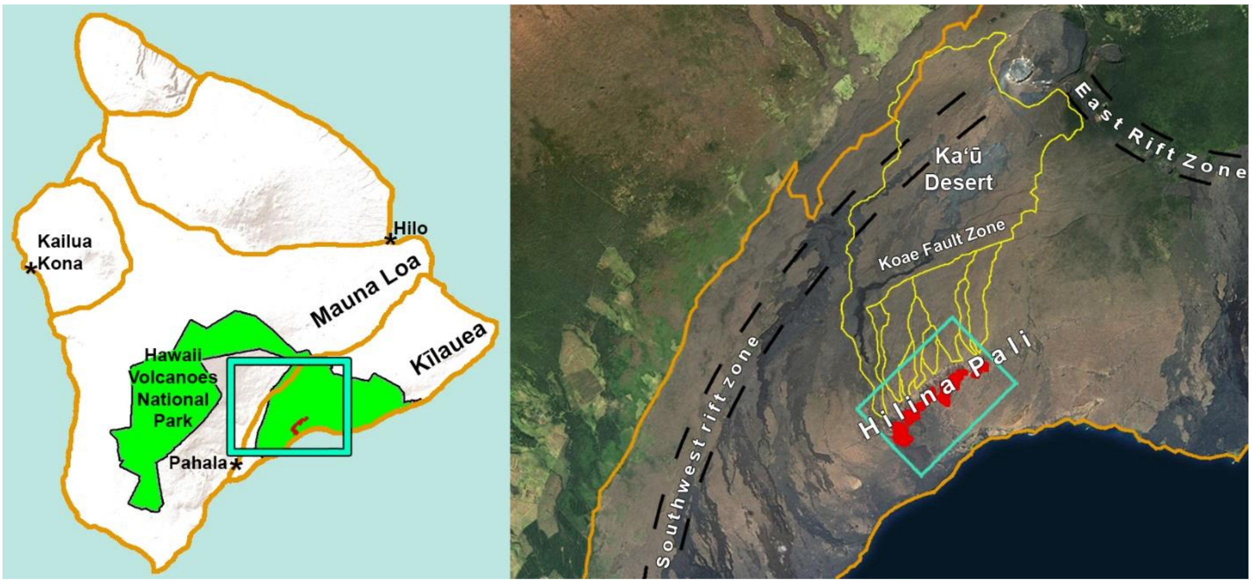

Figure 5.1. Overview of study region. Left: Map of the Island of Hawaii centered on 19.6°N, 155.4°W. Box indicates location of image on right. Right: Global Land Survey 2010 imagery of southeastern Island of Hawaii with features mentioned in text. Alluvial fans along the base of the Hilina Pali escarpment are outlined in red. ArcHydro-derived watersheds (see Section 5.3.2 for discussion) are outlined in yellow. The Koa'e Fault Zone directs all surface runoff from the northern Ka'ū Desert to fan F1. Box indicates the location of Figure 5.2a.

In this report, we describe a series of alluvial fans along the south flank of Kīlauea volcano on the Island of Hawaii. These landforms were included in the Wolfe and Morris (1996) geologic map as Holocene and Pleistocene alluvial and colluvial fill and have been noted in previous studies (Tunison et al., 1994; Craddock et al., 2006; Craddock and Golombek, 2016), but to date have not been studied in detail. We present results from a remote sensing study and field investigation of the fans, and describe our interpretation of the fan deposits as having formed dominantly from sieve deposition associated with the region's the limited availability of fine-grained sediment and steep slopes that assist bedload transport.

5.2. Geologic and climatic setting

Hawaii is the largest and most volcanically active island in the Hawaiian island chain. It is comprised of five volcanoes, the youngest of which is Kīlauea at an elevation of 1200 m. Eruptions occur both from the summit caldera and the two rift zones that radiate from the summit to the southwest and east (Figure 5.1). The north flank of Kīlauea is stabilized against the much larger Mauna Loa volcano, but the south flank is unstable and is moving seaward at a rate of ~6-10 cm/yr (Owen et al., 1995, 2000), though it may move catastrophically, such as the 3 m of displacement that took place during the 7.2 M 1975 Kalapana earthquake (Lipman et al., 1985). At the surface, this slippage is manifested as two normal fault systems, the Koa'e Fault Zone and the much larger Hilina Fault System along the coast. The 42 km long, up to 5 km wide, and ~9 km deep Hilina Fault System's subaerial component is dominated by the 500 m high Hilina Pali escarpment.

Label	**Name**	**Apex latitude** (°N)	**Apex longitude** (°W)	**Fan area** (km^2)	**Fan length** (km)	**Fan Relief** (km)	**Fan slope** (°)	**Alcove area** (km^2)	**Alcove relief** (km)	**Watershed Area** (km^2)
F1	Sand Wash	19.269	155.333	0.38	0.91	0.09	5.6	0.19	0.24	66.34
F2	Pohakaa Arroyo	19.273	155.329	0.27	0.56	0.09	9.0	0.23	0.31	4.67
F3	N/A	19.276	155.326	0.08	0.42	0.14	18.4	0.12	0.25	0
F4	Moo Arroyo	19.276	155.324	0.08	0.30	0.06	10.5	0.08	0.36	1.10
F5	Ahiu Valley	19.279	155.321	0.08	0.31	0.13	22.9	0.15	0.31	1.79
F6	N/A	19.282	155.319	0.06	0.39	0.18	24.7	0.08	0.32	
F7	Nanahu Valley	19.285	155.315	0.27	0.62	0.14	12.4	0.10	0.36	1.07
F8	N/A	19.288	155.309	0.28	0.85	0.14	9.2	0.11	0.35	5.80
F9	N/A	19.289	155.307	0.06	0.35	0.13	19.9	0.05	0.30	
F10	N/A	19.289	155.305	0.03	0.15	0.06	23.0	0.03	0.31	
F11	Kahele Valley	19.291	155.299	0.06	0.40	0.08	11.4	0.05	0.27	1.15
F12	N/A	19.293	155.297	0.09	0.38	0.09	13.1	0.05	0.24	3.57

Table 5.1. Properties of Hilina Pali fans.

Station	Location	Elevation (m)	Distance (km)	Years	Highest Daily Total Precipitation (mm)		Total Annual Precipitation (mm)	
					Decadal average	Decadal max	Decadal average	Decadal max
HALEMAUMAU 52, HI US	19.4°N, 155.28°W	1110	8.2	1951-1959	193.8	291.1	2634.3	3687.8
				1960-1969	148.6	298.2	2630.0	3359.9
				1970-1979	60.8	238.8	2722.9	3603.5
				1980-1989	151.8	328.9	2672.1	3445.0
				1990-1999	126.1	286.0	2755.5	4657.3
				2000-2008	225.0	331.7	2793.6	3372.6
				2011-2012	NoData	NoData	1871.1	1872.0
KEALAKOMO 38.8, HI US	19.29°N, 155.14°W	110	15.5	1996-1998	NoData	NoData	1476.7	2200.4
				2004-2008	NoData	NoData	1576.9	1777.7
KAPAPALA RANCH 36, HI US	19.28°N, 155.45°W	635	18.7	1953-1955	NoData	NoData	1271.9	1470.9
				1983-1988	NoData	NoData	1247.7	1668.5
				1990-1999	NoData	NoData	1532.6	2744.2
				2000-2009	NoData	NoData	1361.9	1937.0
				2010-2010	NoData	NoData	462.5	462.5

Table 5.2. Weather data for the southern Kīlauea region. Distance column indicates the distance from each weather station to an approximate center point of the Kaʻū Desert region (located at 19.33°N, 155.31°W, elevation 890 m).

Twelve distinct fan landforms exist along the base of the Hilina Pali (Figure 5.2 and Table 5.1). The fans are fed by channels that have carved deep alcoves into the Hilina Pali (Figures 5.2 and 5.3) and drain the Kaʻū Desert, on the leeward flank of the Kīlauea volcano. The Kaʻū Desert receives ~1300 mm of rainfall annually (Giambelluca and Sanderson, 1993), so it is not a true desert but rather a chemical desert because of sulfuric aerosol fallout from the summit caldera that inhibits vegetation growth (Schiffman et al., 2000). No weather stations record precipitation in the Kaʻū Desert, but several NOAA weather stations exist in the surrounding area (Table 5.2).

Volcanic eruptions along the Southwest Rift Zone occur frequently, and the Kaʻū Lava Ramp is regularly resurfaced. Geologic mapping and radiometric-derived ages indicate that the oldest surfaces in the Kaʻū Desert are <750 yr old (Wolfe and Morris, 1996) and consist of lavas, splatter cones, and tephra. The Kaʻū Desert is bisected by the 10-20 m high, 12 km long, and 2 km wide Koa'e Fault Zone that connects the rift zones south of the Kīlauea summit caldera ~4 km upslope from Hilina Pali and is the smaller subaerial expression of the south flank slip. The Koa'e system as a whole is likely a long-lived feature (Podolsky and Roberts, 2008), but from lava flow stratigraphy, current rates of seaward displacement, and oral records of native Hawaiians, Duffield (1975) estimated that most of the observable displacement has occurred in the past 500 yr. The water table depth at Kīlauea summit is 490 m (Keller, 1974), and groundwater in the Kaʻū Desert is essentially nonexistent except immediately following precipitation.

The main bedrock formation exposed along the Hilina Pali escarpment is a 300 m thick portion of the Hilina Basalt, consisting of pāhoehoe and ʻaʻā lava flows (95% of exposure) with interspersed ash layers (5% of exposure) (Easton, 1987). Layers of pāhoehoe and ʻaʻā both show evidence for surface weathering, with the pāhoehoe lava layers having lost ~1-10 cm of material and the ʻaʻā clinker zones having been partially to totally weathered to a reddish-brown clay (Easton, 1987). The Hilina Pali is overlain by the ~15 m thick, 31±0.9 ka Pahala ash and the ~50 m thick, < 23 ka Puna Basalt formations, which is capped by the 5-12 m thick, ~500 yr old Keanakākoʻi ash (McPhie et al., 1990). The total thickness and age of the Hilina Basalt is uncertain, but ash layers near the base of the exposed lavas date from ~100 ka (Easton, 1987).

Figure 5.2 (next page). Alluvial fans along the Hilina Pali escarpment. Top: Map of alluvial fans and alcoves. Submeter orthoimagery overlying 10 m USGS DEM. NHD channels are those included in the National Hydrogeography Dataset. Named valleys and channels are indicated. Bottom: Long profiles of fans (2x vertical

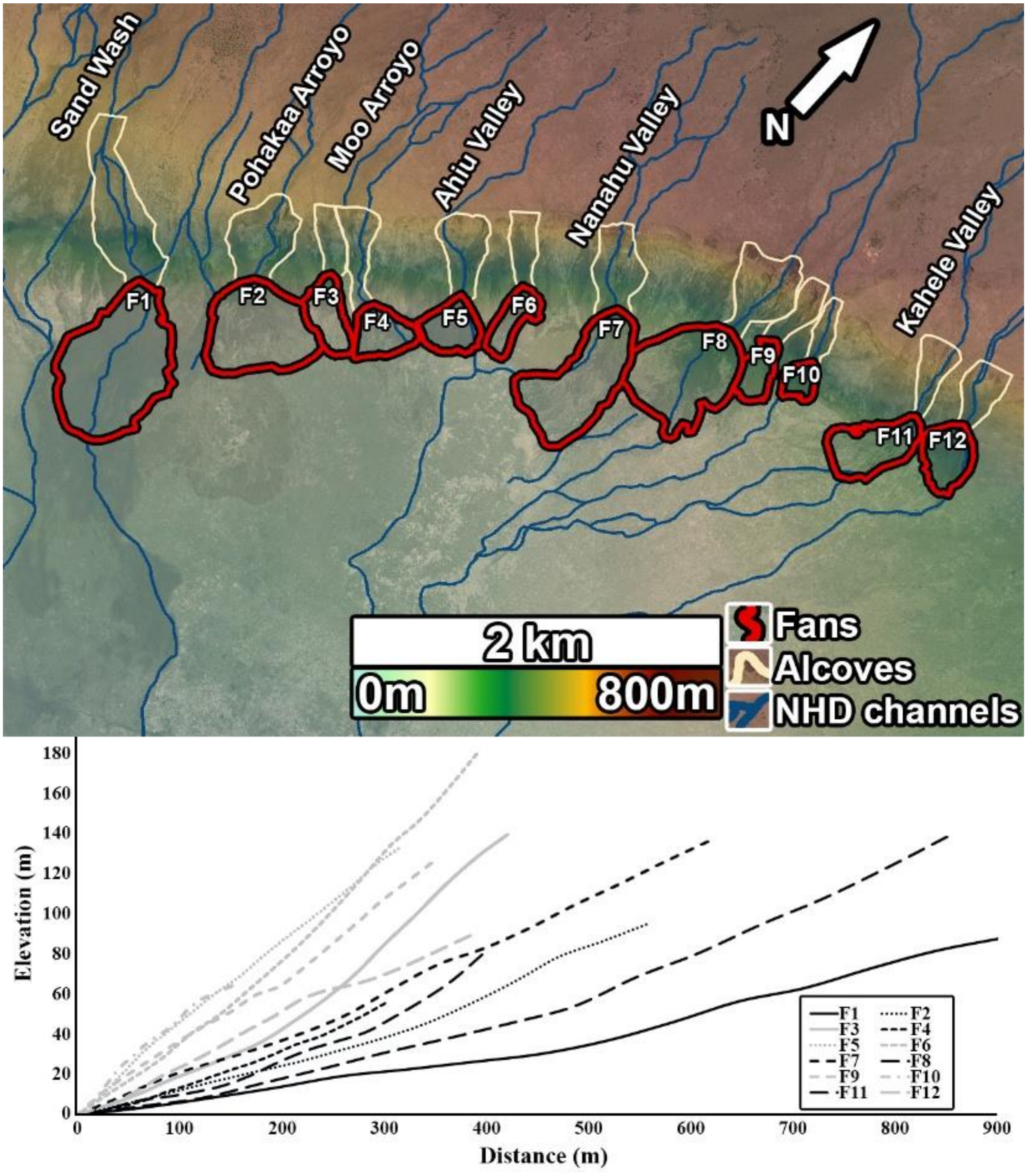

5.3. Methods and data

The primary remote sensing datasets we used in our analyses are a digital elevation model (DEM) with a 10 m horizontal resolution and ~5 m vertical accuracy (Sugarbaker et al., 2016) and public domain aerial orthoimagery with resolution of ~0.25 m (USGS, 2010). We define the fan apex as the location where contours shifted direction from concave (convergent flow) to convex (divergent flow), lateral fan boundaries by an abrupt end of convex form, and fan toes by the sharp change in slope and an end to convex contour orientation. We measured a number of morphometric properties, including fan size, gradient, feeder channel geometry and relief, and watershed area.

We generated longitudinal profiles using 13 points along each transect: the fan toe, five equally spaced points along the fan, fan apex, seven equally spaced points along the alcove, and the upper edge of each alcove where it met the feeder channel. We took the average elevation within a 15 m radius around each point to compensate for the roughness of the fan and alcove surface.

Feeder channels were mapped both visually using the orthoimagery and by using a D8 algorithm within ArcHydro to derive flow accumulations, extract watersheds, and discern flow paths from the DEM. The terrain is difficult to traverse, consisting of a number of overlapping, undulating older lava flows, and the area is also extensive (~30 km^2), so we did not bring heavier surveying tools such as differential GPS, which would have required establishing several base stations. Every 300-500 m along the course of each channel, we measured cross sections using a measuring tape, tracking our location using handheld GPS (horizontal accuracy ~4 m). We determined surface grain size distributions by taking photographs of sediment within a one square meter area and measuring the size of each grain in Adobe Photoshop. In addition, we collected bulk samples of sediment and measured particle size distribution using standard dry sieving techniques (for sand and gravel) and laser diffraction analysis of dispersed samples.

Quantifying the flow rates and discharges responsible for the transport and deposition of fan sediment is necessary for interpreting the fan-forming processes. None of the channels are gauged, and anecdotal reports of discharges during flow events are rare. We used the Manning (5.1) and continuity (5.2) equations to estimate flow velocity U (m/s) and discharge Q (m^3/s):

$$U = \frac{1}{n} R_h^{2/3} S^{1/2} \tag{5.1}$$

$$Q = U A_{XS} \tag{5.2}$$

where R_h is the hydraulic radius (ratio of channel cross-sectional area A_{XS} (m^2) to wetted perimeter), S is slope (m/m), and n ($s/m^{1/3}$) is the Manning-Gauckler roughness coefficient.

We used values of $n = 0.03$, 0.05, and 0.07 for the bedrock floored channels (Chow, 1959). We measured gradient using a Laser Technology TruPulse 200 rangefinder, which has ±0.25° inclination accuracy and ±30 cm distance accuracy. In every instance, laser rangefinder slope measurements of channel sections were within ±2° of the values we extracted from the DEM. Our method of flow depth measurements varied between sites. In some locations, we were able to directly measure a flow depth from vegetation debris or slack water deposits at the high-water mark of channel flow, but at other areas we estimated depth by calculating the required flow shear stress necessary to transport observed sediment on the channel bed. The critical shear stress τ_c (N/m^2) required to transport sediment of diameter D (m) is:

$$\tau_c = \tau^* (\gamma_s - \gamma_f) D \tag{5.3}$$

where γ_s and γ_f are the specific weights (density ρ (kg/m^3) times gravity g (m/s^2)) of sediment and water, respectively, τ_* is the dimensionless boundary shear stress (Shields coefficient), and D is the grain diameter. The shear stress on the channel bed τ_b is:

$$\tau_b = \rho_f g h S \tag{5.4}$$

where h is flow depth (m). At the initiation of sediment motion, $\tau_b = \tau_c$. Equating Eqs. (5.3) and (5.4) yields a threshold flow depth

$$h = \left(\tau_* D \left(\rho_s - \rho_f\right)\right) / (S \rho_f) \tag{5.5}$$

Shields (1936) showed that a value of $\tau_* = 0.045$ is applicable to a wide range of boundary Reynolds numbers, although τ_* has been shown to vary between 0.03 and 0.06, depending on sediment sorting and particle shape (Komar, 1988), so we calculated depths at a range of values.

The primary sources for error in the above calculations are the values of flow depth, bed roughness, and slope. Channels exhibit extreme diversity in terms of roughness and amount of bedload sediment (Figures 5.3c-d), and the channel course is partially defined by lava surface morphology and locations of collapsed lava tubes. We therefore used conservative values and stress that any estimates of discharge are rough approximations. Use of multiple methodologies and realistic required precipitation rates offer some check of discharge reliability.

5.4. Morphologic and morphometric observations

5.4.1. Fan observations

All the fan surfaces are dominated by a ~2 m thick mantle of boulders, cobbles, and gravels (Figure 5.3a). Some boulders are up to a meter in diameter. Gravels are packed between larger grains with no interclast matrix, and there is virtually no sediment finer than coarse sand in the upper few meters. We observed little contrast in sediment size, sorting, or angularity between the proximal, medial, and distal fan regions on the higher gradient fans (those with mean surface slopes >13°), but on the lower gradient fan surfaces particles noticeably decrease in size with distance downfan. The mantle is less obvious in the distal fan deposits, but this is partially due to obscuration by a grass cover.

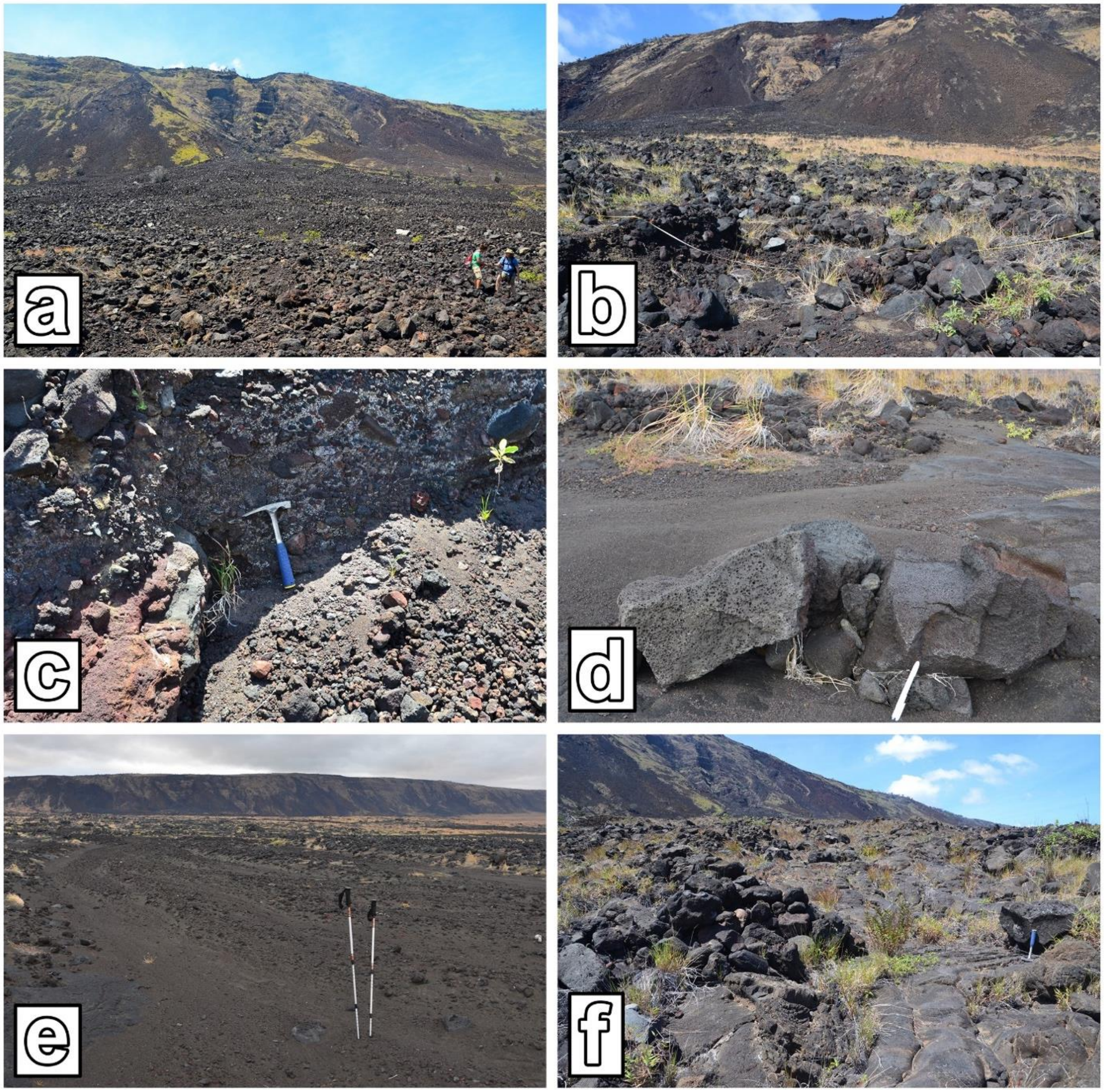

Figure 5.3. Photographs of fans at the base of the Hilina Pali escarpment. Alcoves are visible at the top of (a), (b), and (f). (a) Fan F8. Large blocks, some up to a meter in diameter, make up a mantle capping the fan. (b) Levee deposits on distal portion of fan F2, note tape measure for scale. (c) Fan material at the base of a channel adjacent to a lobe. Deposits are clast supported and unlayered. Flow is to the left. (d) Imbricated clasts just downstream from the toe of fan F1, note pen for scale. Flow is to the right. (e) Gravel and sand splay near toe of fan F1. (f) Bedrock at the base of channel on distal part of fan F11. Note rock hammer for scale at center right.

Viewed in aerial orthoimagery the lower gradient fans feature channels radiating from the fan apex with some degree of sinuosity, but from the ground these can be difficult to discern (Figure 5.4). On the proximal fan, channel locations are defined by radially lobate deposits reminiscent of debris flow material but lacking an interclast matrix. Lobes are typically tens of meters in length, and have frontal dimensions on the order of meters. Channels contain an appreciably higher concentration of gravels than do the lobes, and sediment imbricated in relation to the flow downchannel consists primarily of poorly sorted, angular to subangular, fine gravel to cobble sediment (Figure 5.3). Sediment in the channel bed of the fans was found to contain a higher proportion of finer grained (fine sand) sediment than the feeder channels (Figure 5.5). In the aerial imagery, channels are less than 10 m wide and not generally traceable for more than ~100 m on each fan, but become more organized and discernable past the fan toe. The exception to this is the westernmost fan F1 (see Figure 5.2 and Table 5.1 for labeling notation) that has a main channel that can be traced from the apex to the coastline, albeit with many branches and merges. We did not observe much channel incision into previously-emplaced fan deposits, but in places channel wall exposures did reveal that below the surface boulder-cobble-gravel mantle, sediments are cemented, clast supported, medium sorted, and subangular (Figure 5.3c).

The observed higher gradient fans have sharply defined toes, with very little or no sediment being transported beyond the main fan. The lower gradient fans feature levees that extend outward beyond the fan toe (Figure 5.3b). These consist of gravels and cobbles with a portion of sand that increases with depth, but overall levees are largely grain supported with no interclast matrix. Beyond the fan toes, cobbles and boulders up to 30 cm diameter are imbricated in relation to the downstream direction (Figure 5.3d) and splays of gravel radiate from the channels. We map these as “extended fan”, in that they consist of transported fan material but lie beyond the convex contours that define the fan.

Figure 5.4 (next page). Top: portion of fan F8 (outlined), north is towards the top of image. Circle indicates location of bottom photo. Note light-colored (vegetated) sinuous channels on medial to distal fan deposits. Channels are also present on the proximal fan, but are less obvious from aerial imagery due to lack of vegetation. Bottom: Channel lined by lobate features, photo is looking in the downslope direction.

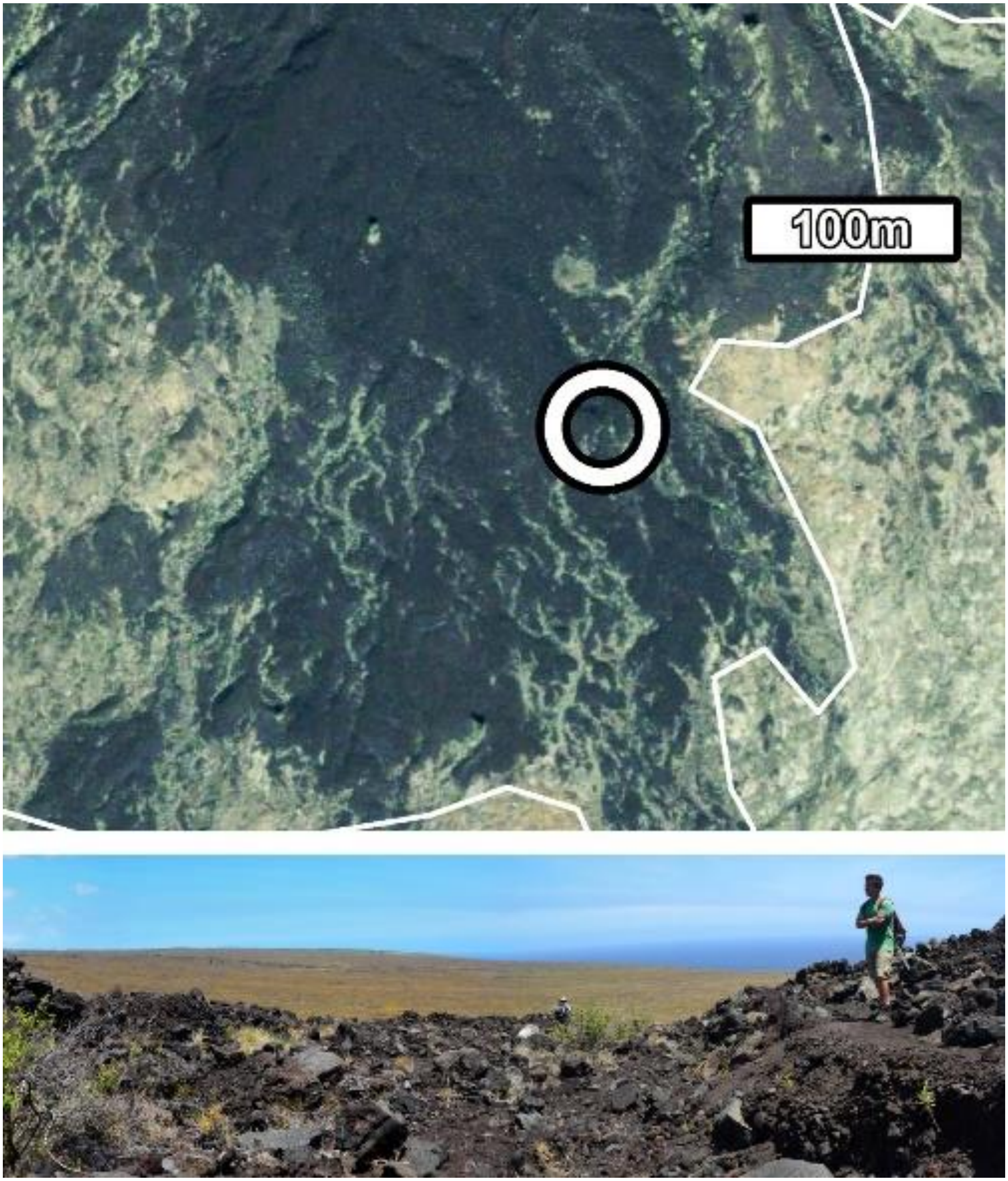
100m

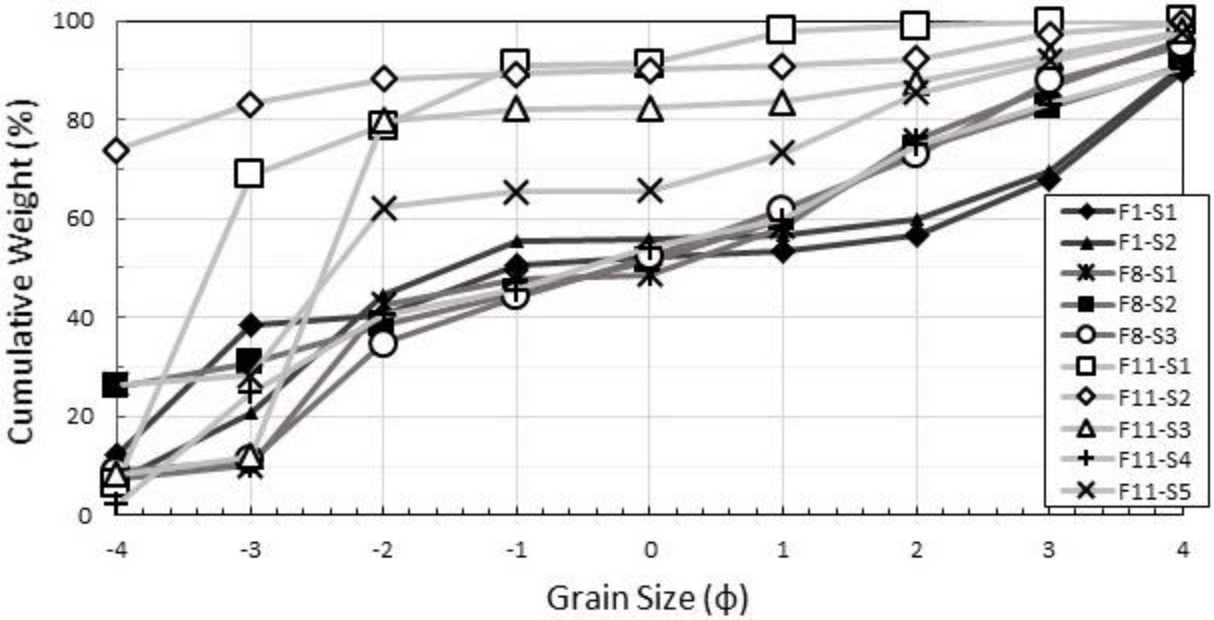

Figure 5.5. Grain size cumulative curve for collected gravel and sand sized sediment. Sediment was measured at 1φ intervals. White markers indicate samples collected at feeder channels, black markers indicate samples collected from fan surfaces.

Lava flows are stratigraphically interspersed with fan deposits. For example, fan F2 is depositing on and reworking the surface of a previously emplaced ‘a‘ā flow along the base of the pali, and portions of fan F11 have been covered by ‘a‘ā lavas. In areas fan channel floors were bedrock channel (Figure 5.3f), having incised through fan material to a layer of previously emplaced lava.

5.4.2. Feeder channel observations

The fans are fed by ephemeral bedrock channels sourced from the Ka‘ū Desert that have carved deep alcoves into the Hilina Pali above each fan, which appear to be the main sources of fan sediments. Upstream from the alcoves, channels erode into lava, ash, and layered scoria deposits (Figure 5.6a). Channel beds occasionally consist of clean, smooth bedrock, but at most locations we observed grain sizes ranging from medium gravel to cobbles tens of centimeters in diameter (Figure 5.6b).

Figure 5.6. Feeder channel observations. Top left: Feeder channel has eroded into previously-emplaced layered scoria. Top right: imbrication of large clasts in bedrock channel feeding fan F11. Bottom: diversity in bed roughness and presence of bedload material in feeder channels. From left to right, channels range from smooth bedrock with no sediment clasts, rough bedrock with no sediment, rough bedrock with sediment (gravels and cobbles) covering channel floor, to smooth bedrock with extensive sediment on the channel bed.

The interaction of channels and lavas makes for a complicated and dynamic system. Lava flows will preferentially flow down eroded fluvial channels, and subsequently the fluvial channels will establish new pathways. Many of the channels we observed have not had time to equilibrate into the landscape, so they have very unsteady local gradients. Separating discernable channels that were primarily fluvial features from those that were primarily lava flow features was often difficult. For example, several feeder channels are located in collapsed lava tubes, and the channel feeding fan F11 is undergoing headward erosion above the main pali escarpment that appears to be driven by the emergence from a lava tube. Consequently, the drainage networks feeding the fans are poorly defined, and are generally not discernable either from aerial imagery or on the ground beyond ~2 km upstream from the main Hilina Pali escarpment. The only exception is the channel network feeding fan F1, which drains a large gully known as Sand Wash that has incised the Keanakākoʻi Tephra deposit directly west of the Kīlauea summit caldera (Craddock et al., 2012). The Koa'e fault zone directs all runoff north of ~19.32°N into the channel feeding F1. Water could be transported below the surface through rock fractures and lava tubes, but the degree to which subsurface water could flow in such a manner to bypass the Koa'e fault zone is poorly constrained.

5.4.3. Hydrology

We focused our hydrology study on fan F11, which is fed by a relatively well-organized channel network that does not intersect with the other fan drainage areas. Many of the other fans share watersheds and channels feeding the fans anastomose. In addition, F11 and its feeder channel were relatively easy to access, and the fan is similar in size, gradient, and grain size to all of the other lower-gradient fans with the exception of F1. The primary channel feeding F11 is bedrock floored with grains ranging in size from medium gravels to large cobbles, which is much smaller than much of the material present on the fan surface. Using the methods described in Section 3, we estimated channel discharges ranging from 2-10 m^3/s (Table 5.3). Multiple methods of discharge calculation yielded similar results within a half order of magnitude. Infiltration rates across most of the Kaʻū Desert are not well constrained. There is a thin (<.25 m) sandy soil cover associated with vegetation over the region within ~1 km distance from the Hilina Pali, but the surface over most of the Kaʻū Desert is solid lava, with permeable structures such as joints and lava tubes that could either store water or transport it downslope to the Hilina Pali. Assuming near-complete runoff, our calculated discharges suggest precipitation rates of 5-30 mm/hr.

Site	D_{84} (m)	Slope (m/m)	Depth (m)		U (m/s)	Q (m^3/s)	Runoff (mm/hr)
			Measured	Calculated			
F1-1	0.49	0.11	0.27	0.23-0.46	0.39-5.50	0.39-6.53	0.19
F1-2	-	0.11	0.28	-	0.52-1.22	0.52-1.22	0.05
F1-3	-	0.07	0.29	-	0.92-2.16	0.92-2.16	0.08
F2-1	0.25	0.02	-	0.77-1.54	0.84-4.77	0.84-62.0	24.22
F8-1	-	0.11	0.23	-	0.82-1.92	0.82-1.92	0.85
F8-2	-	0.11	0.27	-	0.97-2.28	0.97-2.28	1.01
F8-3	0.95	0.07	-	0.73-1.46	1.53-8.60	1.53-71.2	22.57
F8-4	0.26	0.02	0.44	0.81-1.62	0.24-5.08	0.24-86.7	26.98
F11-1	-	0.11	0.14	-	0.70-1.65	0.70-1.65	3.68
F11-2	0.35	0.11	-	0.18-0.36	0.39-4.96	0.39-7.98	13.10
F11-3	0.40	0.07	-	0.31-0.62	0.49-5.07	0.49-9.32	15.35
F11-4	0.35	0.02	-	1.09-2.18	1.30-5.52	1.30-95.3	88.59
F11-5	0.43	0.11	0.23	0.20-0.40	0.97-5.30	0.97-6.74	12.07
F11-6	0.38	0.11	0.20	0.19-0.38	0.93-4.77	0.65-4.47	8.01
F11-7	0.70	0.07	0.38	0.54-1.08	1.06-6.07	1.06-15.9	26.55

Table 5.3. Estimates of flow velocities using equations (5.3) - (5.7). Depths, velocities, and discharges were calculated for a range of roughness coefficients and Shields parameters (see Section 5.3), and we averaged these to obtain runoff rates. The low calculated runoffs for fans F1, F2, and F8 are due to the disorganized mature of their feeder channels and the unconstrained total drainage areas. Fan F11 had the most well-defined channel network.

5.4.4 Morphometry

We used an interpolation function on the DEM to estimate fan and eroded alcove volume, a comparison of which can provide an assessment of the source of fan sediment and a formative timescale. However, observations of lavas interspersed with fan deposits suggests that the estimated volume of fan sedimentary material should be treated with caution. We did find a statistically significant (at the 5% level of significance) high correlation (R^2 = 0.86) between fan surface areas and eroded alcove volumes, leading us to infer that sediment is dominantly sourced from the alcoves rather than transported from farther upstream. Supporting this is our observation that material comprising the fans was much larger than what we observed within the feeder channels upstream from the alcoves. We infer that the young age of the Kaʻū Desert lavas (<750 yr (Wolfe and Morris, 1996)) results in poorly organized channels that cannot effectively erode the surface, the lack of vegetation reduces weathering and transportable sediment production, and aeolian activity quickly removes or reworks any generated sediment. Upon reaching the much steeper Hilina Pali, the channel bed shear stress increases, allowing for the transport of larger sediment, and flow can more easily pluck exposed lava layers along the Hilina Pali than the smooth Kaʻū Desert lavas. Additionally, the highly-fractured lavas could possibly provide conduits for water to seep into the subsurface and travel through lava tubes before discharging at the Hilina Pali escarpment.

Researchers commonly characterize alluvial fans by the relationships between fan gradient or fan area with catchment area, basin relief, and sediment grain size (Harvey, 2011). The individual watersheds feeding each fan are not well constrained. We did not find any statistically significant relations between fan properties and watershed size, relief, or gradient, likely due to lava flows and tectonic activity constantly changing Kīlauea's surface topography. However, regression analyses indicate statistically significant (at the 5% level of significance) relationships between several morphometric parameters (Table 5.4). We report derived watershed areas (using ArcHydro tools on the 10 m DEM) in Table 5.1, but for our morphometric regression analyses we instead used the areas of the alcoves carved into the Hilina Pali. As discussed above, we believe this it is reasonable since the bulk of sediment making up the fans appears to be sourced from the eroded alcoves. The relation between basin area A_b and fan area A_f or gradient G is typically expressed as a power function, $A_f = pA_b^q$, with values for exponent q~0.7 to 1.1 and constant p ~0.7 to 2.11 (Harvey, 2011), a range that excludes the values of q=1.3 and p=2.9 that we derived for the pali fans. We did not find a statistically significant relation between fan gradient and alcove area. This could be due to our use of eroded alcove rather than watershed basin for the source area, as having the entire watershed as a water source affects flood discharge and water to sediment ratios, which will have an effect on fan size and gradient. That our values lie outside the range summarized by Harvey (2011) could be due to the steep nature of the eroded alcoves not fitting well with the area-area relation. Interestingly, values for the pali fans match those obtained from measurements of alluvial fans in southern Argentina described by Milana (2010) as having been formed almost entirely from sieve lobe deposition.

Dependent Variable	**Independent Variable**	***p***	***q***	R^2	***p*-value**
Fan area	Alcove area	2.94	1.34	0.73	0.0004
Fan area	Alcove gradient	0.36	-0.24	0.37	0.0359
Fan area	Basin area[1]	12.81	0.59	0.17	0.2131
Fan area	Basin gradient	0.07	-0.22	0.38	0.0452
Fan gradient	Alcove gradient	1.15	0.42	0.43	0.0215
Fan gradient	Fan area	0.02	-1.25	0.61	0.0028
Fan gradient	Basin relief	0.03	-0.86	0.42	0.0311
Fan surface area	Alcove volume	0.03	0.71	0.86	0.0006

Table 5.4. Morphometric relations fit to the equation $Y = pX^q$, where Y is the dependent variable, X is the independent variable, p is the multiplicative coefficient, and q is the exponent. Fan surface area derived from the 10 m DEM was used as a proxy for volume (see Section 5.4). Basin properties are for the drainage basins found within ArcHydro. [1]Fan area:basin area was not found to be statistically significant (p-value=0.213) but is included for comparison with the fan:alcove analyses.

5.5. Discussion

Our calculated runoff rates suggest heavy rains are responsible for the transport of the observed bedload sediment, which are not uncommon on southern Hawaii. Many of the largest rainfall events are associated with slow-moving, subtropical cyclones known locally as “Kona storms” (Simpson, 1952), named because the winds are often easterlies or, in other words, blow from the Kona side of Hawaii. For example, during a Kona storm on 19 February 1979 the Kaʻū Desert received over 400 mm of rainfall in a 24-hr period (Kodama and Barnes, 1997). Other events that can deliver hundreds of mm/day of precipitation include cold fronts, cold-core upper troposphere toughs, and tropical systems (Kodama and Barnes, 1997). There is very little soil across much of the Ka‘ū Desert, so storms would result in high runoff and channel discharge. Kona storms have been found to be responsible for initiating sediment movement and channel discharge in the continuous deposit of the Keanakāko‘i tephra located near the summit of Kīlauea (Craddock et al., 2012).

The sharply defined toes and lack of channels on the higher gradient fans are indicative of formation by rock falls. The processes responsible for constructing the lower gradient fans is more difficult to discern. In most settings, the dominantly coarse grain size, steep slopes, and low concavity of the fans would suggest an origin from debris flows (Blair and McPherson, 2009). Debris flows are common on alluvial fans due to the long timescales in between flow events during which large volumes of sediment can accumulate in the source area. Debris flows are capable of carrying larger grains than ordinary fluvial flows due to the ability of the suspended sediment to assist in sediment transport. Fine-grained particles (mud or finer) reduce permeability, trapping water within the flow and greatly increasing the internal hydrostatic pressure. Debris-flow initiation can also be affected by the distribution and angularity of larger particles, with medium to coarse sand and angular clasts hindering debris flow initiation by increasing permeability (Blair, 1999). The clearest evidence we observed for debris-flows deposits were sets of paired levees in the distal portions of fans, but these were rare, and do not appear to constitute the bulk of fan sediment. We did not find any deposits in the feeder channels or on the fans that contain a significant portion of sediments fine enough (e.g., mud or silt) to reduce permeability and initiate a transition from fluvial-dominated transport to a debris flow regime. This could be due to secondary winnowing by wind or low intensity runoff, but we also found no evidence of layering indicative of debris flows or distinctive facies within the exposed fan stratigraphy. For these reasons the lower gradient Hilina Pali fans appear to be a rare example of fans that have formed dominantly from sieve deposits. This depositional process was formally defined by Hooke (1967) as a gravelly clast supported, highly permeable, moderately sorted, lobate shaped deposit that forms when water infiltrates before reaching the fan toe. Blair and McPherson (1993) posited that such deposits have not been observed in nature and that so-called sieve lobes form from the winnowing and removal of fines from a matrix-supported debris flow by subsequent water flows. They suggested that the term should be used only to describe hypothetical deposits observed in laboratory experiments. However, Milana (2010) described a series of fans built almost entirely from sieve deposits in San Juan Province, Argentina, and inferred the required formative settings to be “a scarcity of fine sediment, significant bedload, high slope, permeable ground, and discharges moderate enough to allow infiltration.” The Hilina Pali fans meet all of these conditions. The sieve depositional lobes present on these fans are somewhat larger than those described on fans in the Death Valley region or Argentina (Hooke, 1967; Milana, 2010), but this is likely due to the very large sediment size (boulders) of deposited sediment making up the lobes.

There is virtually no soil across most of the Kaʻū Desert, and the limited available sand or finer-sized sediment is primarily reworked tephra that is transported as dunes by the northeasterly trade winds to the southern Kaʻū Desert. There are multiple ash members within the Hilina and Puna Basalts exposed along the Hilina Pali, and the weathered surfaces atop ʻaʻā lava flow layers have weathered to clay-sized sediment (Easton, 1987). Flow may undergo a transition to debris flows when channels erode into these formations, resulting in the observed levees. However, these layers constituted a minor fraction of the total exposure, so the fine-grained sediment constitutes only a minor component of the overall available sediment budget relative to the larger grains produced by fracturing of the lava layers.

We interpret the observed clast-supported deposits at depth as comprising the bulk of the subsurface fan material and were likely also deposited by sieve lobes. Following high intensity rainfall events, such as those associated with Kona storms, the resulting channel flows transport sediment from the eroded Hilina Pali alcoves onto the fans. The steep slopes and high discharges transport large grains onto the fans, but the reduction in gradient rapidly reduces flow competence. Large grains are deposited, creating a sieve that blocks the transport of additional sediment. Water infiltrates into the fan due to the high porosity between large grains, and the channel is choked with sediment. Over time some sand and gravel-sized sediment is transported through the fan and is deposited into the observed splays near the fan toe. Chemical weathering products of basalt, along with aeolian-transported sediment that is trapped in the coarse fan mantle, accumulates at depth in the fan, where it is cemented into a relatively impermeable layer. Water from subsequent flows carries sediment farther forward, over time building up the fans. We therefore infer that the variations in Hilina Pali fan size and gradient correspond with variations in available discharge and sediment size.

5.6. Conclusions

The alluvial fans in southern Hawaii are characterized by their lobate surface morphology and coarse sediment. The fans are fed by channels that drain the Kaʻū Desert, but the bulk of sediment is sourced from the Hilina Pali escarpment. The scarcity of fine grained sediment, steep slopes, and high flow discharges make this region an ideal setting for sieve lobe deposition, and the fans forming along the base of the escarpment appear to be a rare example of fans formed predominately from sieve lobe deposition. Sieve lobe deposition can occur with up to boulder sized sediment given these conditions.

There are several directions for future work at the Hilina Pali fans. Higher resolution topographic data will allow us to better assess variations in sieve lobe and channel dimensions across the fans. This can be done with differential GPS surveys or ground-based lidar (UAV's are not permitted in Hawaii Volcanoes National Park). We will conduct a systematic analysis of grain size distribution with respect to downstream and cross-longitudinal directions to determine how grain size varies with distance downstream and whether there is a grain size difference between "active" and "inactive" fan areas, as well as how grain sizes vary within depositional lobes. The fans along the Hilina Pali exhibit that given high slopes and discharges, sieve lobes can be constructed with boulder sized sediment, and further study is merited to better understand this depositional process.

Acknowledgements

The authors wish to thank Adrian Harvey and three anonymous reviewers for their constructive comments, as well as Scott Lecce's detailed editorial corrections. This work was funded by a predoctoral fellowship awarded to A. Morgan by the Smithsonian Institution, and grant NNX14AN32G awarded to R. Craddock from NASA's Planetary Geology and Geophysics Program. The authors wish to thank Scott Rowland, Peter Mouginis-Mark, and Sarah Fagents for continuing to organize the NASA Planetary Volcanology Field Workshop in Hawaii.

Chapter 6

Summary and future research

The two primary objectives of this dissertation are:

(1) Establish constraints on Mars' climate during the era of fan formation

(2) Characterize the role process has in shaping alluvial fan morphology

These were met by using a synthesis of remote sensing observation, field work, and numerical modeling. This chapter summarizes the main findings within the previous four chapters, and describes a number of ongoing challenges in alluvial fan research and potential research pathways to address them.

6.1. Main conclusions

- Martian alluvial fans are far more widespread than previously reported.
- Large martian alluvial fans formed from a combination of channelized bedload transport and fine-grained overbank mudflows.
- Snowmelt is a viable runoff source to form the martian alluvial fans.
- Significant fluvial geomorphic work occurred during the Hesperian and Amazonian Periods.
- Changes in sediment supply and discharge have a dominant influence on fan surface morphology
- Sieve lobe deposition can produce entire alluvial fans of cobble and boulder sized sediment.

6.2. Conditions during the deposition of martian fans

The primary goal of this dissertation was to constrain the age, dominant sedimentologic processes, and range of environmental conditions during the deposition of alluvial fans on Mars. This was approached using remote sensing data from martian orbiters to document the prevalence of alluvial fans across Mars, and to conduct an in-depth investigation of the sedimentologic and climatic conditions during the formation of the fans in Saheki crater using a field study at an analog fan in the Atacama Desert.

The new global database doubles the number of previously identified fans on Mars, and finds them to be far more geographically widespread than previously reported. I documented ~1300 fan landforms within ~315 craters, and for every fan marked apex location and measured fan gradient, relief, length, area, and catchment area and relief. Martian fans are larger than their terrestrial counterparts, likely due to the lack of tectonic subsidence which allows the fan to prograde as long as it is fed sediment. Measurements of fan morphologies do not appear to correlate with geographic or topographic setting, but fans do show a favored N-S orientation, suggesting a control by solar insolation (Chapter 2). The age of these features was found using two complimentary methods. Assuming the fans formed concurrently, crater statistics yield an age of early Amazonian, and the vast majority of martian fans superpose previously mapped Hesperian and Amazonian terrains.

The alluvial fans in Saheki crater reveal the most detailed record of fan stratigraphy that has been found on Mars. Broad topographic inversion between individual distributaries indicates that the fan consists of a high volume of wind-transportable sediment, and the paucity of dune fields suggests that the dominant size of this material is silt or clay. Linear and platform features radiating from the fan apex are interpreted to be inverted fluvial distributaries, boulders on the fan surface fine with distance down fan, and platform features between ridges appear to be braided or sinuous channels. Together, these observations reveal that the Saheki crater fans were deposited by channelized flows transporting sand, gravel, and occasional boulder sediment as bedload, but the bulk of the deposition (at least in the upper 100 m of deposits) consisted of fine grained mudflows.

The Hesperian and Amazonian Periods have historically been characterized as having a cold and dry climate similar to that of modern Mars (Carr and Head, 2010). The growing body of evidence for fluvial features that formed during this era challenge this paradigm. Crater density counts for the Saheki crater fans yield a mid-Hesperian to possibly early Amazonian age, in agreement with the findings in Chapter 2 as well as work by other researchers (e.g. Grant et al., 2014; Grant and Wilson, 2011). This increasing consistency solidifies the evidence that Mars was hydrologically active during the post-Noachian.

6.3. Linkages between alluvial fan processes and morphology

The second goal of this dissertation was to link alluvial fan process with subsequent morphology. A new alluvial fan landform evolution model was presented that simulates the formation of fine-grained alluvial fans. The model successfully responds to changing boundary conditions, including fan head trenching following an increase in discharge and proximal fan aggradation following an increase in sediment supply. This is a powerful tool that can be used to investigate relations between alluvial fan sedimentation, surface morphology, and stratigraphy.

Sieve lobe deposition was once widely considered to be a major building block in the construction of alluvial fans, but fell out of favor in recent decades due in part to the perceived lack of clear field examples. The coarse-grained fans along the Hilina Pali on the Island of

Hawaii have surface morphologies indicative of debris flow deposits, but the exposed stratigraphy reveals that they are in fact constructed entirely from fluvial flows. The scarcity of fine grained sediment with which to initiate debris flows leads to fluvial transport and deposition of gravels and cobbles as sieve lobes. Discharge estimates show that sediment transport and deposition primarily occur during high precipitation events known locally as Kona storms, which are also the drivers of incision into the nearby Keanakāko'i tephra (Craddock et al., 2012).

6.4. Future work

There a number of questions regarding fan dynamics on Earth and Mars. The fan database presented in Chapter 2 and the fan model in Chapter 5 are powerful tools to use to address some of these open questions. Below I describe work that will expand on the results of each chapter in this dissertation.

6.4.1. Role of pre-existing catchment in initiating martian alluvial fan formation

The lack of correlation between geographic setting and fan properties suggests that other controls, such as initial crater topography, may be a main driver of fan formation. The favored N-S directionality identified in Chapter 2 is a strong indicator of climatic control, and the presence of a pre-eroded alcove in which to build up a snowpack may be a required prerequisite for a martian alluvial fan to form. The orientation of a catchment with respect to solar insolation angle affects weathering and erosion (Blair and McPherson, 2009), and catchment shape influences feeder channel profile, likelihood of flashfloods sediment production, and sediment storage capacity, all of which have an effect on alluvial fan processes.

The role of pre-existing catchment control can be tested using high resolution DEMs to compare the morphometric properties of craters that host fans and those that do not. An additional question is whether the fans identified in the survey formed concurrently, which can be assessed using crater density counts. I am the Co-I on a submitted proposal to the NASA Mars Data Analysis Program to address both of these questions. We will assess whether initial crater morphology is a key control on the development on fan deposits, and constrain fan surface ages using a model developed by the PI to limit the effects of crater erosion on the age statistics (Palucis and Dietrich, 2014). We will test if the fans were built from sustained, long duration surface flows by using similar hydrologic analyses as have been done for the fans in Saheki (Morgan et al., 2014) and Gale (Palucis et al., 2014) craters. Results from this research will place hard limits on the environmental range during the era of alluvial fan formation, which are necessary for to constrain paleoclimate models (Kite et al., 2017a, 2013).

6.4.2. Heterogeneity of martian alluvial fan formative processes

This dissertation provides evidence that martian fans were formed by precipitation-fed, gravity driven alluvial sedimentation. However, the magnitude and duration of activity remains poorly understood, and this is a major factor in Mars' post Noachian habitability potential. Saheki is not the only martian crater to have undergone extensive aeolian deflation, and several of the fans in the database compiled in Chapter 2 have been subjected to large impacts, revealing the interior stratigraphy. The stratigraphic analyses of Saheki crater were limited by the availability of HiRISE coverage, which has expanded considerably in the past few years. There are now numerous examples of inverted channels and superposed impact craters on alluvial fans that are have been imaged in stereo by HiRISE. The Saheki crater study in Chapter 3 highlights the ability of high resolution remote sensing to characterize alluvial fan geomorphology, sedimentology, hydrology, and age, placing constraints on paleoclimate models. In addition, analysis of strike and dip (Lewis and Aharonson, 2006) of these layers can yield insights into the role of lacustrine processes and backwatering effects on fan deposition. More data points, acquired through geomorphic mapping and hydrologic studies will provide quantitative constraints on the timing, duration, regional extent, and heterogeneity of climatic conditions during the era of fan formation on Mars. This will provide a broader context view of the state of Mars' climate during the post-Noachian.

6.4.3. Alluvial fan processes and forms in different climatic regimes

Our ability to characterize flow processes on martian alluvial fans is hindered by gaps in our understanding of terrestrial alluvial fan dynamics, namely the ability to make inferences on flow regime on the basis of surface morphology. Fan processes are generally determined through the detailed facies analysis of fan stratigraphy (Blair, 1999; Blair and McPherson, 2009, 1994; Hooke, 1987; Whipple and Dunne, 1992). These methods are intensive and time consuming. Recent approaches have included the study of variations in fan topography, using the surface as the key to the subsurface. Fan surface morphology can be misleading due to secondary flows and post-depositional weathering (de Haas et al., 2014), but work at fans in the Death Valley fans shows that the upper several meters of stratigraphy reveal similar processes to what is exposed at the surface (Blair, 1999; Staley et al., 2006). An additional question is the variability of flow processes in different climatic settings. I have submitted a proposal as PI to examine links between surface morphology and fan forms using field analogs in two contrasting climatic regimes, Death Valley and Iceland. This will utilize high resolution (cm scale) topographic data acquired from an unmanned aerial aircraft to examine dominant flow processes as exposed on the surface and changes as recorded in the fan stratigraphy. Surface measures that can be used to identify fan process include local relief, expressed as the maximum difference in elevation within a moving window, or the standard deviation of slope, both of which have both been shown to be effective measures of discerning dominant flowing flow processes (Volker et al., 2007).

The interpretation of dominant formative process has significant implications. Permeable sediments in fans formed from dominantly fluvial processes will have a higher aquifer capacity and potentially higher potential as a source for aggregate material than fans dominantly formed from debris flows. Furthermore, alluvial fans offer low gradient surfaces in otherwise steep terrain which can be attractive for human development, but as a geologically active landform fans present risks in the form of debris flows for debris flow fans or flash floods in the case of fluvial fans (Larsen et al., 2001).

6.4.4. Relative importance of climatic versus tectonic effects on fan development

Climatic effects have a major influence on alluvial fan morphology, through changes in base level (i.e. a lake beyond the distal fan), sediment supply, and runoff. In addition, when climatic change modifies sediment supply or flood power, there is a resultant change in depositional regime (Harvey et al., 2005). Model results in Chapter 4 clearly demonstrate the effect of changes in sediment supply and flow discharge to the fan surface. However, studies of ancient alluvial fan stratigraphy show tectonics to play an oversized role relative to climate in modifying the fan (Wagreich and Strauss, 2005). Future revisions to the model to better include tectonics can address this discrepancy between alluvial fan internal geology and surface geomorphology. Characterizing the relative importance of factors is important in how climatic and land use change might affect alluvial fan flooding.

Appendix

Idealized Model for Aeolian Inversion of Saheki Fans

The starting conditions are a hypothetical cross-section of the lower part of fan K2, with the cross-section being taken normal to the dominant flow direction with a 1000 m section taken across the fan perpendicular to the downslope direction and a 100 m vertical extent (Figure 3.29). In this model the uncolored area is envisioned to consist of fine-grained overbank deposits. Interbedded with the overbank deposits are gravel channel deposits scattered randomly within the cross section. The width of each channel is randomly sampled from a uniform distribution from 30 to 80 m, and each channel deposit is 2 m thick. Coordinates for channel deposits are selected randomly within the cross-section, and deposits are added (blue boxes in Figure 3.29) until 5% of the total cross-sectional area (an arbitrary number) is channel gravel. The stack of channel and overbank deposits is then wind-eroded, with the initial surface being a flat surface at the top of the stack (black line). The channel deposits are assumed to be inerodible by wind, but the overbank deposits on a flat surface are eroded at a rate $\dot{z}_{wf}$ of 5.0 m/t (time, t, and the erosion rate $\dot{z}_{wf}$ are in arbitrary but consistent units relative to other simulation parameters). Wind erosion is also assumed to be more rapid on convex slopes due to greater exposure. The wind erosion rate, $\dot{z}_w$ (m/t) relative to a flat surface rate $\dot{z}_{wf}$ is given by:

$$\dot{z}_w = \dot{z}_{wf} \exp(-K_w \nabla^2 z) \tag{A.1}$$

where K_w is a scale constant and has the value 40 m and z is the surface elevation. The value of K_w was selected to rapidly scour ridges no longer capped by gravels, because uncapped hills of layered sediment are rare on the K2 fan.

As time progresses and wind vertically erodes sediment (which is assumed to be entirely removed from the cross-section), diffusive mass wasting occurs using a non-linear relationship (Hanks and Andrews, 1989; Roering et al., 1999, 2001):

$$\vec{q}_m = -\frac{K_m \vec{S}}{\left[1-\left(S/S_c\right)^2\right]} \tag{A.2}$$

where $\vec{q}_m$ is the vector mass wasting flux (volume per unit width of slope in m^2/t) S is slope gradient (as a vector in the numerator), S_c is a critical slope gradient (the angle of repose for loose sediment, set to 0.6 here), and K_m is diffusivity. For these simulations K_m was set at 10.0 m^2/t. Net erosion or deposition rate is given as:

$$\dot{z}_m = -\nabla \bullet \vec{q}_m \, . \tag{A.3}$$

Erosion of the channel gravels is assumed to occur only through mass wasting. The majority of the eroding slope surface is underlain by the overbank deposits. We assume that the gravels make up a minor component of the slope mantle and have no effect upon mass wasting rates or aeolian deflation of the portions of the slope on overbank deposits. Note that we consider the aeolian erosion and the mass wasting to be independent, additive processes. Additive processes are commonly assumed in landform evolution models, such as in modeling drainage basin evolution by mass wasting and fluvial erosion (e.g., Howard, 1994). The net rate of surface change, $\dot{z}$, is the sum of $\dot{z}_w$ plus $\dot{z}_m$.

The absolute values of the rate constants in the model are arbitrary. Their relative values were chosen to reproduce the topographic patterns observed on the wind-eroded surface of the southern Saheki K2 fan (e.g., Figures 3.3 and 3.6 through 3.9). We view the model to be an illustrative portrayal of the pattern of wind erosion and layer exposure pattern, rather than being quantitatively accurate.

References

Abramov, O., Kring, D.A., 2005. Impact-induced hydrothermal activity on early Mars. Journal of Geophysical Research 110, E12S09. doi:10.1029/2005JE002453.

Amundson, R., et al., 2012. Geomorphologic evidence for the late Pliocene onset of hyperaridity in the Atacama Desert. Geological Society of America Bulletin 124, 1048-1070. doi:10.1130/B30445.1.

Anderson, R., Bell, J.F., 2010. Geologic mapping and characterization of Gale Crater and implications for its potential as a Mars Science Laboratory landing site. The Mars Journal 5, 76-128. doi:10.1555/mars.2010.0004.

Andrews, E.D., 1984. Bed-material entrainment and hydraulic geometry of gravel-bed rivers in Colorado. Geological Society of America Bulletin 95, 371-378. doi:10.1130/0016-7606(1984)95<371:BEAHGO>2.0.CO;2.

Ansan, V., et al., 2011. Stratigraphy, mineralogy, and origin of layered deposits inside Terby crater, Mars. Icarus 211, 273-304. doi:10.1016/j.icarus.2010.09.011.

Armitage, J.J., Warner, N.H., Goddard, K., Gupta, S., 2011. Timescales of alluvial fan development by precipitation on Mars. Geophysical Research Letters 38 (L17203). doi:10.1029/2011GL048907.

Balme, M., Berman, D.C., Bourke, M.C., Zimbelman, J.R., 2008. Transverse Aeolian Ridges (TARs) on Mars. Geomorphology 101, 703-720. doi:10.1016/j.geomorph.2008.03.011.

Berman, D.C., Balme, M.R., Rafkin, S.C.R., Zimbelman, J.R., 2011. Transverse Aeolian Ridges (TARs) on Mars II: Distributions, orientations, and ages. Icarus 213, 116-130.

Barnhart, C.J., Howard, A.D., Moore, J.M., 2009. Long-term precipitation and late-stage valley network formation: Landform simulations of Parana Basin, Mars. Journal of Geophysical Research 114, E01003. doi:10.1029/2008JE003122.

Barnhart, C.J., Nimmo, F., Travis, B.J., 2010. Martian post-impact hydrothermal systems incorporating freezing. Icarus 208, 101–117. doi:10.1016/j.icarus.2010.01.013.

Bennett, K.A., Bell, J.F., 2016. A global survey of martian central mounds: Central mounds as remnants of previously more extensive large-scale sedimentary deposits. Icarus 264, 331–341. doi:10.1016/j.icarus.2015.09.041.

Bhattacharya, J.P., Payenberg, T.H.D., Lang, S.C., Bourke, M., 2005. Dynamic river channels suggest a long-lived Noachian crater lake on Mars. Geophysical Research Letters 32, 1–4. doi:10.1029/2005GL022747.

Bibring, J.-P. et al., 2006. Global mineralogical and aqueous mars history derived from OMEGA/Mars Express data. Science 312, 400–404. doi:10.1126/science.1122659.

Birch, S.P.D., Hayes, A.G., Howard, A.D., Moore, J.M., Radebaugh, J., 2016. Alluvial Fan Morphology , Distribution and Formation on Titan, Icarus. doi:10.1016/j.icarus.2016.02.013.

Blair, T.C., 1999. Cause of dominance by sheetflood vs. debris flow processes on two adjoining alluvial fans, Death Valley, California. Sedimentology 46, 1015–1028. doi:10.1046/j.1365-3091.1999.00261.x.

Blair, T.C., 2003 Features and origin of the giant Cucomungo Canyon alluvial fan, Eureka Valley, California. In: M. A. Chan, A. W. Archer, (Eds.), Extreme Depositional Environments: Mega End Members in Geologic Time. Geological Society of America, Denver, CO, pp. Special Paper 370, 105-126. doi:10.1130/0-8137-2370-1.105.

Blair, T.C., McPherson, J.G., 1992. The Trollheim alluvial fan and facies model revisited. Geological Society of America Bulletin 104, 762–769. doi:10.1130/0016-7606(1992)104<0762.

Blair, T.C., McPherson, J.G., 1993. The Trollheim alluvial fan and facies model revisited: Discussion and reply. Geological Society of America Bulletin 105, 563–567. doi:10.1130/0016-7606(1993)105<0563:TTAFAF>2.3.CO;2.

Blair, T.C., McPherson, J.G., 1994. Alluvial fans and their natural distinction from rivers based on morphology, hydraulic processes, sedimentary processes, and facies assemblages. Journal of Sedimentary Research A64, 450–489. doi:10.1306/D4267DDE-2B26-11D7-8648000102C1865D.

Blair, T.C., McPherson, J.G., 1995. Quaternary alluvial fans in southwestern Crete: sedimentation processes and geomorphic evolution: Discussion. Sedimentology 42, 531–535. doi:10.1111/j.1365-3091.1995.tb00390.x.

Blair, T.C., McPherson, J.G., 2009. Processes and forms of alluvial fans. In: Parsons, A.J., Abrahams, A.D. (Eds.), Geomorphology of Desert Environments. Springer Netherlands, Dordrecht, pp. 413–467. doi:10.1007/978-1-4020-5719-9_14.

Bull, W.B., 1962. Relation of textural (CM) patterns to deposition environment of alluvial-fan deposits. Journal of Sedimentary Petrology 32, 211-216. doi:10.1306/74D70C7C-2B21-11D7-8648000102C1865D.

Bull, W.B., 1963. Alluvial-fan deposits in western Fresno County, California. Journal of Geology 71, 243-251. doi:10.1086/626896.

Bull, W.B., 1972. Recognition of alluvial-fan deposits in the stratigraphic record. In: Rigby, J.K., Hamblin, W.K. (Eds.), Recognition of Ancient Sedimentary Environments. Society for Sedimentary Geology, pp. 63–83. doi:10.2110/pec.72.02.0063.

Bull, W.B., 1977. The alluvial-fan environment. Progress in Physical Geography 1, 222–270. doi:10.1177/030913337700100202.

Bull, W.B., 1991. Geomorphic Responses to Climatic Change. Oxford Univ. Press, New York.

Burr, D.M., Enga, M.-T., Williams, R.M.E., Zimbelman, J.R., Howard, A.D., Brennand, T.A., 2009. Pervasive aqueous paleoflow features in the Aeolis/Zephyria Plana Region, Mars. Icarus 200, 52-76.

Burr, D.M., Williams, R.M.E., Wendell, K.D., Chojnacki, M., Emery, J.P., 2010. Inverted fluvial features in the Aeolis/Zephyria Plana region, Mars: Formation mechanism and initial paleodischarge estimates. Journal of Geophysical Research 115 (E07011). doi:10.1029/2009JE003496.

Carr, M.H., 2002. Elevations of water-worn features on Mars: Implications for circulation of groundwater. Journal of Geophysical Research 107, 1–11. doi:10.1029/2002JE001845.

Carr, M.H., 2006. The Surface of Mars, 2nd Ed. Cambridge University Press, Cambridge, 322 p.

Carr, M.H., Head, J.W., 2010. Geologic history of Mars. Earth and Planetary Science Letters 294, 185–203. doi:10.1016/j.epsl.2009.06.042.

Chan, M. A., Yonkee, W. A., Netoff, D. I., Seiler, W. M., Ford, R. L., 2008. Polygonal cracks in bedrock on Earth and Mars: Implications for weathering. Icarus 194, 65-71.

Chen, L., Steel, R.J., Guo, F., Olariu, C., Gong, C., 2017. Alluvial fan facies of the Yongchong Basin: Implications for tectonic and paleoclimatic changes during Late Cretaceous in SE China. Journal of Asian Earth Sciences 134, 37–54. doi:10.1016/j.jseaes.2016.10.010.

Chow, V. Te, 1959. Open-Channel Hydraulics. McGraw-Hill, New York, 700 p.

Christensen, P.R., et al., 2004. The Thermal Emission Imaging System (THEMIS) for the Mars 2001 Odyssey Mission. Space Science Reviews 110, 85–130. doi:10.1023/B:SPAC.0000021008.16305.94.

Costa, J.E., 1984 Physical geomorphology of debris flows. In: J.E. Costa, P.J. Fleisher, (Eds.), Developments and applications of geomorphology. Springer-Verlag, pp. 268-317.

Costa, J.E., 1988. Rheologic, geomorphic, and sedimentologic differentiation of water floods, hyperconcentrated flows, and debris flows. In: Baker, V.R., Kochel, R.C., Patton, P.C. (Eds.), Flood Geomorphology. Wiley-Interscience, pp. 113-122.

Coulthard, T.J., Kirkby, M.J., Macklin, M.G., 2000. Modelling geomorphic response to environmental change in an upland catchment. Hydrological Processes 14, 2031–2045. doi:10.1002/1099-1085(20000815/30)14:11/12<2031::AID-HYP53>3.0.CO;2-G.

Craddock, R.A., Golombek, M.P., 2016. Characteristics of terrestrial basaltic rock populations: Implications for Mars lander and rover science and safety. Icarus 274, 50–72. doi:10.1016/j.icarus.2016.02.042.

Craddock, R.A., Howard, A.D., 2002. The case for rainfall on a warm, wet early Mars. Journal of Geophysical Research 107. doi:10.1029/2001JE001505.

Craddock, R.A., Howard, A.D., Irwin, R.P., Tooth, S., Williams, R.M.E., Chu, P.-S., 2012. Drainage network development in the Keanakāko‘i tephra, Kīlauea Volcano, Hawai‘i: Implications for fluvial erosion and valley network formation on early Mars. Journal of Geophysical Research 117 (E08009). doi:10.1029/2012JE004074.

Craddock, R.A., Irwin, R.P., Williams, R., Swanson, D., Howard, A.D., Quantin, C., Zimbelman, J.R., 2006. Topical martian field studies in the Ka'u Desert, Hawaii. Lunar and Planetary Science Conference, Houston, TX. Abstract 1384.

Craddock, R.A., Maxwell, T.A., Howard, A.D., 1997. Crater morphometry and modification in the Sinus Sabaeus and Margaritifer Sinus regions of Mars. Journal of Geophysical Research Planets 102, 13321–13340. doi:10.1029/97JE01084.

Dade, W.B., Friend, P.F., 1998. Grain-size, sediment-transport regime, and channel slope in alluvial rivers. Journal of Geology 106, 661-675.

Dade, W.B., Verdeyen, M.E., 2007. Tectonic and climatic controls of alluvial-fan size and source-catchment relief. Journal of the Geological Society, London. 164, 353–358. doi:10.1144/0016-76492006-039.

de Haas, T., Ventra, D., Carbonneau, P.E., Kleinhans, M.G., 2014. Debris-flow dominance of alluvial fans masked by runoff reworking and weathering. Geomorphology 217, 165–181. doi:10.1016/j.geomorph.2014.04.028.

De Villiers, G., Kleinhans, M.G., Postma, G., 2013. Experimental delta formation in crater lakes and implications for interpretation of martian deltas. Journal of Geophysical Research: Planets 118, 651–670. doi:10.1002/jgre.20069.

Di Achille, G., Ori, G.G., Reiss, D., Hauber, E., Gwinner, K., Michael, G., Neukum, G., 2006. A steep fan at Coprates Catena, Valles Marineris, Mars, as seen by HRSC data. Geophysical Research Letters 33 (L07204). doi:10.1029/2005GL025435.

Dietrich, W.E., Palucis, M.C., Williams, R.M.E., Lewis, K.W., Rivera-Hernandez, F., Sumner, D.Y., 2017. Fluvial Gravels on Mars. In: Tsutsumi, D., Laronne, J.B. (Eds.), Gravel-Bed

Rivers. John Wiley & Sons, Ltd, Chichester, UK, pp. 755–783. doi:10.1002/9781118971437.ch28.

Dixon, J.C., 2009 Aridic soils, patterned ground, and desert pavements. In: A. J. Parsons, A. D. Abrahams, (Eds.), Geomorphology of Desert Environments. Springer, Dordrecht. pp. 101-122. doi: 10.1007/978-1-4020-5719-9_5.

Duffield, W.A., 1975. Structure and origin, Koae fault system, Kilauea Volcano, Hawaii. U.S. Geological Survey Professional Paper 856.

Easton, R.M., 1987. Stratigraphy of Kilauea Volcano. In: Volcanism in Hawaii. U.S. Geological Survey Professional Paper 1350, pp. 243–260.

Ehlmann, B.L., Edwards, C.S., 2014. Mineralogy of the martian Surface. Annu. Rev. Earth Planet. Sci 42, 291–315. doi:10.1146/annurev-earth-060313-055024.

El Maarry, M.R., Kodikara, J., Wijessoriya, S., Markiewicz, W.J., Thomas, N., 2012. Desiccation mechanism for formation of giant polygons on Earth and intermediate-sized polygons on Mars: Results from a pre-fracture model. Earth and Planetary Science Letters 323-324, 19-26. doi:10.1016/j.epsl.2012.01.016.

El Maarry, M.R., Markiewicz, W.J., Mellon, M.T., Goetz, W., Dohm, J.M., Pack, A., 2010. Crater floor polygons: Desiccation patterns of ancient lakes on Mars? Journal of Geophysical Research 115 (E10006). doi:10.1029/2010JE003609.

Fassett, C.I., Dickson, J.L., Head, J.W., Levy, J.S., Marchant, D.R., 2010. Supraglacial and proglacial valleys on Amazonian Mars. Icarus 208, 86-100. 10.1016/j.icarus.2010.02.021.

Fassett, C.I., Head, J.W., 2008. Valley network-fed, open-basin lakes on Mars: Distribution and implications for Noachian surface and subsurface hydrology. Icarus 198, 37–56. doi:10.1016/j.icarus.2008.06.016.

Fassett, C.I., Head, J.W., 2011. Sequence and timing of conditions on early Mars. Icarus 211, 1204-1214. doi:10.1016/j.icarus.2010.11.014.

Ferguson, R., 2007. Flow resistance equations for gravel- and boulder-bed streams. Water Resources Research 43 (W05427). doi:10.1029/2006WR005422.

Field, J., 2001. Channel avulsion on alluvial fans in southern Arizona. Geomorphology 37, 93-104. doi:10.1016/S0169-555X(00)00064-7.

Forget, F., Wordsworth, R., Millour, E., Madeleine, J.-B., Kerber, L., Leconte, J., Marcq, E., Haberle, R. M., 2013. 3D modelling of the early martian climate under a denser CO2 atmosphere: Temperatures and CO2 ice clouds. Icarus 222, 81-99. doi:10.1016/j.icarus.2012.10.019.

Forsberg-Taylor, N.K., Howard, A.D., Craddock, R.A., 2004. Crater degradation in the Martian highlands: Morphometric analysis of the Sinus Sabaeus region and simulation modeling suggest fluvial processes. Journal of Geophysical Research 109, 1–12. doi:10.1029/2004JE002242.

Frankel, K.L., Dolan, J.F., 2007. Characterizing arid region alluvial fan surface roughness with airborne laser swath mapping digital topographic data. Journal of Geophysical Research: Earth Surface 112. doi:10.1029/2006JF000644.

French, R.H., 1987. Hydraulic Processes on Alluvial Fans. Elsevier Science, Amsterdam, 244 p. doi:10.1002/esp.3290130710.

Frostick, L.E., Reid, I., 1989. Climatic versus tectonic controls of fan sequences: lessons from the Dead Sea, Israel. Journal of the Geological Society, London 146, 527–538. doi:10.1144/gsjgs.146.3.0527.

Garvin, J.B., Sakimoto, S., Frawley, J.J., 2003. Craters on Mars: Global geometric properties from gridded MOLA topography. Sixth International Conference on Mars, Pasadena, CA. Abstract 3277.

Giambelluca, T., Sanderson, M., 1993. The water balance and climatic classification. In: Sanderson, M. (Ed.), Prevailing Trade Winds: Climate and Weather in Hawai`i. University of Hawaii Press, Honolulu, HI, p. 126.

Gillies, J.A., Nickling, W.G., Tilson, M., Furtak-Cole, E., 2012. Wind-formed gravel bed forms, Wright Valley, Antarctica. Journal of Geophysical Research 117 (F04017). doi:10.1029/2012JF002378.

Goldspiel, J.M., Squyres, S.W., 2000. Groundwater sapping and valley formation on Mars Icarus, 148, 176-192. doi:10.1006/icar.2000.6465.

Goldspiel, J.M., Squyres. S.W., 2011. Groundwater discharge and gully formation on martian slopes. Icarus 2011, 238-258. doi:10.1016/j.icarus.2010.10.008.

Golombek, M.P., Grant, J.A., Crumpler, L.S., Greeley, R., Arvidson, R.E., Bell, J.F., Weitz, C.M., Sullivan, R., Christensen, P.R., Soderblom, L.A., Squyres, S.W., 2006. Erosion rates at the Mars Exploration Rover landing sites and long-term climate change on Mars. Journal of Geophysical Research Planets 111. doi:10.1029/2006JE002754.

Goudge, T.A., Milliken, R.E., Head, J.W., Mustard, J.F., Fassett, C.I., 2017. Sedimentological evidence for a deltaic origin of the western fan deposit in Jezero crater, Mars and implications for future exploration. Earth and Planetary Science Letters 458, 357–365. doi:10.1016/j.epsl.2016.10.056.

Gough, D.O., 1981. Solar interior structure and luminosity variations. Sol. Phys. 74, 21–34. doi:10.1007/BF00151270.

Grant, J.A., 2000. Valley formation in Margaritifer Sinus, Mars, by precipitation-recharged ground-water sapping. Geology 28, 223. doi:10.1130/0091-7613(2000)28<223:VFIMSM>2.0.CO;2.

Grant, J.A., Wilson, S.A., 2011. Late alluvial fan formation in southern Margaritifer Terra, Mars. Geophysical Research Letters 38 (L08201). doi:10.1029/2011GL046844.

Grant, J.A., Wilson, S.A., 2012. A possible synoptic source of water for alluvial fan formation in southern Margaritifer Terra, Mars. Planet. Space Sci. 72, 44–52. doi:10.1016/j.pss.2012.05.020.

Grant, J.A., Wilson, S.A., Mangold, N., Calef, F., Grotzinger, J.P., 2014. The timing of alluvial activity in Gale crater, Mars. Geophysical Research Letters 41, 1142–1149. doi:10.1002/2013GL058909.

Greeley, R. White, B., Leach, R., Iversen, J. Pollack, J., 1976. Mars: Wind friction speeds for particle movement, Geophysical Research letters. 3, 417-420. doi:10.1029/GL003i008p00417.

Greeley, R., Guest, J.E., 1987. Geologic Map of the Eastern Equatorial Region of Mars. U. S. Geological Survey Miscellaneous Investigations Series Map. I-1802-B.

Gulick, V.C., 2001. Origin of the valley networks on Mars : a hydrological perspective. Geomorphology 37, 241–268. doi:10.1016/S0169-555X(00)00086-6.

Haberle, R.M., 1998. Early Mars Climate Models. Journal of Geophysical Research 103. doi:10.1029/98JE01396.

Hanks, T.C., Andrews, D.J., 1989. Effect of far-field slope on morphologic dating os scarp-like landforms. Journal of Geophysical Research 94, 565-573.

Harris, R.C., 2004. Giant dessication cracks in Arizona. Arizona Geological Survey. Open-File Report 04-01, 1-93.

Harrison, K.P., and Grimm, R.E., 2009. Regionally compartmented groundwater flow on Mars. Journal of Geophysical Research 114 (E04004). doi: 10.1029/2008JE003000.

Harrison, T.N., Osinski, G.R., Tornabene, L.L., Jones, E., 2015. Global documentation of gullies with the Mars Reconnaissance Orbiter Context Camera and implications for their formation. Icarus 252, 236–254. doi:10.1016/j.icarus.2015.01.022.

Hartmann, W.K., 2007. Martian cratering 9: Toward resolution of the controversy about small craters. Icarus. 189, 274-278. doi:10.1016/j.icarus.2007.02.011.

Hartmann, W.K., Neukum, G., 2001. Cratering Chronology and the Evolution of Mars. Space Science Reviews 96, 165–194. doi:10.1023/A:1011945222010.

Hartmann, W.K., Neukum, G., Werner, S., 2008. Confirmation and utilization of the "production function" size-frequency distributions of Martian impact craters. Geophysical Research Letters 35 (L02205). doi:10.1029/2007GL031557.

Hartmann, W.K., Werner, S.C., 2010. Martian Cratering 10. Progress in use of crater counts to interpret geological processes: Examples from two debris aprons. Earth and Planetary Science Letters 294, 230-237. doi:10.1016/j.epsl.2009.10.001.

Harvey, A.M., 1992. The influence of sedimentary style on the morphology and development of alluvial fans. Israeli Journal of Earth Sciences 41, 123–147.

Harvey, A.M., 1999 The occurrence and role of arid zone alluvial fans. In: D. S. G. Thomas, (Ed.), Arid Zone Geomorphology. Halstead Press, New York, pp. 136-158.

Harvey, A.M., 2004. The response of dry-region alluvial fans to late Quaternary climatic change. In: Alsharhan, A.S., Wood, W.W., Goudie, A.S., Fowler, A., Abdellatie, E.M. (Eds.), Desertification in the Third Millenium. CRC Press, pp. 83–98.

Harvey, A.M., 2011. Dryland Alluvial Fans. In: Thomas, D.S.G. (Ed.), Arid Zone Geomorphology. Wiley & Sons, pp. 333–371.

Harvey, A.M., 2012. The coupling status of alluvial fans and debris cones: a review and synthesis. Earth Surf. Process. Landforms 37, 64–76. doi:10.1002/esp.2213.

Harvey, A.M., Mather, A.E., Stokes, M., 2005. Alluvial fans: geomorphology, sedimentology, dynamics — introduction. A review of alluvial-fan research. In: Harvey, A.M., Mather, A.E., Stokes, M. (Eds.) Alluvial Fans: Geomorphology, Sedimentology, Dynamics. Geological Society of London, Special Publication 251, pp. 1–7. doi:10.1144/GSL.SP.2005.251.01.01.

Harvey, A.M., Wells, S.G., 1994. Late Pleistocene and Holocene changes in hillslope sediment supply to alluvial fan systems: Zzyzz, California. In: Millington, A.C., Pye, K. (Eds.), Environmental Change in Drylands: Biogeographical and Geomorphological Perspectives. Wiley, Chichester, pp. 67–84.

Harvey, A.M., Wells, S.G., 2003. Late Quaternary variations in alluvial fan sedimentologic and geomorphic processes, Soda Lake basin, eastern Mojave Desert, California. In: Enzel, Y., Wells, S.G., Lancaster, N. (Eds.), Paleoenvironments and Paleohydrology of the Mojave and Southern Great Basin Deserts. Geological Society of America Special Paper 368, Boulder, Colorado, pp. 207–230.

Harvey, A.M., Wigand, P.E., Wells, S.G., 1999. Response of alluvial fan systems to the late Pleistocene to Holocene climatic transition: Contrasts between the margins of pluvial

Lakes Lahontan and Mojave, Nevada and California, USA. Catena 36, 255–281. doi:10.1016/S0341-8162(99)00049-1.

Hauber, E., Platz, T., Reiss, D., Le Deit, L., Kleinhans, M.G., Carbonneau, P., De Haas, T., Marra, W.A., 2013. Old or Not So Old: that is the question for deltas and fans in Xanthe Terra, Mars. Lunar and Planetary Science Conference, the Woodlands, TX. Abstract 2513.

Haug, E.W., Kraal, E.R., Sewall, J.O., Van Dijk, M., Diaz, G.C., 2010. Climatic and geomorphic interactions on alluvial fans in the Atacama Desert, Chile. Geomorphology 121, 184–196. doi:10.1016/j.geomorph.2010.04.005.

Hooke, R.L., 1967. Processes on arid-region alluvial fans. Journal of Geology 75, 438–460. doi:10.1086/627271.

Hooke, R.L., 1968. Steady-state relationships on arid region alluvial fans in closed basins. American Journal of Science 266, 609–629.

Hooke, R.L., 1972. Geomorphic Evidence for Late-Wisconsin and Holocene Tectonic Deformation, Death Valley, California. Geological Society of America Bulletin 83, 2073. doi:10.1130/0016-7606(1972)83[2073:GEFLAH]2.0.CO;2.

Hooke, R., 1987. Mass movement in semi-arid environments and the morphology of alluvial fans. In: Anderson, M.G., Richards, K.S. (Eds.), Slope Stability. Wiley, New York, pp. 505–529.

Houston, J., 2002. Groundwater recharge through an alluvial fan in the Atacama Desert, northern Chile: mechanisms, magnitudes and causes. Hydrological Processes. 16, 3019-3035. doi:10.1002/hyp.1086.

Houston, J., 2006. The great Atacama flood of 2001 and its implications for Andean hydrology. Hydrological Processes 20, 591-610. doi:10.1002/hyp.5926.

Howard, A.D., 1980 Thresholds in river regimes. In: D. R. Coates, J. D. Vitek, (Eds.), Thresholds in geomorphology. George Allen & Unwin, London, pp. 227-258.

Howard, A.D., 1994. A detachment-limited model of drainage-basin evolution. Water Resources Research 30, 2261-2285. doi:10.1029/94WR00757.

Howard, A.D., 1996. Modeling Channel Evolution and Floodplain Morphology. In: Anderson, M.G., Walling, D.E., Bates, P.D. (Eds.) Floodplain Processes. John Wiley & Sons, Chichester, pp. 15–62.

Howard, A.D., 2007. Simulating the development of Martian highland landscapes through the interaction of impact cratering, fluvial erosion, and variable hydrologic forcing. Geomorphology 91, 332–363. doi:10.1016/j.geomorph.2007.04.017.

Howard, A.D., 2009. Badlands and gullying. In: A. J. Parsons, A.D. Abrahams, (Eds.), Geomorphology of Desert Environments. Springer Verlag, pp. 233-263.

Howard, A.D., Moore, J.M., 2011. Late Hesperian to early Amazonian midlatitude martian valleys: Evidence from Newton and Gorgonum basins. Journal of Geophysical Research 116, 1–10. doi:10.1029/2010JE003782.

Howard, A.D., Moore, J.M., Irwin, R.P., 2005. An intense terminal epoch of widespread fluvial activity on early Mars: 1. Valley network incision and associated deposits. Journal of Geophysical Research Planets 110, E12S14. doi:10.1029/2005JE002460.

Hunt, C. B., Robinson, T. W., Bowles, W. A., Washburn, A. L., 1966. General geology of Death Valley, California; Hydrologic Basin. U. S. Geological Survey Professional Paper. Report: P 0494-B.

Hynek, B.M., Beach, M., Hoke, M.R.T., 2010. Updated global map of martian valley networks and implications for climate and hydrologic processes. Journal of Geophysical Research 115. doi:10.1029/2009je003548.

Irwin, R.P., Craddock, R.A., Howard, A.D., 2005a. Interior channels in martian valley networks: Discharge and runoff production. Geology 33, 489. doi:10.1130/G21333.1.

Irwin, R.P., Howard, A.D., Craddock, R.A., Moore, J.M., 2005b. An intense terminal epoch of widespread fluvial activity on early Mars: 2. Increased runoff and paleolake development. Journal of Geophysical Research 110, 1–38. doi:10.1029/2005JE002460.

Irwin, R.P., Lewis, K.W., Howard, A.D., Grant, J.A., 2014. Paleohydrology of Eberswalde crater, Mars. Geomorphology 240, 83–101. doi:10.1016/j.geomorph.2014.10.012.

Irwin, R.P., Tanaka, K.L., Robbins, S.J., 2013. Distribution of Early, Middle, and Late Noachian cratered surfaces in the Martian highlands: Implications for resurfacing events and processes. Journal of Geophysical Research: Planets 118, 278–291. doi:10.1002/jgre.20053.

Ivanov, B.A., 2001. Mars/moon cratering rate ratio estimates. Space Science Reviews 96, 87–104. doi:10.1007/978-94-017-1035-0_4.

Jaumann, R. et al., 2007. The high-resolution stereo camera (HRSC) experiment on Mars Express: Instrument aspects and experiment conduct from interplanetary cruise through the nominal mission. Planet. Space Sci. 55, 928–952. doi:10.1016/j.pss.2006.12.003.

Jerolmack, D.J., Mohrig, D., 2007. Conditions for branching in depositional rivers. Geology 35, 463. doi:10.1130/G23308A.1.

Jerolmack, D.J., Mohrig, D., Grotzinger, J.P., Fike, D.A., Watters, W.A., 2006. Spatial grain size sorting in eolian ripples and estimation of wind conditions on planetary surfaces:

Application to Meridiani Planum, Mars. Journal of Geophysical Research 111, E12S02, 10.1029/2005je002544.

Jerolmack, D.J., Mohrig, D., Zuber, M. T., Byrne, S., 2004, A minimum time scale for formation of Holden Northeast fan, Mars, Geophysical Research Letters 31 (L21701). doi:10.1029/2004GL021326.

Johnson, A.M., 1984 Debris Flow. In: D. Brunsden, D. B. Prior, (Eds.), Slope Instability. John Wiley & Sons, Chichester, pp. 257-361.

Karssenberg, D., Bridge, J.S., 2008. A three-dimensional numerical model of sediment transport, erosion and deposition within a network of channel belts, floodplain and hill slope: extrinsic and intrinsic controls on floodplain dynamics and alluvial architecture. Sedimentology 55, 1717–1745. doi:10.1111/j.1365-3091.2008.00965.x.

Kasting, J.F., 1991. CO2 condensation and the climate of early Mars. Icarus 94, 1–13. doi:10.1016/0019-1035(91)90137-I.

Keller, G.V., 1974. Drilling at the Summit of Kilauea Volcano. Golden, CO.

Kiefer, E., Dörr, M. J., Ibbeken, H., and Götze, H. J., 1997. Gravity-based mass balance of an alluvial fan giant: the Arcas Fan, Pampa del Tamarugal, Northern Chile. Revista Geológica de Chile. 24, 165-185.

Kite, E.S., Gao, P., Goldblatt, C., Mischna, M.A., Mayer, D.P., Yung, Y.L., 2017a. Methane bursts as a trigger for intermittent lake-forming climates on post-Noachian Mars. Nature Geoscience. doi:10.1038/ngeo3033.

Kite, E.S., Halevy, I., Kahre, M.A., Wolff, M.J., Manga, M., 2013. Seasonal melting and the formation of sedimentary rocks on Mars, with predictions for the Gale Crater mound. Icarus 223, 181-210. doi:10.1016/j.icarus.2012.11.034.

Kite, E.S., Sneed, J., Mayer, D.P., Wilson, S.A., 2017b. Persistent or repeated surface habitability on Mars during the late Hesperian - Amazonian. Geophysical Research Letters 44, 3991–3999. doi:10.1002/2017GL072660.

Kleinhans, M.G., 2005. Flow discharge and sediment transport models for estimating a minimum timescale of hydrological activity and channel and delta formation on Mars. Journal of Geophysical Research 110 (E12003). doi:10.1029/2005JE002521.

Knighton, A.D., 1998. Fluvial Forms and Processes: A New Perspective. Arnold, London. 400 pp.

Kodama, K., Barnes, G.M., 1997. Heavy Rain events over the south-facing slopes of Hawaii: attendant conditions. Weather Forecast. 12, 347–367. doi:10.1175/1520-0434(1997)012<0347:HREOTS>2.0.CO;2.

Komar, P.D., 1988. Sediment transport by floods. In: Baker, V.R., Kochel, R.C., Patton, P.C. (Eds.), Flood Geomorphology. Wiley-Interscience, New York, pp. 97–111.

Korteniemi, J., Kreslavsky, M. A., 2012. Patterned ground in martian high northern latitudes: Morphology and age constraints. Icarus. doi:10.1016/j.icarus.2013.09.032.

Kraal, E.R., Asphaug, E., Moore, J.M., Howard, A., Bredt, A., 2008. Catalogue of large alluvial fans in martian impact craters. Icarus 194, 101–110. doi:10.1016/j.icarus.2007.09.028.

Kreslavsky, M.A., Head, J.W., 2000. Kilometer-scale roughness of Mars: Results from MOLA data analysis. Journal of Geophysical Research 105, 26695–26711. doi:10.1029/2000JE001259.

Laity, J.E., Malin, M.C., 1985. Sapping processes and the development of theater-headed valley networks on the Colorado Plateau. Geological Society of America Bulletin 96, 203–217. doi:10.1130/0016-7606(1985)96<203:SPATDO>2.0.CO;2.

Lamb, M.P., Dietrich, W.E., Sklar, L.S., 2008. A model for fluvial bedrock incision by impacting suspended and bed load sediment. Journal of Geophysical Research 113 (F03025). doi:10.1029/2007JF000915.

Langer, A.M., Kerr, P.F., 1966. Mojave Playa crusts; physical properties and mineral content. Journal of Sedimentary Petrology 36, 377-396.

Lapotre, M., Lamb, M., 2017. Did Hesperian Amphitheater-Headed Valleys Form by Groundwater Sapping? Lunar and Planetary Science Conference, The Woodlands, TX. Abstract 2860.

Lapotre, M.G.A., Lamb, M.P., Williams, R.M.E., 2016. Canyon formation constraints on the discharge of catastrophic outburst floods of Earth and Mars. Journal of Geophysical Research Planets 121, 1232–1263. doi:10.1002/2016JE005061.

Larsen, M.C., Wieczorek, G.F., Eaton, L.S., Morgan, B.A., Torres- Sierra, H., 2001. Natural hazards on alluvial fans: the debris- flow and flash-flood disaster of northern Venezuela, December 1999. Eos (Washington. DC). 82, 572–573.

Laskar, J., Correia, A.C.M., Gastineau, M., Joutel, F., Levrard, B., Robutel, P., 2004. Long term evolution and chaotic diffusion of the insolation quantities of Mars. Icarus 170, 343-364. doi:10.1016/j.icarus.2004.04.005.

Lasue, J. et al., 2013. Quantitative assessments of the Martian hydrosphere. Space Science Reviews 174. 155-212.

Levy, J., Head, J., Marchant, D., 2009. Thermal contraction crack polygons on Mars: Classification, distribution, and climate implications from HiRISE observations. Journal of Geophysical Research 114 (E01007). doi:10.1029/2008JE003273.

Lewis, K.W., Aharonson, O., 2006. Stratigraphic analysis of the distributary fan in Eberswalde crater using stereo imagery. Journal of Geophysical Research 111, E06001. doi:10.1029/2005JE002558.

Lipman, P.W., Lockwood, J.P., Okamura, R.T., Swanson, D.A., Yamashita, K.M., 1985. Ground deformation associated with the 1975 magnitude-7.2 earthquake and resulting changes in activity of Kilauea Volcano, Hawaii. U.S. Geological Survey Professional Paper 1276, 45 p.

Luo, W., Howard, A.D., 2008. Computer simulation of the role of groundwater seepage in forming Martian valley networks. Journal of Geophysical Research Planets 113, 1–14. doi:10.1029/2007JE002981.

Luo, W., Cang, X., Howard, A.D., 2017. New martian valley network volume estimate consistent with ancient ocean and warm and wet climate. Nature Communications 8, 15766. doi:10.1038/ncomms15766.

Malin, M.C., Bell, J.F., Cantor, B.A., Caplinger, M.A., Calvin, W.M., Clancy, R.T., Edgett, K.S., Edwards, L., Haberle, R.M., James, P.B., Lee, S.W., Ravine, M.A., Thomas, P.C., Wolff, M.J., 2007. Context Camera Investigation on board the Mars Reconnaissance Orbiter. Journal of Geophysical Research 112, E05S04. doi:10.1029/2006JE002808.

Malin, M.C., Carr, M.H., 1999. Groundwater formation of Martian valleys. Nature 397, 589-591. doi:10.1126/science.288.5475.2330.

Malin, M.C., Edgett, K.S., 2000. Evidence of recent groundwater seepage and surface runoff on Mars. Science 288, 2330-2335.

Malin, M.C., Edgett, K.S., 2003. Evidence for Persistent Flow and Aqueous Sedimentation on Early Mars. Science 302, 1931–1934. doi:10.1126/science.1090544.

Mangold, N., 2012. Fluvial valleys on fresh impact ejecta on Mars. Planetary and Space Sciences. 62, 69-85. doi:10.1016/j.pss.2011.12.009.

Mangold, N., Adeli, S., Conway, S., Ansan, V., Langlais, B., 2012a. A chronology of early Mars climatic evolution from impact crater degradation. Journal of Geophysical Research 117 (E04003). doi:10,1029/2011JE004005.

Mangold, N., Forget, F., Maurice, S., Feldman, W. C., Costard, F., 2004. Spatial relationships between patterned ground and ground ice detected by the Neutron Spectrometer on Mars. Journal of Geophysical Research: Planets. 109 (E08001). doi:10.1029/2004JE002235.

Mangold, N., Kite, E.S., Kleinhans, M.G., Newsom, H., Ansan, V., Hauber, E., Kraal, E., Quantin, C., Tanaka, K., 2012b. The origin and timing of fluvial activity at Eberswalde crater, Mars. Icarus 220, 530–551. doi:10.1016/j.icarus.2012.05.026.

Marchant, D.R., Head, J.W., 2007. Antarctic dry valleys: Microclimate zonation, variable geomorphic processes, and implications for assessing climate change on Mars. Icarus 182, 187-222.

Masursky, H., Boyce, J.M., Dial, A.L., Schaber, G.G., Strobell, M.E., 1977. Classification and time of formation of martian channels based on Viking data. Journal of Geophysical Research 82, 4016–4038. doi:10.1029/JS082i028p04016.

Matsubara, Y., Howard, A.D., Burr, D.M., Williams, R.M., Moore, J.M.,2012. Meandering channels in a non-vegetated area: Quinn River, NV as a martian analog. Lunar and Planetary Science Conference, The Woodlands, TX. Abstract 2534.

Matsubara, Y., Howard, A.D., Gochenour, P.J., 2013. Hydrology of early Mars: valley network incision. Journal of Geophysical Research Planets 118. doi:10.1002/jgre.20081.

McEwen, A.S., Bierhaus, E.B., 2006. The importance of cecondary cratering to age constraints on planetary surfaces. Annual Review of Earth and Planetary Science, 34, 535-567. doi:10.1146/annurev.earth.34.031405.125018.

McEwen, A.S., Preblich, B.S., Turtle, E.P., Artemieva, N.A., Golombek, M.P., Hurst, M., Kirk, R.L., Burr, D.M., Christensen, P.R., 2005. The rayed crater Zunil and interpretations of small impact craters on Mars. Icarus 176, 351-381. doi:10.1016/j.icarus.2005.02.009.

McEwen, A.S., et al., 2007. Mars reconnaissance orbiter's high resolution imaging science experiment (HiRISE). Journal of Geophysical Research: Planets 112 (E05S02). doi:10.1029/2005JE002605.

McPhie, J., Walker, G.P.L., Christiansen, R.L., 1990. Phreatomagmatic and phreatic fall and surge deposits from explosions at Kilauea volcano, Hawaii, 1790 A.D.: Keanakakoi Ash Member. Bulletin of Volcanology 52, 334–354. doi:10.1007/BF00302047.

Mellon, M.T., 1997. Small-scale polygonal features on Mars: Seasonal thermal contraction cracks in permafrost. Journal Geophysical Research 102, 25617-25628.

Michael, G.G., Neukum, G., 2010. Planetary surface dating from crater size–frequency distribution measurements: Partial resurfacing events and statistical age uncertainty. Earth and Planetary Science Letters 294, 223-229. doi:10.1016/j.epsl.2009.12.041.

Michael, G.G., 2013. Planetary surface dating from crater size-frequency distribution measurements: differential presentation of data for resurfaced units. Lunar and Planetary Science Conference, The Woodlands, TX. Abstract 2181.

Milana, J.P., 2010. The sieve lobe paradigm: Observations of active deposition. Geology 38, 207–210. doi:10.1130/G30504.1.

Mohrig, D.C., Heller, P.L., Paola, C., Lyons, W.J., 2000. Interpreting avulsion process from ancient alluvial sequences: Guadalope-Matarranya system (northern Spain) and Wasatch Formation, (western Colorado). Geological Society of America Bulletin 112, 1787–1803.

Moore, J.M., Howard, A.D., 2005. Large alluvial fans on Mars. Journal of Geophysical Research 110. doi:10.1029/2004JE002352.

Moore, J.M., Howard, A.D., Dietrich, W.E., Schenk, P.M., 2003. Martian layered fluvial deposits: Implications for Noachian climate scenarios. Geophysical Research Letters 30 (2292). doi:10.1029/2003GL019002.

Morato, Z.M., Broxton, M.J., Beyer, R.A., Lundy, M., Husmann, K., 2010. Ames Stereo Pipeline, NASA's open source automated stereogrammetry software. Lunar and Planetary Science Conference, The Woodlands, TX. Abstract 2364.

Morgan, A.M., Beyer, R.A., Howard, A.D., Moore, J.M., 2012a. The Alluvial Fans of Saheki Crater. Lunar and Planetary Science Conference, The Woodlands, TX. Abstract 2815.

Morgan, A.M., Howard, A.D., Moore, J.M., Hobley, D. E. J., Beyer, R.A., 2012b. Episode(s) of intense alluvial deposition during an era of drought on Mars: Evidence from fans at Saheki (and Gale?). AGU Fall Meeting, San Francisco, CA. Abstract P11B-1830.

Morgan, A.M., Howard, A.D., Hobley, D.E.J., Moore, J.M., Dietrich, W.E., Williams, R.M.E., Burr, D.M., Grant, J.A., Wilson, S.A., Matsubara, Y., 2014. Sedimentology and climatic environment of alluvial Fans in the martian Saheki crater and a comparison with terrestrial fans in the Atacama Desert. Icarus 229, 131–156. doi:10.1016/j.icarus.2013.11.007.

Morgan, G.A., Head, J.W., 2009. Sinton crater, Mars: Evidence for impact into a plateau icefield and melting to produce valley networks at the Hesperian–Amazonian boundary. Icarus 202, 39-59.

Murchie, S.L., et al., 2007. Compact Reconnaisance Imaging Spectrometer for Mars (CRISM) on Mars Reconnaissance Orbiter (MRO). Journal of Geophysical Research 112 (E05S03). doi:10.1029/2006JE002682.

Murchie, S.L., et al., 2009. A synthesis of martian aqueous mineralogy after 1 Mars year of observations from the Mars Reconnaissance Orbiter. Journal of Geophysical Research Planets 114. doi:10.1029/2009JE003342.

Murray, A.B., Paola, C., 1994. A cellular model of braided rivers. Nature 371, 54–57. doi:10.1038/371054a0.

Neal, J.T., Langer, A.M., Kerr, P.F., 1968. Giant dessication polygons of Great Basin playas. Geological Society of America Bulletin 79, 69-90. doi:10.1130/0016-7606(1968)79[69:GDPOGB]2.0.CO;2.

Nemec, W., Postma, G., 1993. Quaternary alluvial fans in southwestern Crete: sedimentation processes and geomorphic evolution. In: Marzo, M., Puigdefábregas, C. (Eds.), Alluvial Sedimentation. Blackwell Publishing Ltd., Oxford, UK, pp. 235–276. doi:10.1002/9781444303995.ch18.

Neukum, G., Ivanov, B.A., Hartmann, W.K., 2001. Cratering Records in the Inner Solar System in Relation to the Lunar Reference System. In: R. Kallenbach, J. Geiss, W.K. Hartmann (Eds.) Chronolology and Evolution of Mars, 55–86.

Nicholas, A.P., Quine, T.A., 2007. Modeling alluvial landform change in the absence of external environmental forcing. Geology 35, 527. doi:10.1130/G23377A.1.

Nicholas, A.P., Sandbach, S.D., Ashworth, P.J., Amsler, M.L., Best, J.L., Hardy, R.J., Lane, S.N., Orfeo, O., Parsons, D.R., Reesink, A.J.H., Sambrook Smith, G.H., Szupiany, R.N., 2012. Modelling hydrodynamics in the Rio Paraná, Argentina: An evaluation and inter-comparison of reduced-complexity and physics based models applied to a large sand-bed river. Geomorphology 169–170, 192–211. doi:10.1016/j.geomorph.2012.05.014.

Owen, S., Segall, P., Freymueller, J., Miklius, A., Denlinger, R., Arnadóttir, T., Sako, M., Bürgmann, R., 1995. Rapid deformation of the South flank of Kilauea volcano, Hawaii. Science (80-.). 267, 1328–1332. doi:10.1126/science.267.5202.1328.

Owen, S., Segall, P., Lisowski, M., Miklius, A., Denlinger, R., Sako, M., 2000. Rapid deformation of Kilauea volcano: global positioning system measurements between 1990 and 1996. Journal of Geophysical Research 105, 18,983–18,998.

Palucis, M.C., Dietrich, W.E., 2014. How small is too small? A model for assessing retention age uncertainties when dating small areas. Workshop on Issues in Crater Studies and Dating of Planetary Surfaces, Laurel, MD. Abstract 9044.

Palucis, M.C., Dietrich, W.E., Hayes, A.G., Williams, R.M.E., Gupta, S., Mangold, N., Newsom, H., Hardgrove, C., Calef III, F., Sumner, D.Y., 2014. The origin and evolution of the Peace Vallis fan system that drains to the Curiosity landing area, Gale Crater, Mars. Journal of Geophysical Research Planets 1–24. doi:10.1002/2013JE004583.

Palucis, M., Dietrich, W., Williams, R., Hayes, A., Parker, T., Sumner, D., Mangold, N., Lewis, K., Newsom, H., 2015. Sequence and relative timing of large lakes in Gale crater (Mars) after the formation of Mount Sharp. Journal of Geophysical Research Planets 1237–1251. doi:10.1002/2014JE004730.

Parker, G., 1978. Self-formed straight rivers with equilibrium banks and mobile bed. Part 2. The gravel river. Journal of Fluid Mechanics 89, 127-146. doi:10.1017/S0022112078002505.

Parker, G., Paola, C., Whipple, K.X., Mohrig, D., 1998. Alluvial Fans Formed by Channelized Fluvial and Sheet Flow. I: Theory. Journal of Hydraulic Engineering 124(10). doi:10.1061/(ASCE)0733-9429(1998)124:10(985).

Parker, G., Wilcock, P.R., Paola, C., Dietrich, W.E., Pitlick, J., 2007. Physical basis for quasi-universal relations describing bankfull hydraulic geometry of single-thread gravel bed rivers. J. Geophys. Res. 112. doi:10.1029/2006JF000549.

Platz, T., Michael, G., Tanaka, K.L., Skinner, J.A., Fortezzo, C.M., 2013. Crater-based dating of geological units on Mars: Methods and application for the new global geological map. Icarus 225, 806–827. doi:10.1016/j.icarus.2013.04.021.

Podolsky, D.M.W., Roberts, G.P., 2008. Growth of the volcano-flank Koa’e fault system, Hawaii. Journal of Structural Geology 30, 1254–1263. doi:10.1016/j.jsg.2008.06.006.

Pollack, J.B., Kasting, J.F., Richardson, S.M., Poliakoff, K., 1987. The case for a wet, warm climate on early Mars. Icarus 71, 203–224. doi:10.1016/0019-1035(87)90147-3.

Pondrelli, M., 2005. Complex evolution of paleolacustrine systems on Mars: An example from the Holden crater. Journal of Geophysical Research 110, E04016. doi:10.1029/2004JE002335.

Pondrelli, M., Rossi, A.P., Marinagleli, L., Hauber, E., Gwinner, K., Baliva, A., Di Lorenzo, S., 2008. Evolution and depositional environments of the Eberswalde fan delta, Mars. Icarus 197, 429-451. doi:10.1016/j.icarus.2008.05.018.

Pondrelli, M., Rossi, A.P., Platz, T., Ivanov, A., Marinangeli, L., Baliva, A., 2011. Geological, geomorphological, facies and allostratigraphic maps of the Eberswalde fan delta. Planetary and Space Science 59, 1166-1178. doi:10.1016/j.pss.2010.10.009.

Pueyo, J.J., Chong, G., Jensen, A., 2001. Neogene evaporites in desert volcanic environments: Atacama Desert, northern Chile. Sedimenology 48, 1411-1431.

Radebaugh, J., Ventra, D., Lorenz, R.D., Farr, T., Kirk, R., Hayes, A., Malaska, M.J., Birch, S., Liu, Z.Y.-C., Lunine, J., Barnes, J., Le Gall, A., Lopes, R., Stofan, E., Wall, S., Paillou, P., 2016. Alluvial and fluvial fans on Saturn's moon Titan reveal processes, materials and regional geology. Geological Society of London, Special Publication 440. doi:10.1144/SP440.6.

Rao, J.S., 1976. Some Tests Based on Arc-Lengths for the Circle. Sankhyā Indian Journal of Statistics 38, 329–338.

Rickenmann, D., Recking, A., 2011. Evaluation of flow resistance in gravel-bed rivers through a large field data set. Water Resources Research 47 (W07538). doi:10.1029/2010WR009703.

Ritter, J.B., Miller, J.R., Enzel, Y., Wells, S.G., 1995. Reconciling the roles of tectonism and climate in Quaternary alluvial fan evolution. Geology 23, 245. doi:10.1130/0091-7613(1995)023<0245:RTROTA>2.3.CO;2.

Robbins, S.J., Hynek, B.M., 2012. A new global database of Mars impact craters ≥1 km: 1. Database creation, properties, and parameters. Journal of Geophysical Research Planets 117, 1–18. doi:10.1029/2011JE003966.

Roering, J.J., Kirchner, J.W., Dietrich, W.E., 1999. Evidence for nonlinear, diffusive sediment transport on hillslopes and implications for landscape morphology. Water Resources Research 35, 853-870.

Roering, J.J., Kirchner, J.W., Dietrich, W.E., 2001. Hillslope evolution by nonlinear, slope-dependent transport; steady state morphology and equilibrium adjustment timescales. Journal of Geophysical Research, B, Solid Earth and Planets 106, 16,499-16,513.

Salcher, B.C., Faber, R., Wagreich, M., 2010. Climate as main factor controlling the sequence development of two Pleistocene alluvial fans in the Vienna Basin (eastern Austria) — A numerical modelling approach. Geomorphology 115, 215–227. doi:10.1016/j.geomorph.2009.06.030.

Schiffman, P., Spero, H.J., Southard, R.J., Swanson, D.A., 2000. Controls on palagonitization versus pedogenic weathering of basaltic tephra: Evidence from the consolidation and geochemistry of the Keanakako'i Ash Member, Kilauea Volcano. Geochemistry, Geophys. Geosystems 1. doi:10.1029/2000GC000068.

Schumm, S.A., Baker, V.R., Bowker, M.F., Dixon, J.R., Dunne, T., Hamilton, D., Merritts, D., Committee on Alluvial Fan Flooding, 1996. Alluvial Fan Flooding. National Academy of Sciences, Washington, D.C.

Segura, T.L., Toon, O.B., Colaprete, A., 2008. Modeling the environmental effects of moderate-sized impacts on Mars. Journal of Geophysical Research 113 (E11007). doi:10.1029/2008JE003147.

Servicio Nacional de Geologia y Mineria, G. d. C., 2003. Mapa Geologico de Chile: Version Digital. Publication Geologica Digital, No. 4.

Shaw, P.A., Thomas, D.S.G., 1989. Playas, pans and salt lakes. In: D. S. G. Thomas, (Ed.), Arid Zone Geomorphology. John Wiley & Sons, New York, pp. 184-205.

Shields, A., 1936. Application of similarity principles and turbulence research to bed load movement. In: Ott, W.P., van Uchelen, J.C. (Eds.), Hydrodynamics Lab. Rep. 167. Calif. Inst. of Technol., Pasadena.

Simpson, R.H., 1952. Evolution of the Kona Storm, a Subtropical Cyclone. Journal of Meteorology 9, 24-35. doi:10.1175/1520-0469(1952)009<0024:EOTKSA>2.0.CO;2.

Smith, G.I., 1957. Core logs from Owens, China, Searles and Panamint basins, California. U.S. Geological Survey Bulletin 1045-A.

Smith, G.I., 1974. Subsurface stratigraphy and geochemistry of Late Quaternary evaporites, Searles Lake, California. U.S. Geological Survey Professional Paper 1043. 1-130.

Smoot, J.P., Castens-Seidel, B., 1995. Sedimentary features produced by efflorescent salt crusts, Saline Valley and Death Valley, California. Sedimentology and Geochemistry of Modern and Ancient Saline Lakes. Society for Sedimentary Geology, pp. 73-90.

Spötl, C., Wright, V.P., 1992. Groundwater Dolocretes from the Upper Triassic of the Paris Basin, France: a Case Study of an Arid, Continental Diagenetic Facies. Sedimentology. 36, 1119-1136. doi:10.1111/j.1365-3091.1992.tb02000.x.

Staley, D.M., Wasklewicz, T.A., Blaszczynski, J.S., 2006. Surficial patterns of debris flow deposition on alluvial fans in Death Valley, CA using airborne laser swath mapping data. Geomorphology 74, 152–163. doi:10.1016/j.geomorph.2005.07.014.

Stock, J.D., 2013. Waters Divided: A History of Alluvial Fan Research and a View of Its Future. In: Shroder, J., Wohl, E. (Eds.), Treatise on Geomorphology. Elsevier, San Diego, pp. 413–458. doi:10.1016/B978-0-12-374739-6.00249-9.

Stock, J.D., Schmidt, K.M., Miller, D.M., 2008. Controls on alluvial fan long-profiles. Geological Society of America Bulletin 120, 619–640. doi:10.1130/B26208.1.

Stoertz, G. E., Ericksen, G., E., 1974. Geology of Salars in Northern Chile. U. S. Geological Survey. Professonal Paper 811, 65 p.

Sugarbaker, L.J., Eldridge, D.F., Jason, A.L., Lukas, V., Saghy, D.L., Stoker, J.M., Thunen, D.R., 2016. Status of the 3D Elevation Program, 2015, Open-File Report. Reston VA. doi:10.3133/ofr20161196.

Sullivan, R., et al., 2008. Wind-driven particle mobility on Mars: Insights from Mars Exploration Rover observations at “El Dorado” and surroundings at Gusev Crater. Journal of Geophysical Research 113 (E06S07) doi:10.1029/2008JE003101.

Sun, T., Paola, C., Parker, G., Meakin, P., 2002. Fluvial fan deltas: Linking channel processes with large-scale morphodynamics. Water Resour. Res. 38, 1–10. doi:10.1029/2001WR000284.

Swenson, J.B., Voller, V.R., Paola, C., Parker, G., Marr, J.G., 2000. Fluvio-deltaic sedimentation: A generalized Stefan problem. European Journal of Applied Mathematics 11 (5), pp. 433–452.

Talling, P.J., 2000. Self-organization of river networks to threshold states. Water Resources Research 36, 1119-1128. doi:10.1029/1999WR900339.

Tanaka, K.L., Skinner, J.A., Dohm, J.M., Irwin, R.P., Kolb, E.J., Fortezzo, C.M., Platz, T., Michael, G.G., Hare, T.M., 2014. Geologic Map of Mars. United States Geol. Surv.

Tanaka, K.L., 1986. The stratigraphy of Mars. Journal Geophysical Research 91(B13), E139-E158. doi:10.1029/JB091iB13p0E139.

Thomas, R., Nicholas, A.P., Quine, T.A., 2007. Cellular modelling as a tool for interpreting historic braided river evolution. Geomorphology 90, 302–317. doi:10.1016/j.geomorph.2006.10.025.

Tunison, J.T., Zimmer, N.G., Gates, M.R., Mattos, R.M., 1994. Fountain Grass Control in Hawai'i Volcanoes National Park 1985-1992. Honolulu, HI.

United States Geological Survey (USGS), 2010. USGS High Resolution Orthoimagery for Hawaii Volcanoes National Park.

Volker, H.X., Wasklewicz, T.A., Ellis, M.A., 2007. A topographic fingerprint to distinguish alluvial fan formative processes. Geomorphology 88, 34–45. doi:10.1016/j.geomorph.2006.10.008.

Wagreich, M., Strauss, P.E., 2005. Source area and tectonic control on alluvial-fan development in the Miocene Fohnsdorf intramontane basin, Austria. In: In: Harvey, A.M., Mather, A.E., Stokes, M. (Eds.) Alluvial Fans: Geomorphology, Sedimentology, Dynamics. Geological Society of London, Special Publication 251, pp. 207-216. doi:10.1144/GSL.SP.2005.251.01.14.

Ward, W.R., 1979. Present obliquity oscillations of Mars - Fourth-order accuracy in orbital E and I. Journal Geophysical Research 84, 237-241. doi:10.1029/JB084iB01p00237.

Warner, N.H., Gupta, S., Calef, F., Grindrod, P., Boll, N., Goddard, K., 2015. Minimum effective area for high resolution crater counting of martian terrains. Icarus 245, 198–240. doi:10.1016/j.icarus.2014.09.024.

Weinberger, R., 1999. Initiation and growth of cracks during dessication of stratified muddy sediments. Journal of Structural Geology 21, 379-386. doi:10.1016/S0191-8141(99)00029-2.

Wells, S.G., Harvey, A.M., 1987. Sedimentologic and geomorphic variations in storm-generated alluvial fans, Howgill Fells, northwest England. Geological Society of America Bulletin 98, 182. doi:10.1130/0016-7606(1987)98<182:SAGVIS>2.0.CO;2.

Wells, S.G., McFadden, L.D., Dohrenwend, J.C., 1987. Influence of late Quaternary climatic changes on geomorphic and pedogenic processes on a desert piedmont, Eastern Mojave Desert, California. Quat. Res. 27, 130–146. doi:10.1016/0033-5894(87)90072-X.

Wentworth, C.K., 1922. A scale of grade and class terms for clastic sediments. Journal of Geology. 30, 377-392.

Werner, S.C., Ivanov, B.A., Neukum, G., 2009. Theoretical analysis of secondary cratering on Mars and an image-based study on the Cerberus Plains. Icarus 200, 406-417. doi:10.1016/j.icarus.2008.10.011.

Werner, S.C., Tanaka, K.L., 2011. Redefinition of the crater-density and absolute-age boundaries for the chronostratigraphic system of Mars. Icarus 215, 603-607. doi:10.1016/j.icarus.2011.07.024.

Werner, S.C., Ody, A., Poulet, F., 2014. The Source crater of martian Shergottite meteorites. Science 343, 1343–1346. doi:10.1126/science.1247282.

Whipple, K.X., Dunne, T., 1992. The influence of debris-flow rheology on fan morphology, Owens Valley, California. Geological Society of America Bulletin. doi:10.1130/0016-7606(1992)104<0887:TIODFR>2.3.CO;2.

Wilkerson, G.V., Parker, G., 2011. Physical Basis for Quasi-Universal Relationships Describing Bankfull Hydraulic Geometry of Sand-Bed Rivers. Journal of Hydraulic Engineering 137. doi:10.1061/(ASCE)HY.1943-7900.0000352.

Williams, K., Toon, O., Heldmann, J., McKay, C., Mellon, M., 2008. Stability of mid-latitude snowpacks on Mars. Icarus 196, 565-577. doi:10.1016/j.icarus.2008.03.017.

Williams, K., Toon, O., Heldmann, J., Mellon, M., 2009a. Ancient melting of mid-latitude snowpack on Mars as a water source for gullies. Icarus 200, 418-425. doi:10.1016/j.icarus.2008.12.013.

Williams, R.M.E., et al, 2013. Martian fluvial conglomerates at Gale crater. Science. 340, 1068-1072. doi:10.1126/science.1237317.

Williams, R.M.E., Deanne Rogers, A., Chojnacki, M., Boyce, J., Seelos, K.D., Hardgrove, C., Chuang, F., 2011. Evidence for episodic alluvial fan formation in far western Terra Tyrrhena, Mars. Icarus 211, 222–237. doi:10.1016/j.icarus.2010.10.001.

Williams, R.M.E., Irwin, R.P., Zimbelman, J.R., 2009b. Evaluation of paleohydrologic models for terrestrial inverted channels: Implications for application to martian sinuous ridges. Geomorphology. 107, 300-315. doi:10.1016/j.geomorph.2008.12.015.

Williams, R.M.E., Malin, M.C., 2008. Sub-kilometer fans in Mojave crater, Mars. Icarus 198, 365–383. doi:10.1016/j.icarus.2008.07.013.

Williams, R.M.E., Zimbelman, J.R., Johnston, A.K., 2006. Aspects of alluvial fan shape indicative of formation process: A case study in southwestern California with application to Mojave Crater fans on Mars. Geophysical Research Letters 33. doi:10.1029/2005GL025618.

Wilson, L., Ghatan, G. J., Head, I. J. W., Mitchell, K. L., 2004. Mars outflow channels: A reappraisal of the estimation of water flow velocities from water depths, regional slopes, and channel floor properties. Journal of Geophysical Research: Planets 109, E09003 1-10. doi:10.1029/2004JE002281.

Wilson, S.A., Zimbelman, J.R., 2004. Latitude-dependent nature and physical characteristics of transverse aeolian ridges on Mars, Journal of Geophysical Research: Planets 109 (E10003). doi: 10.1029/2004JE002247.

Wilson, S.A., Grant, J.A., Howard, A.D., 2012. Distribution of Intracrater Alluvial Fans and Deltaic Deposits in the Southern Highlands of Mars. Lunar and Planetary Science Conference, The Woodlands, TX. Abstract 2462.

Wilson, S.A., Grant, J.A., Howard, A.D., 2013. Inventory of alluvial fans and deltas on Mars. Lunar and Planetary Science Conference, The Woodlands, TX. Abstract 2710.

Wilson, S.A., Howard, A.D., Moore, J.M., Grant, J.A., 2007. Geomorphic and stratigraphic analysis of Crater Terby and layered deposits north of Hellas basin, Mars. Journal of Geophysical Research: Planets 112 (E08009). doi:10.1029/2006JE002870.

Wilson, S.A., Howard, A.D., Moore, J.M., Grant, J.A., 2016. A cold-wet middle-latitude environment on Mars during the Hesperian-Amazonian transition: Evidence from northern Arabia valleys and paleolakes. Journal of Geophysical Research Planets 121, 1667–1694. doi:10.1002/2016JE005052.

Wolfe, E.W., Morris, J., 1996. Geologic map of the island of Hawaii, U.S. Geological Survey Professional Paper.

Wordsworth, R., Forget, F., Millour, E., Head, J.W., Madeleine, J.-B.-B., Charnay, B., Charnaya, B., 2013. Global modelling of the early martian climate under a denser CO2 atmosphere: Water cycle and ice evolution. Icarus 222, 1–19. doi:10.1016/j.icarus.2012.09.036.

Wordsworth, R.D., 2016. The Climate of Early Mars. Annual Reviews of Earth and Planetary Science 44. doi:10.1146/annurev-earth-060115-012355.

Yechieli, Y., Wood, W.W., 2002. Hydrogeologic processes in saline systems: Playas, sabkhas, and saline lakes. Earth-Science Reviews 58, 343-365.

Zimbelman, J.R., Irwin, R.P., Williams, S.H., Bunch, F., Valdez, A., Stevens, S., 2009. The rate of granule ripple movement on Earth and Mars. Icarus 203, 71-76. doi:10.1016/j.icarus.2009.03.033.

Zuber, M.T., Smith, D.E., Solomon, S.C., Muhleman, D.O., Head, J.W., Garvin, J.B., Abshire, J.B., Bufton, J.L., 1992. The Mars Observer Laser Altimeter Investigation. Journal of Geophysical Research 97, 7781–7797. doi:10.1029/92je00341.